INVESTIGATIONS IN EMISSIONS-CONSTRAINED, INTEGRATED GAS-ELECTRIC ENERGY SYSTEMS

A DISSERTATION
SUBMITTED TO THE DEPARTMENT OF ENERGY RESOURCES ENGINEERING
AND THE COMMITTEE ON GRADUATE STUDIES
OF STANFORD UNIVERSITY
IN PARTIAL FULFILLMENT OF THE REQUIREMENTS
FOR THE DEGREE OF
DOCTOR OF PHILOSOPHY

Gregory Von Wald
August 2021

I certify that I have read this dissertation and that, in my opinion, it is fully adequate in scope and quality as a dissertation for the degree of Doctor of Philosophy.

Adam Brandt, Primary Adviser

I certify that I have read this dissertation and that, in my opinion, it is fully adequate in scope and quality as a dissertation for the degree of Doctor of Philosophy.

Ines Azevedo

I certify that I have read this dissertation and that, in my opinion, it is fully adequate in scope and quality as a dissertation for the degree of Doctor of Philosophy.

Sally Benson

Approved for the Stanford University Committee on Graduate Studies.

Stacey F. Bent, Vice Provost for Graduate Education

This signature page was generated electronically upon submission of this dissertation in electronic format. An original signed hard copy of the signature page is on file in University Archives.

Abstract

To mitigate risk of climate disaster, net atmospheric release of greenhouse gases (GHGs) from energy systems must decline to zero by mid-century. Electricity and natural gas are the most widely used end-use energy carriers in existing infrastructure systems that deliver energy to buildings. Such systems serve hundreds of millions of consumers in the United States and billions globally. Electricity and natural gas suppliers are also subject to unique regulatory oversight given their status as a public utility. While the electric power system has a reasonably clear path towards net-zero emissions, the natural gas system lacks a diverse set of low-carbon supply options.

As energy utilities implement climate change mitigation policies, system planners require strategies for achieving affordable emissions reductions. Coordinated planning of electric power and natural gas delivery systems will allow synergistic investment plans to address cross-sector operational constraints, competing uses for net-zero emissions fuels, and shifts in final energy demands across energy carriers. In Chapter 2, we develop a novel optimization program that finds the cost-minimizing mix of infrastructure expansion or reduction across both gas and electric systems to satisfy a sequence of successively tightened, sector-specific emissions constraints. Alongside conventional energy supply resources, our framework allows for central-planning of end-use equipment stocks to allow switching between gas and electric appliances upon failure or premature replacement. The proposed model is used to simulate a range of case study scenarios for a benchmark 25-node gas network coupled to a 24-node power system test network. We find that electrification of greater than 80% of core gas demands is a component of the least-cost solution for indicative energy systems representing Mountain Northwest and Coastal Pacific climate patterns. Despite this substitution, the gas system is maintained to provide energy to difficult-to-electrify customers and to deliver net-zero emissions gas to electricity generators for use in times of peak net electricity demand. Restricting electrification of gas appliances increases reliance on advanced gas technologies, such as power-to-gas transformation, and increases annual system costs by 15% in 2040. Neglecting practical constraints on pipeline blending of hydrogen can produce a misleading result that only transitions 20% of gas demands to electric appliance substitutes, relying on hydrogen blend fractions of greater than 50%. In all cases, we find average costs of delivered gas increase nearly 5-fold across the decarbonization transition in the test system, highlighting the importance of future work to address cost-allocation

strategies for ensuring an equitable, affordable energy transition.

The industrial sector accounts for a large share of natural gas demands and nearly a quarter of global greenhouse gas emissions. These energy demands can be difficult to transition to electric-powered alternatives. Methane pyrolysis could be used to produce low-carbon hydrogen (H_2) for industrial processes while generating a solid carbon product that can be permanently sequestered or sold as a manufacturing feedstock. Chapter 3 analyzes methane pyrolysis via a molten media that continuously catalyzes the reaction and separates the produced carbon. We perform design optimization to evaluate the technoeconomics of this technology. We model a template small-scale 50 MW boiler (10.4 k tonne H_2/year) as a base case for combustion applications, because such boilers are particularly challenging to decarbonize (are expensive to electrify and too small-scale for post-combustion CO_2 capture and sequestration (CCS)). We find that the levelized cost of low-carbon energy using the reactor is \$11.09/MMBTU, equivalent to an abatement cost of \$115/tonne CO_2 avoided. In addition, we examine a policy-informed case study of H_2 production at refineries subject to the California Low Carbon Fuel Standard. In the absence of CO_2 credits, the levelized cost of hydrogen is \$1.75/kg H_2, but when credits are included at recent prices of \$190/tonne CO_2eq., we find a levelized cost of hydrogen as low as \$0.39/kg H_2. Optimization was conducted under a range of economic sensitivities, finding that, as long as catalyst losses can be minimized, methane pyrolysis costs could be competitive with decarbonization methods such as CCS or other low-carbon H_2 production pathways.

Accurate quantification and attribution of GHG emissions liabilities is essential for climate policy but challenging in the case of energy transfers across regulatory jurisdictions. Regulating emissions associated with delivered electricity is further complicated by contractual arrangements for dynamic electricity transfer that confound emissions accounting approaches rooted in the physics of grid operations. In Chapter 4, we present a two-part analysis of greenhouse gas accounting methodologies. First, we evaluate a new methodology adopted by the California Energy Commission to calculate the GHG emissions intensity of retail electricity providers. In the long run, the new regulations better align with the physical nature of grid operation than did past practices, but policymakers should monitor a set of potential challenges as market structures evolve. Second, we propose a novel consumption-based accounting methodology to reconcile the nominal and the physical flows of electricity from generators to consumers. We also compare capacity-factor-based and regression-based approaches for estimating default emissions factors, in the absence of fully specified nominal electricity flows. As a case study, we apply this approach to assess the methods by which California regulators quantify "specified" and "unspecified" electricity imports and their associated GHG emissions. Collectively, these efforts illustrate principles for a comprehensive, empirical accounting framework that could inform efforts to improve the accuracy and consistency of policies regulating regional electricity transfers. Similar techniques will be necessary to track embodied GHG emissions of electricity and gaseous fuel delivered in integrated gas-electric energy systems.

Acknowledgments

As I place this capstone on my academic journey, I feel privileged by circumstance to be the sum-product of all those who have helped to nudge me along this path.

I thank all my teachers, collaborators, and mentors over the years that have helped to chart my course from James Madison University and through Stanford University. I thank Dr. Chris Bachmann for fostering my interdisciplinary ambitions early and often throughout my undergraduate career. I thank Dr. Mohammad Masnadi, Dr. David Chester Upham, and Dr. Evan Sherwin for their invaluable intellectual support, and kindness as I gained my footing as a PhD student. I thank Dr. Danny Cullenward and Dr. Michael Mastrandrea for their guidance, assistance, and insight on the intersection of complex technical questions and the regulatory proceedings where theory meets practice. I also thank Dr. Anatoly Zlotnik and Dr. Kaarthik Sundar for their assistance and patience in collaboration on novel approaches to integrated gas-electric system planning and simulation. I thank Dr. John Weyant for sharing his wealth of insight and serving as my dissertation committee chair. I thank Dr. Michael Wara for lending a critical policy and legal lens to my research and for serving as a member of my dissertation committee. And I owe special thanks to my reading committee members and professors, Dr. Sally Benson and Dr. Ines Azevedo for their sharp critiques, thoughtful insights, and unique perspectives.

I owe the largest debt of gratitude to my advisor, Dr. Adam Brandt. He has provided intellectual support and secured financial support as I followed my nose across an arsenal of interdisciplinary macro-energy systems research questions. His adaptive management style and empathetic leadership is inspiring, and he possesses a rare dedication to not just publish good science, but also to prepare good scientists. Adam gave me enough rope to swing on to new intellectual heights, and I will not soon forget the lessons learned. It has been a joy working together; until our paths cross again: "Ne retardatur quod coepistis explete."

My graduate school experience would not have been complete without internships that allowed me to try on a few of the many hats across the clean energy ecosystem. I thank Brian Bartholomeusz with the TomKat Center for Sustainable Energy for the opportunity to mentor their undergraduate summer researchers. I thank Rachel Peterson and then-Commissioner (now Chair) Liane Randolph for fostering my learning at the California Public Utilities Commission. And I thank Zachary Ming

and the many bright consultants at Energy and Environmental Economics (E3) for the chance to see the models come to life to inform utility investment strategy and regulatory policy.

I also acknowledge the California Council on Science and Technology, the Stanford Center for Carbon Storage, the Precourt Institute for Energy, and the Department of Energy Resources Engineering for the financial support during my course of study. And I thank the Center for Computational Earth Sciences for providing the high-performance computational resources which enabled my work.

I would like to thank all my friends and family, too numerous to name, for the love and laughter over the past five years. I thank my fellow students, colleagues, and friends in the Environmental Assessment and Optimization Group, the Department of Energy Resources Engineering, and specifically the IC/Fish Tank office. I cherish every game of office basketball, all the Friday (and occasionally "small Friday") beers, and I recall fondly every noise complaint we received along the way. I will carry with me the memories and the mild-to-moderate caffeine-dependence.

I am immeasurably indebted to my parents, Donna and Steve, and sister, Melissa, for inspiring in me an incurable curiosity and affording me with every opportunity to pursue my goals. Finally, to my reason, my sunshine, and my super-power, I thank my love, Meghan, for her unflinching support through this years-long rollercoaster ride.

George Box, the British statistician, is often referenced for his famous quotation noting that "all models are wrong, but some are useful." Though true, I much prefer his subsequent guidance as it applies to building models and in all aspects of life: "It is inappropriate to be concerned about mice when there are tigers abroad." It is my sincere hope that this imperfect work is useful for the next to embark on this tiger hunt.

Thank you for reading.

Contents

List of Tables

List of Figures

Chapter 1

Introduction

1.1 Motivation

To mitigate risk of climate disaster, net atmospheric release of greenhouse gases (GHGs) must decline to zero by mid-century [1, 2]. Technological and economic systems for production, conversion, and consumption of energy account for nearly three-quarters of anthropogenic GHG emissions [3]. Therefore, large-scale mitigation of GHG emissions requires transitioning to net-zero emissions energy systems [4].

Electricity and natural gas are the most widely used end-use energy carriers in existing infrastructure systems. These systems deliver energy to buildings housing hundreds of millions of consumers in the United States and billions globally. Given their status as public utilities and natural monopolies, electricity and natural gas providers are also often subject to unique and comprehensive regulatory oversight, permitting cost-of-service regulation [5] and investment planning to protect the public interest [6, 7].

The electric power system has a clear path towards net-zero emissions by utilizing a suite of renewable and emissions-free energy resources, ranging from wind and solar to nuclear-powered or carbon-capture enabled electricity generators [8]. While the costs of clean electricity may be high in some cases (e.g., when serving demand with expensive seasonal backup technologies), the technical roadblocks are generally well understood and options exist. The natural gas system, on the other hand, lacks a diverse set of low-carbon supply options to satisfy "direct-use" (or "core") gas demands in the residential, commercial, and industrial sectors (as distinguished from natural gas consumed by electricity generators). Biogenic methane (CH_4) can be produced via the anaerobic breakdown of organic matter in landfills, wastewater treatment plants, or agricultural/livestock waste management [9]. In addition, well-understood mechanisms for water electrolysis can be used to generate hydrogen (H_2) from clean sources of electricity, though at high cost given current technologies. Synthesizing this H_2 with carbon dioxide (CO_2) of atmospheric origin enables the production of hydrocarbons

with net-zero emissions on a life-cycle basis. These options are collectively called "electro-fuels". It is widely thought that electro-fuels production facilities will be a large source of flexible and price-responsive demand for electricity during times of renewable over-generation (e.g., mid-day surplus solar energy converted to H_2).

Alternatively, continued use of fossil natural gas may be paired with direct carbon-capture at the point of consumption or atmospheric carbon removal to offset the emissions. Lastly, current natural gas demands could be transitioned to the electricity system directly by replacing gas-fired equipment with electric alternatives. Economy-wide analyses consistently find that two core tenants of cost-effective decarbonization include: (1) electrification of current diffuse, small-scale natural gas direct-uses in buildings, and (2) equipping remaining large point-sources of GHG emissions with carbon-capture technologies for permanent geologic sequestration [10].

Natural gas and electrical energy infrastructure systems have become increasingly intertwined on operational and planning time scales [11, 12, 13], and this trend may be accelerated by the transition to clean energy. The persistence of low-cost natural gas in North America has motivated investment in new gas-fired generation capacity [14]. Flexible, gas-fired power plants have been essential to balance net load[1] fluctuations that arises from increasing use of variable renewable generation. This is seen widely in the current California energy system, where high solar penetration necessitates reliance on flexible natural gas-fired power generation to ramp as the sun sets in the evening.

Importantly, nearly all gas-sector emissions mitigation options involve direct competition with or integration with the electric power sector. Biomethane and other sustainable biofuels are highly valuable to zero-emissions electricity systems for providing firm[2] power generation [15] and are extremely supply-limited relative to current natural gas demands [9]. The production of electro-fuels at scale or the removal of atmospheric carbon dioxide (i.e., direct air capture) for permanent sequestration will require large amounts of low-cost clean electricity and heat. And widespread electrification of current gas demands raises concerns about the cost of meeting increased electricity demand, specifically during seasonal periods of low renewables generation or during exacerbated peaks in demand.

Electro-fuels offer flexibility in the timing and location of electricity consumption, relative to the demand for the final energy service. Production and transport of electro-fuels may help circumvent transmission constraints in the electricity system. Long-duration storage of electro-fuels may help to satisfy seasonal swings in net electricity demand [16] or serve direct-use demands that peak in the winter. Alternatively, rather than have electro-fuel powered generators that turn on for one week out of the year, we may plan flexible electro-fuels production facilities that shut down for the week of scarcity (see [17] for more on these trade-offs in fixed costs and capacity utilization).

As decarbonization strategies include the transition of gas demands to the electricity system and

[1] Net load is equal to total demand for electricity less any available electricity generation from renewable sources

[2] Firm, or "dispatchable," electricity sources are those that can be turned on to generate power when needed and for as long as needed.

the conversion of surplus clean electricity into gaseous fuels, new modeling techniques are required to jointly plan for the integrated public-interest energy system of the future. Traditional energy systems planning models focus exclusively on supply-side resources in generation and transmission expansion optimization for a single energy infrastructure system, electricity [18] or natural gas [19]. Integrated investment planning, co-optimized across natural gas and electric power systems, is essential to jointly consider cross-sector competition for limited bio-energy resources, direct substitution of electric appliances for legacy gas-fired equipment, or flexible production of electro-fuels for direct-use gas demands or to generate electricity during time periods of (or in locations with) scarce wind and solar generation. In addition, integrated gas-electric system planning is necessary to account for the potential economic feedback associated with modeled declines in natural gas deliveries and the impact on cost-effective investment decisions.

Maintaining redundant sets of energy infrastructure can improve system resiliency, and be highly valuable to provide essential energy services during times of stress on the electricity system. However, if gas system deliveries decline without comparable reductions in system fixed costs, the price per unit of gas delivered to consumers may need to increase to cover these costs. Increasing natural gas rates may then drive further customer defections and electrification [20], causing a so-called "rate spiral." While the welfare-maximizing solution may entail hybrid[3] reliance on a gas distribution infrastructure, an unplanned transition may result in complete defection. Legacy natural gas infrastructure, including pipelines and underground storage facilities, could become "stranded assets." Further, the equity impact of rate spirals presents a critical challenge for policymakers as low-income customers may be less likely to have the capital necessary to transition away from natural gas appliances.

Some industrial demands for natural gas for high-temperature heat are challenging to transition to electric equipment or may be associated with process emissions such as that of cement production. Point-source carbon capture technologies may be used to reduce the climate impact of these energy demands. Simultaneously, consumer-driven adoption of carbon capture would support throughput in gas systems and potentially provide an alternative avenue for recovery of fixed infrastructure costs that mitigates a rate spiral in residential and commercial sectors.

Lastly, the investment and system design decisions determined by planning optimization techniques must be implemented by market actors, subject to regulatory scrutiny. In complex networked systems of energy transfer, electricity and gas are dynamically transferred across regulatory jurisdictions. The nominal supply portfolio for an energy provider is the outcome of a set of financial arrangements, contractual off-takes, and spot market transactions. However, the delivery of energy is mediated by the nonlinear physics of energy system operation. It is a mathematical impossibility to precisely attribute a particular generation source to any specific customer as electricity does not

[3]Hybrid gas-electric solutions may retain gas distribution for direct provision of energy services during times of power system stress or failure.

flow from a source to a sink; all generators work in concert to energize the grid and supply all demands. Similarly, fuel injected to the natural gas pipeline system will quickly become well-mixed and the molecules delivered to a particular customer bear little resemblance to the contractual arrangements. The allocation of emissions liabilities across a set of regulated entities presents a challenging computational and policy challenge - regulators must reconcile the nominal supply portfolio with the physical emissions consequences of a regulated entity's energy consumption.

1.2 Scope of work

The transition to net-zero emissions natural gas and electric power systems must accommodate three parallel trends:

- increasing integration across gas and electric energy systems,
- the challenge of difficult-to-decarbonize industrial energy demands,
- the regulatory and accounting structures which track and assess their emissions liabilities or promote the development of low-carbon resources.

The goal of this dissertation is to present new modeling frameworks that help elucidate features of cost-effective transitions to deeply-decarbonized, integrated gas-electric energy systems. We develop and implement three model formulations that enable design and simulation of low-carbon energy systems, providing insight for the policy and economic decisions that will shape the transition.

The core research contributions of this work are as follows:

- *Provide a comprehensive review of the current state of modeling for coordinated planning and operations of integrated gas-electric energy systems.* With the increased availability of low-cost domestic natural gas supplies, the rise of gas-fired electricity generation has increased the interactions and integration between our energy infrastructure systems. We offer an introduction to this literature and summarize the important model innovations and short-comings.
- *Develop a novel optimization program for practical least-cost planning of integrated gas-electric systems.* Regulators and utilities need new tools and techniques for ensuring a cost-effective transition across all regulated fuels. The proposed model formulation for coordinated planning of electric power and natural gas delivery systems will allow synergistic investment plans to address cross-sector operational constraints, competing uses for net-zero emissions fuels, and shifts in final energy demands across energy carriers.
- *Evaluate the techno-economics of breakthrough technologies for decarbonization of industrial energy demands.* Methane pyrolysis offers one option for decarbonization of current gas end-uses. Here, we evaluate the technoeconomic performance of a catalytic molten-media methane

pyrolysis systems via optimization of the energy system design. Using these results, we provide insight regarding how methane pyrolysis might compete economically with other options for reducing industrial emissions in two specific use cases: fuel-switching at distributed medium-scale combustion applications and substitution for conventional sources of H_2 in oil refining.

- *Evaluate regulatory frameworks adopted for accounting for the greenhouse gas emissions associated with retail electricity sales.* To avoid legal challenges, sub-national climate policies often regulate the emissions intensity attribute associated with delivered retail sales of electricity. In 2020, the California Energy Commission adopted a new mathematical approach to estimating this value in cases where a retail provider's total purchases of electricity exceed their retail sales. Here, we evaluate the implications of this approach relative to other options.

- *Develop a harmonized approach to greenhouse gas accounting in highly integrated energy systems across regulatory jurisdictions and fuels.* We adapt existing approaches to greenhouse gas emissions accounting to reflect the nominal (or contractual) arrangements for electricity purchases. This allows harmonized quantification of emissions associated with so-called "specified" electricity transfers, "unspecified" electricity transfers, and emissions leakage associated with the contractual arrangement for electricity transfer from unregulated jurisdictions.

1.3 Outline

The body of this dissertation is composed of three chapters, representing three separate frameworks for modeling decarbonized gas and electric energy systems. Each chapter presents a self-contained analysis which either has been, or is in the process of being, published; as such, each chapter includes its own literature review and conclusions. Each chapter also utilizes its own self-contained nomenclature, as defined in Appendix Chapters A, B, and C.

In Chapter 2 we design and implement a least-cost system planning optimization program for integrated gas-electric energy systems. This model incorporates elements of traditional electricity sector capacity expansion optimization alongside decision variables for the natural gas distribution sector, in order to identify the central planner solution under a range of sensitivity scenarios.

In Chapter 3 we conduct technoeconomic optimization and analysis of a novel technology for low-emissions utilization of natural gas. We use technoeconomic optimization to illustrate how methane pyrolysis in molten catalyst media bubble column reactors may be a cost-competitive option for capture of solid carbon and production of hydrogen. A version of this work has been previously published in [21].

In Chapter 4 we investigate novel approaches to tracking and accounting for greenhouse gas emissions associated with dynamic transfers of electricity, reconciling the contractual portfolio of electricity supplies with a physical interpretation of power sector operations. Approaches like this

will be of increasing importance as contractual electricity arrangements are used also to produce nominally net-zero emissions gaseous fuels for decarbonizing the gas distribution sector. A version of this work has been previously published in [22] (Sect. 4.2) and [23] (Sect. 4.3).

In Chapter 5 we summarize key findings and policy implications of this body of work. We conclude with a discussion of future research directions.

Chapter 2

Cost-optimal planning for integrated gas-electric grids

2.1 Introduction

Emissions of greenhouse gases (GHGs) must decrease rapidly in coming decades to mitigate the impacts of climate change [2, 24]. The resulting decarbonized energy systems of the future will likely rely on a mix of renewable energy, zero-emissions or carbon capture-enabled thermal generation, energy storage, and chemical fuels such as hydrogen (H_2) or synthetic methane (CH_4) produced from renewable electricity. Large investments in these technologies will be required in order to reliably satisfy demand for electrical, thermal, and chemical energy over all hours of the year [4]. The specific mix that will prevail in the end is profoundly uncertain, and depends on a complex set of technology characteristics, technological learning rates, and local implementation details. It is in this fog of uncertainty that energy delivery system planners and operators (e.g., grid operators or gas distribution system operators) are currently designing and investing in long-lived infrastructure.

Importantly, these operators cannot simply invest in a "greenfield" system that meets a mid-century decarbonization target. An enormous set of interlinked systems already exists, and deliverability must be maintained across all hours during the transition. In the intervening years, investments in emerging carbon-reducing and efficiency-promoting energy technologies will impact the function of electricity and natural gas transmission systems. Consequently, it is critical to determine investment priorities that minimize system-level infrastructure and operating costs for the desired end system while also assuring resource adequacy and reliability during the transition.

The conceptual "energy hub" was first proposed as a framework for designing optimal greenfield energy systems to satisfy environmental goals, unconstrained by existing infrastructure [25]. Using well-understood mathematical models for the physics of electrical power and hydraulic gas flows [26,

27], integrated energy systems optimization models were proposed for joint simulation of optimal power flows in multi-carrier networks [28, 29, 30]. More recent efforts have included district heating or hydrogen alongside electricity and gaseous fuels networks [31]. Such multi-carrier energy systems will play a critical role in balancing low-carbon energy supplies and demands across sectors and carriers [32]. However, as timelines shrink to minimize climate risks, designing and implementing a least-cost greenfield multi-carrier energy system to achieve emissions goals becomes less feasible.

Electricity and natural gas are the most widely used energy carriers in existing infrastructure systems. They deliver energy to buildings housing hundreds of millions of consumers in the United States and billions globally. Natural gas and electrical energy infrastructure systems have become increasingly intertwined on operational and planning time scales [11, 12, 13], and this trend may be accelerated by the transition to clean energy. The persistence of low-cost natural gas in North America has motivated investment in new gas-fired generation capacity [14], and flexible, gas-fired power plants will be essential to balance net load fluctuations that arises from increasing use of variable renewable generation. Climate goals in gas distribution must be satisfied by reducing the life-cycle GHG emissions of fuels delivered. This may be accomplished by using biomethane, pipeline blending of hydrogen, or catalytic methane production using clean electricity and captured carbon dioxide. Alternatively, end customers will reduce their gas consumption by transitioning – at least partially – to electric appliances. As regulators and utilities confront these trends, comprehensive frameworks are needed for coordination of system operations and investment planning [6, 7].

In this chapter, we develop a novel mixed-integer quadratically-constrained program to fill a practical gap in the multi-carrier energy system planning literature. The proposed framework conducts multi-period system planning across integrated, gas-electric energy systems. The modeling context is planning under strict sector-specific GHG emissions constraints that tighten over time. We employ time series aggregation (data reduction) techniques to allow for solutions that jointly simulate operations across representative days [33, 34]. This reduced temporal complexity allows us to jointly consider detailed electricity sector operations constraints, nonlinear gas system steady-state flows, and the transition of final energy demands across carriers. Such detail would not be practical if all days in a template year or years were modeled.

Importantly, this model treats endogenous stock turnover of legacy appliance populations, allowing the model to shift end use appliances between gas and electric supply networks. This appliance-investment planning allows for joint consideration of direct electrification of current gas consumption alongside electro-fuel (or power-to-gas) resources which decouple the timing and location of electricity production from the provision of final energy services using the gas grid as a buffer. A simple formulation for spatially-resolved hydrogen concentration tracking allows us to illustrate the critical role of permissible gas quality on optimal decarbonization investments. A realistic implementation of sector-specific GHG emissions constraints allows endogenous allocation of constrained resources (such as sustainable bio-energy) across competing end-uses in the electricity and natural gas sectors.

With the presented model and illustrative case study scenarios, we lay the groundwork for an array of future analyses addressing critical questions of practical importance to the transition to a deeply decarbonized energy system.

Below, we review previous studies on gas-electric system modeling, operational planning, optimal expansion, and emissions reduction. We then outline in detail the critical gaps in previous analyses and computational methods that this study aims to fill. In Section 2.3, we present the model formulation for co-optimized gas-electric system planning. In Section 2.4, we describe all data inputs and assumptions required to simulate a case study implementation of the model. In Section 2.5, we present the data inputs and assumptions for a "toy" network case study along with the least-cost planning and operational decisions. We discuss the results, key conclusions, and areas for further study in Section 2.7.

2.2 Background

There is a growing body of work on coordinated expansion planning and operational scheduling optimization of integrated energy systems to generate and deliver electricity, natural gas, hydrogen, and/or heat. For comprehensive recent reviews on this previous work, we refer the reader to He et al. (2018) [35], Farrokhifar et al. (2020) [36], and Huang et al. (2020) [37].

Using models for co-optimized gas and electric flows, several researchers have investigated the value of coordination and optimal control of the two integrated networks [38, 39, 40, 41]. The fidelity of simulation used for optimizing control varies from convexified steady-state simulations [42, 43] to transient flow models [44, 45]. Moreover, uncertainty frameworks have been proposed for the integrated gas-electric operations optimization [46] and gas expansion planning optimization problems [47]. Several studies have analyzed whether the inclusion of power-to-gas conversion facilities can further reduce operational costs of integrated gas-electric energy systems [48, 49, 50]. Although studies anticipate reduced curtailment of renewables and decreased operational costs with the addition of such facilities, they do not examine whether the economic benefits exceed the capital costs of their installation.

A related body of work has investigated coordinated expansion planning between the electric power and natural gas systems. Expansion planning scope can include generation, transmission [51, 52], and distribution-level decisions [53]. Bi-level optimization approaches have been used to iteratively solve the planning and operations sub-problems in order to converge to a solution [54]. Convex relaxations have been proposed for the gas expansion planning problem [55] and implemented for joint expansion planning of gas and power systems [56], while fully linearized approaches are employed to solve large-scale systems [57]. Recent work has incorporated power-to-gas [58, 59, 60, 54] or combined heat and power [61] resources in integrated planning optimization. However, many of these studies are only applicable to cases where district energy systems infrastructure

already exists for delivery of power, gas, and heat to buildings [62, 63], irrespective of the local conversion equipment. One study explicitly optimizes the distribution-level heat demands across appliance technologies, but only examines new-build infrastructure decisions [64]. Planning for the potential early retirement of legacy equipment presents an important challenge for system planners and regulators. Further, assuming the existence or cost-effective development of an entirely new set of networked infrastructure for energy delivery, whether it be district heat or hydrogen, is often unrealistic in cases where legacy buildings must be transitioned to zero-carbon energy sources.

Many planning studies simulate operations for a set of independent steady-states [43] or use clustering to reduce 8760 hourly data points in the planning year down to a tractable set of representative hourly steady-states [60] or representative days [65]. However, these approaches typically treat each evaluated operational period as a stand-alone simulation and not in sequence to allow for transfer of energy across simulated hours or days. As systems rely on increasing shares of weather-dependent renewable resources, these asynchronous developments will be critical to ensuring system feasibility. To our knowledge there is no published global optimization formulation that enables flexible simulation of representative time periods while retaining their sequencing in the calendar year to allow for inter-day, inter-week, and seasonal energy storage.

The capability to tractably solve planning optimization over several sequential multi-year periods is critical for enabling realistic integrated resource planning proceedings. Researchers have proposed various models to optimize gas-electric system planning across multiple investment periods using genetic algorithms [66], linearized expansion co-planning [53], or Bender's decomposition techniques [61]. However, the primary focus of these studies and others is on serving incremental load growth across a time horizon [67, 60, 65] rather than transformative energy transition to satisfy environmental constraints.

Carbon emissions constraints have been included in operational optimizations [68, 69] and in multi-objective planning optimization problems [70], as components of the objective function at a fixed cost [71, 72, 73] or as constraints subject to an emissions cap [74, 75]. Berger et al. (2020) propose a temporally resolved expansion planning model to satisfy economy-wide demands for energy subject to carbon emissions constraints [76]. However, no transmission networks are contemplated in that study, and final energy demands are exogenously specified, which limits the ability of their formulation to identify and exploit synergies across gas and electricity systems or to use endogenous appliance fuel switching as a model decision to optimally make use of renewable and gaseous fuels. Further, implementation of such emissions-constrained optimization programs in practical policy proceedings may require moving beyond system-wide emissions constraints and towards sector-specific accounting of GHG emissions. The goal of our study is to extend previously proposed formulations to enable a richer variety of future scenario analyses that account for how system operations will adjust in response to the optimized structural changes.

In summary, our model has the following novel features not-before seen in the coordinated gas-electric transition literature:

- Inclusion of endogenous appliance stock turnover model to address capital longevity and existing infrastructure
- Inclusion of associated building retro-fit costs to accommodate the transition of gas demands to the electric power system
- Inclusion of endogenous fuel switching as a model decision, not as an externally-specified case definition
- Inclusion of linking constraints across representative operational time periods to allow for long-term storage of energy
- Inclusion of a simplified, linear gas component tracking formulation for ensuring adequate quality delivered to consumers
- Inclusion of sector-specific emissions intensity constraints to endogenously assess cross-sector competition for constrained net-zero emissions gas supplies
- Ex-post computation of average costs of delivered gas, electricity, and electro-fuels (as an integrated linear system of equations) indicative of how cost-of-service regulated volumetric rates may evolve across the transition.

2.3 Model formulation

The objective of the proposed method is to identify the cost-optimal trajectory of capacity investment decisions for a set of coupled energy infrastructures that deliver electricity and gaseous energy, across a multi-period time horizon with progressively declining GHG emissions constraints. To conduct integrated, multi-period gas-electric systems planning, we synthesize methods from studies on electricity sector capacity expansion modeling [77, 78], coordinated gas-electric operations optimization [38, 56], and economy-wide decarbonization pathway simulation techniques [10, 79].

System design decisions include the expansion or retirement of electricity generators, producers of net-zero emissions gas, and electricity or gas storage. The proposed model also endogenously models the natural stock-rollover of end-use appliance populations, allowing for endogenous model decisions on transitions in final energy demands across energy carriers. Each unit has an associated location on the gas network and on the electricity grid where the unit's net energy supplies or demands interface with each infrastructure system and can be transferred through modeled networks of gas pipelines and electricity transmission lines, respectively.

For each modeled annual or multi-year investment period, the program jointly determines cost-optimal operations of the integrated gas-electric energy system across a set of representative operational periods (i.e., days) to ensure that energy demands can be satisfied, subject to hourly operational constraints such as availability of renewable electricity generation, energy storage charging and discharging, and generator characteristics.

The least-cost integrated system planning problem is expressed mathematically as the coordinated optimization program in Eq. (2.1). The objective function sums total societal costs across all evaluated investment periods $\mathcal{I}$ and their associated expansion investment costs C_i^{exp} [$/year], the fixed costs of transmission & distribution infrastructure C_i^{inf} [$/year], and variable system operating costs C_i^{op} [$/year]. All future costs are discounted to present value using ϑ_i, a societal cost discount factor described in Section 2.3.8. The full problem formulation is given by:

$$
\begin{aligned}
\min \quad & \sum_{i \in \mathcal{I}} \vartheta_i (C_i^{exp} + C_i^{inf} + C_i^{op}) \quad \text{using (2.72), (2.64), (2.67), and (2.71)} \\
\text{s.t.} \quad & \text{supply/demand capacity expansion constraints: (2.5)-(2.6)} \\
& \text{appliance turnover and replacement constraints: (2.14), (2.16)} \\
& \text{power flow constraints: (2.18)-(2.19)} \\
& \text{power system operating constraints: (2.20)-(2.26)} \\
& \text{gas system operating constraints: (2.30)-(2.32), (2.40)} \\
& \text{gas flow constraints: (2.34), (2.36), (2.38), (2.39)} \\
& \text{gas energy balance: (2.41)-(2.47)} \\
& \text{gas quality constraints: (2.49)-(2.50)} \\
& \text{storage operations constraints: (2.51)-(2.59)} \\
& \text{emissions constraints: (2.60)-(2.63)}
\end{aligned}
\tag{2.1}
$$

In the forthcoming Sections 2.3.1-2.3.2, we present the mathematical notation employed throughout this paper. Sections 2.3.3-2.3.7 explain the decision variables and constraints employed in Eq. (2.1). We compute the objective function terms in Section 2.3.8. Finally, we describe model outputs in Section 2.3.9.

2.3.1 Network topology

The network topology of an integrated gas-electric system consists of separate gas and electric networks that interact through a limited set of coupling units that enable energy flows between the two carriers. A schematic illustration of an integrated gas-electric network is presented in Figure 2.1.

The power grid is defined by a graph $(\mathcal{N}_P, \mathcal{E}_P)$ with $N_P = |\mathcal{N}_P|$ nodes denoting buses connected

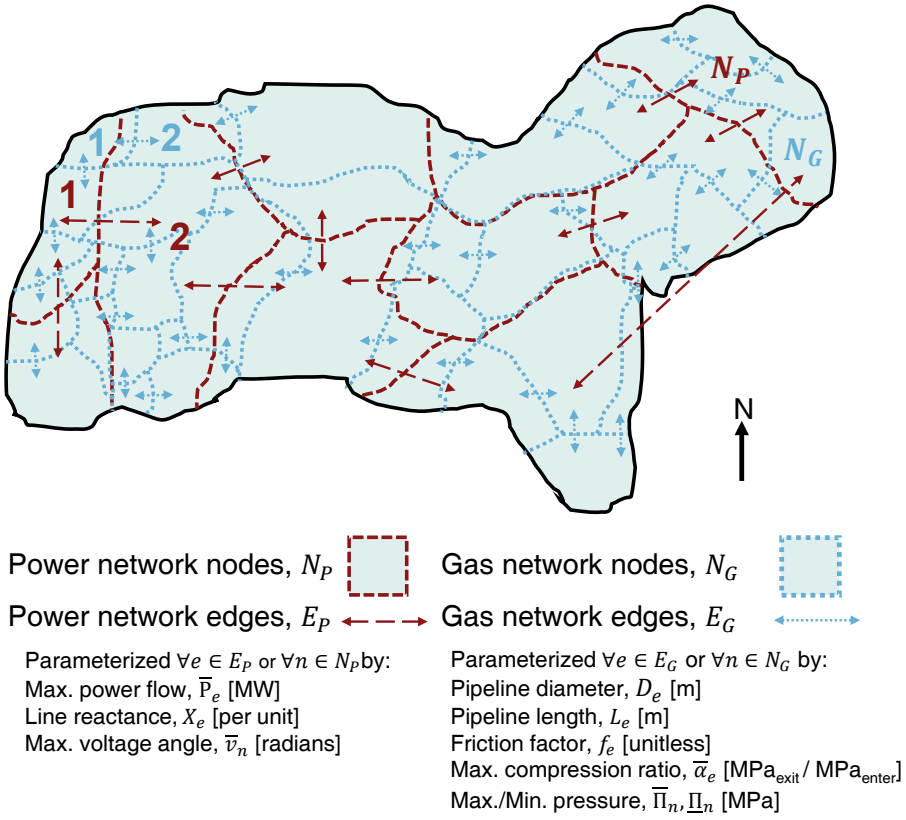

Figure 2.1: Schematic illustration of an integrated gas-electric energy system composed of overlaid electric and gas networks with nodes, interconnected by edges that allow for energy transfer between connected nodes. Each edge has an associated maximum transfer capacity, as dictated by the physical parameters for gas pipeline and electric transmission networks.

by $E_P = |\mathcal{E}_P|$ edges denoting power lines, and the gas pipeline network is defined by a graph $(\mathcal{N}_G, \mathcal{E}_G)$ with $N_G = |\mathcal{N}_G|$ nodes denoting junctions connected by $E_G = |\mathcal{E}_G|$ edges denoting pipelines. Nodal boundaries are represented in Figure 2.1 with dashed (electric system) and dotted (gas system) lines. Edges are presented here as bi-directional arrows, specified by an origin and a terminus node, indicating energy transfer capabilities between the connected nodes.

These networks are defined separately, and interact through a set of energy supply and demand units $\mathcal{X}$, such as electricity generators, that are connected to an associated node on the gas network as well as an associated node on the electric network. To facilitate matrix notation, network topology for the electric power and gas grids are characterized by nodal-edge incidence matrices A^P and A^G of dimension $N_P \times E_P$ and $N_G \times E_G$, respectively:

$$\text{Power: } A^P_{n,e} = \begin{cases} 1 & \text{if edge } e \text{ leaves node } n \\ -1 & \text{if edge } e \text{ enters node } n \end{cases} \quad \text{Gas: } A^G_{n,e} = \begin{cases} 1 & \text{if edge } e \text{ leaves node } n \\ -1 & \text{if edge } e \text{ enters node } n \end{cases} \tag{2.2}$$

Each column of A^P and A^G represents an edge, with positive and negative values indicating the edge's origin and terminus nodes. Consequently, each row characterizes a node, and indicates all of the edges that nominally enter or exit that node.

Each existing or candidate resource is mapped to a node on the electricity and gas systems. In Figure 2.2 we illustrate the sets of energy supply and demand units that may operate at each specific node on the gas and electric system and the associated decision variables and parameters that govern their contribution to nodal energy supplies and/or demands.

2.3.2 Temporal notation

In the presented model formulation, variables and parameters are indexed across time in three nested timescales. We consider indexing across combinations of investment time horizons $i \in \mathcal{I}$, representative operational periods $r \in \mathcal{R}$, and linked operational time steps $o \in \mathcal{O}$ for each operational period. Let us denote the sizes of these sets by $I = |\mathcal{I}|$, $R = |\mathcal{R}|$, and $O = |\mathcal{O}|$. We use the multi-index $(i, r, o) \in \mathcal{I} \times \mathcal{R} \times \mathcal{O}$, and denote $\mathcal{T} \equiv \mathcal{I} \times \mathcal{R} \times \mathcal{O}$ for ease of exposition. For specific values of $i \in \mathcal{I}$, $r \in \mathcal{R}$, and $o \in \mathcal{O}$, we will then write $(i, r, o) \in \mathcal{T}$.

Each representative period also has an associated weight $w_{(i,r)}$ that reflects the proportion of operational conditions that it represents. We use these weights to evaluate operational costs on an annual basis, and to limit the annual availability of some supply-constrained resources.

To offer a concrete example, a case may optimize across 5 linked investment years, using 8 representative days to represent each year. Each representative day is composed of 24 hourly time steps. In that case, $I = 5$, $R = 8$, and $O = 24$. The total times steps modeled is then $5 \times 8 \times 24 = 960$. The proposed modeling framework can flexibly accommodate different investment periods, representative periods, and operational time steps of any length. However, for simplicity,

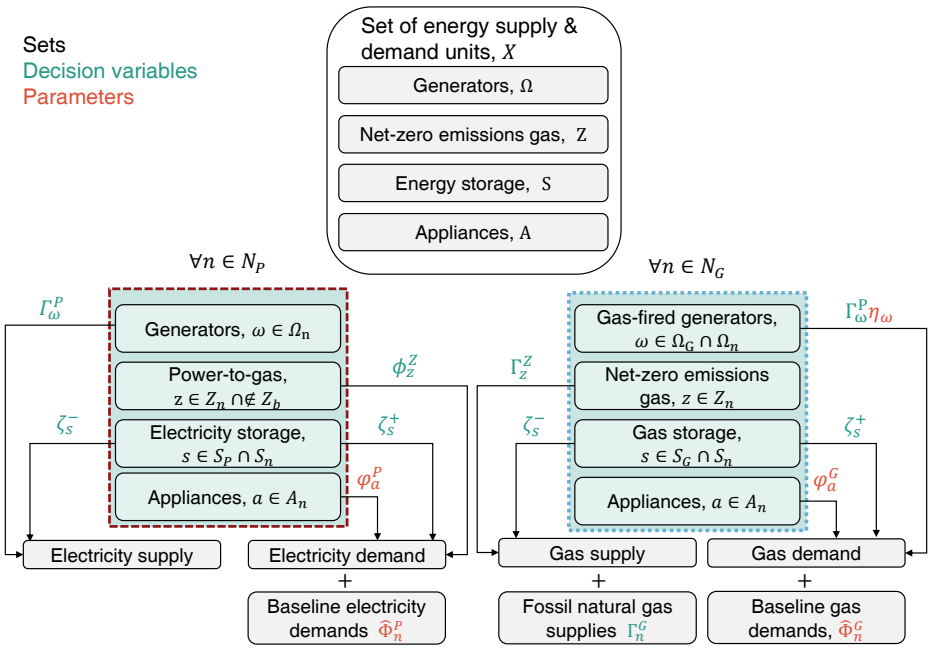

Figure 2.2: Schematic illustration of integrated gas-electric energy system nodes.

we will discuss the model formulation using investment years and representative days composed of operational hours. This approach to time series reduction allows for large reductions in problem complexity while retaining important operational characteristics. However, use of representative days introduces challenges when modeling constraints or resources that bind across time horizons that extend longer than the length of each representative day (i.e., minimum generator up- or down-time constraints or long-duration energy storage) [34, 80].

In order to accommodate operational constraints that relate adjacent time periods, we retain the contiguous sequencing of time periods as a sequence $\mathcal{C}$ of length $N_C = |\mathcal{C}|$ that consists of elements taken from the set $\mathcal{R}$ of representative time periods. We can define a projection $\sigma : [N_C] \rightarrow \mathcal{R}$, where we use the shorthand $[N] \equiv \{1, 2, \ldots, N\}$, so that the sequence of operational periods $c \in \mathcal{C}$ for a time horizon can be defined using representative periods according to

$$\mathcal{C} = \{\sigma(1), \sigma(2), ..., \sigma(N_C)\}. \tag{2.3}$$

The proposed approach to time series reduction with representative periods mapped to their contiguous sequence is presented in Figure 2.3. In this cartoon illustration, each investment year is reduced for operational purposes to a set of representative days (denoted by color) composed of operational hours. The representative periods are then mapped back to their original sequencing in the calendar year based on the actual days assigned to each representative day via a clustering

algorithm. Note that in this illustrative example, representative days are found that capture seasonal features, differences between weekends and weekdays, and potential multi-day extreme periods.

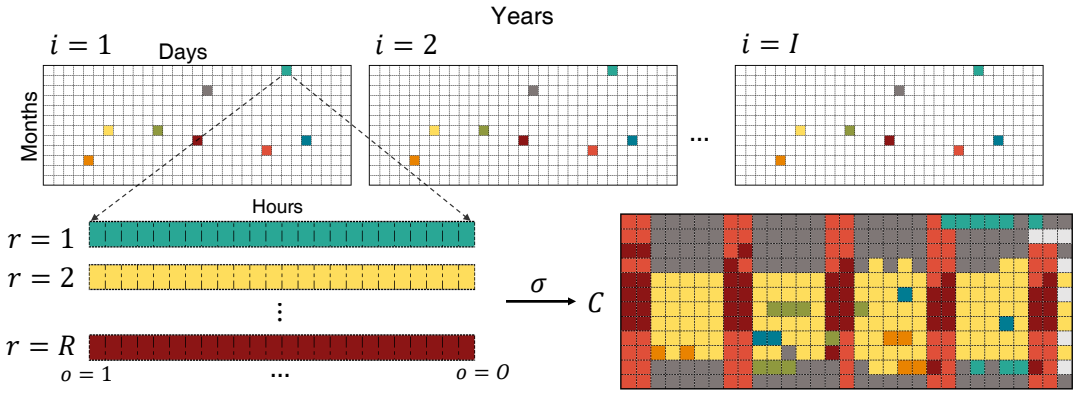

Figure 2.3: Schematic illustration of time series reduction from investment years $\mathcal{I}$ to representative days $\mathcal{R}$ composed of operational hours $\mathcal{O}$. The representative periods are then cast back to their sequence in the original calendar year $\mathcal{C}$ via σ.

Our approach provides the proposed model a flexible framework for experimenting with temporal resolution. In this computational analysis, we use representative days to examine annual operations, i.e., $N_C = 365$. However, the framework can accommodate representative periods of any length (number of days or hours), while preserving the calendar sequence on which constraints that relate adjacent periods can be imposed throughout an annual or multi-year simulation horizon. The investment years in the considered set $\mathcal{I}$ are associated with actual calendar years in Y. For example, our computational case study (described in Section 2.5) tracks $|\mathcal{I}| = 5$ investment time horizons staggered at 5-year increments from a base year of 2020. Thus, the calendar years considered here are

$$Y = \{2020, 2025, 2030, 2035, 2040\}. \tag{2.4}$$

2.3.3 Design decisions

Design decision variables evaluate the expansion or retirement of units in the candidate set $\mathcal{X}$, which includes electricity generators, electrical and gaseous energy storage, new sources of net-zero emissions gas, i.e., biomethane and power-to-gas conversion, and end-use consumer appliances. These decision variables are included for each modeled investment time period $i \in \mathcal{I}$. Constraints must be defined in order to delimit annual expansion of new units to lie between zero and a maximum annual rate of development. In addition, we must constrain the total expansion to remain below a maximum number of units. We also constrain the retirement of existing units to not exceed the

number of legacy units and any previously developed units. Finally, for simplicity of exposition, we compute the number of units in operation during a given investment year. These constraints are given by

$$\delta_{i,x} \geq 0, \;\; \zeta_{i,x} \geq 0, \;\; m_{i,x} \geq 0 \qquad \forall i \in \mathcal{I}, x \in \mathcal{X} \qquad (2.5a)$$

$$\delta_{i,x} \leq \overline{\delta}_x (Y_i - Y_{i-1}), \qquad \forall i \in \mathcal{I}, x \in \mathcal{X} \qquad (2.5b)$$

$$\sum_{i \in \mathcal{I}} \delta_{i,x} \leq \overline{\Delta}_x, \qquad \forall x \in \mathcal{X} \qquad (2.5c)$$

$$\zeta_{i,x} \leq \hat{m}_x + \sum_{j \in [i-1]} (\delta_{j,x} - \zeta_{j,x}) \qquad \forall i \in \mathcal{I}, x \in \mathcal{X} \qquad (2.5d)$$

$$m_{i,x} = \hat{m}_x + \sum_{j \in [i]} (\delta_{j,x} - \zeta_{j,x}) \qquad \forall i \in \mathcal{I}, x \in \mathcal{X}. \qquad (2.5e)$$

Here, Eq. (2.5a) introduces the decision variables for expansion $\delta_{i,x}$ [units], retirement $\zeta_{i,x}$ [units], and existing units in operation $m_{i,x}$ [units] and ensures these variables take on non-negative values. Eq. (2.5b) ensures that the expansion decision in each time period $\delta_{i,x}$ does not exceed maximum annual expansion rates $\overline{\delta}_x$ [units/year] multiplied by the number of years represented by the current investment period evaluation $(Y_i - Y_{i-1})$[years]. Eq. (2.5c) requires that total expansion across the modeled investment horizon does not exceed the maximum allowable development for each candidate set of units $\overline{\Delta}_x$ [units]. Eq. (2.5d) ensures that the number of units retired, $\zeta_{i,x}$ does not exceed the number of existing legacy units, $\hat{m}_x$ [units], plus any previously-constructed units less any previous retirements $\sum_{j \in [i-1]} (\delta_{j,x} - \zeta_{j,x})$. Finally, Eq. (2.5e) evaluates the total number of units in service $m_{i,x}$ in any investment period.

Note that for simplicity of exposition we use the notation $j \in [i]$ as short-hand for the more pedantic $j = 1 \ldots i$.

When modeling investment decisions across extended time horizons, we endogenously include any planned or expected retirements of units or appliance failures. Each class of unit included in the set $\mathcal{X}$ may have a different cumulative failure function $f_{j,x,i}$ to describe the cumulative fraction of units of kind x installed during investment year j that will fail before or during investment year i. For example, electricity generators that are modeled in small populations may have their failure or retirement modeled as a discrete occurrence at their expected lifetime. However, populations of thousands of appliances may have their failure modeled as a continuous function with fractional shares exiting the operating stock in between each investment year.

Here, we compute the cumulative number of expected retirements as the sum of legacy units $\hat{m}_x$ by the legacy unit failure function $\hat{f}_{i,x}$ [cum. units failed / initial units in service] and previously expanded units $\sum_{j \in [i-1]} \delta_{j,x}$ by the modeled cumulative failure function $f_{j,x,i}$ [cum. units failed / initial units installed]. In every modeled investment year, the retirements in the current investment

period must exceed those cumulative expected retirements, less any previous retirement decisions, i.e. $\sum_{j\in[i-1]}\zeta_{j,x}$. This constraint is expressed as

$$\zeta_{i,x} \geq \hat{m}_x \hat{f}_{i,x} + \sum_{j\in[i-1]} \delta_{j,x} f_{j,x,i} - \sum_{j\in[i-1]} \zeta_{j,x} \qquad \forall i \in \mathcal{I}, x \in \mathcal{X} \tag{2.6}$$

For units in the generators, storage, and net-zero emissions gas production sets we govern the expected retirement using the following relationships:

$$\hat{f}_{i,x} = \{1|Y_i \geq \tilde{Y}_x + \tau_x\} \qquad \forall i \in \mathcal{I}, x \in \Omega \cup \mathcal{S} \cup \mathcal{Z} \tag{2.7a}$$

$$f_{i,x,j} = \{1|Y_i \geq Y_j + \tau_x\} \qquad \forall i \in \mathcal{I}, x \in \Omega \cup \mathcal{S} \cup \mathcal{Z}. \tag{2.7b}$$

To endogenously evaluate the expected retirement deadlines of existing and candidate resource expansion, we leverage the set of calendar years Y defined in Eq. (2.4). Indicator functions are used to indicate when legacy units $\hat{m}_x$ have reached their expected lifetime τ_x [years], based on their calendar year of installation $\tilde{Y}_x$ with the expression $\{1|Y_i \geq \tilde{Y}_x + \tau_x\}$. A similar function is used to indicate when previously expanded units $\delta_{j,x}$ have reached their expected lifetime, i.e., $\{1|Y_i \geq Y_j + \tau_x\}$.

These indicator functions are mathematically implemented as defined in Eq. (2.8) for two values x and y. This expression ensures that if x is greater than or equal to y, this value equals one. If x is less than y, this value equals zero:

$$\{1|x \geq y\} = 1 - \max\{\min\{y - x, 1\}, 0\} \tag{2.8}$$

Another collection of constraints relates investment decisions made by direct-use gas customers in residential, commercial, or industrial sectors. We model these decisions using a set of appliances $a \in \mathcal{A} \subset \mathcal{X}$ (each of which satisfy a particular energy end-use service $u \in \mathcal{U}$) across the set of modeled investment periods $i \in \mathcal{I}$. Examples of appliances include gas furnaces, air-source heat pumps, gas-fired or electric resistance water heaters, and gas or electric stoves. Corresponding energy end-use services may include space heating, water heating, and cooking.

The same unit stock-tracking constraint set (Eq. (2.5)-(2.6)) is employed for the appliances $\mathcal{A} \subset \mathcal{X}$, however we use different failure functions applied to legacy unit populations and expansion decisions.

We endogenously model appliance failure fractions using the standard Poisson distribution approach, where the failure fraction is specified by the average appliance lifetime τ_a [years]. Cumulative

failure fractions in each investment year i for each appliance population installed in a previous investment period j are pre-computed according to Eq. (2.9).

$$f_{i,a,j} = \sum_{k \in [Y_i - Y_j]} e^{-\tau_a} \frac{\tau_a^k}{k!} \qquad \forall i \in \mathcal{I},\ a \in \mathcal{A},\ j \in \mathcal{I}. \tag{2.9}$$

Here, we sum across the failure fractions occurring in each year between the install year Y_j and the current investment year Y_i using the appliance's expected lifetime τ_a.

The cumulative failure fraction of the initial appliance population in each modeled investment time period $\hat{f}_{i,a}$ can be similarly pre-computed using simplified assumptions about the historical growth rate of appliance sales $\hat{g}_a$ [%/year] and the number of existing appliances at the beginning of the modeled time horizon $\hat{m}_a$ (i.e., in service during the base calendar year $\hat{Y}$).

The appliance population size at the beginning of the modeled time horizon is assumed to be a function of the cumulative failure (as specified by the same Poisson failure function) of all previous appliance sales $\tilde{M}_{a,k}$ [units/year] (for each historical year k):

$$\hat{m}_a = \sum_{k \in [\text{inf}]} \tilde{M}_{a,k} \left(1 - \sum_{j \in [k]} \left(e^{-\tau_a} \frac{\tau_a^j}{j!} \right) \right) \qquad \forall a \in \mathcal{A} \tag{2.10a}$$

$$\tilde{M}_{a,k} = \frac{\hat{M}_a}{(1+\hat{g}_a)^k} \qquad \forall k \in \mathcal{K},\ a \in \mathcal{A}. \tag{2.10b}$$

As shown above, we cast all historical sales, $\tilde{M}_{a,k}$ [units/year], as a function of appliance sales in the beginning of the modeled time horizon $\hat{M}_a$ [no. units] using an assumed historical growth rate $\hat{g}_a$ [%/year].

We can, therefore, substitute Eq. (2.10b) into Eq. (2.10a):

$$\hat{m}_a = \sum_{k \in [\text{inf}]} \hat{M}_a (1+\hat{g}_a)^{-k} \left(1 - \sum_{j \in [k]} \left(e^{-\tau_a} \frac{\tau_a^j}{j!} \right) \right) \qquad \forall a \in \mathcal{A}. \tag{2.11}$$

and rearrange the above to infer the appliance sales in the base year as solely a function of (1) an assumed historical growth rate in sales $\hat{g}_a$ and (2) the initial appliance population $\hat{m}_a$, provided that appliance failures are characterized by a Poisson distribution:

$$\hat{M}_a = \hat{m}_a \sum_{k \in [\text{inf}]} \frac{(1+\hat{g}_a)^k}{1 - \sum_{j \in [k]} \left(e^{-\tau_a} \frac{\tau_a^j}{j!} \right)} \qquad \forall a \in \mathcal{A}. \tag{2.12}$$

We use this term to pre-compute the expected cumulative failure fraction of existing appliances $\hat{f}_{i,a}$

on a forward-basis in every modeled investment time period:

$$\hat{f}_{i,a} = 1 - \frac{1}{\hat{m}_a}\hat{M}_a \sum_{k\in[\text{inf}]} (1+\hat{g}_a)^{-k} \left(1 - \sum_{j\in[k+(Y_i-\hat{Y})]} e^{-\tau_a}\frac{\tau_a^j}{j!}\right) \qquad \forall i \in \mathcal{I},\ a \in \mathcal{A}. \tag{2.13}$$

In essence, we are dividing the existing population of appliances $\hat{m}$ into a set of vintages based on assumed prior sales, which allows us to use the same vintage tracking and failure functions for *both* appliances pre-existing at the start of the simulation and those added in our investment time periods.

Next, we add constraints that ensure that in each investment time period, and for each energy end-use, the population of appliance units (at every node) must exceed the total demand for that energy service. This constraint set applies across both sets of electricity and gas system nodes as these networks may have different spatial resolution. In this manner, we ensure that, whether the replaced appliances are fueled by gas or electricity, the same demand for energy end-use services is met at any level of spatial granularity considered. We enforce this requirement as

$$\sum_{a\in(\mathcal{A}_u\cap\mathcal{A}_n)} m_{i,a} \geq \sum_{a\in(\mathcal{A}_u\cap\mathcal{A}_n)} \hat{m}_a(1+g_u)^{(Y_i-\hat{Y})} \qquad \forall i \in \mathcal{I}, u \in \mathcal{U}, n \in (\mathcal{N}_P \cup \mathcal{N}_G). \tag{2.14}$$

Eq. (2.14) evaluates (for each investment period) the total number of appliances that can satisfy the required energy end-use and exist at the specified node (i.e., $a \in \mathcal{A}_u \cap \mathcal{A}_n$). This quantity equals the number of appliances installed and not retired in this investment year $m_{i,a}$. This value must be greater than the original number of appliances satisfying this energy service, $\hat{m}_a$, escalated by an assumed growth rate in demand for this energy service g_u [%/year]. The number of intervening calendar years between each investment period is calculated using the elements of Y as originally explained in Eq. (2.4).

Note that if a more granular population of appliances is modeled, the set of energy end-use services $\mathcal{U}$ will need to be similarly expanded to differentiate across. For example, a future model might disaggregate demand for space heating equipment in older, leakier homes vs. newer or recently retrofitted homes. The subset of candidate appliances that can act as direct substitutes in each of these use cases may be different, despite the fact that all appliances satisfy a "space heating" need. For example, heat pumps may be a viable choice in newer more efficient homes but not in older leakier homes.

To isolate the impact of co-optimized appliance-level investment planning decisions on decarbonization pathways, in sensitivity analysis cases we can enforce "persistence" of appliance replacements by fuel type. In this circumstance, we remove the flexibility to serve demand growth and appliance replacements with any appliance that satisfies the same energy end-use service. Instead,

in these sensitivity cases, appliances that fail must be replaced by appliances that use the same end fuel type (gaseous or electrical), and demand growth rates are applied uniformly across all existing appliance populations. These requirements are given in Eq. 2.15.

$$m_{i,a} \geq \hat{m}_a (1 + g_u)^{\left(Y_{(i)} - \hat{Y}\right)} \qquad \forall a \in \mathcal{A}, i \in \mathcal{I}. \tag{2.15}$$

Note that these constraints are only included as limited sensitivity cases, and all baseline runs allow for end use switching between gas and electric energy carriers.

All appliance-level energy demands are modeled using parameterized hourly gas and electricity consumption profiles $\varphi^G_{(r,o),a}$ [MW] and $\varphi^P_{(r,o),a}$ [MW], respectively. These energy demands are incremental to a baseline of immutable temporal gas and electricity demands $\hat{\Phi}^G_{(i,r,o),n}$ [MW] and $\hat{\Phi}^P_{(i,r,o),n}$ [MW], that represent any nodal energy demands that are not modeled at the appliance-level. These quantities are related to the realized nodal gas and electricity loads $\Phi^G_{(i,r,o),n}$ [MW] and $\Phi^P_{(i,r,o),n}$ [MW], respectively, by

$$\Phi^G_{(i,r,o),n} = \hat{\Phi}^G_{(i,r,o),n} + \sum_{a \in \mathcal{A}_n} \varphi^G_{(r,o),a} m_{i,a} \qquad \forall n \in \mathcal{N}_G, \quad \forall (i,r,o) \in \mathcal{T}, \tag{2.16a}$$

$$\Phi^P_{(i,r,o),n} = \hat{\Phi}^P_{(i,r,o),n} + \sum_{a \in \mathcal{A}_n} \varphi^P_{(r,o),a} m_{i,a} \qquad \forall n \in \mathcal{N}_P, \quad \forall (i,r,o) \in \mathcal{T}. \tag{2.16b}$$

We use the above Eq. (2.14)-(2.16) to explicitly model the potential transition of residential and commercial gas demands through adoption of electric appliances for space heating, water heating, and cooking. However, the presented framework is extensible to any number of residential, commercial, or industrial energy end-uses.

2.3.4 Power system operational decisions

Here we describe the models we use to reflect operational decision-making for electric power transmission. Power system constraints are given on an hourly resolution, for 24 operational time steps $o \in \mathcal{O}$ in each operational time period $r \in \mathcal{R}$ based on the unit commitment problem for day-ahead scheduling. We describe the constraint set we use to represent the physics of power flow and the engineering and operational limitations for the power grid below. We use an integer-relaxed unit commitment and dispatch model to represent scheduled and dispatched generation or demand from each power system resource. The set of constraints in this formulation is based on standard formulations of the unit commitment problem that have been used in numerous variations [81, 82, 83].

Power flow constraints

In steady-state, active power flow on a loss-less edge $e \in \mathcal{E}_P$ directed from node $n \in \mathcal{N}_P$ to $m \in \mathcal{N}_P$ is represented by a single algebraic equation, using nodal voltages V_n, V_m [kV], transmission line reactance X_e [Ω], and nodal voltage angles v_n, v_m [radians]:

$$P_e = \frac{|V_n||V_m|}{X_e} \sin(v_n - v_m) \qquad \forall e \in \mathcal{E}_P. \tag{2.17}$$

In our analysis, we employ three simplifying assumptions: (1) line resistances are negligible compared to line reactances, (2) the voltage amplitude is equal for all nodes on a per unit basis (i.e., $|V_n| \approx |V_m| \approx$1 p.u.), and (3) the voltage angle differences between neighboring nodes are small (i.e., $\sin(v_n - v_m) \approx (v_n - v_m)$) [84]. Under these circumstances, the physical power flows on each line can be modeled using the linearized DC power flow equations, which relate the per-unit line reactance X_e [p.u.] and nodal voltage angles v_n [rad.] to the power flow on each line P_e [MW] using a base power $\hat{P} = 100$MW. Eq. (2.17) can be defined over the entire power network ($\forall e \in \mathcal{E}_P$) using the incidence matrix A^P. We also cast the power flow constraint set across all operational time steps i.e., $\forall (i, r, o) \in \mathcal{T}$:

$$P_{(i,r,o),e} = \hat{P}\left(\frac{-1}{X_e}\right) \sum_{n \in \mathcal{N}_P} A^P_{n,e} v_{(i,r,o),n} \qquad \forall (i,r,o) \in \mathcal{T},\ \forall e \in \mathcal{E}_P. \tag{2.18}$$

The electrical energy balance at each node is enforced using

$$\sum_{\omega \in \Omega_n} \Gamma^P_{(i,r,o),\omega} - \sum_{e \in \mathcal{E}_P} A^P_{n,e} P_{(i,r,o),e} + \sum_{s \in \mathcal{S}_P \cap \mathcal{S}_n} (\psi^-_{(i,r,o),s} - \psi^+_{(i,r,o),s}) - \Phi^P_{(i,r,o),n} - \sum_{z \in \mathcal{Z}_n} \Phi^Z_{(i,r,o),z} = 0,$$
$$\forall (i,r,o) \in \mathcal{T},\ \forall n \in \mathcal{N}_P, \tag{2.19}$$

where $\mathcal{Z}_n$ is the set of net-zero emissions gas units at a node $n \in \mathcal{N}_G$. The above relation ensures that the sum of local generation supplies $\Gamma^P_{(i,r,o),\omega}$ [MW], net electricity transfers $\sum_{e \in \mathcal{E}_P} A^P_{n,e} P_{(i,r,o),e}$ [MW], and net storage discharge $(\psi^-_{(i,r,o),s} - \psi^+_{(i,r,o),s})$ [MW] matches local demands $\Phi^P_{(i,r,o),n}$ [MW] and any demand $\Phi^Z_{(i,r,o),z}$ [MW] for production of net-zero emissions gaseous fuel. In short: supply must match demand at the nodal level, net of transfers.

A collection of inequality constraints then delimits the engineering and operational limits of power flow in the grid. Transmission of electric power is limited by lower and upper bounds on power flows across each line $P_{(i,r,o),e}$ [MW] and voltage angle differentials $v_{(i,r,o),n}$ [radians], of the form

$$-\overline{P}_e \leq P_{(i,r,o),e} \leq \overline{P}_e \qquad \forall (i,r,o) \in \mathcal{T},\ \forall e \in \mathcal{E}_{\mathcal{P}} \tag{2.20a}$$

$$-\overline{v} \leq \sum_{n \in \mathcal{N}_P} A^P_{n,e} v_{(i,r,o),n} \leq \overline{v} \qquad \forall (i,r,o) \in \mathcal{T},\ \forall e \in \mathcal{E}_{\mathcal{P}} \tag{2.20b}$$

Lastly, in order to ensure a unique solution, the voltage angle at a designated slack bus must be fixed to equal 0:

$$v_{(i,r,o),0} = 0 \qquad \forall (i,r,o) \in \mathcal{T}. \tag{2.21}$$

Unit commitment constraints

Next, we apply constraints to control the unit-commitment and dispatch of electricity generators and power-to-gas conversion units. The below constraints introduce these operational decision variables and govern the amount of power generation (or demand) according to the number of units active during each operational time step.

$$0 \leq \nu_{(i,r,o),x},\ \ \nu^+_{(i,r,o),x},\ \ \nu^-_{(i,r,o),x} \leq m_{i,x} \qquad \forall (i,r,o) \in \mathcal{T},\ \forall x \in \Omega \cup \mathcal{Z} \tag{2.22a}$$

$$\nu_{(i,r,o),x} u_x \underline{\Gamma}_x \leq \Gamma^P_{(i,r,o),x} \leq \nu_{(i,r,o),x} u_x \overline{\Gamma}_x \qquad \forall (i,r,o) \in \mathcal{T},\ \forall x \in \Omega \tag{2.22b}$$

$$\nu_{(i,r,o),x} u_x \underline{\Phi}_x \leq \Phi^Z_{(i,r,o),x} \leq \nu_{(i,r,o),x} u_x \overline{\Phi}_x \qquad \forall (i,r,o) \in \mathcal{T},\ \forall x \in \mathcal{Z} \tag{2.22c}$$

$$\nu_{(i,r,o),x} u_x \underline{\gamma}_{(i,r,o),x} \leq \Gamma^P_{(i,r,o),x} \leq \nu_{(i,r,o),x} u_x \overline{\gamma}_{(i,r,o),x} \qquad \forall (i,r,o) \in \mathcal{T},\ \forall x \in \Omega \tag{2.22d}$$

$$\nu_{(i,r,o+1),x} = \nu_{(i,r,o),x} + \nu^+_{(i,r,o),x} - \nu^-_{(i,r,o),x} \qquad \forall (i,r,o) \in \mathcal{T},\ \forall x \in \Omega \tag{2.22e}$$

Eq. (2.22a) introduces non-negative decision variables for units committed $\nu_{(i,r,o),x}$ [no. units], started up $\nu^+_{(i,r,o),x}$ [no. units], and shut down $\nu^-_{(i,r,o),x}$ [no. units] in each operational time step. This constraint also requires these variables to be less than or equal to the total number of units that exist in that investment period, $m_{i,x}$.

In the full integer unit-commitment model formulation, all of the above defined variables ν, ν^+, ν^- would all be constrained to take on integer values (i.e., $\in \mathbb{Z}$). Here, we relax these to continuous variables to reduce computational burden.

In Eq. (2.22b), the power dispatch $\Gamma^P_{(i,r,o),x}$ for each generator is delimited by the maximum and minimum stable power output, $\overline{\Gamma}_x$ and $\underline{\Gamma}_x$ on a per unit [p.u.] basis, multiplied by unit size u [MW/unit] and the number of units committed $\nu_{(i,r,o),\omega}$units. The dispatchable electricity demand $\Phi^Z_{(i,r,o),z}$ for each net-zero emissions gas producer is similarly constrained in Eq. (2.22c). Eq. (2.22d) bounds fixed profile, or non-dispatchable, generation units, such as wind and solar, by minimum and maximum availability, $\underline{\gamma}_{(i,r,o),\omega}$ and $\overline{\gamma}_{(i,r,o),\omega}$, that constrains generation on a per unit basis in each

evaluated time point. For example, generation from a weather-dependent resource must be less than or equal to the available power in that time step, but could go as low as zero, if curtailment is economic. Other non-dispatchable units bound by this constraint set could include combined heat and power facilities with a minimum amount of load during particular time steps. For conventional thermal units with stable fuel supplies, Eq. (2.22d) will not bind output (i.e., $\underline{\gamma}_{(i,r,o),\omega} = 0$ and $\overline{\gamma}_{(i,r,o),\omega} = 1$) and the minimum or maximum per unit output will be solely constrained by Eq. (2.22b).

Finally Eq. (2.22e) ensures that the number of units committed in each subsequent operational time step $\nu_{(i,r,o+1),\omega}$ is equal to the previous unit commitments $\nu_{(i,r,o),\omega}$ plus units started $\nu^{+}_{(i,r,o),\omega}$, less any units shut down $\nu^{-}_{(i,r,o),\omega}$.

Generator operational constraints

Next, we include maximum ramp rate constraints to bound the hourly change upward and downward in output for each generator. We use the same form of these constraints as that which was implemented in a previous study [77], given by

$$\begin{aligned}
&\Gamma^{P}_{(i,r,o),\omega} - \Gamma^{P}_{(i,r,o-1),\omega} \leq u_\omega \overline{\rho}_\omega (\nu_{(i,r,o),\omega} - \nu^{+}_{(i,r,o),\omega}) \\
&\quad \ldots + u_\omega \min\{\overline{\Gamma}_\omega, \max\{\underline{\Gamma}_\omega, \overline{\rho}_\omega\}\} \nu^{+}_{(i,r,o),\omega} - u_\omega \underline{\Gamma}_\omega \nu^{-}_{(i,r,o),\omega} \qquad \forall (i,r,o) \in \mathcal{T},\ \forall \omega \in \Omega, \quad (2.23a) \\
&\Gamma^{P}_{(i,r,o-1),\omega} - \Gamma^{P}_{(i,r,o),\omega} \leq u_\omega \overline{\rho}_\omega (\nu_{(i,r,o),\omega} - \nu^{+}_{(i,r,o),\omega}) \\
&\ldots + u_\omega \min\{\overline{\Gamma}_\omega, \max\{\underline{\Gamma}_\omega, \overline{\rho}_\omega\}\} \nu^{-}_{(i,r,o),\omega} - u_\omega \underline{\Gamma}_\omega \nu^{+}_{(i,r,o),\omega} \qquad \forall (i,r,o) \in \mathcal{T},\ \forall \omega \in \Omega. \quad (2.23b)
\end{aligned}$$

In Eq. (2.23a), the maximum hourly change in generator output is bounded by the maximum ramp rate $\overline{\rho}_\omega$ [p.u./hour] multiplied by the number of units committed and not newly started up in this time step, i.e., $\nu_{(i,r,o),\omega} - \nu^{+}_{(i,r,o),\omega}$. Units that are newly started up may increase output to the greater of their minimum stable power output $\underline{\Gamma}_\omega$ and their ramp rate $\overline{\rho}_\omega$, not to exceed the maximum stable power output $\overline{\Gamma}_\omega$. Finally, any units shut down $\nu^{-}_{(i,r,o),\omega}$ during the time step may decrease power output from the minimum stable power output $\underline{\Gamma}_\omega$ to zero.

The net downward change in generation output is similarly constrained by Eq. (2.23b). Thermal generation units typically have maximum ramp rates $\overline{\rho}_\omega$ determined by their operational characteristics and flexibility to increase output on-demand, while variable renewable generation units increase generation output with the empirical resource availability specified by $\overline{\gamma}_{(i,r,o),\omega}$ and described in Eq. (2.22d) (i.e., $\overline{\rho}_\omega = 1$).

To enforce ramp rate constraints across representative time periods, we use the set $\mathcal{C}$ as defined in Eq. (2.3) to map representative time days to an appropriate sequence within a calendar year of operations. We then apply constraints that limit the change in generation output between the final hour of a representative day (here O, or 24 in our case for day $c-1$) to the first hour of the

subsequent day (with respect to the represented calendar sequence) (hour 1 in day c). These take the form

$$\Gamma^P_{(i,c,1),\omega} - \Gamma^P_{(i,c-1,O),\omega} \leq u_\omega \overline{\rho}_\omega (\nu_{(i,c,1),\omega} - \nu^+_{(i,c,1),\omega}) \\ \ldots + u_\omega \min\{\overline{\Gamma}_\omega, \max\{\underline{\Gamma}_\omega, \overline{\rho}_\omega\}\} \nu^+_{(i,c,1),\omega} - u_\omega \underline{\Gamma_\omega} \nu^-_{(i,c,1),\omega}, \qquad \forall i \in \mathcal{I},\ \forall c \in \mathcal{C},\ \forall \omega \in \Omega \quad (2.24a)$$

$$\Gamma^P_{(i,c-1,O),\omega} - \Gamma^P_{(i,c,1),\omega} \leq u_\omega \overline{\rho}_\omega (\nu_{(i,c,1),\omega} - \nu^+_{(i,c,1),\omega}) \\ \ldots + u_\omega \min\{\overline{\Gamma}_\omega, \max\{\underline{\Gamma}_\omega, \overline{\rho}_\omega\}\} \nu^-_{(i,c,1),\omega} - u_\omega \underline{\Gamma_\omega} \nu^+_{(i,c,1),\omega}, \qquad \forall i \in \mathcal{I},\ \forall c \in \mathcal{C},\ \forall \omega \in \Omega. \quad (2.24b)$$

Next, we develop a novel approach to represent constraints on the minimum up-time $\overline{\upsilon}$ [hours] and down-time $\underline{\upsilon}$ [hours] for generators in adjacent representative time periods. To dynamically accommodate minimum up- or down-times that exceed the length of multiple representative time periods, we define two vectors:

$$\tilde{Y} = \Big(\underbrace{0}_{O \text{ times}} \quad \underbrace{1}_{O \text{ times}} \quad \ldots \quad \underbrace{W}_{O \text{ times}} \Big), \qquad \tilde{X} = \underbrace{\Big(O \quad O-1 \quad \ldots \quad 1 \Big)}_{\text{W times}}. \qquad (2.25)$$

The above vectors are used to express constraints that involve any required number of previous time periods, depending on the relative magnitude of O and $\underline{\upsilon}$ or $\overline{\upsilon}$. $\tilde{Y}$ dynamically identifies the representative time period $r \in \mathcal{R}$ to which to apply the constraint, and $\tilde{X}$ identifies the position $o \in \mathcal{O}$ within the representative time period. For this purpose, $W \in \mathbb{N}$ is a natural number greater than the largest number of representative time periods required to cast the constraint across to accommodate the up/down-time, or $W \geq \frac{\max\{\overline{\upsilon}, \underline{\upsilon}\}}{O}$. The minimum up- and down- time constraints are then given by

$$\nu_{(i,c,o),\omega} \geq \sum_{k \in [\overline{\upsilon}_\omega]} \nu^+_{i,c-\tilde{Y}_{k-o+O},\tilde{X}_{k-o+O},\omega} \qquad \forall (i,o), \in (\mathcal{I} \times \mathcal{O}),\ \forall c \in \mathcal{C}, \qquad (2.26a)$$

$$m_{i,\omega} - \nu_{(i,c,o),\omega} \geq \sum_{k \in [\underline{\upsilon}_\omega]} \nu^-_{i,c-\tilde{Y}_{k-o+O},\tilde{X}_{k-o+O},\omega} \qquad \forall (i,o) \in (\mathcal{I} \times \mathcal{O}),\ \forall c \in \mathcal{C}. \qquad (2.26b)$$

The minimum up-time constraint given in Eq. (2.26a) bounds the number ν of units committed in every operational time step from below by the number ν^+ of units started up across the previous $\overline{\upsilon}$ hourly time steps. In other words, any units that are started up must remain committed for at least $\overline{\upsilon}$ hourly time steps. Similarly, the minimum down-time constraint given in Eq. (2.26b) computes the number of units offline, i.e., those not committed, in a given time step as the difference between units that exist during this investment period, i.e., $m_{i,x}$, and committed units ν. The number of units

offline must be equal to or greater than the number of units shut-down ν^- across the preceding $\underline{\upsilon}$ hourly time steps. Note that depending on the number and sequence of representative time periods, some constraints specified by Eq. (2.24) and Eq. (2.26) may be identical, and could be automatically removed from the optimization during pre-solve.

2.3.5 Gas system operational decisions

Here we describe the models we use to reflect operational decision-making for natural gas transmission. The natural gas pipeline constraints are given in steady-state for each operational time period $r \in \mathcal{R}$, because practical decision making for gas systems is done assuming balancing of supplies and consumption on a daily time-scale. The compressibility of natural gas enables operations that use "line-pack" and renders instantaneous balancing of injections into and withdrawals from a pipeline system unnecessary. We describe the physical flow modeling as well as the engineering and operating constraints for natural gas delivery systems below.

Gas flow constraints

We use a form of the gas flow equations taken in a previous study on integrated power and natural gas system operations [85]. The flow of gas through a pressurized network of pipes is governed by coupled partial differential equations for mass conservation and momentum conservation, given by:

$$\frac{\partial Q}{\partial x} + \frac{\pi D^2}{4 R_{CH_4} T Z \rho_0} \cdot \frac{\partial \mathrm{p}}{\partial t} = 0, \tag{2.27a}$$

$$\frac{\pi^2 D^5}{16 f R_{CH_4} T_{\mathrm{std}} Z \rho_0^2} \cdot \frac{\partial \mathrm{p}}{\partial x} + Q|Q| = 0. \tag{2.27b}$$

In the above equations that relate pressure p and flow Q, we assume an ideal gas equation of state. The parameters include the diameter D [m], specific gas constant for methane R_{CH_4} [J/kg-K], gas temperature T [°K], gas compressibility Z, pipeline length L [m], friction factor f, standard temperature $T_{\mathrm{std}} = 300$ [°K], and gas density at standard conditions ρ_0 [kg/m^3]. In steady-state, gas flow on an edge $e \in \mathcal{E}_G$ directed from node $n \in \mathcal{N}_G$ to $m \in \mathcal{N}_G$ is then represented by a single algebraic momentum conservation equation

$$Q_e|Q_e| = \frac{K_e}{L_e}(\mathrm{p}_n^2 - \mathrm{p}_m^2) \qquad \text{where} \quad K_e = \frac{\pi^2 D_e^5}{16 f_e R_{CH_4} T_{STP} Z \rho_0^2}. \tag{2.28}$$

In the above flow equation, the diameter D_e and friction factor f_e depend on the pipeline segment e, so that the coefficient K_e is edge dependent. The nodal pressures P_n and P_m are given in units of Pa, and Q_e is molar flow of gas in units of standard m^3/s. Eq. (2.28) can be defined over the

entire network using the incidence matrix of the graph. We also wish to reproduce the physical gas flow constraints for all operational time periods i.e., $\forall (i,r) \in (\mathcal{I} \times \mathcal{R})$. Because flow is a function of squared pressure, we can replace the term p_n^2 for each node $n \in \mathcal{N}_G$ with squared pressure decision variables defined as Π_n in units of Pa^2. We therefore use the physical flow constraint

$$Q_{(i,r),e}|Q_{(i,r),e}| = K_e \sum_{n \in \mathcal{N}_G} A^G_{n,e} \Pi_n \qquad \forall (i,r) \in (\mathcal{I} \times \mathcal{R}),\ \forall e \in \mathcal{E}_G. \tag{2.29}$$

The squared pressure variables are constrained by maximum and minimum values for each node,

$$\underline{\Pi}_n \leq \Pi_{(i,r),n} \leq \overline{\Pi}_n \qquad \forall (i,r) \in (\mathcal{I} \times \mathcal{R}),\ \forall n \in \mathcal{N}_G, \tag{2.30}$$

and the gas flow rates at every evaluated time point $Q_{(i,r),e}$ are constrained by minimum and maximum values for each edge according to

$$-\overline{Q}_e \leq Q_{(i,r),e} \leq \overline{Q}_e \qquad \forall (i,r) \in (\mathcal{I} \times \mathcal{R}),\ \forall e \in \mathcal{E}_G. \tag{2.31}$$

Henceforth, we will work with the relation (2.29) for physical gas flow.

We suppose that each directed pipeline segment that is represented by an edge $e \in \mathcal{E}_G$ in the gas network may or may not have a compressor at its start node. Here, we introduce an auxiliary pressure squared variable, $\hat{\Pi}_{(i,r),e}\ \forall e \in \mathcal{E}_G$, to allow for pressure boosting to occur at the start of a pipeline. This compression pressure for each edge is constrained to be no less than the nodal pressure $\Pi_{(i,r),n}$ at the start node, and no greater than the product of the same pressure and the maximum compression ratio $\overline{\alpha}_e$ of this compressor. In the case where the pipeline does not possess a compressor at its start node, the maximum compression ratio is $\overline{\alpha}_e = 1$, so in effect the auxiliary compression pressure variable is constrained to equal the nodal pressure at the start node. To define the required constraints, we use indicator functions to identify the start and end nodes for each edge using the nodal-edge incidence matrix $A^G_{n,e}$ defined in Eq. (2.2). For an edge $e \in \mathcal{E}_G$ that is directed from start node $n \in \mathcal{N}_G$ to end node $m \in \mathcal{N}_G$, the start node is identified using $\{1|A^G_{n,e} = 1\}$ and the exit node is identified using $\{1|A^G_{n,e} = -1\}$. The constraints then take the form

$$\hat{\Pi}_{(i,r),e} \leq \overline{\alpha}_e \sum_{n \in \mathcal{N}_G} \{1|A^G_{n,e} = 1\} \Pi_{(i,r),n} \qquad \forall (i,r) \in (\mathcal{I} \times \mathcal{R}),\ \forall e \in \mathcal{E}_G, \tag{2.32a}$$

$$\hat{\Pi}_{(i,r),e} \geq \sum_{n \in \mathcal{N}_G} \{1|A^G_{n,e} = 1\} \Pi_{(i,r),n} \qquad \forall (i,r) \in (\mathcal{I} \times \mathcal{R}),\ \forall e \in \mathcal{E}_G. \tag{2.32b}$$

Generalizing the gas flow equation to apply to edges with and without compressors, the square of the gas flow is a function of the difference between the squared pressure $\hat{\Pi}_{(i,r),e}$ at the start node and the squared pressure $\{1|A^G_{n,e} = -1\}\Pi_{(i,r),n}$ at the end node, resulting in the constraint

$$Q_{(i,r),e}|Q_{(i,r),e}| = K_e \left(\hat{\Pi}_{(i,r),e} - \sum_{n \in \mathcal{N}_G} \{1|A^G_{n,e} = -1\}\Pi_{(i,r),n} \right) \qquad \forall (i,r) \in (\mathcal{I} \times \mathcal{R}),\ \forall e \in \mathcal{E}_G. \tag{2.33}$$

Because flow directions are not known a priori, Eq. (2.33) is non-convex [51]. To handle the non-convexity and enable the use of relaxed mixed-integer programming formulations, we introduce binary variables $y_{(i,r),e} \in \{0,1\}$ that indicate the gas flow direction relative to the nominal flow direction assigned in the nodal-branch incidence matrix $A^G_{n,e}$. This enables the application of disjunctive constraints that depend on flow direction:

$$y_{(i,r),e} = \begin{cases} 1 & \text{if } Q_{(i,r),e} \geq 0 \\ 0 & \text{otherwise} \end{cases} \qquad \forall (i,r) \in (\mathcal{I} \times \mathcal{R}),\ \forall e \in \mathcal{E}_G \tag{2.34a}$$

$$(y_{(i,r),e} - 1)\overline{Q}_e \leq Q_{(i,r),e} \leq y_{(i,r),e}\overline{Q}_e \qquad \forall (i,r) \in (\mathcal{I} \times \mathcal{R}),\ \forall e \in \mathcal{E}_G. \tag{2.34b}$$

The binary variables are also included into the physical flow equation, in order to define the sign of the pressure drop across each pipeline, relative to the nominal direction indicated in $A^G_{n,e}$. This results in a straightforward, non-negative quadratic expression of gas flow:

$$Q^2_{(i,r),e} = (2y_{(i,r),e} - 1)K_e \left(\hat{\Pi}_{(i,r),e} - \sum_{n \in \mathcal{N}_G} \{1|A^G_{n,e} = -1\}\Pi_{(i,r),n} \right) \qquad \forall (i,r) \in (\mathcal{I} \times \mathcal{R}),\ \forall e \in \mathcal{E}_G \tag{2.35}$$

Furthermore, we employ a McCormick relaxation to convexify Eq. (2.35). This is a well-known convex relaxation used by Borraz-Sanchez, et al. (2016) to represent steady-state gas flows in a pipeline network with unknown flow directions [56].

The McCormick relaxation is used to represent a product of two variables x and y by an auxiliary variable λ that is delimited within an envelope $\langle x, y \rangle^{Mc}$, which is defined by a collection of inequalities that involve the maximum and minimum possible values for x, given by $\overline{x}$ and $\underline{x}$, as well as y, given by $\overline{y}$ and $\underline{y}$. The McCormick relaxation is then given by the constraint set

$$\lambda \leq \overline{x}y + x\underline{y} - \overline{x}\underline{y}, \tag{2.36a}$$

$$\lambda \leq x\overline{y} + \underline{x}y - \underline{x}\overline{y}, \tag{2.36b}$$

$$\lambda \geq \underline{x}y + x\underline{y} - \underline{x}\underline{y}, \tag{2.36c}$$

$$\lambda \geq \overline{x}y + x\overline{y} - \overline{x}\overline{y}, \tag{2.36d}$$

which will tightly constrain $\lambda = xy$, in cases where x or y are binomial variables.

We employ the above formulation to represent the product in Eq. (2.35). Here, $x = (2y_{(i,r),e}-1)$ has an upper bound of $\overline{x} = 1$ and a lower bound $\underline{x} = -1$.

Similarly, $y = \left(\hat{\Pi}_{(i,r),e} - \sum_{n\in\mathcal{N}_G}\{1|A^G_{n,e} = -1\}\Pi_{(i,r),n}\right)$ has an upper bound $\overline{y} = \left(\overline{\Pi} - \underline{\Pi}\right)$ and lower bound $\underline{y} = \left(\underline{\Pi} - \overline{\Pi}\right)$. This fully specifies the above constraint set as defined in Eq. (2.36), and can be used in concert with the equality constraint to represent Eq. (2.35) by the relaxed constraint set presented in Eq. (2.37) and Eq. (2.38).

$$Q^2_{(i,r),e} = K_e\lambda_{(i,r),e} \qquad \forall(i,r) \in (\mathcal{I}\times\mathcal{R})\,,\ \forall e \in \mathcal{E}_G, \tag{2.37}$$

$$\lambda_{(i,r),e} \in \left\langle 2y_{(i,r),e}-1,\ \left(\hat{\Pi}_{(i,r),e} - \sum_{n\in\mathcal{N}_G}\{1|A^G_{n,e} = -1\}\Pi_{(i,r),n}\right)\right\rangle^{Mc}, \qquad \forall(i,r) \in (\mathcal{I}\times\mathcal{R})\,,\ \forall e \in \mathcal{E}_G. \tag{2.38}$$

Applying the above approach, Eq. (2.35) can be fully convexified using Eq. (2.38) as defined by Eq. (2.36) and by relaxing the equality in Eq. (2.37) to

$$Q^2_{(i,r),e} \leq K_e\lambda_{(i,r),e} \qquad \forall(i,r) \in (\mathcal{I}\times\mathcal{R})\,,\ \forall e \in \mathcal{E}_G. \tag{2.39}$$

The above constraints can be used in a convex quadratic programming formulation.

Lastly, to ensure a unique solution, we enforce a slack node pressure at the designated slack node N:

$$\Pi_{(i,r),\mathrm{N}} = \tilde{\Pi} \qquad \forall(i,r) \in (\mathcal{I}\times\mathcal{R}) \tag{2.40}$$

Note that in the above mathematical formulation, we assume that (for the purposes of gas flow simulation) the gas mixture in the pipeline will have the attributes of methane (CH_4). For planning purposes, this is an acceptable simplification to simulate the multi-component gaseous flow through

a pipeline.

Gas energy balance

Next, we note that gaseous fuels vary in energy content depending on their molar composition. Net-zero emissions gases, in particular, could range from synthetic natural gas drop-in substitutes to pure hydrogen. Gas customers will have appliances and equipment tuned to operate using gas that satisfies adopted pipeline specifications or is broadly aligned with historical deliveries. We use the proposed model to illustrate the potential effect of gas quality or hydrogen blending constraints on the least-cost resource expansion and system operation decisions.

In order to permit such gas quality constraints, and to approximate the flow of gases in the networked system, we introduce a set of gas components $g \in \mathcal{G}$ each with an associated molar weight M_g [kg/kmol] and energy content x_g [MJ/kg].

Each potential source of gas in the system is parameterized by a set of mole fractions for each component $g \in \mathcal{G}$, for nodal fossil natural gas supplies $\chi^G_{n,g}$ [%], for gas storage resources $\chi^S_{s,g}$ [%], and for net-zero emissions gas supplies $\chi^Z_{z,g}$ [%].

Local natural gas supplies at each node $\Gamma^G_{(i,r),n}$ [MW] are assumed to be of a fixed composition indicated by the parameters $\chi^G_{n,g}$ [%]. These gas injections are constrained to remain below the maximum local production capability or import at the boundary "slack" node $\overline{S}_n$ [MW]:

$$\Gamma^G_{(i,r),n} \leq \overline{S}_n \qquad \forall (i,r) \in (\mathcal{I} \times \mathcal{R}),\ \forall n \in \mathcal{N}_G. \tag{2.41}$$

Additionally, in order to avoid introducing component tracking for gas storage reservoirs (and the associated computational burden), we assume that these resources charge and discharge the same gas composition $\chi^S_{s,g}$ [%] as fossil natural gas available at the slack node $\chi^G_{n,g}$ [%].

Decision variables are included to track the nominal flows $q_{(i,r),e,g}$ [kmol/sec] and nodal off-takes $\phi_{(i,r,o),n,g}$ [kmol/sec] across the system. All gas component flows must be in the same direction as the natural gas flow on each pipeline, and local gas component deliveries must be non-negative. These constraints are specified as

$$(y_{(i,r),e} - 1)\overline{Q}_e \leq q_{(i,r),e,g} \leq y_{(i,r),e}\overline{Q}_e \qquad \forall (i,r) \in (\mathcal{I} \times \mathcal{R}),\ \forall e \in \mathcal{E}_G,\ \forall g \in \mathcal{G} \tag{2.42a}$$

$$\phi_{(i,r),n,g} \geq 0 \qquad \forall (i,r) \in (\mathcal{I} \times \mathcal{R}),\ \forall n \in \mathcal{N}_G,\ \forall g \in \mathcal{G} \tag{2.42b}$$

The sum of all nominal molar gas flows $q_{(i,r),e,g}$ [kmol/sec] (by their molar mass M_g [kg/kmol]) must equal the total mass flow implicated by the gas flow $Q_{(i,r),e}$ [standard m^3/sec], adjusted to a mass-basis using the number of moles occupied by a m^3 at standard conditions ($V_m = 40.87$ [moles/m^3]) and the molar mass of methane M_{CH_4} [kg/mole] (as this was originally employed in

estimating the physical parameters of steady-state gas pipeline network operation):

$$\sum_{g\in\mathcal{G}} M_g q_{(i,r),e,g} = Q_{(i,r),e}(M_{CH_4} V_m), \qquad \forall (i,r) \in (\mathcal{I}\times\mathcal{R}),\ \forall e \in \mathcal{E}_G. \tag{2.43}$$

Similarly, the sum of all nominal molar gas component deliveries $\phi_{(i,r,o),n,g}$ [kmol/sec] by their molar mass M_g [kg/kmol] and energy content x_g [MJ/kg] must equal total consumption of gaseous energy at every node:

$$\sum_{g\in\mathcal{G}} x_g M_g \phi_{(i,r,o),n,g} = \left(\Phi^G_{(i,r,o),n} + \sum_{\omega\in\Omega_G\cap\Omega_n} \eta_\omega \Gamma^P_{(i,r,o),\omega}\right), \qquad \forall (i,r,o)\in\mathcal{T},\ \forall n\in\mathcal{N}_G. \tag{2.44}$$

The total consumption is assessed as total core gas demands $\Phi^G_{(i,r,o),n}$ [MW] plus any gas used for electricity generation $\eta_\omega \Gamma^P_{(i,r,o),\omega}$ [MW].

A molar balance for every gas component is enforced at every gas node, accounting for local nominal off-takes, local production, and any transfers:

$$\begin{aligned}
&\frac{\chi^G_{n,g}}{M_n x_n}\Gamma^G_{(i,r),n} + \sum_{z\in\mathcal{Z}_n} \frac{\chi^Z_{z,g}}{M_z x_z}\Gamma^Z_{(i,r,o),z} + \\
&\quad \dots \sum_{s\in\mathcal{S}_G\cap\mathcal{S}_n} \frac{\chi^S_{s,g}}{M_s x_s}\left(\psi^-_{(i,r,o),s} - \psi^+_{(i,r,o),s}\right) = \phi_{(i,r,o),n,g} + \sum_{e\in\mathcal{E}_G} A^G_{n,e} q_{(i,r),e,g}, \\
&\quad \dots \forall (i,r,o)\in\mathcal{T},\ \forall g\in\mathcal{G},\ \forall n\in\mathcal{N}_G.
\end{aligned} \tag{2.45}$$

where the molar weight M_z [kg/kmol] and energy content x_z [MJ/kg] of gas produced by each potential gas supply is computed using the mole fraction composition $\chi_{z,g}$ [%] as:

$$M_z = \sum_{g\in\mathcal{G}} M_g \chi_{z,g}, \qquad \forall z\in\mathcal{Z}\cup\mathcal{S}_G\cup\mathcal{N}_G \tag{2.46a}$$

$$x_z = \sum_{g\in\mathcal{G}} x_g M_g \chi_{z,g}, \qquad \forall z\in\mathcal{Z}\cup\mathcal{S}_G\cup\mathcal{N}_G. \tag{2.46b}$$

Finally, the total energy balance is enforced at every gas node. The energy balance constraints are defined to ensure that modeled operations are feasible in steady-state across each representative time period (day in our case), i.e., $\forall (i,r)\in(\mathcal{I}\times\mathcal{R})$. Local natural gas supplies $\Gamma^G_{(i,r),n}$ [MW] less net gaseous energy outflows must be equal to the average gas demands of utility customers $\Phi^G_{(i,r,o),n}$ [MW], generators $\eta_\omega\Gamma^P_{(i,r,o),\omega}$ [MW] and net charging to gas storage $(\psi^+_{(i,r,o),s} - \psi^-_{(i,r,o),s})$ [MW], less

any local production $\Gamma^{Z}_{(i,r,o),z}$ [MW] of net-zero emissions gases. This constraint is given by

$$\Gamma^{G}_{(i,r),n} - \sum_{g\in\mathcal{G}}\sum_{e\in\mathcal{E}_G} A^{G}_{n,e} x_g M_g q_{(i,r),e,g} - \frac{1}{O}\sum_{o\in\mathcal{O}} \Phi^{G}_{(i,r,o),n} + \sum_{\omega\in\Omega_G\cap\Omega_n} \eta_\omega \Gamma^{P}_{(i,r,o),\omega} + \\ \dots \sum_{s\in\mathcal{S}_G\cap\mathcal{S}_n} \left(\psi^{+}_{(i,r,o),s} - \psi^{-}_{(i,r,o),s}\right) - \sum_{z\in\mathcal{Z}_n} \Gamma^{Z}_{(i,r,o),z} = 0, \\ \forall (i,r) \in (\mathcal{I}\times\mathcal{R}),\ \forall n \in \mathcal{N}_G. \tag{2.47}$$

In Eq. (2.47), $\mathcal{Z}_n$ denotes the set of net-zero emissions gas production units at a node $n \in \mathcal{N}_G$. Note that differently from the electricity system, supply must equal demand in the gas system only at the daily level, not with the hourly frequency of the electric grid energy supply-demand balance.

The modeling framework allows users to select one of three constraint formulations for ensuring acceptable gas quality.

First, in the least-constrained case, we impose no additional restrictions on the blending of different gas components.

Second, we impose annual, system-wide restrictions on production of gas components that may experience infrastructural limits on blending governed by materials constraints in gas transmission, distribution, and consumption infrastructure. This ensures, for example, that the amount of hydrogen delivered for consumption by the system across the modeled investment year does not exceed the maximum mole fraction acceptable by existing infrastructure. The constraint is given as

$$\sum_{r\in\mathcal{R}} w_{(i,r)} \sum_{o\in\mathcal{O}}\sum_{n\in\mathcal{N}_G} \phi_{(i,r,o),n,g} \le \overline{\chi_g} \sum_{r\in\mathcal{R}} w_{(i,r)} \sum_{o\in\mathcal{O}}\sum_{n\in\mathcal{N}_G}\sum_{h\in\mathcal{G}} \phi_{(i,r,o),n,h} \\ \forall i \in \mathcal{I}, \forall g \in \mathcal{G}. \tag{2.48}$$

Third, the most restrictive gas quality formulation applies gas quality constraints across every simulated operational day, for each node and transmission pipeline.

Every nominal flow $q_{(i,r),e,g}$ [kmol/sec] must be constrained to abide by molar blend limitations governed by materials considerations in transmission infrastructure.

$$q_{(i,r),e,g} \le \overline{\chi_g} \sum_{h\in\mathcal{G}} q_{(i,r),e,h} + (1 - y_{(i,r),e})\overline{Q}_e, \qquad \forall (i,r) \in (\mathcal{I}\times\mathcal{R}),\ \forall g \in \mathcal{G},\ \forall e \in \mathcal{E}_G, \tag{2.49a}$$

$$q_{(i,r),e,g} \ge \overline{\chi_g} \sum_{h\in\mathcal{G}} q_{(i,r),e,h} - y_{(i,r),e}\overline{Q}_e, \qquad \forall (i,r) \in (\mathcal{I}\times\mathcal{R}),\ \forall g \in \mathcal{G},\ \forall e \in \mathcal{E}_G. \tag{2.49b}$$

These constraints are formulated to limit the nominal molar flows $q_{(i,r),e,g}$ to remain below a maximum molar fraction for each component $\overline{\chi_g}$, applied to the sum of all nominal gas flows. Eq. (2.49a) will bind in cases where flows are positive (i.e., $y_{(i,r),e} = 1$), and Eq. (2.49b) will bind in cases where flows are negative (i.e., $y_{(i,r),e} = 0$).

In addition, maximum and minimum heating value constraints are implemented by ensuring that the total molar off-take at any node is within acceptable bounds, relative to the total energy delivered:

$$\underline{x} \sum_{g \in \mathcal{G}} M_g \phi_{(i,r,o),n,g} \leq \sum_{g \in \mathcal{G}} x_g \phi_{(i,r,o),n,g} \leq \overline{x} \sum_{g \in \mathcal{G}} M_g \phi_{(i,r,o),n,g}, \qquad \forall (i,r,o) \in \mathcal{T},\ \forall n \in \mathcal{N}_G. \quad (2.50)$$

The delivered amount of energy is computed as the sum of molar off-takes $\phi_{(i,r,o),n,g}$ [kmol/sec] multiplied by their component molar heating value x_g [MJ/kmol]. Eq. (2.50) introduces minimum $\underline{x}$ and maximum $\overline{x}$ limits on heating value of gas delivered (on a mass basis) [MJ/kg]. This constraint applies these values to the total mass of gas delivered at each node using the molar off-takes $\phi_{(i,r,o),n,g}$ [kmol/sec] multiplied by their component molar mass values M_g [kg/kmol].

This simplified version of the gas quality tracking problem does not enforce mixing at every node. However, this approach does ensure that no transmission interchange or delivered gas composition will ever exceed the guidelines. As long as permissible blend fractions are small, we do not expect this to meaningfully impact the physics of gas flow. Further, as long as the maximum permissible blend fraction of hydrogen is uniform across the network, there should be no obtainable objective function improvement by deviating from a well-mixed solution to preferentially transport hydrogen to particular nodes on the network.

2.3.6 Energy storage operational decisions

Energy storage units can be used to balance time-varying energy supplies and demands in dynamic systems. Historically, the natural gas industry has leveraged geologic gas storage fields to satisfy large seasonal swings in gas demand without commensurate cycles in gas extraction and processing [86, 87]. In the electric power sector, the majority of energy storage takes the form of hydroelectric generators, which can capture and control geophysical flows of water with reservoirs to generate electricity. However, increasing electricity generation from weather-dependent renewable energy supplies will likely require a suite of new electrochemical, gravitational, or thermal energy storage units to smooth out real-time fluctuations in generation and to shift bulk energy generation from periods of abundance to scarcity periods on diurnal, weekly, multi-weekly, and possibly seasonal time scales. Here, we introduce two sets of electrical and gaseous energy storage units, denoted by $\mathcal{S}_P$ and $\mathcal{S}_G$, respectively. Constraints are required to track the state of charge of each storage resource, based on charge and discharge dispatch decisions across the simulated operational time horizon and technology efficiency characteristics. These constraints are expressed as

$$\Psi_{(i,r,o+1),s} = \Psi_{(i,r,o),s} + \eta_s^+ \psi^+_{(i,r,o),s} - \frac{\psi^-_{(i,r,o),s}}{\eta_s^-} - \eta_s^l \Psi_{(i,r,o),s} \qquad \forall (i,r,o) \in \mathcal{T},\ \forall s \in \mathcal{S}_P \cup \mathcal{S}_G, \tag{2.51a}$$

$$\Psi_{(i,r,o),s} \leq d_s u_s m_{i,s} \qquad \forall (i,r,o) \in \mathcal{T},\ \forall s \in \mathcal{S}_P \cup \mathcal{S}_G. \tag{2.51b}$$

Eq. (2.51a) tracks the amount of energy in storage at the end of each time step $\Psi(i,r,o+1),s$ by incrementing or decrementing the state of charge $\Psi_{(i,r,o),s}$ from the previous time step by any charging $\psi^+_{(i,r,o),s}$ or discharging $\psi^-_{(i,r,o),s}$ dispatch, adjusted by the respective charging and discharging efficiencies η_s^+, η_s^- [%]. An hourly loss rate η_s^l [%/hour] is also applied to the amount of energy in storage during the previous time step (e.g., battery self-discharge). Eq. (2.51b) constrains the amount of energy stored to not exceed the maximum energy capacity of the storage resource (i.e., the duration d_s [hours] by the unit size u_s [MW/unit] by the number of units in operation during the present investment period, given by $m_{i,s}$ [units].

Here, we model gas and electrical energy storage units with the same constraint set but note that this abstracts away important transient features of gas storage operation as identified by [87]. To conservatively model gas storage operating dynamics, we include constraints that require a constant charge/discharge rate for the duration of each representative day:

$$\psi^+_{(i,r,o+1),s} = \psi^+_{(i,r,o),s} \qquad \forall (i,r,o) \in \mathcal{T},\ \forall s \in \mathcal{S}_G, \tag{2.52a}$$

$$\psi^-_{(i,r,o+1),s} = \psi^-_{(i,r,o),s} \qquad \forall (i,r,o) \in \mathcal{T},\ \forall s \in \mathcal{S}_G. \tag{2.52b}$$

However, more complex models for gas storage operation can be accommodated by the proposed model formulation in future work.

A constraint set is also necessary to bound the charge and discharge capabilities based on nameplate installed power capacity and technology efficiency characteristics (i.e., constraints on power rates [MW], not energy [MWh]). Here, we ensure that the storage charge rate does not exceed the permissible range, which is limited by the installed nameplate storage power capacity [MW] and the total remaining energy capacity in the storage resource. These limits are given by

$$\psi^+_{(i,r,o),s} \leq \frac{1}{\eta_s^+} u_s m_{i,s} \qquad \forall (i,r,o) \in \mathcal{T},\ \forall s \in \mathcal{S}_P \cup \mathcal{S}_G, \tag{2.53a}$$

$$\psi^+_{(i,r,o),s} \leq d_s u_s m_{i,s} - \Psi_{(i,r,o),s} \qquad \forall (i,r,o) \in \mathcal{T},\ \forall s \in \mathcal{S}_P \cup \mathcal{S}_G. \tag{2.53b}$$

Installed storage power capacity is calculated in Eq. (2.53a) by applying the unit size u_s (in units

of maximum instantaneous power output $\text{MW}_{electric}$ for electrical storage and $\text{MW}_{thermal}$ for gas storage) to the number of units in operation during the current investment time period $m_{i,s}$. Eq. (2.53b) further constrains the charging to the installed energy storage capacity. Next, we similarly ensure that the storage discharge rate does not exceed the permissible range, which is limited by the installed nameplate storage power capacity as well as the amount of energy in storage using the following constraints:

$$\psi^{-}_{(i,r,o),s} \leq \eta^{-}_{s} u_s m_{i,s} \qquad \forall (i,r,o) \in \mathcal{T},\ \forall s \in \mathcal{S}_P \cup \mathcal{S}_G, \tag{2.54a}$$

$$\psi^{-}_{(i,r,o),s} \leq \Psi_{(i,r,o),s} \qquad \forall (i,r,o) \in \mathcal{T},\ \forall s \in \mathcal{S}_P \cup \mathcal{S}_G. \tag{2.54b}$$

Finally, because storage units are modeled as continuous, they may represent multiple discrete storage units with some charging and some discharging simultaneously. As such, we must constrain the total amount of storage power capacity used for charging and discharging simultaneously, to ensure this value does not exceed the installed power capacity. This constraint is formulated as

$$\frac{1}{\eta^{-}_{s}} \psi^{-}_{(i,r,o),s} + \eta^{+}_{s} \psi^{+}_{(i,r,o),s} \leq u_s m_{i,s} \qquad \forall (i,r,o) \in \mathcal{T},\ \forall s \in \mathcal{S}_P \cup \mathcal{S}_G. \tag{2.55}$$

In deeply-decarbonized energy systems, long-duration and seasonal energy storage may also have a role to play in managing seasonal availability of solar and wind generation [16]. However, as described in Section 2.3.2, co-optimization of design and operational decision variables may require simulation of operations for only a subset of representative time periods. The discrete nature of these selected time periods generally prohibits transfer of energy between simulated representative time periods. However, some selected periods may represent times of surplus where energy storage units should experience net inflows of energy to be available during other represented periods during times of scarcity.

Inspired by approaches previously described by [78, 88, 89], we include constraints to track cumulative, sequential state of charge across the full time series using the subset of simulated, representative time periods $r \in \mathcal{R}$, as mapped to their sequence in a calendar year $\mathcal{C}$ (as described in Eq. (2.3)). This sequential state of charge variable is defined for each storage resource as $\Upsilon_{c,s}$ [MWh] by

$$\Upsilon_{c,s} = \Psi_{i,\sigma(1),1,s} + \sum_{k \in [c]} (\Psi_{i,\sigma(k),O,s} - \Psi_{i,\sigma(k),1,s}) \qquad \forall c \in \mathcal{C},\ \forall s \in \mathcal{S}_P \cup \mathcal{S}_G. \tag{2.56}$$

Here, we compute the cumulative, sequential state of charge $\Upsilon_{c,s}$ at the end of each operational

time period in the full calendar sequence of periods simulated. This value is equal to the initial state of charge $\Psi_{i,\sigma(1),1,s}$ plus the net change in energy stored $(\Psi_{i,\sigma(k),O,s} - \Psi_{i,\sigma(k),1,s})$ summed across all preceding operational time periods in the calendar sequence. Recall that $\sigma(k)$ indicates the representative day $r \in \mathcal{R}$ that is associated with position k in the represented calendar sequence $\mathcal{C}$. In this way, Eq. (2.56) computes the state of charge at the transition between each representative period in sequence.

We also include constraints to ensure storage charge and discharge behavior over the course of each representative period would not violate maximum energy capacity when mapped to the cumulative, sequential state of charge variable. In other words, if we were to compute $\Upsilon_{c,s}$ at every operational time step, rather than at the transition between each operational time period, this value must remain between zero and the installed storage energy capacity. We do this by including auxiliary variables to first identify the maximum and minimum nominal states of charge, $\overline{\Psi}_{(i,r),s}$ and $\underline{\Psi}_{(i,r),s}$, respectively, which are accessed over the course of each simulated representative period:

$$\underline{\Psi}_{(i,r),s} \leq \Psi_{(i,r,o),s} \qquad \forall (i,r,o) \in \mathcal{T},\ \forall s \in \mathcal{S}_P \cup \mathcal{S}_G, \tag{2.57a}$$

$$\overline{\Psi}_{(i,r),s} \geq \Psi_{(i,r,o),s} \qquad \forall (i,r,o) \in \mathcal{T},\ \forall s \in \mathcal{S}_P \cup \mathcal{S}_G. \tag{2.57b}$$

Next, we implement constraints on $\Upsilon_{c,s}$ to delimit its value to the permissible range, using the difference between the nominal initial storage state of charge $\Psi_{i,\sigma(c+1),1,s}$ and the maximum and minimum states accessed:

$$\Upsilon_{c,s} + (\overline{\Psi}_{i,\sigma(c+1),s} - \Psi_{i,\sigma(c+1),1,s}) \leq d_s u_s m_{i,s} \qquad \forall c \in \mathcal{C},\ \forall s \in \mathcal{S}_P \cup \mathcal{S}_G, \tag{2.58a}$$

$$\Upsilon_{c,s} - (\Psi_{i,\sigma(c+1),1,s} - \underline{\Psi}_{i,\sigma(c+1),s}) \geq 0 \qquad \forall c \in \mathcal{C},\ \forall s \in \mathcal{S}_P \cup \mathcal{S}_G. \tag{2.58b}$$

In Eq. (2.58a), the cumulative, sequential state of charge, plus any deviation to the maximum nominal state of charge accessed across the following representative period (i.e., $\overline{\Psi}_{i,\sigma(c+1),s} - \Psi_{i,\sigma(c+1),1,s}$) must not exceed the installed storage energy capacity. Here, again, the total energy capacity is calculated by multiplying the storage duration d_s by unit size u_s and by the cumulative number of installed (and not retired) units i.e., $m_{i,s}$. Similarly, in Eq. (2.58b), $\Upsilon_{c,s}$, less the deviation to the minimum nominal state of charge accessed over the course of the following representative period (i.e., $\Psi_{i,\sigma(c+1),1,s} - \underline{\Psi}_{i,\sigma(c+1),s}$), must remain non-negative.

Finally, we apply periodicity constraints to ensure that the final cumulative, sequential state of charge $\Psi_{\|C\|,s}$ is greater than or equal to the initial energy in storage $\Delta_{i,\sigma(1),1,s}$. This constraint applies for each modeled investment year. This requirement is

$$\Upsilon_{\|\mathcal{C}\|,s} \geq \Psi_{i,\sigma(1),1,s} \qquad \forall (i,r,o) \in \mathcal{T},\ \forall s \in \mathcal{S}_P \cup \mathcal{S}_G. \tag{2.59}$$

2.3.7 Policy and economic constraints

In addition to constraints on energy network operations and design, which have been examined in various optimization formulations in previous studies, here we include constraints that reflect specific policies and regulations that may arise in future scenarios. Gas and electric utilities may be subjected to unique GHG accounting conventions and regulatory constraints. The relative scope, magnitude, and pace of these environmental targets may govern the least-cost investment strategy. In the proposed model formulation, constraints on GHG emissions are included separately for the electricity sector $\overline{\beta}_i^P$ and gas sector $\overline{\beta}_i^G$ on an emissions-intensity basis, in terms of net GHG emissions per unit of energy delivered [$\frac{tCO_2e}{\text{MWh}}$].

Electric power entities are liable for all emissions associated with generation of electricity, less any net-zero emissions gas that is procured by electricity sector entities. Gas sector entities are liable only for the emissions associated with combustion of natural gas distributed to serve direct-use gas demands.

This constraint set evaluates these criteria over entire investment periods, and is formulated as

$$\sum_{r\in\mathcal{R}}\sum_{o\in\mathcal{O}}\sum_{\omega\in\Omega} w_{(i,r)}\Gamma^P_{(i,r,o),\omega}\eta_\omega\beta_\omega - \beta^G\xi_i^P \leq \overline{\beta}_i^P \sum_{r\in\mathcal{R}}\sum_{o\in\mathcal{O}}\sum_{\omega\in\Omega} w_{(i,r)}\Gamma^P_{(i,r,o),\omega} + \varepsilon_i^P \qquad \forall i \in \mathcal{I}, \tag{2.60a}$$

$$\beta^G\left(\sum_{r\in\mathcal{R}}\sum_{o\in\mathcal{O}}\sum_{n\in\mathcal{N}_G} w_{(i,r)}\Phi^G_{(i,r,o),n} - \xi_i^G\right) \leq \overline{\beta}_i^G \sum_{r\in\mathcal{R}}\sum_{o\in\mathcal{O}}\sum_{n\in\mathcal{N}_G} w_{(i,r)}\Phi^G_{(i,r,o),n} + \varepsilon_i^G \qquad \forall i \in \mathcal{I}. \tag{2.60b}$$

Emissions from electricity generation are assessed using generator output $\Gamma^P_{(i,r,o),\omega}$ [MWh/hr], heat rate η_ω [MMBtu/MWh], and fuel emissions factor β_ω [kg CO_2e/MMBtu]. Nominal allocation of net-zero emissions gas production ξ_i^P [MWh/year] can be used to offset some of the emissions of gas use in generation at the emissions factor of natural gas β^G [kg CO_2e/MWh]. The emissions intensity for electricity is assessed with respect to total generation (including electricity used to produce electro-fuels such as electrolytic hydrogen or electro-methane) and must remain below the constraint for the investment time period $\overline{\beta}_i^P$ [kg CO_2e/MWh], plus any negative emissions offsets ε_i^P [kg CO_2e/year].

Gas sector entities are liable for the emissions associated with combustion of natural gas distributed to serve direct-use gas demands $\Phi^G_{(i,r,o),n}$ [MWh/hr], assessed at the emissions factor of natural gas β^G [kg CO_2e/MWh], less any gas sector net-zero emissions gas procurements ξ^G_i [MWh/year]. Any emissions from natural gas used for electricity generation are accounted for on the power sector constraint (Eq. (2.60a)). The emissions intensity of the delivered portfolio is assessed with respect to the core gas demands served and must not exceed the maximum allowable emissions intensity for each investment period $\overline{\beta}^G_i$ [kg CO_2e/MWh], plus any negative emissions offsets or atmospheric carbon removal ε^G_i [kg CO_2e/year].

As discussed above, slack variables are included to allow for violation of this constraint set at a fixed cost in the objective function for the power sector ε^P_i and the gas sector ε^G_i. This model feature can be used for a range of sensitivity testing and allows for emissions costing representative of either negative emissions technologies for atmospheric carbon removal, a social cost of carbon, or a prohibitively high value to allow model feasibility under scenarios where emissions constraints would make the problem infeasible. For simplicity of explanation, we will refer to these slack variables as use of negative emissions technologies for atmospheric carbon removal.

$$\varepsilon^P_i \geq 0, \qquad \varepsilon^G_i \geq 0 \qquad \forall i \in \mathcal{I} \tag{2.61a}$$

$$\varepsilon^P_i \leq \overline{\varepsilon}_i \sum_{r\in\mathcal{R}} \sum_{o\in\mathcal{O}} \sum_{\omega\in\Omega} w_{(i,r)} \Gamma^P_{(i,r,o),\omega} \eta_\omega \beta_\omega \qquad \forall i \in \mathcal{I} \tag{2.61b}$$

$$\varepsilon^G_i \leq \overline{\varepsilon}_i \beta^G \sum_{r\in\mathcal{R}} \sum_{o\in\mathcal{O}} \sum_{n\in\mathcal{N}_G} w_{(i,r)} \Phi^G_{(i,r,o),n} \qquad \forall i \in \mathcal{I} \tag{2.61c}$$

In Eq. (2.61), the use of negative emissions offsets in each sector is constrained by a maximum share $\overline{\varepsilon}_i$ [%] of gross emissions liabilities. For the electric power sector, this is equal to the gross sum of emissions from electricity generators. For the gas sector, this is equal to the total gas deliveries $\Phi^G_{(i,r,o),n}$ [MWh] by the emissions factor for natural gas β^G [kg CO_2/MWh].

To support the allocation of emissions liabilities across energy systems, total net-zero emissions fuel production must be nominally allocated to either gas or electricity sector entities to offset emissions liabilities resulting from gaseous fuel combustion. This is stipulated by the following constraints:

$$\xi^G_i \geq 0, \;\; \xi^P_i \geq 0 \qquad \forall i \in \mathcal{I}, \tag{2.62a}$$

$$\xi^G_i + \xi^P_i \leq \sum_{r\in\mathcal{R}} \sum_{o\in\mathcal{O}} \sum_{z\in\mathcal{Z}} w_{(i,r)} \Gamma^Z_{(i,r,o),z} \qquad \forall i \in \mathcal{I}, \tag{2.62b}$$

$$\xi^P_i \leq \sum_{r\in\mathcal{R}} \sum_{o\in\mathcal{O}} \sum_{\omega\in\Omega_G} w_{(i,r)} \Gamma^P_{(i,r,o),\omega} \eta_\omega \qquad \forall i \in \mathcal{I}, \tag{2.62c}$$

$$\xi^G_i \leq \sum_{r\in\mathcal{R}} \sum_{o\in\mathcal{O}} \sum_{n\in\mathcal{N}_G} w_{(i,r)} \Phi^G_{(i,r,o),n} \qquad \forall i \in \mathcal{I}. \tag{2.62d}$$

Eq. (2.62a) introduces two non-negative decision variables for nominal allocation of net-zero emissions fuel use to the electricity and the gas sectors, denoted by ξ_i^P and ξ_i^G, respectively. Eq. (2.62b) constrains the sum of allocations to remain below total net-zero emissions fuel production $\Gamma^Z_{(i,r,o),z}$. Eq. (2.62c) ensures electricity sector allocation ξ_i^P [MWh/year] does not exceed use in gas-fired generators $\Omega_G \subset \Omega$, and Eq. (2.62d) requires that gas sector allocation ξ_i^G [MWh/year] does not exceed the endogenously assessed gas demands served $\Phi^G_{(i,r,o),n}$ [MWh/year].

In addition to constraints on the rate of expansion included in Eq. (2.5), some bio-energy resources may experience economic limitations on annual supply because of competition with non-modeled end-uses such as liquid fuels for transportation. We include such constraints on biomethane facilities ($z \in \mathcal{Z}_b$) to limit total annual biomethane use to an assumed maximum availability $\overline{b}$ [MWh/year], using equation

$$\sum_{r\in\mathcal{R}}\sum_{o\in\mathcal{O}}\sum_{z\in\mathcal{Z}_b} w_{(i,r)}\Gamma^Z_{(i,r,o),z} \leq \overline{B} \qquad \forall i \in \mathcal{I}. \tag{2.63}$$

2.3.8 Objective function

The objective function to be minimized in multi-period system planning is equal to the sum of the fixed costs of investment, the fixed costs of incremental transmission and distribution infrastructure, and the variable costs of system operation.

Fixed investment costs

The fixed investment costs are computed by summing the annualized fixed costs for the integrated energy system, given by

$$C_i^{exp} = \sum_{x\in\mathcal{X}}\sum_{j\in[i]} \left(\kappa_x(C^{cap}_{j,x}\delta_{j,x} + C^b_{j,x})\{1|Y_i \leq Y_j + \tau_x\}\right) + C^{FOM}_{i,x} m_{i,x} \qquad \forall i \in \mathcal{I}. \tag{2.64}$$

This term includes the annualized capital costs of expanded units $C^{cap}_{j,x}$, the fixed operations and maintenance costs $C^{FOM}_{i,x}$. Note that the annualized capital cost of unit expansion are included in C_i^{exp} for all investment periods across the duration of the developed unit's expected lifetime τ_x [years].

Here, we include the customer costs of any building infrastructure upgrades required to accommodate the transition to electric appliances $C^b_{i,a}$ [$] (e.g., meter or electrical panel upgrades, re-wiring, or building envelope retrofits). These costs are incurred only upon the first installation of a new piece of equipment and not on replacement investment decisions. As such, this is a variable bound below by the number of new installs that do not represent replacement of incremental appliance-failures

occurring across from the previous investment year.

$$C^b_{i,a} \geq 0 \qquad \forall i \in \mathcal{I}, \forall a \in \mathcal{A}. \tag{2.65a}$$

$$C^b_{i,a} \geq c^b_{i,a} \left(\delta_{i,a} - \sum_{j \in [i-1]} (f_{i,a,j} - f_{i-1,a,j}) \delta_{j,a} \right) \qquad \forall i \in \mathcal{I}, \forall a \in \mathcal{A}. \tag{2.65b}$$

The new appliance sales $\delta_{i,a}$ are adjusted downward by the number of new sales that may represent like-for-like replacements based on the failures of previously installed appliances of this kind. We sum across all previous investment years and take the difference between the cumulative failure fraction in the current investment year $f_{i,a,j}$ and that of the preceding investment year $f_{i-1,a,j}$ and assume that this quantity of new appliance sales would not require the associated building infrastructure costs $c^b_{i,a}$ [\$/unit] having already incurred this cost in a previous modeled investment year.

Here, we also use a capital recovery factor κ_x [year^{-1}]. Capital recovery factors are calculated for each resource using the economic lifetime τ_x and a weighted average cost of capital ι^{WACC}:

$$\kappa_x = \frac{\iota^{WACC}(1+\iota^{WACC})^{\tau_x}}{(1+\iota^{WACC})^{\tau_x} - 1} \qquad \forall x \in \mathcal{X} \tag{2.66}$$

Fixed infrastructure costs

Planning and operational decisions may incur fixed transmission and distribution infrastructure costs. We compute the fixed infrastructure costs,

$$C^{inf}_i = C^{peak} \sum_{n \in \mathcal{N}_P} (\overline{\Phi}^P_{i,n} - \max_{(r,o)} \hat{\Phi}^P_{(i,r,o),n}) + \sum_{n \in \mathcal{N}_G} C^{dist}_n \qquad \forall i \in \mathcal{I}, \tag{2.67}$$

as the sum of fixed re-investment and maintenance costs for electricity and gas transmission and distribution systems. Here, we use an assumed cost of distribution infrastructure C^{peak} [\$/MW-yr] that scales with the peak electricity demand of the system. The peak hourly demand at the nodal level $\overline{\Phi}^P_{i,n}$ [MW] is the maximum of all modeled temporal demands $\Phi^P_{(i,r,o),n}$, and satisfies

$$\overline{\Phi}^P_{i,n} \geq \Phi^P_{(i,r,o),n} \qquad \forall (i,r,o) \in \mathcal{T}, n \in \mathcal{N}_P. \tag{2.68}$$

The cost of gas distribution system maintenance and operations C^{dist}_n [\$/yr] is also included for each node and scales with the number of residential or commercial customers served at that node.

In sensitivity scenarios where gas distribution retirement is permitted, we introduce a binary

variable for each distribution node to indicate whether this node is delivering gas to distribution-level customers:

$$\zeta_{i,n} \in \{0,1\} \qquad \forall i \in \mathcal{I},\ \forall n \in \mathcal{N}_G \tag{2.69a}$$

$$(1-\zeta_{i,n})M \geq \sum_{a \in \mathcal{A}_n} \varphi^G_{(r,o),a} m_{i,a} \qquad \forall i \in \mathcal{I},\ \forall n \in \mathcal{N}_G. \tag{2.69b}$$

This indicator variable $\zeta_{i,n}$ may take on a value of 1 if and only if the appliance-level gas demands at a node are equal to zero. Note that this does not include any baseline gas demands assumed to occur at the transmission-level. For this model functionality to reflect reality, all distribution-level gas demands must be modeled at the appliance-level.

In these cases, the gas distribution retirement variables $\zeta_{i,n}$ are also included in the calculation of fixed infrastructure costs:

$$C^{inf}_i = C^{peak} \sum_{n \in \mathcal{N}_P} (\overline{\Phi}^P_{i,n} - \max_{(r,o)} \hat{\Phi}^P_{(i,r,o),n}) + \sum_{n \in \mathcal{N}_G} (1-\zeta_{i,n}) C^{dist}_n \qquad \forall i \in \mathcal{I}. \tag{2.70}$$

We must note that the current formulation does not include any costs associated with decommissioning existing gas distribution infrastructure. However, future iterations of this work may incorporate this feature using the gas system shut-down indicator variable $\zeta_{i,n}$.

Operational costs

Eq. (2.71) assesses the annual variable costs C^{op}_i [$/year] for the set of simulated operations, using the representative weight of each representative time period, $w_{(i,r)}$. The cost of operation includes the costs of serving core gas demands $\Phi^G_{(i,r,o),n}$ with natural gas at commodity costs C^G_i [$/MWh], the fuel costs $C^{fuel}_{i,\omega}$ [$/MMBtu] of generation units and variable costs of operation $C^{VOM}_{i,x}$ [$/MWh] of generators and net-zero emissions fuel production units incurred across simulated operational time steps. Here, some of the assessed costs of commodity gas are offset by nominal allocation of net-zero emissions fuel production (i.e., $\xi^P_i + \xi^G_i$). Finally, we also include the cost of negative emissions to offset CO_2 emissions exceeding the sector-specific constraint assessed at a penalty of $C^{CO_2}_i$ [$/kg CO_2]. The resulting expression is

$$\begin{aligned} C^{op}_i = &\sum_{r \in \mathcal{R}} \sum_{o \in \mathcal{O}} w_{(i,r)} \sum_{n \in \mathcal{N}_G} C^G_i \Phi^G_{(i,r,o),n} + \sum_{z \in \mathcal{Z}} C^{VOM}_{i,z} \Gamma^Z_{(i,r,o),z} \\ &\ldots + \sum_{\omega \in \Omega} (C^{fuel}_{i,\omega} \eta_\omega + C^{VOM}_{i,\omega}) \Gamma^P_{(i,r,o),\omega} - C^G_i(\xi^P_i + \xi^G_i) + C^{CO_2}_i(\varepsilon^G_i + \varepsilon^P_i) \qquad \forall i \in \mathcal{I}. \end{aligned} \tag{2.71}$$

Present value discounting

When evaluating the objective function over investment periods that span multiple decades, we apply a discounting factor d that represents the societal value of delaying costs. In other words, this can be thought of as the risk-less rate of return available to capital at the societal level, ι^{soc}. The discount factor for each investment period is given by:

$$\vartheta_i = \sum_{j \in [Y_{i+1} - Y_i]} \frac{1}{(1+\iota^{soc})^{\left(Y_i + j - \tilde{Y}\right)}} \qquad \forall i \in \mathcal{I}. \tag{2.72}$$

Here, we assume that each simulated investment period is representative of the annual costs of each calendar year until the following investment period simulation.

2.3.9 Model outputs

Model outputs allow for comparison across sensitivity scenarios and regional case studies to explore features of least-cost transitions in integrated gas-electric energy systems. Outputs of the proposed model include the investment and operational decision variables, total system costs, and the average costs of energy.

Investment and operational decisions

Capacity investment decisions are the primary model output, providing insight into the least-cost mix of energy supply and demand units to satisfy an emissions constraint trajectory. These investment decisions include the timing and location of infrastructure expansion and retirement decisions for electricity generators, net-zero emissions gas production units, energy storage technologies, and consumer appliances.

Optimal system operations decisions also lend insight regarding the implications of a cost-effective transition to deeply decarbonized systems. Total annual electricity generation by fuel type and generation curtailment values are identified across the modeled time horizon. In addition, the model outputs the composition of gaseous fuel resources used to serve core gas demands or to fuel gas-fired electricity generators. The share of net-zero emissions gas that is directed for nominal consumption in the gas sector and the electricity sector to satisfy sector-specific emissions constraints.

In addition to annual metrics, operational patterns may be visualized for electricity grid dispatch during specific days or weeks of operation. Of particular interest are the weeks of the year with peak total electricity demand and peak net electricity demand (after subtracting available renewable energy generation) as these periods stress the system. In the integrated gas-electric system operations, we also observe particular times when remaining core gas demands are largest as these may offer directional insight regarding appliance electrification decisions.

Total system costs

Total system costs can be accessed on an annualized basis for each modeled investment year, by technology or location using the unit-specific expansion, retirement, and operations decisions. Annual total system costs can be partitioned by sector-specific components including electricity generation, storage, transmission & distribution, net-zero emissions gas production, gas transmission & distribution infrastructure, and customer appliance investments.

The electric power sector costs are partitioned across generation capacity costs $C_i^{gen.,P}$, fuel costs $C_i^{fuel,P}$, costs of electrical storage $C_i^{stor.,P}$, and transmission and distribution infrastructure $C_i^{T\&D.,P}$ as presented in Eq. (2.73).

$$C_i^{gen.,P} = \sum_{j\in[i]} \sum_{x\in\Omega} \kappa_x C_{j,x}^{cap} \delta_{j,x} \{1|Y_i \leq Y_j + \tau_x\} + C_{i,x}^{FOM} m_{i,x} \qquad \forall i \in \mathcal{I} \qquad (2.73a)$$

$$C_i^{fuel,P} = \sum_{r\in\mathcal{R}} \sum_{o\in\mathcal{O}} w_{(i,r)} \sum_{\omega\in\Omega} (C_{i,\omega}^{fuel} \eta_\omega + C_{i,\omega}^{VOM}) \Gamma_{(i,r,o),\omega}^{P} - C_i^G \xi_i^P \qquad \forall i \in \mathcal{I} \qquad (2.73b)$$

$$C_i^{stor.,P} = \sum_{j\in[i]} \sum_{x\in\mathcal{S}_P} \kappa_x C_{j,x}^{cap} \delta_{j,x} \{1|Y_i \leq Y_j + \tau_x\} + C_{i,x}^{FOM} m_{i,x} \qquad \forall i \in \mathcal{I} \qquad (2.73c)$$

$$C_i^{T\&D.,P} = C^{peak} \sum_{n\in\mathcal{N}_P} (\overline{\Phi}_{i,n}^{P} - \max_{(r,o)} \hat{\Phi}_{(i,r,o),n}^{P}) \qquad \forall i \in \mathcal{I}. \qquad (2.73d)$$

The gas sector costs are partitioned across the costs of net-zero gas generation units $C_i^{gen.,G}$, commodity fuel costs of natural gas for core demands $C_i^{fuel,G}$, investment and operating costs of gas storage units $C_i^{stor,G}$, and transmission and distribution infrastructure $C_i^{T\&D.,G}$. These computations are presented in Eq. (2.74).

$$\begin{aligned} C_i^{gen.,G} &= \sum_{z\in\mathcal{Z}} \sum_{j\in[i]} \kappa_z C_{j,z}^{cap} \delta_{j,z} \{1|Y_i \leq Y_j + \tau_x\} + C_{i,z}^{FOM} m_{i,z} \\ &\quad \ldots + \sum_{r\in\mathcal{R}} \sum_{o\in\mathcal{O}} w_{(i,r)} \sum_{z\in\mathcal{Z}} C_{i,z}^{VOM} \Gamma_{(i,r,o),z}^{Z} \qquad \forall i \in \mathcal{I} \qquad (2.74a) \end{aligned}$$

$$C_i^{fuel,G} = \sum_{r\in\mathcal{R}} \sum_{o\in\mathcal{O}} \sum_{n\in\mathcal{N}_G} w_{(i,r)} C_i^G \Phi_{(i,r,o),n}^{G} - C_i^G \xi_i^G \qquad \forall i \in \mathcal{I} \qquad (2.74b)$$

$$C_i^{stor,G} = \sum_{j\in[i]} \sum_{x\in\mathcal{S}_G} \kappa_x C_{j,x}^{cap} \delta_{j,x} \{1|Y_i \leq Y_j + \tau_x\} + C_{i,x}^{FOM} m_{i,x} \qquad \forall i \in \mathcal{I} \qquad (2.74c)$$

$$C_i^{T\&D.,G} = \sum_{n\in\mathcal{N}_G} (1 - \zeta_{i,n}) C_n^{dist} \qquad \forall i \in \mathcal{I}. \qquad (2.74d)$$

The costs of customer appliance investments are calculated in a similar manner, summing capital investment in appliances:

$$C_i^{apps} = \sum_{j\in[i]} \sum_{x\in\mathcal{A}} \kappa_x (C_{j,x}^{cap} \delta_{j,x} + C_{j,x}^{b}) \{1|Y_i \leq Y_j + \tau_x\} \qquad \forall i \in \mathcal{I}. \qquad (2.75)$$

Lastly, we include the cost of any GHG emissions that exceed the permitted emissions intensity for gas and electric power entities C_i^{NETs} assessed at a cost representing the cost of negative emissions offsets for carbon removal or the social cost of carbon.

$$C_i^{NETs} = C_i^{CO_2}(\varepsilon_i^G + \varepsilon_i^P) \qquad \forall i \in \mathcal{I} \tag{2.76}$$

Note that these are coarse representations of system costs and do not account for the interactive effects to avoid double-counting any costs. For example, the fuel costs of generators do not include the cost of net-zero emissions gas as these are included in a separate tranche of system costs.

Average costs of energy

The model also computes the average cost of delivered energy for both the gas and electric sectors. This metric offers a first-order estimate of how volumetric energy rates may evolve across the modeled investment horizon. However, this computation requires assumptions regarding the share of cross-sector investments (i.e., net-zero emissions fuels) that may be borne by ratepayers of each energy system. In this work, investment and operating costs of net-zero emissions fuel production units are amortized across total production of net-zero emissions gas. Any electricity consumption to generate electro-fuels is assessed at the average cost of delivered electricity. This average cost of net-zero emissions gas is allocated proportionately to the gas and electricity revenue requirements according to the nominal share of net-zero emissions gas production assigned to each entity in the computation of sector-specific emissions liabilities.

For simplicity of exposition, we introduce quantities for total annual generation of electrical power $\mathbf{\Gamma}_i^P$ [MWh/year], deliveries of gas $\mathbf{\Phi}_i^G$ [MWh/year], production of net-zero emissions gas $\mathbf{\Gamma}_i^Z$ [MWh/year] and consumption of electric power for production of electro-fuels $\mathbf{\Phi}_i^Z$ [MWh/year]:

$$\mathbf{\Gamma}_i^P = \sum_{r\in\mathcal{R}}\sum_{o\in\mathcal{O}}\sum_{\omega\in\Omega} w_{(i,r)}\Gamma^P_{(i,r,o),\omega} \qquad \forall i \in \mathcal{I} \tag{2.77a}$$

$$\mathbf{\Phi}_i^G = \sum_{r\in\mathcal{R}}\sum_{o\in\mathcal{O}}\sum_{n\in\mathcal{N}_G} w_{(i,r)}\Phi^G_{(i,r,o),n} \qquad \forall i \in \mathcal{I} \tag{2.77b}$$

$$\mathbf{\Gamma}_i^Z = \sum_{z\in\mathcal{Z}}\sum_{r\in\mathcal{R}}\sum_{o\in\mathcal{O}} w_{(i,r)}\Gamma^Z_{(i,r,o),z} \qquad \forall i \in \mathcal{I} \tag{2.77c}$$

$$\mathbf{\Phi}_i^Z = \sum_{r\in\mathcal{R}}\sum_{o\in\mathcal{O}}\sum_{z\in\mathcal{Z}} w_{(i,r)}\Phi^Z_{(i,r,o),z} \qquad \forall i \in \mathcal{I} \tag{2.77d}$$

Using the total societal cost terms defined in Eq. (2.73) - (2.74), we define the average costs of delivered electric power μ_i^P [$/MWh] and gas μ_i^G [$/MWh] as a function of the average cost of

net-zero emissions gas production μ_i^Z [$/MWh].

$$\mu_i^P = \frac{C_i^{gen,P} + C_i^{fuel,P} + C_i^{stor,P} + C_i^{T\&D,P} + C_i^{CO_2}\varepsilon_i^P + \xi_i^P(\mu_i^Z - C_i^G)}{\mathbf{\Gamma}_i^P} \qquad \forall i \in \mathcal{I} \quad (2.78a)$$

$$\mu_i^Z = \frac{C_i^{gen,G} + \mathbf{\Phi}_i^Z \mu_i^P}{\mathbf{\Gamma}_i^Z} \qquad \forall i \in \mathcal{I} \quad (2.78b)$$

$$\mu_i^G = \frac{C_i^{fuel,G} + C_i^{stor,G} + C_i^{T\&D,G} + C_i^{CO_2}\varepsilon_i^G + \xi_i^G(\mu_i^Z - C_i^G)}{\mathbf{\Phi}_i^G} \qquad \forall i \in \mathcal{I} \quad (2.78c)$$

The average cost of electric power μ_i^P is estimated in Eq. (2.78a) to be the sum of variable operating costs $C_i^{fuel,P}$, negative emissions offsets $C_i^{CO_2}\varepsilon_i^P$, and the incremental cost of net-zero emissions gas purchases ξ_i^P, assessed at the average cost of net-zero emissions gas production μ_i^Z, relative to the cost of commodity gas C_i^G already included in $C_i^{fuel,P}$. These costs are then levelized across total electricity generation $\mathbf{\Gamma}_i^P$.

The cost of net-zero emissions gas μ_i^Z is then cast in Eq. (2.78b) as a function of electric power costs μ_i^P. The cost of net-zero emissions gas is equal to the sum of capital investments and operating costs of net-zero emissions production $C^{gen,G}$ and the costs of all electric power inputs $\mathbf{\Phi}_i^Z$ (as assessed at the average cost of electricity). These costs are levelized across the total production of net-zero emissions gas $\mathbf{\Gamma}_i^Z$.

The average costs of gas delivered μ_i^G can be straightforwardly computed in Eq. (2.78c) using the fuel costs of commodity natural gas to serve core demands $C_i^{fuel,G}$, the costs of gas storage $C_i^{stor,G}$, the costs of distribution infrastructure $C_i^{T\&D,G}$ and the costs of negative emissions offsets for the gas sector $C_i^{CO_2}\varepsilon_i^G$. In addition, the gas sector purchases of net-zero emissions gas ξ_i^G are assessed at the incremental cost of net-zero emissions gas μ_i^Z relative to commodity gas costs C_i^G. These costs are levelized for recovery across all core gas demands served $\mathbf{\Phi}_i^G$.

The term in Eq. (2.78b) is substituted in Eq. (2.78a) to compute the value of μ_i^P in closed form. Subsequently, the average cost of net-zero emissions gas μ_i^Z can be computed using Eq. (2.78b) and the value of μ_i^P. Finally, the average cost of gas delivered μ_i^G can be computed using Eq. (2.78c) and the value of μ_i^Z.

The above equations are solved ex-post after system optimization to assess how average costs of delivered energy could evolve across the transition. An alternative approach where net-zero emissions gas production units are exposed to the wholesale cost of electricity (estimated as the variable cost of generation) rather than the average cost of delivered electricity is presented in Appendix Section A.5.

Note that while all costs are included in the societal cost objective function (and the total system cost model outputs presented in Section 2.3.9), appliance costs are excluded from the average cost of energy calculations outlined in Eq. (2.78). The cost of appliances and associated building retro-fits are borne directly by the customer and not included in the revenue requirement for an energy utility.

However, future work may also account for utility subsidies for appliance investments or the required building upgrades in the computation of average rates.

These results are key to interpreting the economic implications and feasibility of the identified least-cost transition pathways. The optimal transition trajectory may include a small amount of gas consumption spread across customers with particular system costs associated with their transition to electricity. However, the distribution of such costs across ratepayers will determine the stability of this solution. A welfare-maximizing actor may electrify their gas demands, regardless of the associated system costs incurred by electricity providers, especially if tariff designs do not adequately pass marginal system cost impacts onto consumers.

2.4 Data & assumptions

To solve the above optimization program for realistic case studies, a range of input data and assumptions are required. Section 2.4.1 describes data and assumptions for any existing or candidate energy demands. Section 2.4.2 presents all data inputs for existing and candidate supplies of gaseous and electrical energy. Section 2.4.3 describes the required data and assumptions to specify a gaseous or electrical energy storage unit. In Section 2.4.4, we discuss the data required to fully specify the gas and electricity network configurations and the associated infrastructure costs. Section 2.4.5 describes the assumptions required for policy constraints. In Section 2.4.6 we discuss the assumed parameters for discounting costs to present value in the model.

2.4.1 Energy demand

Hourly demands for gas and electricity are modeled at each node in the system. The total energy demanded at each location and each time point includes a set of modeled appliance-level demands and a baseline of immutable energy demands.

Baseline energy demands

Each baseline nodal energy demand for gas or electricity will have associated attributes including a peak hourly demand [MW], total annual energy demand [MWh/year] (also expressed as average energy demand [MW_a]), and a temporal profile.

For electricity demands, plausible shapes and quantities can be generated using historical data from grid operators [90, 91] or from bottom-up simulations of electricity demands [92, 93]. In this work, we use state-level electricity demand simulations generated by NREL's Electrification Futures Study (EFS) [93]. NREL's EFS employs the Demand Side Grid Model (dsgrid) to complete detailed bottom-up simulations of electricity demand under different appliance adoption scenarios for transitioning gas demands to the electricity system. Reference scenario simulations for the base year 2018 are used to represent the shape of current electricity demands in various geographies and climate zones across the United States.

For indicative case study simulations, it may be useful to normalize electricity demands of the template system to allow for generalized comparison across regions. Baseline energy demand profiles may be normalized to the maximum hourly electricity demand or to the average hourly electricity demand such that the hour-to-hour shape of electricity demand can be retained and applied to various case study systems that range in size.

Empirical data on hourly gas consumption is often not recorded or made public. Baseline profiles for gas demand could be constructed from bottom-up aggregation of simulated equipment-level demands [92]. Alternatively, baseline gas demands can be modeled as constant demands, representative of gas consumption at large commercial or industrial facilities with high capacity utilization

factors.

Appliance energy demands

Appliance-level energy demands are modeled for a subset of gas and electricity final energy demands. Each modeled appliance requires an assumed hourly gas and electricity consumption profile [MWh/hour], capital cost [$], and costs of any necessary building upgrades associated with the installation of the appliance [$]. For specific case studies, these appliance populations will also be specified by their total initial values [no. units], historical sales growth rates [%/year], and location at a gas node and an electric node. The realistic appliance population in a modeled region will be incredibly diverse. For the purposes of model demonstration, we abstract appliances to indicative templates. Legacy end-use appliances modeled in this work include residential and commercial gas furnaces, gas water heaters, and gas cooking. Candidate appliances include air-source heat pumps for space heating, heat pump water heaters, and electric cooking alternatives.

To generate plausible assumptions for hourly appliance energy demand, we first estimate the energy required to satisfy the demand for the provided end-use energy service on an annual basis. Second, these annual energy demands are down-scaled to hourly values that capture temporal trends in demand for energy services as well as potential temporal variations in appliance efficiency as a function of ambient temperature.

In order to ensure consistency across substitutable gas and electric appliances, we benchmark the annual demand for energy services using the EIA's Residential Energy Consumption Survey (RECS) and Commercial Building Energy Consumption Survey (CBECS) data for gas demand. For residential appliances, average site energy consumption by census region and division (Table CE5.4 [94]) is used to estimate average annual gas consumption for the listed energy end-uses (space heating, water heating, and cooking). For commercial appliances, we use natural gas energy intensity by end-use [MMBtu/ft^2] (Table E7 [95]) paired with an assumed median building floor area [ft^2] (Table B2 [95]). Next, using an assumed average seasonal efficiency of the gas-fired equipment serving each end-use, we estimate the annual demand for energy services. Finally, an average seasonal efficiency assumption for the substitute electric equipment is applied to this demand for energy services to estimate the corresponding annual demand for each modeled electric appliance that may displace a gas-fired unit.

For space heating, gas furnace efficiency will vary depending on the vintage and technology of the appliance. Gas furnace efficiency can range from 62% to over 90% in the most efficient condensing furnace technologies [96]. Electric heat pumps can allow for energy efficiencies in excess of 100% as they use electricity to move heat rather than generate heat. However, heat pump efficiency will gradually decline as the difference between source and sink temperature increases. During extreme cold, heat pump technologies may rely on back-up electric resistance elements. Reasonable assumptions for seasonal average heat pump coefficient of performance can range from 2.25 to

Technology	Energy Service	Unit size [various]	Life time τ_a [years]	Annual energy consumption [MWh / year]	Energy efficiency [MWh service / MWh fuel]
Template Residential Appliances					
Gas furnace	Residential Space Heating	4 ton	18 - 20	7.7 - 19	0.62 - 0.90
Gas water heater	Residential Water Heating	50 gal.	13 - 18	4.4 - 6.5	0.60 - 0.96
Gas cooking	Residential Cooking	4 9,500 BTU-burner	19	0.73 - 0.94	0.25
Air-source electric heat pump	Residential Space Heating	4 ton	19 - 25	0.95 - 9.8	1.75 - 5
Electric heat pump water heater	Residential Water Heating	50 gal.	15	1.5 - 3.5	1.8 - 3
Electric induction cooking	Residential Cooking	4 5kW-burner	19	0.37 - 0.47	0.50
Template Commercial Appliances					
Gas furnace	Commercial Space Heating	10 ton	16	25 - 60	0.62 - 0.90
Gas water heater	Commercial Water Heating	199 kBTU/ hour	13	9.8 - 20	0.60 - 0.96
Gas cooking	Commercial Cooking	24 9,500 BTU-burner	12	14 - 35	0.25
Air-source electric heat pump	Commercial Space Heating	10 ton	16	3.1 - 31	1.75 - 5
Electric heat pump water heater	Commercial Water Heating	74 kBTU/ hour	17	2.0 - 11	1.8 - 3
Electric induction cooking	Commercial Cooking	24 5 kW-burner	19	7 - 18	0.50

Table 2.1: Operating characteristics for modeled template appliances.

3.5 [97], however these are highly sensitive to ambient climate. RMI (formerly Rocky Mountain Institute) completed building energy simulations for representative locations in all 48 contiguous states in order to evaluate the emissions impacts of electrifying space heating. The "heating season-weighted" coefficients of performance range from 2.06 (in Fargo, ND) to 4.06 (in Los Angeles, CA) depending on the regional climate [98]. Hybrid gas-heat pump furnaces are commercially available and often selected in cold-climates over full-electrification for their resilience to extreme cold weather.

Gas-fired water heater efficiencies can range similarly from 60% to 96% depending on whether they are storage or tank-less (instantaneous) gas water heaters and whether they extract the latent heat of condensation from gas combustion products. Electric resistance water heaters will have a thermal conversion efficiency of close to 100% with losses only associated with storage tanks [97]. Tankless water heaters can reduce thermal losses, and improve efficiency. However, tankless electric water heaters require much larger power draws on the order of 13-36 kW depending on the rate of hot water demand (2.54 - 7.03 gallons per minute, respectively). Heat pump water heaters can have coefficients of performance exceeding 3 [97] however field studies find more realistic COPs ranging from 1.8 - 2.3, depending on the degree of reliance on electric resistance elements [99]. Also, heat pump water heaters draw heat from their ambient environment and can lower the surrounding temperature considerably (especially in confined spaces), potentially increasing the demand for space heating. These interactive effects have been modeled in building energy simulation tools [100], but are omitted for simplicity in the proposed modeling framework. The interactive effects between water heating and space heating are considered to be negligible for the system-scale planning study proposed here. Incorporating this feature would require building-level tracking of appliance populations, in order to apply different energy demand profiles for air source heat pumps that exist in buildings with heat pump water heaters. For a more thorough review of the efficiency characteristics and considerations for modeling heat pump water heaters see [101]. Hybrid gas-fired heat pump water heaters have been developed [102], analyzed [103] and demonstrated in recent field studies [104], however these technologies are not widely available and are omitted from the current study.

For cooking energy demands, electric induction is often cited as the most efficient cooking technology. Induction cook tops have fewer losses as they heat the cooking implement directly rather than via conductive heat transfer. As such, induction cooking can transfer up to 90% of the electricity consumed to the cooked items, while traditional electric and gas cooking systems are referenced at 74% and 40% efficient, respectively [105, 106]. Experimental results for gas stove efficiencies confirm this value, ranging between 32 - 47% [107]. Electric ovens have cooking efficiencies of 12-14%, compared to a gas oven efficiency of 6-7% [106, 108]. Cooking energy efficiency values will vary depending on ambient conditions, sizing of cookware, and user cooking behavior. For simplicity, we assume that half of the cooking energy is consumed in stoves and half in ovens and that both will be powered by the same fuel. We use default values of 51% for electric cooking and 25% for gas

cooking appliances.

Next, annual energy demands are down-scaled to hourly values. Several sources are used to generate plausible values for appliance energy demand normalized to annual consumption. This work employs template building energy simulations conducted with EnergyPlus or Building Energy Optimizer (BEOpt) [109]. Simulations are available for a set of template residential and commercial buildings [109]. A recent study used linear regression analysis and empirical heat pump efficiency correlations to estimate hourly gas demands by census district [92]. Gas-fired appliances are assumed to operate with similar temporal efficiency characteristics as resistance electric appliances. While some gas appliances will operate less efficiently or with greater losses during different weather conditions, in general, these effects are assumed to be small relative to the annual energy efficiency differences [97]. However, the impact of ambient conditions on heat pump efficiency is expected to be larger and non-negligble as use of resistance back-up may trigger large peaks in electricity demand during cold weather. As such, we use the modeling efforts of [92] to generate plausible profiles for electric heat pump energy consumption for space heating by state.

NREL's EFS [93] also produces hourly electricity demand simulations at the state-level using the dsGRID modeling tool. Electricity demand data is provided for several end-use services such as water heating, space heating and cooling, and clothes drying/dish washing under a range of technology adoption scenarios across a transition away from direct-gas use. However, the available electricity demand profiles aggregate several different technologies providing the same service. And key gaseous energy demands, such as cooking, are combined with a wide range of energy services in the "Other" category. Note also that the EFS data combines space heating and cooling electricity demands. To model the transition of space heating demands currently served by gas furnaces, these profiles must be normalized to heating demand only. Here, we use a proxy to indicate whether an hourly energy demand is providing heating or cooling services. Future work may explore opportunities to leverage these efforts to generate representative consumption profiles for appliances of various technology types and in various geographic climate zones.

Default appliance sizing, cost, and lifetime assumptions are based on the academic literature [110, 96], Building Energy Optimization (BEopt) data [111], commercially available technologies [112, 113, 114, 115, 116], and NREL EFS data [97, 117]. Installed cost assumptions for each template appliance candidate are presented in Appendix Section A.2.

Some electric appliances may require substantial building envelope retrofits, electrical panel upgrades, or other rewiring of building electrical infrastructure. These costs can exceed the upfront capital cost of the appliance alone and present substantial barriers to adoption. Such building infrastructure upgrade costs are highly uncertain and case-specific, and often depend on the age of the building. Parametric scenarios can be used to test sensitivity of results to the upgrade cost assumptions for each appliance type. Upgrading a home electrical panel to handle 200 amps can cost up to $4,000 [118]. Alternatively, new 50 amp sub-panels could be installed for $500, but may

require rewiring which can cost over$1,400 in labor and materials. Heat pump water heaters must be installed in areas that remain between 40 °F to 90 °F and are surrounded by at least 1,000 cubic feet of air [119]. As such, renovations to existing closet spaces may be required to accommodate these appliances. Finally, building envelope retrofits may be necessary to fix a leaky home or building before switching to an electric heat pump for space heating. These efficiency retrofits can range in cost from $11 to $34 per square foot [120].

To further complicate things, in some cases it can be challenging to allocate infrastructure upgrade costs to a single appliance as it may be the combination of several modeled (i.e., heat pump water heaters) or non-modeled (i.e., electric vehicle adoption) investments that trigger the need for rewiring or panel upgrades. It is similarly challenging to account for the increased property value and the myriad of health and quality of life benefits that may accompany such building energy efficiency improvements. Given these uncertainties, we provide the modeler the maximal amount of flexibility to parametrically specify the cost of building infrastructure upgrades that accompany appliance investment decisions.

For the purposes of model demonstration, we abstract appliances to indicative templates with annual consumption informed by the RECs and CBECs surveys [95, 94] and hourly consumption profiles based on a set of template building energy consumption simulations for a typical meteorological year [109]. However, the proposed modeling framework is extensible to inclusion of highly-detailed appliance population breakdowns if these data are available. Additional sources for more detailed building and/or appliance stock information could include the American Community Survey [121], the County Business Patterns data [122], and the Federal Energy Management Agency's Hazus General Building Stock [123] (as used in [92] and described in [124]). In addition, future work should aim to incorporate correlations that exist between modeled appliance demands, the assumed baseline energy demands, and the availability of renewable energy resources. Recent research efforts in this regard have developed approaches using the NREL's ResStock tool to conduct detailed building-level simulation of appliance populations and their potential grid impacts [125]. Future efforts in gas-electric system planning should move towards use of such statistically-representative tools to generate a set of appliance consumption profiles for residential and commercial appliances (using ResStock and ComStock, respectively).

Finally, there is a large set of equipment and appliances that fall outside of the scope of the natural gas and electric power sectors that may also be transitioned to the electric system. In some regions, fuel oil and liquified petroleum gas providers currently satisfy the heat demands of many customers. Adoption of electric vehicles across the transportation sector is also a crucial strategy for achieving cost-effective, decarbonized economies. Suppliers of liquid fuels are not typically subject to the same regulatory oversight as natural gas and electric utilities. As such, these investment decisions, operational characteristics, and emissions consequences are not included in the presented optimization program. However, the transition of these final energy demands to the electricity system

may alter the least-cost strategy found for the natural gas and electric sectors, when modeled in isolation. In future work, the novel quantitative approach presented here for endogenous evaluation of equipment failure and replacement alongside centrally-planned system design and operations decisions may accommodate the inclusion of other sectors such as liquid fuels providers.

2.4.2 Energy supply

Candidate and existing energy supply units are modeled for the electricity system and the gas system. Here, we describe the operating characteristics for each of these sets of modeled energy supplies and the associated cost assumptions.

Electrical energy supply

Energy supply units in the electricity system can include conventional thermal generators, such as nuclear-fueled plants, coal-fired plants, gas-fired combustion turbines or combined-cycle gas-fired generators. Every generation unit will be specified by a nodal location on the electricity system, a nodal location on the gas network, and the set of operating characteristics included in Table 2.2. Here, we present technology-average default values for each parameter and modeled generator type, however the modeling framework is flexible to include additional technology-classes or unit-level specification of generators and their attributes.

Representative unit sizes for generation plants are referenced from [15] with solar and wind plants modeled as continuous. When integer unit-commitment variables (see Eq. (2.22)) are relaxed, these unit sizes do not play a role in meaningfully constraining dispatch operations. Operating lifetime assumptions are referenced from [15], however empirical values can be estimated by using EIA Form 860 data in future work [126]. Plausible unit ramp rates, stable power output bounds, and minimum up/down-times are referenced from [15]. Heat rate assumptions for new generators are referenced from NREL's ATB [127]. Default average heat rates for legacy generating fleets are referenced from the EIA Electric Power Annual with data for 2019 [128]. Unit-specific average heat rates can be estimated from empirical data available in EIA Form 923 [129]. While unit heat rate will vary in time and across seasons as a function of operational patterns and ambient temperatures, for simplicity we use constant average heat rates applied to all generation output to assess fuel consumption and emissions factors. Fuel emissions factors are referenced from the Environmental Protection Agency's Greenhouse Gas Inventory assumptions [130] with an assumed carbon capture efficiency of 90% [15]. If more granular heat rate and emissions factor data are desired, the EPA's Air Markets Program Database (AMPD) provides hourly data at the unit-level for gross generation output, fuel consumption, and CO_2 emissions [131].

Additional generator characteristics specified for a given case study include the number of existing legacy generators of that class and their associated installation year, to evaluate natural retirement. Each generator can have an assumed maximum total expansion across the modeled investment

Electricity generators							
Resource	Unit size u_ω [MW]	Life time τ_ω [years]	Max./Min. power output [p.u.]	Max. hourly ramp rate [p.u./hour]	Min. up/down time [hours]	Heat rate for new / legacy units η_ω [MMBtu / MWh]	Fuel emissions factor β_ω [tCO_2 / MMBtu]
Natural gas combustion turbine (CT)	50	55	0.1/1	1	1/1	9.51/ 11.10	53.1
Natural gas-fired combined cycle (CC)	100	55	0.3/1	0.7	2/1	6.40/ 7.63	53.1
Coal	200	75	0.5/1	0.3	24/12	10.3/ 10.00	97.7
Nuclear	500	60	0.5/1	0.25	36/36	10.46/ 10.44	0
Solar PV	1	30	0/1	1	1/1	0/0	0
Wind	1	30	0/1	1	1/1	0/0	0
NGCC+CCS	500	55	0.4/1	0.6	4/3	7.53/ n.a.	5.31

Table 2.2: Assumed design and operating characteristics for electricity generators.

time horizon [no. units] and a maximum rate of expansion [no. units/year]. These will vary by geography and are often excluded in high-level planning studies to first identify the least-cost resource mix absent such limits. However, these optional attributes can be used to characterize land-use constraints or local opposition to generation expansion.

All generators also have specified parametric assumptions for minimum and maximum temporal availability $\underline{\gamma}, \overline{\gamma}$ [on a per unit basis]. The minimum generation $\underline{\gamma}$ will equal 0 in all time steps for all generating units that are not associated with a so-called "must-run" commitment. Such units could include combined heat and power plants that must burn fuel to satisfy on-site heat demands. The maximum temporal generation $\overline{\gamma}$ will be equal to 1 in all time steps for all generating units that are not associated with weather-dependent or seasonal production limitations. Most commonly, this will be applied to solar and wind generators that rely on the instantaneous availability of energy from the ambient weather conditions. However, some coal-fired generating stations have associated seasonal generation constraints due to air quality regulations [23]. For fuel-secure, fully-dispatchable units, the maximum per unit availability will be equal to 1 and the minimum per unit availability will be equal to 0 in all time steps.

Temporal availability of electricity production from variable renewable energy generators is specified using either historical generation data for the region of interest or simulated production data for specific locations. Historical data is available for total hourly generation by fuel-type from EIA's Form 930 Operating System Dashboard [90] (from July 2015 - present) and, in some cases, grid operator websites [132, 133]. Some entities also publish simulated production data across many historical weather-years for use in probabilistic generation resource adequacy studies [134, 135].

To produce hourly capacity availability factors for each variable renewable resource, we divide total generation in each hour by the amount of generation capacity installed at the time. Installed capacity values for each historical month are estimated using EIA Form 860 data and can be aggregated to the state-, balancing authority-, or regional-level as needed [126]. This approach abstracts away some spatial resource heterogeneity to produce a class-average, regional renewable energy profile that is often sufficient for planning studies.

Where low-quality data exist for installed capacity or hourly generation, increasing the regional scope can produce a plausible result that is less sensitive to missing or erroneous data points. If no high-quality empirical data exist for a desired region from any of the above sources, NREL's System Advisory Model (SAM) [136] allows for granular simulation of hourly and sub-hourly production profiles for specific locations, as specified by a latitude and longitude.

All capital, operating, and fuel cost assumptions for electricity generators are referenced from the NREL's ATB [127]. NREL's ATB synthesizes the best available data in the literature from government, professional, and academic sources to conduct bottom-up cost modeling for each generation technology.

Net-zero emissions gas production				
Technology	Unit size u_z [MW]	Life time τ_z [years]	Hydrogen energy fraction (LHV basis) [%]	Conversion efficiency η_z [MWh gas / MWh elec.]
Biomethane	1	40	0	n.a.
Electrolytic hydrogen	5	20	100	0.65
Electro-methane	5	20	0	0.45

Table 2.3: Operating characteristics for power-to-gas units.

Gaseous energy supply

Energy supplies for the natural gas system include fossil natural gas supplies at the system boundary or locally available at specific gas nodes and endogenously modeled production of net-zero emissions fuels such as biomethane, hydrogen, or electro-methane.

Supply of natural gas are assumed to be available from outside of the region at the designated "slack" node. Local supplies of fossil natural gas can also be included by modifying the maximum supply rate available at a given node $\hat{S}$. Commodity costs of natural gas are estimated based on NREL's ATB [127]. For this work, we use annual average values in order that the same commodity cost of natural gas can be assigned to all operations for a given investment year. The cost of gas will fluctuate seasonally, however the impact of these variations on the least-cost system design decisions across a multi-decade planning horizon remains an area of future work. As legacy supply chains for energy are reshaped by the transition to net-zero emissions energy systems, observed seasonal features in commodity pricing may not be wholly indicative of future patterns.

Net-zero emissions fuel production units will have an associated gas node, electrical node, and operating characteristics such as conversion efficiency, hydrogen fraction, and operating lifetimes. Default values are presented in Table 2.3. Note that electrolytic fuels are not technically net-zero emissions until the electricity supply comes from net-zero emissions sources. However, for simplicity of exposition, we will refer to this family of fuels as net-zero emissions gases.

Biomethane production facilities convert biogenic organic material into a raw biogas through anaerobic digestion or a raw syngas through gasification. These gases are then processed to remove bulk inert components (most commonly carbon dioxide and nitrogen) and trace contaminants (hydrogen sulfide, siloxanes, etc.) required purity specifications for consumption. The most common sources of biogas include landfills and wastewater treatment facilities, both of which utilize anaerobic digestion. In the United States, these facilities are, in general, already required to capture and flare waste methane. As such, many facilities use biogas productively for on-site generation of electricity and heat. Biogas can also be purified or converted into biomethane by removing the carbon dioxide

components. When methane purity greater than 95% is achieved, biomethane is considered a drop-in interchangeable fuel with fossil natural gas and can be introduced to the common-carrier pipeline.

Several technoeconomic studies have estimated the available supplies and levelized cost of biomethane production [137]. This body of work indicates that sources of biomethane with capture equipment already in place (i.e., existing landfills and anaerobic digesters at waste-water treatment facilities) will offer the lowest-cost biomethane resource, with costs ranging from \$5 to \$20/MMBtu (\$17 to \$68/MWh thermal). Smaller-scale, distributed animal waste resources lie at the most expensive end of the supply curve with costs exceeding \$60/MMBtu (\$200/MWh thermal) [137].

Sustainable sources of biomethane are typically supply-constrained and can be subjected to annual limitations in Eq. (2.63). These limitations will be region-specific and subject to large uncertainties as the current model formulation does not endogenously consider competing demands for sustainable biofuels in the transportation sector. Biogas from anaerobic digestion will likely be most cost-effectively converted to a gaseous fuel as it is already 50% methane. However, syngas from biomass gasification may be converted to longer-chain hydrocarbons to produce liquid fuels at similar unit energy costs by tuning the ratio of hydrogen to carbon entering the fuel synthesis reactor. Given the relatively high value of liquid fuels per MJ and the lack of good options for replacing some transport demands (most notably jet fuel), it is possible that transport applications will be able to outbid gas consumers for biomass-based fuels.

Here, we use simple volumetric limits on the supply of biomethane, mimicking a de facto price floor and supply cap imposed by higher-value demands for bio-energy in liquid fuels. However, competition between the liquid and gaseous fuels markets for sustainable bioenergy resources is a factor that should be accounted for more explicitly in future energy systems planning optimization work.

In this work, we assume natural sources of waste methane will be captured and available in a continuous fashion. To model this, we assume a levelized cost of biomethane equal to \$15/MMBtu (\$51.20/MWh) and convert this to an equivalent fixed operating cost for a facility with a 100% capacity utilization factor. In other words, a 1 MW biomethane production facility can produce as much as 8760 MWh per year and will have an associated fixed operating cost of \$448/kW-year with no modeled variable operating and maintenance costs. In this manner, the model will preferentially dispatch these resources with high utilization factors, reflective of the, generally, continuous nature of biomethane production.

For hydrogen, we primarily consider proton exchange membrane electrolyzers as expert elicitation studies suggest these are likely the dominant technology by 2030, achieving lower capital costs and facilitating cost-effective intermittent operation [138]. For a most comprehensive overview of electrolyzer technologies, their capital and operating costs, and efficiency characteristics we defer to [139], [140] and [141]. We assume that electrolytic hydrogen production facilities will blend 100% hydrogen into the natural gas system, and produced oxygen is assumed to be vented to the

atmosphere.

Electrolyzer conversion efficiencies are expected to improve over time. Near-term projects have been referenced between 40 and 69% [142] but are likely to achieve efficiencies closer to 60% [139]. By mid-century it is anticipated that efficiencies will reach or exceed 70% [139]. However, as we model a single set of operating parameters for all units in each technology class, we use an estimate of 65% (consistent with the 2035 scenario in [143] and the "Next-decade" case in [141]). Future model extensions may accommodate changing technology characteristics with more granular equipment vintage tracking or by including multiple classes of electrolyzer technology, which become available in a future investment year (see Section 2.7.1).

The capital cost trajectory for electrolyzers is highly uncertain and a wide range of estimates exist in the literature. Here, we assume a moderate case where these capital costs scale linearly from \$1,025/kW$_e$ in 2018 to \$570/kW$_e$ in 2030 and to \$485/kW$_e$ in 2050 based on the analysis in [141]. Fixed operating cost estimates generally range from 2-5% of capital investment with the cost of stack replacements across a 20-year plant life estimated at 50-60% of investment cost [142]. Other studies also suggest stack replacement intervals of 7-10 years with costs equal to 15% of installed capital cost [143]. Here, we adopt the same approach taken by [141] and consistent with [143] and assume fixed annual operating costs (including stack replacements) equal to 7.5% of capital investment. The largest variable cost of hydrogen production will be the endogenously-evaluated cost of input electricity. As such only small additional variable costs are modeled to account for the cost of water (0.08 \$/kg H_2) and estimated costs of compression [140].

For electro-methane production, we assume electrolytic hydrogen is combined with climate-neutral carbon dioxide to produce a net-zero emissions methane-rich fuel gas that can act as a drop-in substitute for fossil natural gas. The conversion efficiencies for electrolyzers are the same as outlined above. Reverse water-gas shift reactors are used to convert a stream of hydrogen and carbon dioxide into a syngas with larger mole fractions of carbon monoxide and hydrogen. This syngas can be passed into a Fischer-Tropsch fuel synthesis reactor to generate hydrocarbons such as methane, ethane, and butane. Taken together, this yields an all-in electricity-to-fuel efficiency of 45%. This is in general agreement with other studies that find efficiencies of 33-41% [144].

The capital cost of a fuel synthesis reactor to convert carbon dioxide and electrolytic hydrogen to methane is assumed to decline linearly from \$1,770/kW$_{\text{fuel}}$ in 2018 to \$1,010/kW$_{\text{fuel}}$ in 2030 and further to \$760/kW$_{\text{fuel}}$ in 2050 based on the analysis of [142] and [141]. Assuming the same electrolytic efficiency of 65% and applying a fuel synthesis efficiency of 70%, these costs are converted to [\$/kW$_e$].

Recent studies have found that optimally-designed electrofuels plants will include storage of heat, hydrogen, and carbon dioxide to achieve high utilization factors for capital-intensive carbon capture and catalytic upgrading equipment [145, 141]. These effects are non-negligible, but challenging to incorporate endogenous to the system-wide planning optimization. Instead, we create a simplified

"black box" representation that considers these cost components of electro-methane as variable costs assuming a fixed capacity factor utilization of fuel synthesis equipment and a fixed cost of climate-neutral carbon dioxide. These capital costs are levelized across an assumed 20-year plant life using a capital recovery factor of 0.1, reflective of a 7% internal rate of return. The fixed operating costs for fuel synthesis reactors are assumed to be 10% of invested capital, inclusive of any necessary investments in hydrogen or carbon dioxide storage for system design optimization. These fixed costs are then levelized across an assumed 75% utilization factor.

Costs of climate-neutral carbon dioxide for fuel synthesis are assumed to decline linearly from present day values of \$600/tCO_2 in 2018 to \$130/tCO_2 in 2040 [141]. The fuel synthesis reactor is assumed to have a carbon dioxide conversion efficiency of 95% [142, 141]. Other studies suggest lower carbon efficiencies for Fischer-Tropsch reactors, ranging from 65%-89% [144], however here, we assume unconverted CO_2 can be recirculated to achieve higher conversion fractions. These costs are accounted for in the variable cost of electro-methane presented in Appendix A.2, and the only explicitly-modeled electro-methane capital and fixed operating costs is that of the electrolyzer. In future work, the set of decision variables may be extended to co-optimize capture of climate-neutral carbon dioxide, generation of net-zero emissions hydrogen, production of electro-fuels, and any intermediate storage of energy or chemicals (as implemented in [141]).

In this work, we only explicitly track hydrogen and assume the remainder of gas in the pipeline network can be modeled as methane. We limit hydrogen transmitted through a pipeline or delivered for consumption at a node to less than 20 mol.% of the mixture [146]. However, ongoing research continues to examine the materials limitations of hydrogen delivery and consumption.

Future work may extend the component tracking formulation to account for additional constituents, such as carbon dioxide or ethane, and their impacts on heating value, specific gravity, and gas interchangeability indices. Optimized blending of liquified petroleum gases or inert components, like nitrogen, could be used to control gas quality and ensure combustion interchangeability for all end-use customers. Alternatively, more rigorous formulations for the pooling problem could be included (see Appendix Section A.4 for more). Future modeling extensions may also consider additional sources of low-emissions hydrogen from natural gas steam methane reforming or methane pyrolysis equipped with carbon capture technologies. These are not modeled in the current work, but are easily accommodated in future study as net-zero emissions gas units.

2.4.3 Energy storage

In this work, we model energy storage units for gas and electrical energy, each specified by an associated gas node, electricity node, and set of operating characteristics presented for a set of template technology types in Table 2.4. Note that there is an ever-expanding set of storage technologies under development to serve the range of market niches that may exist in a decarbonized energy system. In this work, we parameterize each storage technology using a generalized set of specifications for

Storage						
Technology	Unit size u_s [MW]	Duration [hrs]	Life time τ_s [years]	Charge efficiency η_s^+ [MWh to storage / MWh elec.]	Discharge efficiency η_s^- [MWh elec. / MWh from storage]	Loss rate η_s^l
Lithium ion battery	1	4	15	0.92	0.92	1% per month
Long-duration storage	50	720	55	0.63	0.53	0.01% per year
Subsurface gas storage	1300	1200	75	0.96	0.995	0.01% per year

Table 2.4: Operating characteristics for energy storage units

technology charge and discharge efficiencies and hourly loss rates.

First, we model a short-duration electricity storage candidate based on 4-hour duration lithium-ion battery technology. We use technology cost assumptions from the NREL's 2020 ATB [127] and their referenced sources [147]. Lithium-ion charge/discharge efficiencies and estimated lifetimes are referenced from [15] and [127].

Second, we model a long-duration electricity storage candidate based on electrolysis paired with underground hydrogen storage [16] and a hydrogen-fueled combined cycle gas turbine. Electrolyzer cost and efficiency assumptions are explained in Section 2.4.2. Parasitic energy consumption for compression for underground storage can exceed 8% of hydrogen energy (on an LHV basis) and can be as high as 16% for tank storage [148]. Energy required for compression [149] and any potential compression losses [150] are applied to the electrolyzer conversion efficiency to estimate the storage charging efficiency of 63%. Capital costs of the underground hydrogen storage are assumed to scale with total volumetric energy capacity and remain constant across our planning horizon at \$0.35/kWh [151] (escalated to 2018\$). A hydrogen combined-cycle gas turbine is modeled after a natural gas combined-cycle turbine and assumed to perform at similar LHV efficiency (53%) and cost per [127].

Third, underground natural gas storage fields are also modeled and are sized based on the average facility in the United States [152]. These facilities are modeled using the same set of operating parameters as electrical energy storage, however there may be important transient features that are not addressed by this model simplification as shown by [87]. The only associated efficiency losses are in compression of natural gas [149] and minor modeled losses of 0.01% per year from the subsurface [16]. In order to approximate the limits on flexible charging and discharging of gas storage, we require that gas storage facilities have the same charge/discharge rate in all hours across each representative day. This approach is consistent with the average gas pipeline flows evaluated in steady-state across each representative day in Section 2.3.5 and the gaseous energy balance enforced across each representative day in Section 2.3.5.

All storage technologies are modeled as flexible units without any parametric limitations on the rate of change of charge or discharge (i.e., hourly ramp rates, minimum up- or down-times). These attributes may be important for some less flexible gaseous and thermal energy storage technologies and can be accommodated in future work by adapting the constraint set in Eq. (2.23) to apply to storage charge/discharge variables ψ^+, ψ^-.

Some energy storage technologies may be flexibly designed to optimize the storage duration, with different power capacity for charging and discharging. For example, the modeled long-duration hydrogen storage may separately size the electrolyzer, the storage tank, and the combustion turbine to fit the system's needs. This functionality is included in similar models in the literature and has been used to identify the storage attributes which offer the greatest system value [15]. In future versions of this work, decision variables may be included for all three storage technology attributes: charge power capacity [MW], energy storage capacity [MWh], and discharge power capacity [MW]. In addition, electro-chemical storage capacity is expected to degrade over time and as a function of cycling behavior. This feature is not included in the current model formulation, but could be accommodated in future work.

2.4.4 Transmission and distribution

Network topology

The transfer of gas and electricity between nodes on each system is governed by the network configuration as described in Section 2.3.1. Here, we describe the parameters for each edge that are required to fully specify a network configuration. We also describe the approach to estimate costs associated with transmission and distribution infrastructure operation, maintenance, and re-investment.

Electricity transmission lines are specified by an origin node, a terminus node, and a maximum power flow. If the steady-state DC power-flow models in Eq. (2.18) are employed, the network must also be specified by a base MVA, line impedance on a per unit basis, and a designated slack (or reference) bus with its voltage angle constrained to equal 0. Template examples of such power networks are available from the IEEE.

Gas transmission pipelines are specified by an origin node, a terminus node, a pipeline diameter, length, and friction factor. Each transmission pipeline will also have a maximum compression ratio $\overline{\alpha}$. Compression ratios for gas transmission compressors are always greater than 1 and typically below 2, however multi-stage compression units can be used to produce larger maximum compression ratios [153]. If a compressor does not exist on the pipeline then both compression ratio bounds are equal to 1.

Generating transmission network topology data sets can be challenging as this information is generally withheld due to security concerns. Previous work by this author has used geographic information systems (GIS) data sources to generate plausible network connections between potential sources of gas and regional demands at the zip-code level [9]. Pipeline network data sets have

also been created for a 24-pipeline template system [38], the Belgian gas network [47], and the Transcontinental pipeline [154]. However, when using GIS data, it can be challenging to identify where distribution-level off-takes exist and where transmission-level features may be intersecting, but do not exchange energy. Missing network connections due to slight misalignment in two transmission features can result in infeasible networks with stranded sections of energy demands. In addition, important topology information may be abstracted away when features (such as parallel, but not connected pipelines) are lumped together as a single network edge. For the most recent overview of approaches in synthetic pipeline and electricity network creation see [154].

Infrastructure costs

In this work, fixed costs of energy transmission and distribution (T&D) infrastructure investment and maintenance are abstracted behind exogenous assumptions based on system attributes indicative of the capacity of generic T&D infrastructure and correlated with the revenue requirement of an energy utility provider.

For the electricity system, the capacity of transmission and distribution infrastructure will roughly scale with the instantaneous peak in energy demand on the system. These correlations have been identified in the academic literature [155] and are widely used to estimate the value of distributed energy resources or the avoided costs due to energy efficiency measures [156, 157, 158]. Other regulatory proceedings have generated utility-specific values for the marginal cost of transmission and distribution capacity [159].

In California, the marginal costs of transmission capacity are estimated using utility-specific data either from the General Rate Case or Commission data requests. These calculations produce utility-specific results that range from \$11.75 to \$28.52 per kW-year [159]. The marginal costs of distribution infrastructure are partitioned into the near-term and the long-run marginal costs using different data sources. Project deferral data allows such estimates for the near-term marginal costs. These values can range as low as \$3.66/kW- (for San Diego Gas & Electric territory) to \$29.13/kW-y (for Southern California Edison) [159]. For long-run marginal costs of distribution capacity, General Rate Case data are used to estimate the costs of meeting incremental peak-coincident electricity demands. This produces a wider range of estimates spanning \$19.48 to \$206.57 per kW-y in the case of California utilities [159].

For the generalized purpose of this model, we abstract these factors behind a single default cost value – the incremental cost of non-modeled electricity transmission and distribution infrastructure to serve peak demands is assumed to be \$21/kW$_{\text{peak}}$-year and \$52/kW$_{\text{peak}}$-year, respectively [155].

For the gas system, fixed costs of gas distribution system maintenance are estimated based on EIA Form 176 filings by natural gas distribution companies [160]. We estimate the fixed costs of system maintenance and re-investment as the difference between total revenues collected and the costs of fuel delivered. We use city-gate natural gas prices from EIA for each state and separately

estimate the fixed costs of distribution allocated to the residential and commercial sectors. We assume the industrial sector bears a negligible share of distribution costs in their rates.

Proportionate monthly deliveries are estimated for each state based on EIA RECS [94] and CBECS [95] data, paired with temporal profiles for energy consumption by end use from EFS data [93]. These hourly profiles offer a rough estimate of the relative monthly gas consumption and are meant to capture the coarse relationships between the cost of natural gas and the relative demand for distribution-level end-uses. This likely represents an over-estimate of the degree to which gas distribution companies are exposed to the monthly city-gate price as long-term contracts and gas storage facilities are used to hedge price exposure.

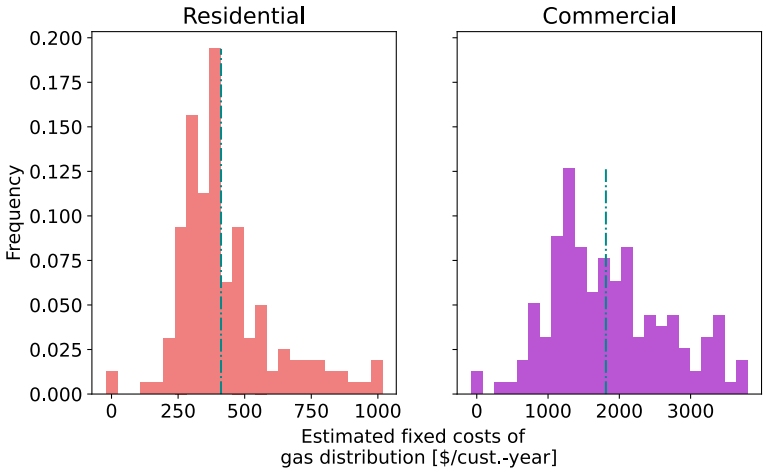

Figure 2.4: Distribution of estimated gas distribution utility fixed costs for the year 2019.

Figure 2.4 presents the distribution of estimated fixed system costs for residential and commercial sectors across gas companies and averaged across states. Note that revenues collected from particular sectors may not perfectly align with cost causation principles, and some degree of customer class subsidization is expected. Further, long-term contracts for natural gas and use of seasonal gas storage fields allow distribution companies to reduce exposure to the seasonal fluctuation in city-gate prices. However, to a first-order, these offer plausible estimates for the cost-of-service of gas distribution.

The proposed model does not currently implement expansion variables for gas or electric transmission units. However, future work may do so as outlined in Appendix Section A.3. Introducing expansion and retirement of transmission assets would allow for more explicit fixed cost considerations, using the characteristics of the network assets in the gas and electricity systems. The most widely cited cost estimates for development of new electric transmission can be found in [161]. Cost estimates for gas pipeline projects is published by the EIA [162] and can be used to inform estimates for new transmission pipeline expansion as a function of pipeline length and diameter. Transmission expansion scenarios should be modeled with extreme caution, however, as these projects are more

Electricity		Gas	
Source	Emissions intensity [kg CO_2/MWh elec.]	Source	Emissions intensity [kg CO_2/MWh fuel]
Solar/Wind	0	Biomethane	0
Coal-fired generation	1,006	Electrolytic H_2 (Solar)	0
Natural Gas-fired CT	504	Electrolytic H_2 (Natural Gas-fired CC)	523
Natural Gas-fired CC	340	Electro-methane (Natural Gas-fired CC+CCS)	89
Natural Gas-fired CC+CCS	40	Fossil Natural Gas	181

Table 2.5: Greenhouse gas emissions intensity for a variety of indicative electricity and gaseous energy sources for conceptual comparison with system-wide targets.

often constrained by regulatory, social, and political barriers than the relative economics. As such, even as new transmission is routinely found to play a keystone role in cost-effective decarbonized energy systems [163, 164], scenarios for integrated gas-electric energy system planning should be cognizant of the limitations that may exist on regional transfer of energy with existing infrastructure.

2.4.5 Energy policy constraints

Emissions intensity constraints are included for the electricity sector and the gas sector. Sub-national climate policies target net-zero economy-wide emissions by 2045 [165] or 2050 [166, 167] with specific targets for the emissions associated with retail electricity sales [168]. However, many climate policies lack meaningful enforcement of interim targets and no current law requires such emissions reductions in the natural gas sector.

To fully specify Eq. (2.60), every modeled investment year must have a corresponding emissions intensity limit for both the electricity and the gas sector entities. Each case study will have parameters for emissions intensity trajectories either informed by current policy, voluntary targets, or indicative decarbonization scenarios. This modeling framework offers a maximal degree of flexibility to test the impact of pace and timing of such sector-specific emissions constraints. For context, we present a sampling of emissions intensity estimates in Table 2.5 for typical sources of delivered electricity and gas using the characteristics outlined in Table 2.2 and 2.3.

Model functionality is also included to test the impact of permitting negative emissions technologies for atmospheric carbon removal. Some existing climate policies permit some use of negative emissions offsets bound by 7% of a regulated entities emissions liabilities [169]. However, large uncertainties exist about the bio-physical limitations of cost-effective carbon removal [170, 171] and the permanence of existing offset projects [172, 173]. For all results presented here, negative emissions

offsets or atmospheric carbon removal are not permitted. As such, these variables are constrained to maximum shares of emissions liabilities equal to 0%.

Note that we do not model or account for the costs or climate impacts of any non-CO_2 co-pollutants or the associated public health consequences. This remains an important area for future study. Specifically, as heat pump technologies become a keystone feature of decarbonized energy systems, the life-cycle impacts of refrigerants will be important to include. We also do not include natural gas leakage from production, transmission, and distribution systems [174] or from gas-fired appliances [175]. Methane leakage may account for non-negligible life-cycle climate impacts for intentionally produced methane [176]. However, this feature can be accommodated by the presented modeling framework in future studies.

Further, as illustrated in Table 2.5, emissions impacts of electro-fuels may be significant if not generated using clean electricity. The current model implementation applies a net-zero emissions intensity to any direct-use of electro-fuels. This represents a policy scenario where contractual arrangements are made by electro-fuels production facilities to operate with 100% emission-free electricity. In the proposed modeling framework, liabilities for any upstream emissions associated with the production of net-zero emissions fuel are accounted for in total emissions of electricity generation. This represents a model simplification to avoid double-counting of GHG emissions liabilities, and to reflect one plausible regulatory future.

Finally, we treat biomethane as a climate-neutral fuel with an assessed emissions intensity of 0 [kg CO_2/MWh]. Current biomethane projects are typically credited for the high global warming potential methane emissions avoided through capture and productive use of methane [9]. This can result in net negative life-cycle carbon intensity values. The implicit assumption of our study is that the anthropogenic release of methane from waste management and agricultural facilities is or will soon be regulated to be zero. As such, the baseline from which any emissions benefit is evaluated for incremental productive use of biomethane is zero, rather than the unmitigated release of methane.

2.4.6 Present value discounting

All modeled costs must be discounted to present value, in a variety of contexts, to account for both the realistic cost of interest-bearing capital required for investments and the societal value of delayed capital outlays, allowing for. A rich literature exists on the many dimensions of discount rates, however, here we simply aim to address the risk-adjusted cost of capital for infrastructure investments and the potential risk-free capital accumulation for delay of capital outlays.

For all capital investments, we use a weighted average cost of capital to amortize upfront capital costs across the economic lifetime of infrastructure. The weighted average cost of capital here represents a reasonable value for this illustrative analysis [177]. In practice, each candidate generator, storage, or power-to-gas resource will have a different cost of capital based on the respective share of debt and equity financing and the level of associated technical and regulatory risk. Further, consumer

investments in appliances will experience a higher discount rate than corporate investments with access to lower cost financing.

In the objective function, we use a societal discounting factor d, reflective of the societal value of delaying costs. This value may range from 0% to 7% depending on the view taken by the modeler. A higher societal discount rate will allocate greater weight in the objective function to near-term transition costs and neglect long-term costs of the net-zero emissions end-state. A discount rate of 0% will place much larger emphasis on the long-run costs of operating and reinvesting in the decarbonized energy system. Discount rate assumptions will play a larger role in situations with rapidly changing technology costs that may enable a more cost-effective long-term solution by relying on infrastructure that are currently uneconomic.

Similar bipartite discounting framework have been employed in other energy systems planning optimization programs to account for different contexts when discounting future dollars to present value [178].

2.5 Case study implementation

To illustrate this approach to co-optimized system planning, we extend an integrated energy system composed of the IEEE 24-bus electricity transmission network coupled with a 25-node pipeline network from a previous study [38], which is shown in augmented form for this study in Figure 2.5. We modify this system with the addition of candidate electricity generators, net-zero emissions gas sources, and energy storage units. We also explicitly model a set of appliance-level energy demands and their candidate replacements. This indicative network allows us to demonstrate full model functionality and illustrate how local heterogeneity in energy resource availability and delivery networks can impact the cost-effective investment decisions.

All cost assumptions are inflation adjusted to consistent 2018 USD.

2.5.1 Sensitivity scenarios

We use and modify the program in Eq. (2.1) to evaluate the least-cost decarbonization path for two indicative regional gas-electric networks, under two appliance-investment cases, and three gas quality constraint formulations.

All sensitivity scenarios are presented in Figure 2.6 with a description of model formulation adjustments adopted for each case.

First, we construct two gas-electric system load and renewable energy scenarios, representative of two different climate regions in the United States: the Mountain Northwest, and the Coastal Pacific regions. These two regions provide a diverse set of renewable resource availability and final energy demand characteristics. Each system has unique energy demand characteristics (i.e., magnitude and

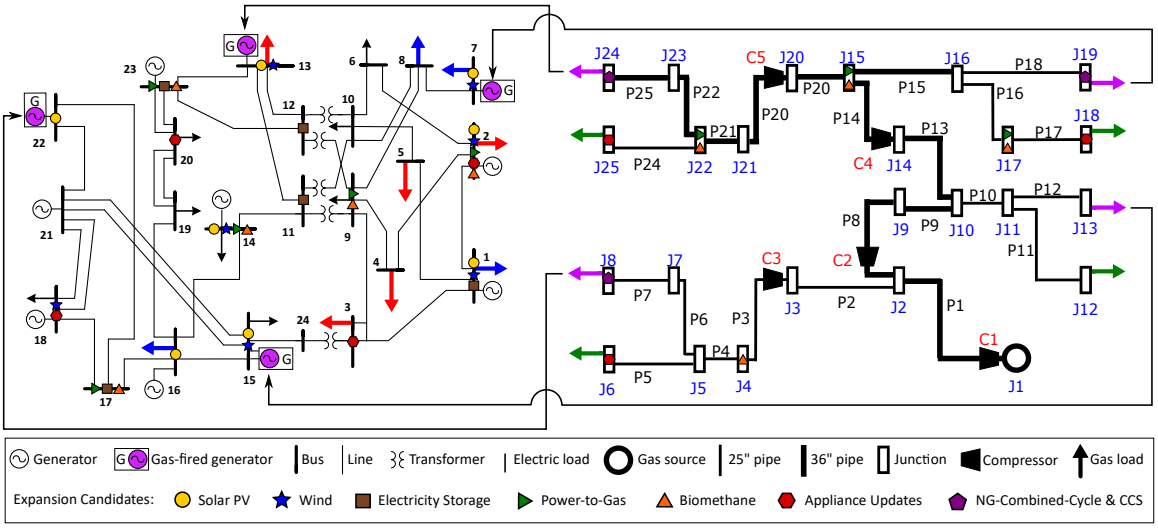

Figure 2.5: Schematic of gas-electric energy system used in the computational study. Expansion candidates are indicated at each bus (resp. junction) for the power (resp. gas) networks.

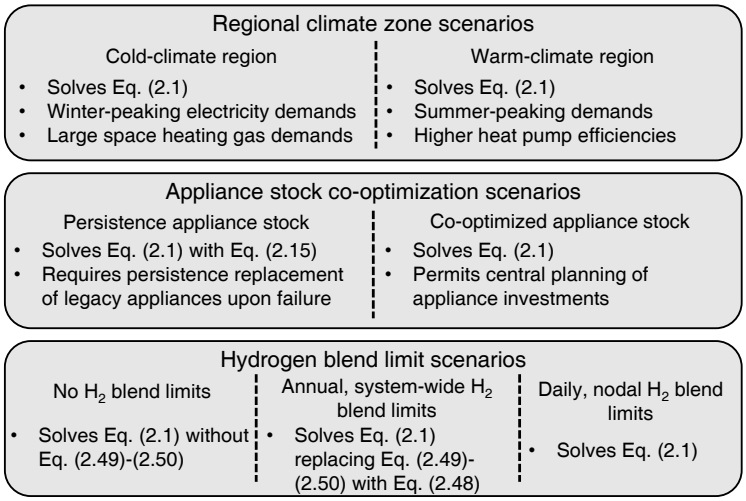

Figure 2.6: Schematic illustration of the case study scenarios explored in this analysis and the constraints added or removed from Eq. (2.1)

temporal profile). Both systems have identical candidate units and network topology as presented in Figure 2.5. The model formulation presented in Eq. (2.1) is solved for each system.

Second, we illustrate the impact of appliance investment planning. The most restrictive appliance-investment case assumes a fixed appliance stock, replaced on a persistence basis to satisfy demand growth, by enforcing Eq. (2.15). The second scenario introduces appliance-level investment decisions for policy-driven electrification by removing Eq. (2.15) from the constraint set.

Third, we test three degrees of gas quality constraint implementation to illustrate the impact of locational and temporal hydrogen blending limitations on the least-cost result. The first case excludes all gas quality constraints, assuming gas infrastructure can accept any degree of hydrogen blending. In the second case, we include Eq. (2.48) to ensure that over the course of each investment year, the system-wide hydrogen injection does not exceed acceptable blend limits. Finally, in the third case, we use the full formulation as presented in Eq. (2.1). This includes gas quality constraints (Eq. (2.49) - (2.50)), introducing more granular spatial and temporal constraints on the blending of hydrogen.

For all cases, we use high-performance computing resources in order to simulate full representative years of operations for each of the five modeled investment periods (i.e., $I = 5, R = 365, O = 24$). The problem is implemented in JuMP [179], a toolkit for mathematical programming in the Julia language [180]. The solver used is Gurobi, which can directly solve the convex quadratic optimization problem using a second order cone programming solver using interior point methods. The model is solved on 128 core AMD 7742 processors with 800 GB of accessible RAM. Solve times for a 24-node coupled network range from approximately 12,000 to 24,000 seconds (3-6 hours) depending on problem classification.

Because of the computational complexity of the time-extended planning and operations co-optimization, we adopt a key modeling simplification. Specifically, we fix gas pipeline flow directions $y_{(i,r),e} = 1$. In our opinion, this is an acceptable reduction in complexity for demonstration of the method and to highlight broader features of such systems under deep decarbonization constraints. However, future work should explore model reduction techniques to allow for tractable simulation of such bi-directional gas flows (alongside detailed representations of operations) to adapt to an evolving spatial allocation of low-carbon gas resources. This would add a large number of binary variables and make the problem much harder to solve.

2.5.2 Data

Energy demand

Hourly profiles for baseline electricity demands are assumed for a Mountain Northwest (i.e., winter-peaking) and a Coastal Pacific (i.e., summer-peaking) system, using simulated state-level electricity demands from NREL's Electrification Futures Study (EFS) [117]. Demand profiles for the Mountain Northwest system are based on the aggregated state-level profiles of Washington, Montana,

and North Dakota. For the Coastal Pacific system, we use data for California. Hourly electricity demands are normalized to average annual energy consumption and scaled to the average nodal energy demands presented in Table 2.6.

Base case nodal electricity demands (Mountain Northwest/Coastal Pacific)						
Node	Baseline		Existing appliances		Candidate appliances	
	Average [MW]	Peak [MW]	Average [MW]	Peak [MW]	Average [MW]	Peak [MW]
1	100	145/175	0/0	0/0	0/0	0/0
2	50	50/50	0/0	0/0	58.9/22.8	385/85
3	50	50/50	0/0	0/0	58.9/22.8	385/85
4	75	108/131	0/0	0/0	0/0	0/0
5	70	101/122	0/0	0/0	0/0	0/0
6	130	187/227	0/0	0/0	0/0	0/0
7	75	75/75	0/0	0/0	58.9/22.8	385/85
8	170	245/300	0/0	0/0	0/0	0/0
9	175	253/306	0/0	0/0	0/0	0/0
10	200	289/350	0/0	0/0	0/0	0/0
11	0	0	0/0	0/0	0/0	0/0
12	0	0	0/0	0/0	0/0	0/0
13	200	200/200	0/0	0/0	58.9/22.8	385/85
14	194	280/340	0/0	0/0	0/0	0/0
15	317	458/555	0/0	0/0	58.9/22.8	385/85
16	110	159/192	0/0	0/0	0/0	0/0
17	0	0	0/0	0/0	0/0	0/0
18	50	50/50	0/0	0/0	58.9/22.8	385/85
19	190	274/332	0/0	0/0	0/0	0/0
20	50	50/50	0/0	0/0	58.9/22.8	385/85
21	0	0	0/0	0/0	0/0	0/0
22	0	0	0/0	0/0	58.9/22.8	385/85
23	0	0	0/0	0/0	0/0	0/0
24	0	0	0/0	0/0	0/0	0/0

Table 2.6: Assumed nodal electricity demands for the network case study.

Gas distribution demands exist at nodes 6, 8, 12, 13, 18, 19, 24, and 25 on the pipeline network. Each distribution node is assumed to have 50,000 residential customers and 2,000 commercial customers, each of which use gas appliances for space heating and water heating. Half of these customers are also assumed to have gas cooking energy demands. As noted in Section 2.3.1, the gas and electric networks have disjoint sets of nodes. If electrified, the appliance energy demands at nodes 6, 8, 12, 13, 18, 19, 24, and 25 on the gas system will operate at nodes 18, 22, 3, 15, 2, 7, 13 and 20 on the electricity network, respectively.

We assume the presence of baseline gas demands evenly distributed across the same set of gas demand nodes that are not modeled at the appliance level. These are representative of potential industrial or petrochemical demands that are not easily transitioned to direct-use of electricity but

may compete with other core gas demands for limited climate-neutral resources. For this case study, these are assumed to be constant across the year such that baseline gas demands equal 10% of system average baseline electricity demand. In an industrial heavy case study this fraction could of course be higher. These initial gas demands are characterized in Table 2.7.

Base case nodal gas demands (Mountain Northwest/Coastal Pacific)						
Node	Baseline		Existing appliances		Candidate appliances	
	Average [MW]	Peak [MW]	Average [MW]	Peak [MW]	Average [MW]	Peak [MW]
6	27.5/27.5	27.5/27.5	164/80.6	528/372	0/0	0/0
8	27.5/27.5	27.5/27.5	164/80.6	528/372	0/0	0/0
12	27.5/27.5	27.5/27.5	164/80.6	528/372	0/0	0/0
13	27.5/27.5	27.5/27.5	164/80.6	528/372	0/0	0/0
18	27.5/27.5	27.5/27.5	164/80.6	528/372	0/0	0/0
19	27.5/27.5	27.5/27.5	164/80.6	528/372	0/0	0/0
24	27.5/27.5	27.5/27.5	164/80.6	528/372	0/0	0/0
25	27.5/27.5	27.5/27.5	164/80.6	528/372	0/0	0/0

Table 2.7: Assumed nodal gas demands for the network case study.

Legacy end-use appliances in the system include residential and commercial gas furnaces, gas water heaters, and gas cooking. Candidate appliances include air-source heat pumps for space heating, heat pump water heaters, and electric cooking alternatives. Total annual energy demand estimates per household or per commercial building are based on the Energy Information Administration (EIA) RECS and CBECS, respectively [94, 95], and are presented in Table 2.8. We assume annual average gas and electric appliances efficiencies for template class-average appliances [97, 111, 105]. We use DOE building energy simulations to generate plausible hourly consumption profiles for space heating, water heating, and cooking appliances [109] as described in Section 2.4. Further, we use state-level simulations from [92] to generate plausible profiles for air-source heat pump operation with reliance on back-up electric resistance during periods of extreme cold weather. For the Mountain Northwest region, we use appliance demand profiles from Montana. For the Coastal Pacific region, we use California building simulation data.

Appliance capital cost assumptions are based on a synthesis of Building Energy Optimization (BEopt) data [111], commercially available technologies [112, 113, 114, 115, 116], and NREL's EFS [97, 117]. Installed cost assumptions for each appliance candidate are presented in Appendix A.2.

Energy supply

Existing generation units are inspired by the IEEE 24-bus data set, including a set of coal-fired, gas-fired, and nuclear-powered generators. These legacy generators are assumed to retire naturally at their expected lifetime (per Eq. (2.6)). Candidates for generation expansion include solar photovoltaics (PV), wind turbines, and natural gas-fired combined cycle generators equipped with carbon

Residential Appliances (Mountain Northwest/Coastal Pacific system)					
Technology	Electricity nodes	Gas nodes	Existing units [no. per node]	Energy demand [MWh/ year]	Energy efficiency [%]
Gas furnace	2, 3, 7, 13, 15, 18, 20, 22	6, 8, 12, 13, 18, 19, 24, 25	100,000	19/6	0.80
Gas water heater	2, 3, 7, 13, 15, 18, 20, 22	6, 8, 12, 13, 18, 19, 24, 25	100,000	6/5	0.80
Gas cooking	2, 3, 7, 13, 15, 18, 20, 22	6, 8, 12, 13, 18, 19, 24, 25	50,000	0.9/0.7	0.25
Air-source electric heat pump	2, 3, 7, 13, 15, 18, 20, 22	6, 8, 12, 13, 18, 19, 24, 25	0	7.6/1.4	2.0/3.5
Electric heat pump water heater	2, 3, 7, 13, 15, 18, 20, 22	6, 8, 12, 13, 18, 19, 24, 25	0	2.2/1.6	2.2/2.5
Electric induction cooking	2, 3, 7, 13, 15, 18, 20, 22	6, 8, 12, 13, 18, 19, 24, 25	0	0.45/0.35	0.50
Commercial Appliances (Mountain Northwest/Coastal Pacific system)					
Technology	Electricity nodes	Gas nodes	Existing units [no. per node]	Energy demand [MWh/ year]	Energy efficiency [%]
Gas furnace	2, 3, 7, 13, 15, 18, 20, 22	6, 8, 12, 13, 18, 19, 24, 25	4,000	56/27	0.80
Gas water heater	2, 3, 7, 13, 15, 18, 20, 22	6, 8, 12, 13, 18, 19, 24, 25	4,000	11/20	0.80
Gas cooking	2, 3, 7, 13, 15, 18, 20, 22	6, 8, 12, 13, 18, 19, 24, 25	2,000	14/32	0.25
Air-source electric heat pump	2, 3, 7, 13, 15, 18, 20, 22	6, 8, 12, 13, 18, 19, 24, 25	0	22/6.2	2.0/3.5
Electric heat pump water heater	2, 3, 7, 13, 15, 18, 20, 22	6, 8, 12, 13, 18, 19, 24, 25	0	4/6.4	2.2/2.5
Electric induction cooking	2, 3, 7, 13, 15, 18, 20, 22	6, 8, 12, 13, 18, 19, 24, 25	0	7/16	0.50

Table 2.8: Assumed set of modeled appliance-level energy demands for network case study.

capture (NG-CC+CCS). Each generator type requires assumptions for a range of characteristics including fuel type, heat rate, maximum hourly ramp rate, minimum stable output, maximum stable output, minimum up time and minimum down time, and year of entry into service (if an existing resource). These are presented in Table 2.2 and Table 2.9 presents the specific locations and characteristics of all legacy and candidate generators in the network.

For hourly solar and wind availability, we use data specific to the regional system simulated. For the Mountain Northwest system, we use historical data for solar and wind production from the Northwest region of the United States (as defined by the EIA's Operating System Dashboard [90]). Total installed capacity for this set of balancing authorities in 2019 is estimated from EIA Form 860 data to be 3.9 GW of solar photovoltaic and 13.9 GW of wind generating capacity. This produces annual average capacity factors for 2019 of 17.6% for solar and 25.2% for wind. In the Coastal Pacific system, we use data from the EIA Form 930 Operating Dashboard [90] for historical solar and wind production for the year 2019. These generation values were normalized to total installed capacity of solar (13 GW) and wind (6 GW) generators in the California Independent System Operator (CAISO) balancing authority as reported in EIA Form 860 [126]. These sources produce an annual average capacity factor of 24.6% for solar and 30% for wind. Assumed capital and operating costs for electricity generators and fuel costs are referenced from the NREL's ATB for 2020 [127] as described in Section 2.4 and presented in Appendix A.2.

We include three kinds of net-zero emissions gas: biomethane, electrolytic hydrogen, and electromethane with operating characteristics specified in Section 2.4. For this case study, we limit annual production of biomethane in the base case scenarios to not exceed 30% of total initial core gas demands. All capital and operating cost assumptions are outlined in Section 2.4.

Energy storage

We model three technology options for electrical and gaseous energy storage, as described in Section 2.4.3. First, we model a short-duration electricity storage candidate based on 4-hour duration lithium-ion battery technology [127, 147, 15]. Candidate lithium-ion batteries exist at nodes 1, 11, 12, 17, and 23 on the electricity system. Second, we model a long-duration electricity storage candidate based on electrolysis paired with underground hydrogen storage [16] and a hydrogen-fueled combined cycle gas turbine. Long-duration electricity storage candidates are assumed to exist at nodes 1, 11, 12, 17, and 23 on the electricity system. Legacy underground natural gas storage fields are assumed to exist at gas system nodes 3 and 14, and are sized based on the average facility in the United States [152]. These facilities are assumed to be maintained to allow for seasonal shifting of gaseous energy, with only modest losses from compression upon charging.

Note that electrical energy storage resources have no interaction with the gas network and gaseous energy storage facilities have no interaction with the electric network. Therefore, the gas grid location for electricity storage units (and the electric power grid nodal location specified for gas storage units)

Electricity generators					
Technology	Electricity node	Gas node	Unit size [MW]	Existing units	Max. new unit expansion (annual/total)
Natural gas CT	1	1	50	10	2/100
Coal	1	1	200	1	0/0
Natural gas CT	2	1	50	10	2/100
Coal	2	1	200	1	0/0
Natural gas CC	7	19	100	10	1/100
Natural gas CC	13	24	100	10	1/100
Natural gas CC	15	13	100	10	1/100
Coal	16	1	200	1	0/0
Nuclear	18	1	500	1	1/1
Natural gas CT	22	8	50	10	1/100
Coal	23	1	200	1	0/0
Solar PV	1	1	50	10	2/100
Wind	1	1	50	10	2/100
Solar PV	2	1	50	10	2/100
Wind	1	2	50	10	2/100
Solar PV	7	1	50	10	2/100
Wind	1	7	50	10	2/100
Natural gas CC-CCS	4	19	200	0	1/1
Natural gas CC-CCS	13	24	200	0	1/1
Solar PV	13	24	50	10	2/100
Wind	13	24	50	10	2/100
Natural gas CC-CCS	14	13	200	0	1/1
Solar PV	14	13	50	10	2/100
Wind	14	13	50	10	2/100
Natural gas CC-CCS	15	13	200	0	1/1
Solar PV	15	13	50	10	2/100
Wind	15	13	50	10	2/100
Solar PV	16	13	50	10	2/100
Wind	18	13	50	10	2/100
Natural gas CC-CCS	22	8	200	0	1/1
Solar PV	22	8	50	10	2/100
Solar PV	20	8	50	10	2/100

Table 2.9: Network case study configuration of electricity generation units.

Net-zero gas production units					
Technology	Electricity node	Gas node	Unit size [MW]	Existing units [no.]	Max. new unit expansion (annual/total)
Biomethane	17	5	10	0	2/10
Biomethane	23	20	10	0	2/10
Electrolytic hydrogen	14	15	10	0	4/20
Electrolytic hydrogen	9	10	10	0	4/20
Electrolytic hydrogen	17	3	10	0	4/20
Electrolytic hydrogen	23	22	10	0	4/20
Electrolytic hydrogen	2	17	10	0	4/20
Electro-methane	14	15	10	0	2/10
Electro-methane	9	10	10	0	2/10
Electro-methane	17	3	10	0	2/10
Electro-methane	23	22	10	0	2/10
Electro-methane	2	17	10	0	2/10

Table 2.10: Case study network configuration of net-zero emissions gas production units.

Electricity storage units					
Technology	Electricity node	Gas node	Unit size [MW]	Existing units	Max. new unit expansion (annual/total)
Lithium-ion battery	1	1	10	0	5/200
Long-duration H_2 storage	1	1	50	0	2/20
Lithium-ion battery	11	1	10	0	5/200
Long-duration H_2 storage	11	1	50	0	2/20
Lithium-ion battery	12	1	10	0	5/200
Long-duration H_2 storage	12	1	50	0	2/20
Lithium-ion battery	17	1	10	0	5/200
Long-duration H_2 storage	17	1	50	0	2/20
Lithium-ion battery	23	1	10	0	5/200
Long-duration H_2 storage	23	1	50	0	2/20
Lithium-ion battery	18	1	5	0	10/200
Lithium-ion battery	3	1	5	0	10/200
Lithium-ion battery	2	1	5	0	10/200
Lithium-ion battery	20	1	5	0	10/200
Gas storage units					
Technology	Electricity node	Gas node	Unit size	Existing units	Max. new unit expansion (annual/total)
Underground gas storage	1	3	1300	1	0/0
Underground gas storage	1	14	1300	1	0/0

Table 2.11: Case study network configuration of energy storage resources.

does not impact results or operational behavior. All cost and operating characteristic assumptions for these energy storage candidates are described in further detail in Section 2.4.3.

Transmission and distribution infrastructure

The gas and electric energy systems modeled here are toy systems inspired by the IEEE 24-bus network and a indicative 24-node gas pipeline network designed by [38]. For completeness, the modeled gas pipeline network topology is described in Table 2.12 and the modeled electric grid topology is described in Table 2.13.

Origin node	Terminus node	Diameter [m]	Length [m]	Friction factor	Max compression ratio [MPa/MPa]
1	2	0.9144	100	0.01	2
2	3	0.635	30	0.01	1
3	4	0.635	5	0.01	2
4	5	0.635	15	0.01	1
5	6	0.635	10	0.01	1
5	7	0.635	5	0.01	1
7	8	0.635	10	0.01	1
2	9	0.9144	5	0.01	2
9	10	0.9144	60	0.01	1
10	11	0.635	5	0.01	1
11	12	0.635	8	0.01	1
11	13	0.635	6	0.01	1
10	14	0.9144	80	0.01	1
14	15	0.9144	10	0.01	2
15	16	0.9144	20	0.01	1
16	17	0.635	3	0.01	1
17	18	0.635	6	0.01	1
16	19	0.635	5	0.01	1
15	20	0.9144	40	0.01	1
20	21	0.9144	5	0.01	2
21	22	0.9144	20	0.01	1
22	23	0.9144	5	0.01	1
23	24	0.9144	16	0.01	1
22	25	0.635	8	0.01	1

Table 2.12: Case study network configuration of gas pipeline interconnections.

As described in Section 2.4, the incremental cost of non-modeled electricity distribution and transmission infrastructure to serve peak demands is assumed to be \$52/kW_{peak}-year and \$21/kW_{peak}-year, respectively [155]. Fixed costs of gas distribution system maintenance are estimated based on Energy Information Administration (EIA) Form 176 filings by natural gas distribution companies [160]. Using the distribution of 2019 data across all reporting gas distribution utilities, we assume that fixed costs of gas distribution scale roughly with the number of core customers on each node.

Origin node	Terminus node	Max rated power flow [MW]	Reactance [p.u.]
1	2	175	0.014
1	3	175	0.211
1	5	175	0.065
2	4	175	0.127
2	6	175	0.192
3	9	175	0.119
3	24	400	0.084
4	9	175	0.104
5	10	175	0.088
6	10	175	0.061
7	6	175	0.061
8	9	175	0.165
8	10	175	0.165
9	11	400	0.084
9	12	400	0.084
10	11	400	0.084
10	12	400	0.084
11	13	500	0.048
11	14	500	0.042
12	13	500	0.048
12	23	500	0.097
13	23	500	0.087
14	16	500	0.059
15	16	500	0.017
15	21	500	0.049
15	21	500	0.049
15	24	500	0.052
16	17	500	0.026
16	19	500	0.023
17	18	500	0.014
17	22	500	0.105
18	21	500	0.026
18	21	500	0.026
19	20	500	0.04
19	20	500	0.04
20	23	500	0.022
20	23	500	0.022
21	22	500	0.068

Table 2.13: Case study network configuration of electricity transmission interconnections.

In this work, we assume costs of $350 per residential customer per year and $1,200 per commercial customer per year. This results in fixed costs of gas distribution C_n^{dist} equal to $20 million per year for each of the eight gas nodes which serve distribution-level demands. See Section 2.4 for further information on these assumptions.

Energy policy constraints

Emissions constraints on the electricity system decline from a loosely constrained emissions intensity of 500 $\frac{kgCO_2}{MWh}$ in 2020 to a deeply decarbonized energy system bound to 0 $\frac{kgCO_2}{MWh}$ on a net basis in 2040. A similar proportionate trajectory is followed in the gas sector from 200 $\frac{kgCO_2}{MWh}$ to 0 $\frac{kgCO_2}{MWh}$. This trajectory is modeled across 5 planning stages with interim targets as outlined in Table 2.14. Identical emissions intensity targets are imposed across both regional systems and for all sensitivity scenarios.

Emissions intensity target [kg CO_2/MWh]		
Year	Power	Gas
2020	500	300
2025	200	150
2030	75	50
2035	25	15
2040	0	0

Table 2.14: Greenhouse gas emissions intensity targets for the evaluated investment time horizon for the network case study.

Present value discounting

For all capital investments, we use a weighted average cost of capital of 7% (i.e. $\iota^{WACC} = 0.07$). The weighted average cost of capital here represents a reasonable value for this illustrative analysis [177]. In practice, each candidate generator, storage, or power-to-gas resource will have a different cost of capital based on the respective share of debt and equity financing and the level of associated technical and regulatory risk. Further, consumer investments in appliances will experience a higher discount rate than corporate investments with access to lower cost financing. In the objective function, we use a societal discounting factor of 1% (i.e., $\iota^{soc} = 0.01$), reflective of the societal value of delaying costs. Sensitivity tests can be conducted to assess the sensitivity of results to discount rate assumptions.

2.6 Results & discussion

In all computational case study scenarios, we find the optimal decarbonization investment plan includes a diverse set of renewable and low-emissions electricity generation sources. These electricity supplies are complemented by development of short duration electrical energy storage to smooth out

diurnal features in availability of weather-dependent generation. To satisfy emissions constraints in the gas sector, we find biomethane resources are developed to their fullest extent, as constrained by Eq. (2.63), and electrolytic hydrogen is blended to the maximum permissible fraction, as specified by Eq. (2.49). In addition, in all cases, net-zero emissions gas resources are allocated for consumption in the gas sector and by electricity generators. Fueling carbon-capture enabled gas-fired generators with biomethane or electro-methane results in net negative GHG emissions per unit of electricity. These arrangements are used to offset some of the emissions resulting from imperfect carbon capture efficiencies and continued use of un-captured combustion turbines during times of low renewable electricity generation.

When appliance stock co-optimization is considered alongside realistic hydrogen blending constraints, we find that direct-electrification of nearly all current gas distribution demands is a key feature of the optimized system plan for deep decarbonization. However, the pace, timing, and location of appliance investments will be determined by system-specific characteristics and will vary across geographies with different weather patterns or local network topology constraints. However, we find that misleading and structurally different investment plans can be obtained if integrated gas-electric systems are naively planned assuming a static appliance stock or ignoring infrastructural limits on hydrogen blending.

Here, we present the results of three sensitivity scenarios. In Section 2.6.1, we explore the differences between decarbonization strategies for test systems with different regional weather conditions. Next, Section 2.6.2 highlights the importance of co-optimizing the distribution of final energy demands and accounting for the natural failure and replacement cycle of existing appliance stocks. Finally, in Section 2.6.3 we explore the impact of neglecting practical infrastructure limits on hydrogen blending and acceptable gas quality.

2.6.1 Regional climate zones

Regional weather patterns shape existing gas and electricity energy demands and will affect the least-cost gas-electric system decarbonization pathway. Cost-optimal investment decisions will be affected by the degree of coincidence of gaseous energy demands with both the availability of renewable energy resources and the timing of the peak in existing electricity demands. In addition, heat pump technologies for space heating perform less efficiently in colder regions, and reliance on back-up resistance heat can create large winter peaks in electricity demand during extreme weather events.

As depicted in Figure 2.7, the Coastal Pacific system relies on a larger amount of solar capacity (paired with more investment in electricity storage). The Coastal Pacific system has significantly lower generation capacity needs overall as the electrification of gas appliances has a smaller impact on peak electricity demands. Figure 2.8 shows the week of operations that contains each system's peak hourly electricity demand. The Mountain Northwest peak happens during a winter week (week 52 of the year, from December 24 to December 31]) with low solar output which drives a large need

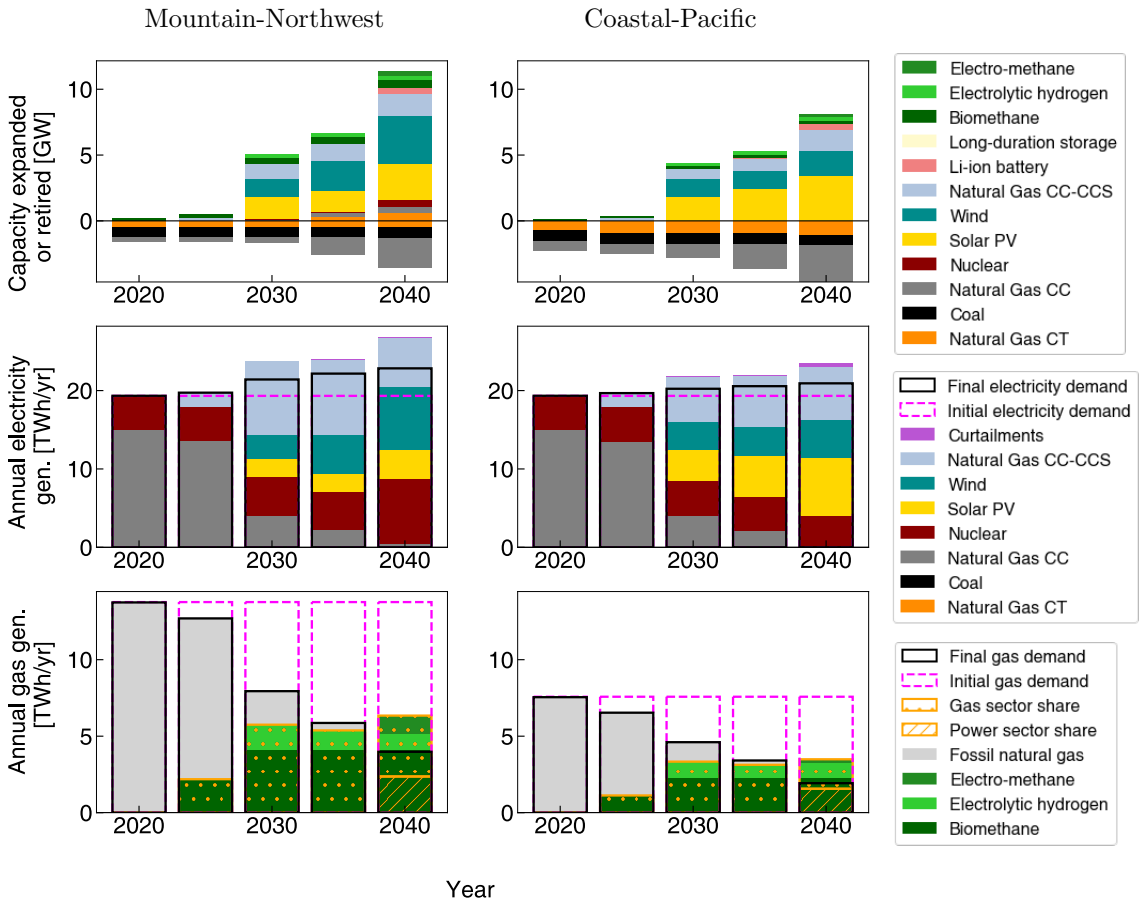

Figure 2.7: Comparative results of time-extended planning optimization of a Mountain Northwest (left) and Coastal Pacific (right) integrated energy system for capacity (top), generation (middle), and gas production (bottom).

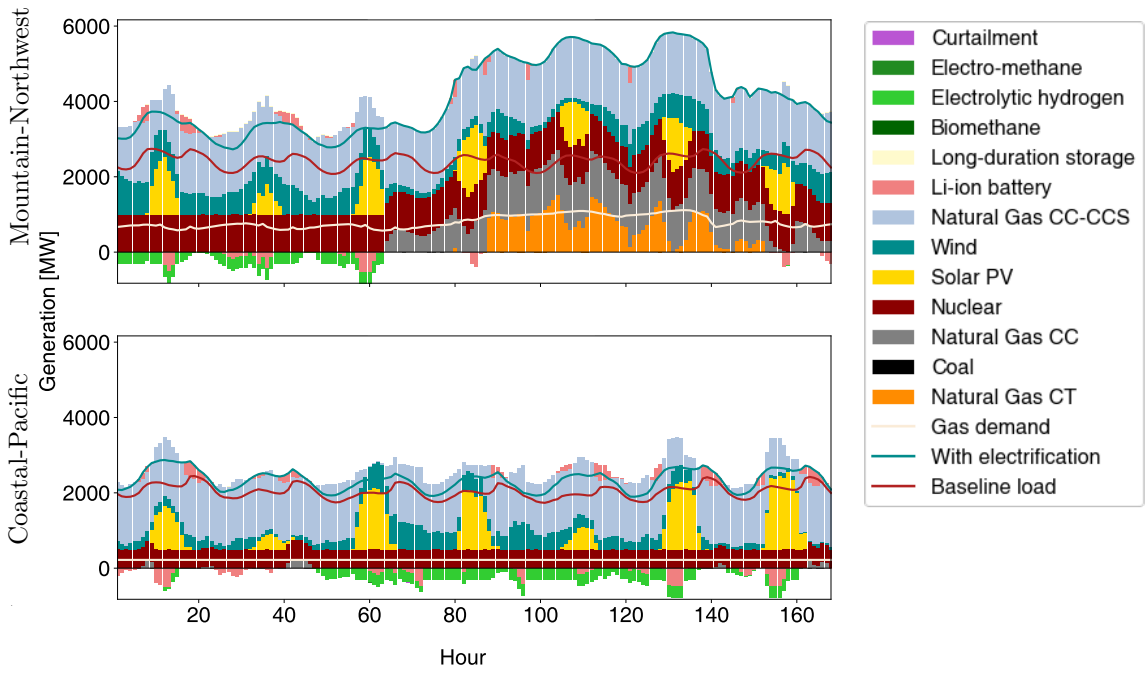

Figure 2.8: Comparative results of hourly electricity grid operations of a Mountain Northwest (top) and Coastal Pacific (bottom) integrated energy system for the week with the peak electricity demand. Results presented include appliance investment optimization. Note that the Coastal Pacific system peak occurs during the summer, when electrified gas demands are low, whereas the Mountain Northwest system peak is further exacerbated by electrification during a time when renewables output is low.

for reserve gas-fired capacity. The Coastal Pacific peak occurs during a late-summer week (week 34 of the year, from August 14 to August 21 with high solar availability and minimal appliance-level demands for space heating.

Figure 2.9 shows the appliance stock composition across the modeled investment time horizon. Here, we see that the loading order in which appliances are optimally transitioned from gas to electricity differs slightly between the two regions. In the Mountain Northwest region, cooking energy demands are the first to begin the transition, while in the Coastal Pacific region commercial space heating demands are preferentially electrified.

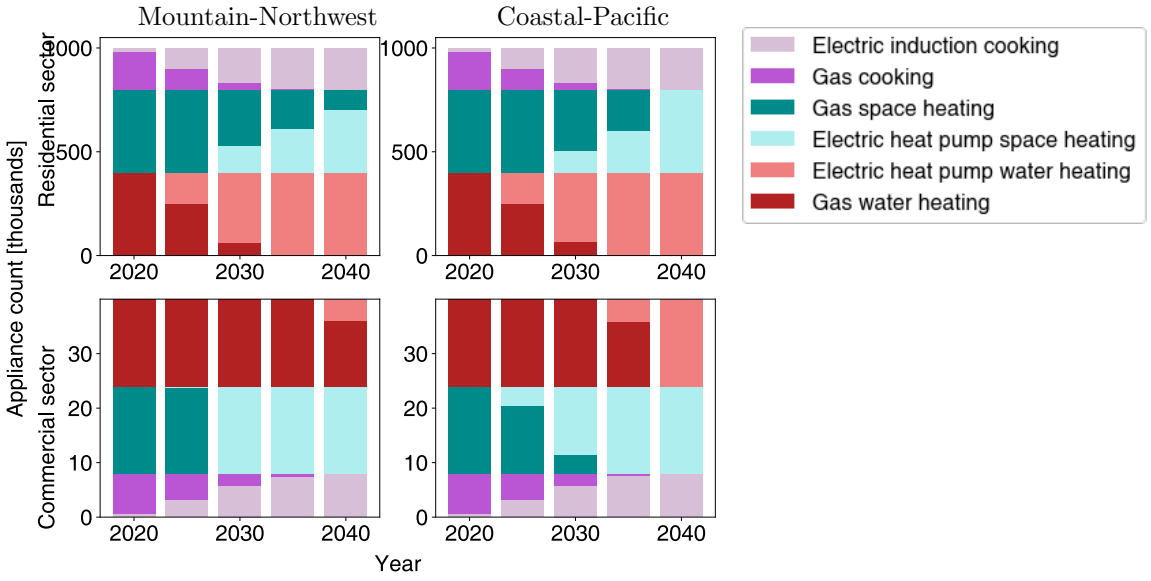

Figure 2.9: Comparative results of appliance stocks for a Mountain Northwest (left) and Coastal Pacific (right) integrated energy system. Results presented include appliance investment optimization. In both climate regions, we find appliance electrification to be a feature of optimal decarbonization pathways. However, the pace and sequencing of electrification investments differs depending on system characteristics.

Despite minor differences in the interim trajectory, we find the final appliance stock for each region is nearly identical. In both cases, the residual non-electrified demands include a portion of residential space heating demands. This could be due to a range of factors including local transmission constraints, coincidence of these energy demands with poor availability of renewable electricity generation, and/or the magnitude of capital costs relative to the potential emissions reductions.

Importantly, as presented in Figure 2.9, we find that premature retirement of some customer equipment is a component of the least-cost investment trajectory. In part, this may be because investment periods are evaluated at 5-year increments, exacerbating the step-function changes observed in the appliance stock. However, this result is indicative of the kinds of energy demands

that may be cost-effectively transitioned without waiting for emergency replacement at end-of-life. In the both climate cases, we find residential water heating demands and commercial space heating demands are preferentially electrified through premature retirements. However, a significant share of customer equipment continues to leverage the gas system until fairly stringent emissions intensity constraints begin to bind (and lower-cost net-zero gaseous fuel options have been fully exploited).

The pace and magnitude of appliance electrification specified by a central planner optimization can be highly sensitive to system-specific characteristics. This case study presents just one result of how the proposed modeling framework can jointly consider this array of factors endogenously and alongside all other candidate decarbonization technologies.

2.6.2 Appliance investment planning

Central planning of appliance investments allows for optimized allocation of final energy demands across energy carriers. Constraining the program to replace appliances on a persistence basis illustrates how systems may be naively planned based on the current distribution of customer equipment. In these comparative scenarios, we find the magnitude and composition of the least-cost resource mix changes depending on whether the appliance stock can be shifted across energy carriers to satisfy emissions constraints at lower cost, as present in Figure 2.10.

Under persistence appliance stock assumptions, we find gigawatts of electrolytic hydrogen and electro-methane units are developed to convert clean electricity to gaseous fuel for residential and commercial demands. This scenario retains the smallest amount of flexible thermal generation capacity, retiring all legacy generators and building the least new gas-fired generation capacity. In this system, power-to-gas units satisfy the role of dispatchable electricity generators to integrate gigawatts of variable renewable energy generators. Power-to-gas units ramp flexibly to ensure demand does not exceed supply, while satisfying all gas demands on a daily basis. This dynamic operation of power-to-gas conversion and injection into the pipeline system is observed in Figure 2.11. Future work should consider more detailed modeling of transient features in gas system operations to ensure the planned system can be feasibly operated. A combination of on-site gas storage tanks and system line-pack management will likely accommodate this flexible behavior, albeit at incremental cost.

With appliance investment optimization permitted, we find the optimal system plan shifts most final energy demands to the electricity system to reduce the amount of net-zero emissions gas production required. This results in a decreased need for generation capacity, even as final electricity demand increases due to appliance electrification. We observe more fossil fuel capacity investments in this case to satisfy electricity demand during times of low renewable energy output. Notably, some production of electro-methane for direct consumption remains a component of the least-cost resource mix. This result indicates that, despite the poor conversion efficiency of power-to-gas relative to direct electrification, the incremental fixed cost of some appliance electrification may outweigh any operational savings. This result also highlights the gas system's potential dual value as an energy

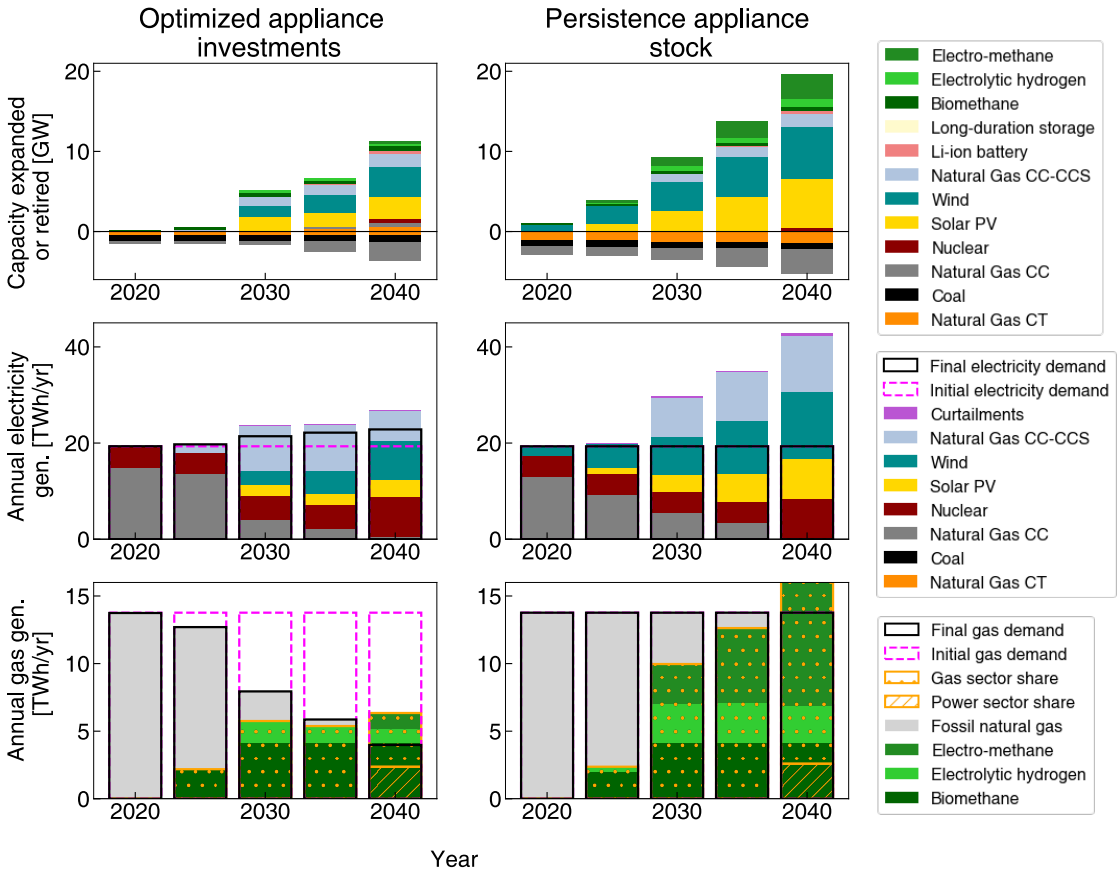

Figure 2.10: Comparative results of time-extended planning optimization of a Mountain Northwest energy system with co-optimized appliance investments (left) and persistence appliance investments (right) for capacity (top), generation (middle), and gas production (bottom). Naive system planning, assuming static appliance populations, results in substantially larger generation and electrofuels production capacity to supply residential and commercial gas demands with net-zero emissions energy.

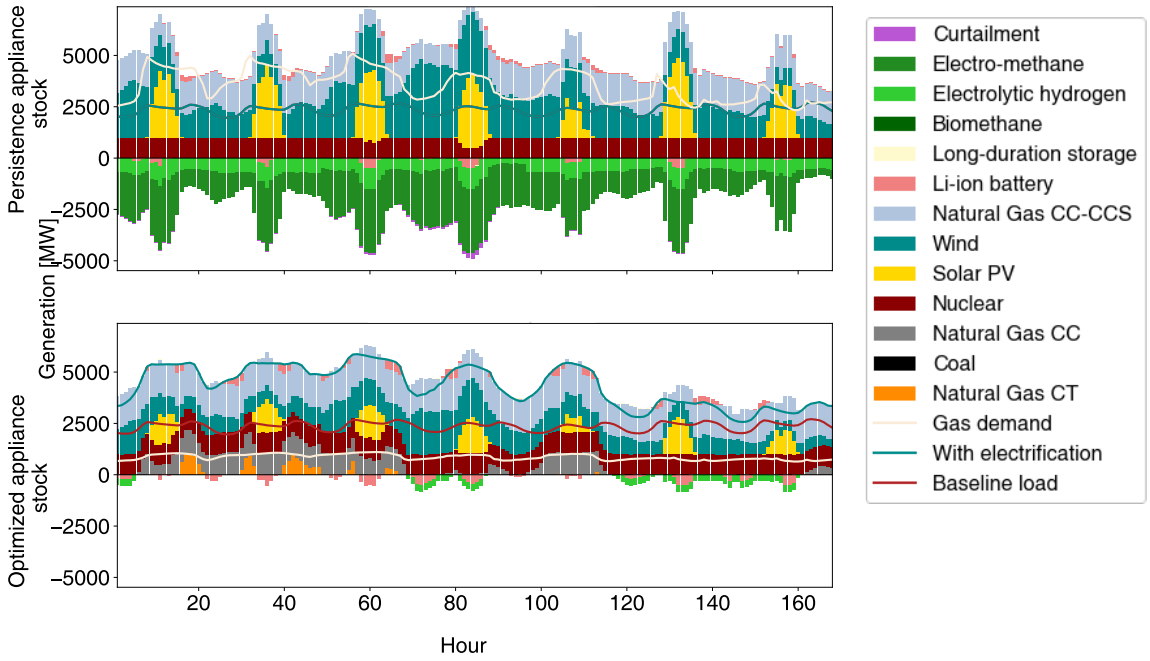

Figure 2.11: Hourly dispatch for a simulated week of operations during a typical winter week (week 6 of the year, from February 13 to February 20) in a Mountain Northwest integrated energy system for the two appliance-investment scenarios explored. Note that electro-methane units are operated flexibly throughout the day to integrate intermittent renewable energy supplies, serving a similar role that firm generation capacity does in the case with co-optimized appliance investments.

transmission and energy storage asset. The flexibility to balance gas demands with less granular temporal resolution (relative to electricity demands) allows the gas delivery network to double as a short-duration storage resource for renewable electricity, converted to electro-fuels.

The volume of net-zero gaseous fuels, as presented in the bottom panel of Figure 2.10, is determined by the share of gas demands that are electrified, the quantity of non-electrifiable direct-use gas demands, and the amount of net-zero emissions gas needed for use in the electricity sector. We find that biomethane resources are developed to their fullest extent in all decarbonization scenarios. We also find that net-zero emissions gases are routinely allocated for nominal consumption across both the power and gas sectors. Nominal use of biomethane or other climate-neutral fuels in carbon capture-enabled generators allows for negative emissions that offset some utilization of uncaptured gas-fired plants and imperfect carbon-capture efficiencies. An important contribution of the proposed modeling framework is the endogenous evaluation of this cross-sector economic tradeoff between allocating available net-zero emissions fuels to the power or gas sector. Here, we show that even as the system relies on electro-methane, there is sufficient value in the power sector to allocate net-zero emissions gas for use in thermal generators rather than substituting this capacity with additional renewable electricity generators.

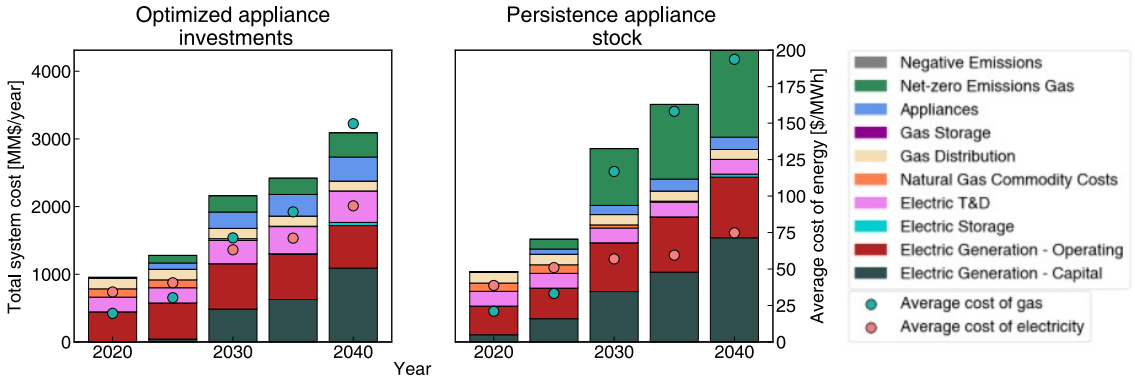

Figure 2.12: Total system costs and average costs of delivered energy for each modeled investment year for optimized appliance stock assumptions (left) and persistence appliance stock (right). In the persistence appliance stock case, total system costs are increased due to a large need for expensive electro-fuels to satisfy residential and commercial gas demands. These costs are avoided in the optimized appliance stock case through centrally-planned electrification of gas appliances. Note also that average costs of delivered gas increase 5-fold across the transition (in both cases for different reasons) due to more expensive net-zero emissions gas supplies (left) and declining total gas deliveries across which to recover fixed costs (right).

Examining the total system costs in Figure 2.12, we find that the persistence appliance stock case has larger system costs primarily because of the costs of net-zero emissions gas. When the appliance stock is co-optimized, the costs of net-zero emissions gas generation units and the electricity generation capacity necessary to produce these electro-fuels are reduced through appliance

electrification. These savings exceed the countervailing increase in appliance costs and transmission and distribution infrastructure costs on the electricity grid.

As highlighted in Figure 2.12, recovering fixed costs of gas distribution system maintenance, operation and re-investment across declining gas deliveries produces an upward spiral in the average cost of gas. If these costs are recovered entirely through volumetric rates, it is possible that this spiral in gas rates will drive further defection from the gas distribution system, even if such a result is sub-optimal from a societal cost perspective. As shown in Figure 2.9, gas appliances may continue play a large role in serving space heating, water heating, and cooking demands until stringent emissions intensity standards are in place on the gas sector.

The presented cost-minimization illustrates a practical approach to centralized planning of decarbonized integrated gas-electric energy systems. However, in practice, appliance investment decisions will be made by a heterogeneous set of agents based on a confluence of economic incentives, regulations, and consumer preference. The total societal costs will be allocated across and borne by gas ratepayers, electricity ratepayers, and appliance-purchasing consumers. The allocation of societal costs across different welfare-maximizing agents could produce a realized trajectory that confounds the societal cost-minimizing plan. Future work should aim to examine approaches to cost-allocation and rate-making that align the central planner solution with the welfare-maximizing behavior of individual customers.

2.6.3 Gas quality and hydrogen blending

The introduction of pure hydrogen to natural gas infrastructure is one strategy to reduce the GHG emissions intensity of gaseous fuel delivered to customers. However, gas interchangeability limits generally apply to end-use equipment and materials integrity concerns exist for high-pressure transmission, compression, and distribution equipment. Limited blends of hydrogen may be acceptable, however the particular location and timing of such injections is important for ensuring safety of downstream equipment. Here, we illustrate how relaxations in such gas quality constraints can lead to different strategies for multi-sector decarbonization planning.

In Figure 2.13, we show that when no constraints are included on hydrogen blending, the least-cost decarbonization trajectory includes a large reliance on electrolytic hydrogen. This solution limits electrification of end-use appliances, displacing less than 30% of initial gas demand with electric alternatives. This indicates that transitioning to energy infrastructure systems that can accommodate high hydrogen fractions could provide system value in a decarbonized gas-electric energy system (if savings exceed the incremental cost of compliant infrastructure).

The reliance on direct-use of blended hydrogen drops sharply when annual blend limits are included at the system-level (see Figure 2.13 center). The level of centrally-planned electrification in this case resembles that of the fully-constrained scenario with daily, spatially-resolved hydrogen blend limits imposed. In the fully-constrained case (see Figure 2.13 right), we find the largest amount

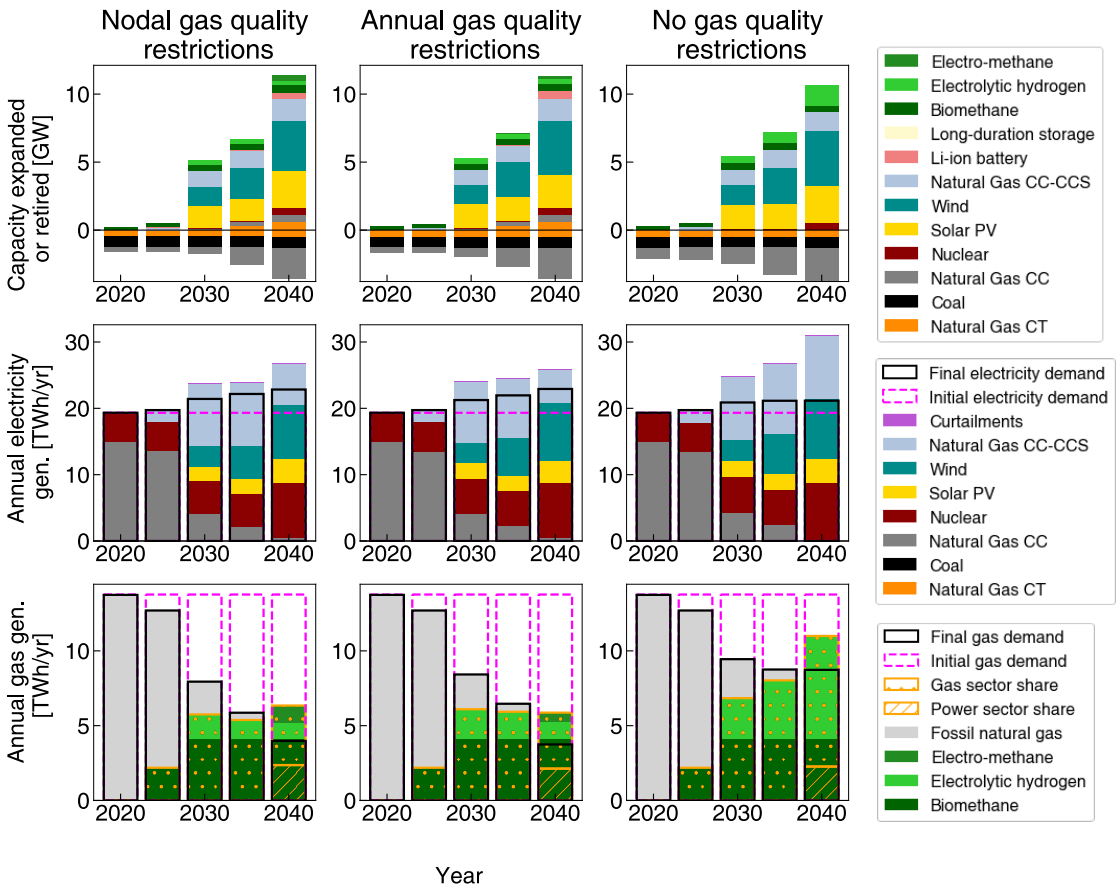

Figure 2.13: Comparative results for increasing degrees of hydrogen blend limits ranging from fully-constrained hydrogen blending (left), to hydrogen blend fractions constrained on an annual, system-wide basis (center), to un-constrained introduction of hydrogen (left). Results presented for a Mountain Northwest integrated energy system with appliance investment optimization for capacity (top), generation (middle), and gas production (bottom).

of electro-methane is required to satisfy gas quality limits as hydrogen blending is further limited.

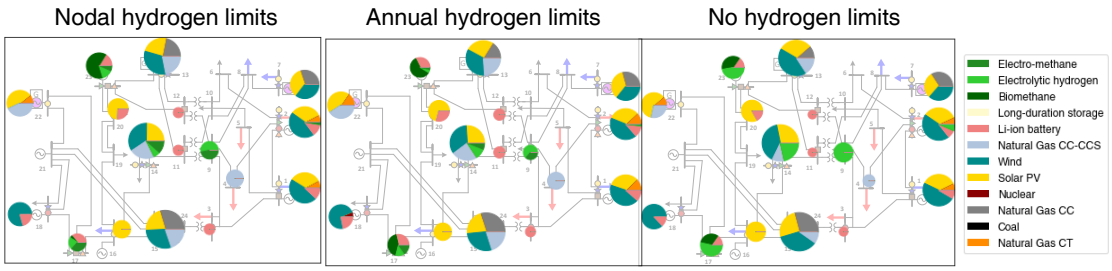

Figure 2.14: Spatial allocation of capacity development in 2040 for three different approaches to hydrogen blend limitations. Note that as we move from fully-constrained hydrogen blending (left) to annual, system-wide blend fraction constraints (center) we see the spatial distribution of electrolyzer capacity expansion shift towards from the most advantageous locations on the electricity system as the gas quality constraints no longer retain the nodal limits. As we further loosen the system constraints to unlimited hydrogen blends delivered (right), we observe significant increases in electrolyzer capacity development as a smaller share of appliances are transitioned to the electricity system.

In addition, the proposed model can identify the spatial distribution of least-cost expansion investments and how these decisions are altered by constraints such as hydrogen blend limits. The availability of clean electricity will be geographically concentrated in regions with large supplies of low-cost renewable electricity generators. However, just as transmission constraints may exist on the electricity grid, similar constraints are likely to limit the large-scale conversion of clean electricity to hydrogen for blending directly into the transmission network due to local constraints on concentration.

In Figure 2.14 we see that the unconstrained hydrogen blending case develops large electrolytic hydrogen capacity in the most advantageous locations on the electricity transmission network. Incorporating annual, system-wide blend limits (see the center panel of Figure 2.14), we find electrolytic hydrogen generation capacity decreases significantly paired with increased expansion of other local biomethane or electro-methane production capacity. However, in the most constrained case (left panel of Figure 2.14), using spatially-resolved, daily hydrogen blend limitations, we find that while the most cost-effective or technically-favorable nodes see decreased investment in capacity for electrolytic hydrogen generation, other nodes see slight increases to allow for distributed injection accounting for the technical limitations of the gas network to accept hydrogen.

Future work should leverage models like this to further explore the system design space in order to identify the potential role for gas system infrastructures that can accommodate high-blends of hydrogen. Omitting gas quality constraints entirely (i.e., assuming full interchangeability) produces a least-cost solution that relies heavily on direct blending of hydrogen and entails significantly less planned electrification of core gas demands. Future work could compare the associated cost of

upgrading downstream infrastructure to permit such hydrogen blends to the savings of relying on less expensive electrolytic hydrogen as compared to drop-in synthetic electro-methane fuels or direct appliance electrification.

2.7 Conclusions

As policymakers and businesses contend with the growing threat of climate change, energy providers require new techniques and strategies for reducing the net GHG emissions of the gas and electricity resource mix. Here, we propose a practical approach for co-optimized system planning of integrated gas-electric energy systems. This novel formulation extends previously-published methods for coordinated expansion planning and operations, with an enhanced focus on modeling the multi-period transition trajectory, subject to legacy infrastructure limitations and successively tightened constraints on GHG emissions. We demonstrate this method for an indicative gas-electric system subject to sector-specific GHG emissions constraints under a range of sensitivity cases.

We find that direct-electrification of nearly all current gas distribution demands is a core component of the optimized system plan for achieving deep decarbonization. However, we find that misleading and structurally different investment plans can be obtained if integrated gas-electric systems are naively planned assuming a static appliance stock or ignoring infrastructural limits on hydrogen blending. In appropriately constrained problems, the incremental costs of electric appliances and any associated electricity system infrastructure are smaller than the additional costs of electro-fuels production to serve the legacy gas appliance population. However, the pace, timing, and location of appliance electrification is determined by system-specific characteristics and can vary across geographies with different weather patterns or local network topology constraints.

Notably, electro-methane production is included in the cost-optimal investment plan prior to full electrification of residential gas demands. This indicates that in some cases, despite the poor conversion efficiency of electro-fuels (relative to direct electrification), the incremental fixed costs of marginal appliance electrification may outweigh any operational savings. Finally, in all computational case study scenarios we find net-zero emissions gas resources are allocated for consumption by power sector entities, indicating the value of biomethane and electro-fuels to provide firm net-zero emissions electricity generation, offsetting net emissions from imperfect carbon capture efficiencies and un-captured combustion turbines. It is important that future work on gas system decarbonization incorporate such cross-sector competition for limited sustainable net-zero emissions gaseous fuels.

Finally, we observe that in all cases, the transition to a decarbonized energy system entails a nearly 5-fold increase in the average costs of delivered gas. This arises due to some combination of increased reliance on expensive electro-fuels for net-zero emissions gas supply and the declining volumetric deliveries as gas appliances are transitioned to the electricity system. The allocation of

societal costs across different welfare-maximizing agents could produce a realized trajectory that confounds the societal cost-minimizing plan. Future work should aim to examine approaches to cost-allocation and rate-making that align the central planner solution with the welfare-maximizing behavior of individual customers.

The proposed modeling framework will accommodate a number of future investigations. The sector-specific emissions constraint formulations will allow for study on the consequences of resource limitations in sustainable bio-energy for optimal allocation across the power and gas sectors. In addition, the approximate gas component tracking will allow future work to elucidate the role of hydrogen blending for direct-use in pipeline systems. Finally, we note that planning decisions at the consumer equipment-level are not made by a central planner, but by a series of agents with economic incentives and personal preferences. Future analysis should leverage sequential or iterative optimization routines to incorporate agent-based decision-making respective of evolving volumetric rates for delivered gas or electricity. This study represents a first step towards practical system planning of cost-effective, safe, and reliable integrated energy systems under strict greenhouse gas emissions constraints.

2.7.1 Future model extensions

We recommend several model extensions to support future analysis of least-cost emissions mitigation in integrated gas-electric energy systems.

Gas component tracking and quality In general, more robust formulations for gaseous fuel component and attribute tracking may be necessary for analysis of multi-fuel systems with higher blends of hydrogen or other non-methane gases.

The climate impacts of non-CO_2 pollutants should be accounted for in future analyses. Methane leakage from gas distribution systems will account for a larger share of life-cycle GHG emissions as supply portfolios shift towards net-zero emissions gaseous fuels [176]. Further, as total throughputs decline, it is possible that natural gas leakage quantities will grow as a share of total gas produced and procured. Depending on the leak mechanism, maintaining a network of pipelines at pressure may result in a fixed leakage rate that is only a weak function of total deliveries. However, calculating the GHG impacts of leakage most carefully will require more rigorous component-tracking formulations to differentiate the climate impact of hydrogen relative to methane or other non-methane components.

In addition, the current modeling approach is not highly-resolved enough to account for the impact of hydrogen blends on the operation and carbon capture-rate of gas-fired generators with post-combustion CCS technologies. However, such model functionality will necessarily introduce non-linearity as the variable carbon content of fuel delivered will be multiplied by the total fuel consumed to compute the gross emissions from a gas-fired generator. In Appendix A.4 we present a

preliminary model formulation extension to account for the well-mixed mole-weighted attributes of gas delivered at various locations on the network.

Planning under uncertainty Accounting for low probability, high-impact events will be of importance as the costs of such events can be astronomical. In particular, as we model the prospective retirement or shut-down of gas distribution systems.

The maintenance and re-investment in gas distribution systems may represent a stranded asset and a sunk cost. However, it also represents a hedge against an uncertain future that may include higher costs renewable electricity due to transmission constraints, and lower-cost negative emissions technologies for carbon removal offsetting continued use of fossil fuels.

A 1 in 100 year weather event, despite it's low frequency, can alter the total system cost minimizing solution if the expected costs (economic and otherwise) of not having redundant energy infrastructure during such tail events are disproportionately large. Future work on gas-electric systems planning optimization should consider strategies to plan under uncertainty to account for low-probability, extreme events.

Exploring liquefied gaseous fuel alternatives Redundant energy delivery infrastructure systems can provide immense value during power system failures. However, the total energy throughput by such back-up energy systems will be small, with very high levelized costs of energy delivered. For such systems, the primary variable of importance is the fixed costs of system investment and maintenance.

It is possible that existing gas distribution systems provide a low-cost alternative for peak-shaving and improving distribution system resiliency. Hybrid gas-electric appliances for space or water heating can switch fuels to continue providing service during power outages, or during times of scarcity in the electricity sector. However, hybrid liquefied petroleum gas (LPG)-electric appliances may offer identical resiliency and reliability benefits as gas-electric hybrids without requiring the maintenance and re-investment in an expansive (but low-throughput) gas pipeline system. Bio-LPG and electro-LPG will rely on the same feed-stocks as biomethane (from gasification sources) and electro-methane and may be produced at similar cost and complexity [142]. Future work may consider introducing distributed LPG alternatives as a means to satisfy resiliency objectives and offer flexibility during times of scarce renewable electricity generation.

Practical case studies The proposed model formulation should be put into practice for realistic case studies of integrated gas-electric utilities or regions. As highlighted in Section 2.4, it can be challenging to generate realistic data sets for gas and electricity infrastructure at meaningful resolution due to security concerns and practical availability of data. However, even coarse study of particular geographies and climate zones may elucidate the circumstances that support a future for the gas distribution utility in a net-zero emissions energy system.

Model formulation extensions may be required to allow for more robust accounting of greenhouse gas emissions liabilities for the practical set of gaseous energy end-uses. Specifically, combined heat and power (CHP) facilities represent a key aspect of integrated gas-electric energy systems that are not fully accounted for in the proposed modeling framework. Specifically, partitioning the cross-sector emissions liabilities of a combined heat and power facility is a non-trivial accounting exercise. However, this is of great importance as CHPs can account for a large share on gas demands delivered to large commercial customers such as universities, hospitals, and other campuses. Accounting for these gas deliveries and emissions liabilities in the above framework is challenging. Electrification of the heat demands served by a CHP will also similarly increase electricity demands by an amount equal to the power that was produced on-site from gas combustion.

Additional model formulation updates may be necessary to characterize each technology vintage with different operational attributes, such as energy efficiency or fixed maintenance costs. Here, we have collapsed all technology vintages into singular technology classes with uniform operating attributes. This allows for substantive reductions in the number of decision variables required for the computationally intensive stock-rollover simulation and optimization. However, for novel technologies with quickly changing operating parameters, it may be prudent to include expanded vintaging of equipment populations.

Lastly, future work should account for the realistic appliance adoption decisions made by private actors that are not directly subject to the regulatory commission jurisdiction. The central-planner optimization formulation is only useful inasmuch as it reflects a reality where a central regulatory commission may approve or deny investment plans of regulated entities. However, for investment decisions that lie outside of this scope, we must consider the interactions between the central-planner solution and a welfare-maximizing behavior of unregulated entities. For appliance investment decisions by private consumers, this is traditionally a parameter specification subject to sensitivity testing. In Appendix Section A.6 we present characteristics of a preliminary model formulation for endogenous evaluation of cost-allocation and rate-making strategies.

Chapter 3

Molten-media pyrolysis design optimization

3.1 Introduction

As noted by the 2018 Intergovernmental Panel on Climate Change (IPCC) special report on global warming of 1.5 °C, net economy-wide greenhouse gas (GHG) emissions must decrease to levels near zero by mid-century to minimize risk of catastrophic environmental and economic damages [181]. According to the International Energy Agency, carbon dioxide (CO_2) emissions from the industrial sector reached 24% of global emissions in 2017 [182]. Therefore, substantial reductions in industrial sector CO_2 emissions are required in order to mitigate climate change.

There are multiple technically feasible options for decreasing emissions from the industrial sector. One option is the use of CO_2-capture technologies to separate and permanently sequester CO_2 produced from combustion of fossil fuels. However, the economics of operating these technologies at small scale is challenging and retrofits are costly. The Global CCS Institute produces estimates for the costs of CO_2 avoided for a variety of CCS use-cases. For large-scale, post-combustion capture for a natural gas fired generator, estimated costs are \$89/tonne CO_2 avoided [183].

Another option for decreasing emissions from some segments of the industrial sector is fuel-switching to a low-carbon fuel such as hydrogen (H_2) or leveraging low-carbon H_2 for industrial processes. H_2 can be produced from steam methane reforming (SMR) combined with CCS (SMR-CCS) or from water electrolysis. Recent academic work has estimated abatement costs for SMR-CCS to be \$100/tCO_2 and for electrolysis from zero emissions electricity sources to be above \$500/tCO_2 at scales of 100 kilotonnes per year (kt/y) [184].

Regulatory policies have been introduced to motivate the development of emissions mitigation projects. In support of CCS, the United States adopted the 45Q tax credits that increased incentives

for CCS at industrial facilities, providing as much as $50/tonne of carbon dioxide placed in permanent geologic sequestration [185, 186]. However, this incentive may not be sufficient for gigatonne scale deployment of CCS technology [187]. Another supporting policy is the Low Carbon Fuel Standard (LCFS) program in California, which has provisions to award credits for the use of renewable H_2 and incorporation of innovative, emissions reduction technologies at oil refineries to reduce the carbon intensity of the transportation sector [188].

One emerging technology for emissions reduction is methane pyrolysis. Methane pyrolysis can be used before combustion to split methane into solid carbon – which can be sequestered or used – and an H_2-rich gas that could be used in combustion applications or for chemical processes (e.g. hydrotreating in oil refineries). Prior work on methane pyrolysis used solid catalysts to cause the endothermic reaction to proceed at industrially feasible rates, however deposition of solid carbon can quickly deactivate a solid catalyst [189]. One solution to this challenge is to use a bubble column as the reaction environment, with a molten media providing an efficient heat transfer medium and acting as a catalyst [190]. The generated carbon floats to the surface as a fine solid, avoiding deactivation of the catalyst. This solid carbon can be transported to sites for permanent sequestration or sold as a manufacturing feedstock. This could provide a flexible supply chain of carbon that could serve a wide array of use cases. Further, this process may be applicable to a wider range of scales because it is a comparatively simple process with a single vessel and disposal of the product does not require a high-pressure pipeline network (i.e., solid carbon can be stockpiled and disposed at will).

In this work we evaluate the technoeconomic performance of a catalytic molten-media methane pyrolysis systems via optimization of the energy system design. That is, we do not perform technoeconomic analysis of a few set cases, but instead optimize high-level chemical process models of the system to understand the technoeconomics of an optimal configuration. Using these results, we provide insight regarding how methane pyrolysis might compete economically with other options for reducing industrial emissions in two specific use cases: fuel-switching at distributed combustion applications and substitution for conventional sources of H_2 in oil refining. While engineering challenges remain regarding the high temperature separation of solid carbon from molten metals, purity and microstructure of solid carbon for resale, and minimization of operational losses of the catalyst, our work demonstrates at a high level that further research and development in these areas may be warranted.

This work has been previously published in [21].

3.2 Background

Many technologies exist for the capture of carbon dioxide from flue gas streams. Capture mechanisms generally fall into one of four categories: absorption, adsorption, cryogenic distillation, and

membrane separation. After capture, CO_2 is compressed to supercritical conditions and transmitted via pipeline to sites for permanent geologic sequestration. Costs of CO_2 transmission exhibit significant economies of scale due to the large fixed costs of building pipelines [191]. In addition, the large fixed capital costs of separation and purification equipment raises questions about the economics of CCS operation at smaller, distributed scales. Enhanced oil recovery has provided the largest market to date for captured CO_2. Some proposals for net-zero-emissions energy systems of the future include a carbon-neutral fuel produced from captured CO_2 [4]. However, the options for carbon utilization have been limited in the past by the low-energy state of CO_2. Any value-added chemical product will require substantial energy inputs.

Some industrial sector emissions can be attributed to emission of CO_2 from material processing. For example, between 50-60% of CO_2 emissions from cement production result from the calcination of calcium carbonate to calcium oxide [192, 193]. Additionally, the iron and steelmaking industry accounts for 31% of industrial emissions, with a substantial portion of these emissions coming from reduction of metal oxides with use of metallurgical coke [194]. However, much of the remainder of industrial sector emissions are a consequence of combusting carbon-based fuels for heat and power generation. In the United States over half of 2017 GHG emissions attributed to the industry sector were a consequence of fossil fuel combustion [195]. In oil refineries approximately 65% of CO_2 emissions are from fired heaters and boilers [196], and the largest emission source in the pulp and paper industry is fired boilers [197]. As such, a nontrivial portion of GHG emissions from the industrial sector could be mitigated by fuel-switching to low-carbon fuels such as hydrogen.

There are a variety of chemical processes by which H_2 could be produced for fuel-switching in industrial energy applications [198]. Fossil-based pathways use natural gas as a principal energy feedstock to produce H_2 while power-to-gas pathways leverage electric power as the primary energy input to generate H_2 by splitting water molecules. The most common commercial H_2 production method is steam methane reforming (SMR).

SMR is a two-step process consisting of the catalytic decomposition of methane into carbon monoxide (CO) and hydrogen (H_2) followed be the water-gas shift reaction converting the CO into CO_2 and H_2. The methane decomposition is endothermic, requiring 206 kJ/mol CH_4 while the water-gas shift is slightly exothermic, yielding 41 kJ/mol CO. On net, this set of reactions will yield 4 moles of H_2 for every mole of CH_4 and require 41 kJ/mol H_2 produced along with energy for separation and heat exchange. However, in a carbon constrained future, SMR facilities would need to be outfitted with CCS in order to mitigate CO_2 emissions associated with the produced H_2.

$$CH_4 + H_2O + 206 \text{ kJ} \longrightarrow CO + 3H_2 \tag{3.1}$$

$$CO + H_2O \longrightarrow CO_2 + H_2 + 41 \text{ kJ} \tag{3.2}$$

An oft-suggested alternative is water electrolysis wherein an electric current is used to split water molecules into H_2 and oxygen (O_2). While this can provide emissions free H_2 if electricity inputs are from zero-carbon sources, it is also a thermodynamically-unfavorable reaction, requiring 235 kJ/mol H_2 produced. Further, due to the substantial energy inputs, if the electricity consumed is not 100% emissions-free, the carbon intensity of H_2 from electrolysis can rival and exceed that of SMR.

$$H_2O + 235 \text{ kJ} \longrightarrow H_2 + \frac{1}{2}O_2 \tag{3.3}$$

Methane pyrolysis is a chemical process where the carbon is stripped from the methane, yielding gaseous H_2 and solid carbon. This reaction is endothermic, requiring 75 kJ/mol CH_4, and produces two moles of H_2 from every mole of methane, thus requiring 37.5 kJ/mol H_2. Energy inputs for pyrolysis could be provided through combustion of methane, releasing 0.05 mol. CO_2/mol. H_2 (assuming 85% LHV efficiency). Alternatively, produced H_2 could be combusted to provide a self-sustaining auto-thermal process, however this requires combustion of 18% of produced H_2 to sustain the reaction.

$$CH_4 + 75 \text{ kJ} \longrightarrow 2H_2 + C \tag{3.4}$$

However, pyrolysis technology traditionally involves a solid catalyst which can become deactivated over time via deposition of carbon on the catalyst surface. The catalyst must be regenerated [199], typically by oxidizing the carbon, which yields CO_2 emissions and imposes additional costs. Solid catalyst deactivation through sintering and unwanted solid-state reactions between the metallic catalyst and the oxide support at elevated temperatures also occur [200, 201]. One technology that may solve the some of the challenges associated with conventional methane cracking is using liquid metals or salts as the heat transfer medium and reaction catalyst.

In 1930, Tyrer patented a continuous process for producing hydrogen via decomposition in a molten iron bath, introducing air into a separate, but connected, chamber to oxidize the carbon and fuel the endothermic pyrolysis reaction [202]. More recently, Steinberg proposed the use of a liquid metal bubble column to facilitate the thermal decomposition of methane into hydrogen and solid carbon [203]. Serban et al. conducted several experiments of methane cracking in molten tin and lead baths, and Paxman et al. investigated the use of solar thermal energy to fuel a molten media methane pyrolysis reactor [204, 205]. A transient bubble-scale model was built to simulate the reaction kinetics and identify the residence time required for a desired methane conversion [205]. Similarly, Zheng and Xu conducted thermodynamic analysis of a system for hydrogen production via solar thermally heated liquid metal methane pyrolysis [206]. Catalan and Rezaei presented a novel

treatment that couples empirical hydrodynamic models from the literature with an equilibrium-constrained kinetic model for non-catalytic methane decomposition [207].

Researchers at the Karlsruhe Institute of Technology have conducted a variety of experiments and analyses of methane pyrolysis [189, 199]. Plevan et al. model methane decomposition with a first order reaction kinetic and compare this to their experimental results [208]. Geißler et al. conducted additional experiments on a liquid tin bubble column reactor with a packed bed and find maximum hydrogen yields of 78% [209, 210]. Finally, Postels et al. published a life cycle assessment of H_2 produced via liquid-metal technology suggesting that methane cracking technologies could realize 64% emissions reductions relative to steam methane reforming [211]. However, these non-catalytic processes require longer residence times, requiring either a larger reactor volume or lower CH_4 conversion rates.

Upham et al. conducted the first experiments using liquid metal catalysts alloyed with low melting temperature metals in order to convert methane into hydrogen and solid carbon [190]. The characterization of the kinetics of reaction provide important data points for system-level analysis. Utilizing an alloy of nickel (Ni) and bismuth (Bi), the authors observed methane conversion exceeding 95% at 1050 C [190]. Parkinson et al. present a technoeconomic analysis of a system such as this for comparison with steam methane reforming and electrolysis for industrial hydrogen production [184, 212]. Recent experimental work has demonstrated that molten salts (such as MnCl2-KCl) can similarly act as catalysts for CH_4 pyrolysis [213]. This study found high H_2 selectivity and CH_4 molar conversion efficiencies exceeding 40% with small residence times [213]. Other efforts to model molten media methane pyrolysis reactors have employed a membrane bubble column reactor model, identifying ultra-high conversion of CH_4 and separation of H_2 before the bubbles reach the top of the reactor [214]. This reduces any metal losses that may be observed by vaporization. Molten salts have also been used on top of molten metals to reduce metal loss [215].

Some industrial processes may not be well-suited for traditional CO_2 capture techniques. Thus, at the intersection of CO_2 capture and fuel-switching lies a methane pyrolysis process that produces H_2-rich fuel gas to be used in industrial boilers and burners or as a direct substitute for more carbon-intensive H_2 feedstocks. Capturing the solid carbon also provides a material feedstock that could serve multiple markets. This work presents a novel coupled hydrodynamic and kinetic model formulation for a catalytic molten-media methane pyrolysis system. Leveraging this model, we use optimization to evaluate the project economics of a molten-media methane pyrolysis technology and illustrate how this technology may compare with more conventional options for decarbonizing industrial energy services.

3.3 Methods

3.3.1 Modeling molten media methane pyrolysis

To analyze the technoeconomics of a catalytic liquid-media methane pyrolysis system, we develop a thermodynamic energy systems model and optimize design variables. The objective function to minimize is the levelized energy price required to achieve a net present value (NPV) of zero at the specified internal rate of return (IRR).

In this work, methane pyrolysis is modeled as depicted in Figure 3.1. The two use-cases explored are fuel-switching of high-temperature combustion devices such as boilers or burners and blending of low-carbon H_2 for oil refining. The base case scale selected was 50 MW_{LHV} to correspond to an industrial boiler of 170 MMBTU/hour at 85% efficiency on a lower heating value (LHV) basis [216]. This system produces approximately 10.4 kilotonnes of H_2 per annum (kta). Such a system could act as a modular unit that could operate between the natural gas pipeline and an existing combustion device that has been retrofitted to accept gaseous fuels with large mole fractions of H_2. In the case of an oil refinery, this scale of production would be appropriate for displacing onsite steam methane reforming at a small refinery or providing supplemental H_2 capacity. The scales of typical H_2 production facilities co-located with oil refineries in California ranges from 40kta to 100kta [217]. Alternatively, the produced H_2 could be blended directly into the natural gas pipeline in order to reduce the climate impact of all downstream uses [146], although gas interchangeability and pipeline integrity challenges remain in blending H_2 into distribution pipeline systems.

The primary feedstock for the system is natural gas from the transmission pipeline at a molar flow rate, $\dot{n}_g0$ [kmol/s], and a pressure, P_g0 [Pa]. For the purposes of this work, this stream is assumed to be 100% CH_4 as data for catalytic reaction rates are not available for the full profile of hydrocarbons and other compounds present in pipeline-grade natural gas. A heat exchanger is used to pre-heat the inlet stream of CH_4, scavenging the sensible energy from the hot product gas, and reducing thermal energy inputs to the reactor. The inlet temperature of the CH_4, T_g0, is assumed to be 10 °C and the inlet temperature of the H_2 blend, T_g2, is assumed to be equal to that of the reactor, T_r0. The exit temperature of the methane, T_g1, and of the hydrogen blend, T_g3, are design variables determined by the optimization. In order to minimize any CH_4 decomposition in the heat exchanger tubes, the pre-heat temperature is constrained to not exceed 700 °C.

$$T_{g1} \leq 700 \tag{3.5}$$

The energy balance between the gas streams is performed using the integral of empirical specific heat correlation equations provided in the Supporting Information (Appendix B) [218]. Mass

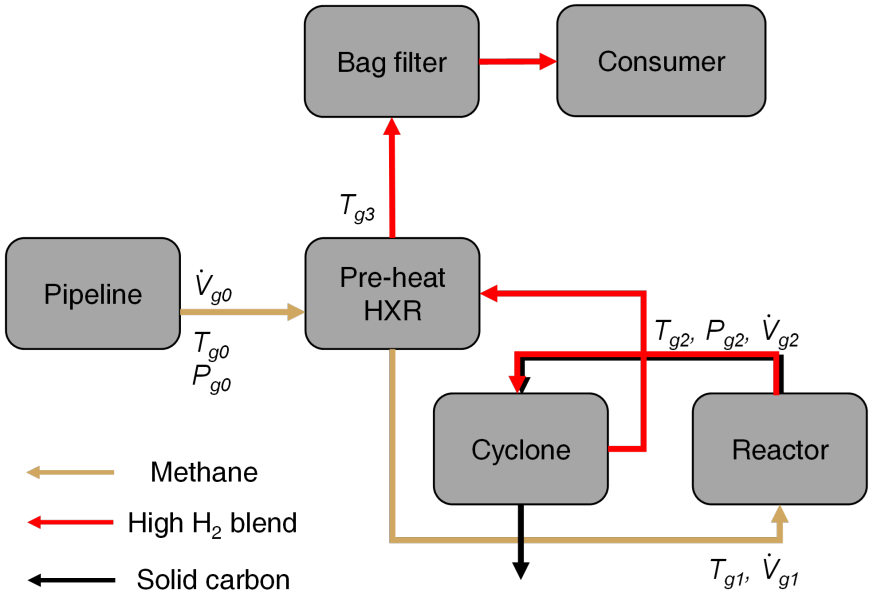

Figure 3.1: Process block diagram depicting all components of the methane pyrolysis energy system for decarbonization of industrial energy uses.

fractions of the hot gas are denoted as x_{H_2} and x_{CH_4}.

$$Q_{HXR,C} = \dot{m}_{g1} \int_{T_{g0}}^{T_{g1}} c_{p,CH_4}(T)\, dT \tag{3.6}$$

$$Q_{HXR,H} = \dot{m}_{g1} \left(x_{H_2} \int_{T_{g2}}^{T_{g3}} c_{p,H_2}(T)\, dT + x_{CH_4} \int_{T_{g2}}^{T_{g3}} c_{p,CH_4}(T)\, dT \right) \tag{3.7}$$

$$Q_{HXR,C} = Q_{HXR,H} \tag{3.8}$$

The heat exchanger design is governed by the log-mean temperature difference (LMTD_{HXR}) of the gas streams. The heat transfer coefficient, U_{HXR} is estimated based on correlations from Ulrich (2004) for high-pressure, gas-gas heat exchangers [219]. The required heat exchange area, A_{HXR} [m^2], is governed by the gas temperature design variables which determine the heat transferred, Q_{HXR} [W]. We assume negligible pressure drop across this heat exchanger such that $P_g1 = P_g0$.

$$A_{HXR} = \frac{Q_{HXR}}{U_{HXR} LMTD_{HXR}} \tag{3.9}$$

After pre-heat, the CH_4 stream is introduced to the bubble-column, with a volumetric flow rate, $\dot{V}_{g1}$ [m3/s], calculated according to ideal gas assumptions.

$$\dot{V}_{g1} = \frac{\dot{N}_{g0} R T_{g1}}{P_{g1}} \tag{3.10}$$

The reactor is a vertically-oriented pressure vessel with a volume, V_R [m3], specified by two design variables: a radius, R [m], and a height, H [m]. The fluid dynamics of two-phase bubble columns is a topic of ongoing study [220]. While empirical correlation equations have been proposed to represent the behavior of various bubble columns, few are directly applicable in the density regime indicative of a liquid metal system. The correlations proposed by Kataoka and Ishii (1987) for gas holdup have been experimentally validated in molten metal baths and are used in previous optimization modeling of such methane pyrolysis reactors [221, 207]. The gas holdup is cast as a function of the superficial gas velocity, j_g [m/s], mean drift velocity $V_g j$ [m/s], and a unitless distribution parameter for round ducts, C_0. Eq. (3.11) presents the gas holdup correlation equation for a system with no recirculation of the molten media, and using dimensionless superficial gas velocity, j_g^+, and drift velocity, $V_g j^+$.

$$\epsilon_1 = \frac{j_g^+}{C_0 j_g^+ + V_{gj}^+} \tag{3.11}$$

$$j_g^+ = \frac{j_g}{\left(\frac{\sigma g(\rho_m - \rho_{CH_4})}{\rho_m^2}\right)^{0.25}} \tag{3.12}$$

$$V_g^+ = \frac{V_{gj}}{\left(\frac{\sigma g(\rho_m - \rho_{CH_4})}{\rho_m^2}\right)^{0.25}} \tag{3.13}$$

$$C_0 = 1.2 - 0.2\sqrt{\frac{\rho_{CH_4}}{\rho_m}} \tag{3.14}$$

Here, σ is the surface tension of the molten media (0.318 N/m for bismuth at 1000 °C), g is the gravitational constant (9.8 m/s2), and $(\rho_m - \rho_{CH_4})$ is the difference between the molten media density (9000 kg/m3) and the density of the methane entering the reactor (4.38 kg/m3 for CH_4 at 1100 °C and 30 bar). Finally, we use the drift flux correlations for churn-turbulent flow and values

of $j_g^+ \leq 0.5$ as proposed by Ishii (1977) [222].

$$V_{gj}^+ = \sqrt{2} \text{ for churn-turbulent flow} \tag{3.15}$$

The gas holdup at the reactor entrance ϵ_1 is constrained to be no greater than 12.5%. Previous work has assumed gas holdup of 25% at the column entrance, analogous with other commercial-scale bubble columns [184]. In order to account for the mole creation and uncertainties associated with bubble columns with such dense liquids, a more conservative approach is taken here which ensures that even under 100% conversion of CH_4 to H_2, the gas holdup at the reactor exit will not exceed 25%.

$$\epsilon_1 \leq 0.125 \tag{3.16}$$

As the CH_4 bubbles rise through a molten media with density ρ_m, increase in temperature, and convert at a fraction η_{CH_4} to H_2, the pressure drops to P_g2 and the volumetric flow rate expands to $\dot{V}_g2$.

$$P_{g2} = P_{g1} - \rho_m g H \tag{3.17}$$

$$\dot{V}_{g2} = \frac{\left(2\eta_{CH_4}\dot{n}_{g0} + (1-\eta_{CH_4})\,\dot{n}_{g0}\right) R T_{g2}}{P_{g2}} \tag{3.18}$$

The dynamics inside the reactor are modeled as a kinetically-controlled, plug-flow reactor in steady state. The rate of reaction is modeled using the Arrhenius equation, informed by experimentally derived kinetic data. From Upham et al., we use as our base case a Ni-Bi melt with 27 mol % of Ni [190]. This reaction was found to exhibit an activation energy, E_a = 208 kJ/mol CH_4 and a pre-exponential factor, A, of 7.88*106 mL cm-2 s-1 [190]. These parameters can be modified to represent various desired media, including molten salts as explored in recent work [213]. The rate constant, k, is evaluated using the Arrhenius equation.

$$k = A e^{\frac{-Ea}{k_B T_{r0}}} \tag{3.19}$$

The rate of reaction, r [mol s^{-1} m^{-3}] is calculated by multiplying this rate constant by the concentration of the reactants, in this case, CH_4, and accounting for the reactive surface area per unit volume. Assuming a population of spherical bubbles, the ratio of surface area to volume can be applied to the pre-exponential factor.

$$r = \frac{3A}{r_b} e^{\frac{-Ea}{k_B T_{r0}}} C_{CH_4} \tag{3.20}$$

As the concentration of CH_4, the gas holdup, and the bubble radius are not constant across the reactor, we apply a differential model for a plug-flow reactor to determine the CH_4 molar conversion efficiency, η_{CH_4} [kmol CH_4 converted/kmol CH_4 entering reactor]. The rate of reaction will equal the change in molar flow of CH_4 per unit increase in reactant volume.

$$\frac{d\dot{n}_{CH_4}}{dV_{CH_4}} = \frac{3}{r_b} A \left(e^{\frac{-E_a}{k_B T}} \right) C_{CH_4} \tag{3.21}$$

We redefine the differential term for CH_4 flow rate in terms of the change in CH_4 conversion efficiency η_{CH_4} (22) and similarly redefine the differential term for reactant volume in terms of the reactor volume V_R and gas holdup ϵ (23). The gas holdup throughout the reactor will be proportionate to the CH_4 conversion efficiency due to mole creation. We ignore the effects of pressure across the reactor as, for the high pressure system explored, the effects of hydrostatic pressure of the molten media will be small.

$$d\dot{n}_{CH_4} = \dot{n}_{CH_4,0} d\eta_{CH_4} \tag{3.22}$$

$$dV_{CH_4} = \epsilon dV_R = \epsilon_1 \left(1 + \eta_{CH_4}\right) dV_R \tag{3.23}$$

As noted above, the concentration of CH_4 is also not constant across the bubble column reactor and will vary as a function of the CH_4 conversion efficiency achieved.

$$C_{CH_4} = C_{CH_4,0} \frac{1 - \eta_{CH_4}}{1 + \eta_{CH_4}} \tag{3.24}$$

Similarly, as the bubbles react and decompose into H_2 and carbon, the average bubble radius will expand, increasing the catalytic surface area.

$$r_b = r_{b,1} \left(1 + \eta_{CH_4}\right)^{1/3} \tag{3.25}$$

Substituting Eqs. (3.22)-(3.25) into Eq. (3.21) and separating terms for integration, we produce our constraint for ensuring CH_4 conversion efficiency abides by the reaction kinetics of a differential

bubble column (26). This model was also validated against the behavior of a plug-flow reactor in a commercial process simulation software (Aspen HYSYS®) (see Appendix B).

$$\int_0^{\eta_{CH_4}} \frac{(1+\eta)^{1/3}}{1-\eta}\, d\eta = \frac{3A\,()\,C_{CH_4,0}V_R\epsilon_1}{r_{b,1}\dot{n}_{CH_4,0}} \tag{3.26}$$

As carbon will be continuously removed from the system, it is unclear whether equilibrium concentrations will govern the maximum attainable mole fraction of H_2 produced. Past experimental studies suggest that continuous removal of carbon limits the reverse reaction, so we do not include any equilibrium constraints [190]. Additionally, recent work has found that bubble column design improvements can allow for H_2 mole fractions that exceed equilibrium values [214]. To ensure that adequate reductions in carbon emissions are realized, a constraint is imposed on the minimum molar conversion of CH_4, ($\underline{\eta_{CH_4}}$). A minimum molar conversion efficiency of $\underline{\eta_{CH_4}} = 90\%$ is used in the base case, and sensitivity is explored to increased purity requirements.

$$\eta_{CH_4} \geq \underline{\eta}_{CH_4} \tag{3.27}$$

Using the molar conversion efficiency of CH_4 ($\eta_(CH_4)$), the product molar flow rate ($\dot{n}_g 2$), and mole fractions of H_2 (y_{H_2}), and CH_4 (y_{CH_4}), in the product gas can be calculated. A molar conversion efficiency of 90% corresponds to a product gas mixture with 95 mol.% H_2 due to the mole creation of H_2 and the precipitation of solid carbon.

$$\dot{n}_{g2} = \dot{n}_{g0}\,(2\eta_{CH_4} + (1-\eta_{CH_4})) \tag{3.28}$$

$$y_{H_2} = \frac{2\eta_{CH_4}}{2\eta_{CH_4} + (1-\eta_{CH_4})} \tag{3.29}$$

$$y_{CH_4} = 1 - y_{H_2} \tag{3.30}$$

Thermal energy input for the endothermic reaction is introduced to the reactor through electric resistive heating elements lining the reactor walls. The resistive heating elements are silicon carbide (Si-C) elements with resistivity of 0.016 Ω-cm at 1100 °C [223]. The molten bath is assumed well-mixed and isothermal at operating temperature. In the range of superficial gas velocities explored, the bubbly flow will be aptly characterized as turbulent with sufficient mixing to affirm the assumption of isothermal conditions [207]. Resistive elements are encased in MgO-C ceramic layer to insulate electrical current from the bath. As such, the temperature of the Si-C resistors is governed by the required heat conduction through the MgO-C layer in order to maintain steady-state, and constrained by the maximum operating temperature of such heating elements (1625 C per [224]).

Heat transfers into and losses from the reactor are determined using a radial thermal conduction model.

A layer of carbon insulation is included to ensure the outer pressure vessel temperature does not exceed operating limits for carbon steel. This layered design is presented conceptually Figure 3.2. All design temperatures for the reactor $(T_{r1}, T_{r2}, T_{r3}, T_{r4})$ are determined during model solve model in order to satisfy the steady-state radial conduction model. This model ensures that enough heat enters the reactor to drive the reaction and computes the heat loss from reactor side walls. The amount of necessary heat input to the reactor is a function of the conversion efficiency η_{CH_4} and the reaction enthalpy, ΔH_{rxn}, of 75 $kJ/molCH_4$ as well as the amount of sensible heat required to raise the temperature of the inlet CH_4 stream from T_g1 to T_r0, for a mass flow rate calculated with the molar mass of CH_4, M_{CH_4}. This heat input, $\dot{Q}_(reactor, in)$ [W], must be driven by the temperature gradient from the isothermal ceramic heating elements into the isothermal molten bath.

$$\dot{Q}_{reactor} = \Delta H_{rxn}\eta_{CH_4}\dot{n}_{g0}c_{p,CH_4}(T)dT = \frac{2\pi R^2 k_{MgO}(T_{r1} - T_{r0})}{L_{MgO}} + \frac{2\pi H k_{MgO}(T_{r1} - T_{r0})}{\log\frac{R+L_{MgO}}{R}} \quad (3.31)$$

A multi-layer radial conduction model is employed. In this manner, the rate of heat transfer out of the ceramic layer can be calculated. The heat transfer through each layer is computed as part of the constraint set during optimization. Solving this set of equations in steady state determines the temperature at each layer and provides an estimate for heat losses from the reactor shell. The full system of equations for the multi-layer conduction model can be found in Appendix B.

$$\dot{Q}_{loss} = \dot{Q}_{steel} = \dot{Q}_{insulation} = \dot{Q}_{ceramic} \quad (3.32)$$

The elemental carbon saturates the molten bath and precipitates on any non-equilibrium surface. Carbon accumulation on the surface of the liquid is removed primarily through entrainment in the gaseous flow. As shown in Figure 3.1, a cyclone is used to separate the solid carbon from the stream of product gas. The cyclone is sized based on the resultant volumetric gas flow rate leaving the reactor, V_{g2} [m3/s]. In order to ensure removal of the solid carbon through gas entrainment, we introduce a design variable for the exit radius of the reactor, r_e [m]. An exit radius must be found such that the superficial velocity of product gas leaving the reactor is large enough to satisfy conditions necessary for homogenous, dilute phase entrainment of the generated mass flux of solid carbon, $G_s = \dot{m}_(Csolid)/(\pi r_e^2 \rho_p)$. The transition to homogenous dilute flow can be estimated at the superficial velocity V_{mp} [m/s] using empirical models from Bi & Grace (1995) [225].

$$V_{mp} = 10.1(gd_p)^{0.347}(\frac{G_s}{\rho_{H_2}})^{0.310}(\frac{d_p}{D})^{-0.139}Ar^{-0.021} \quad (3.33)$$

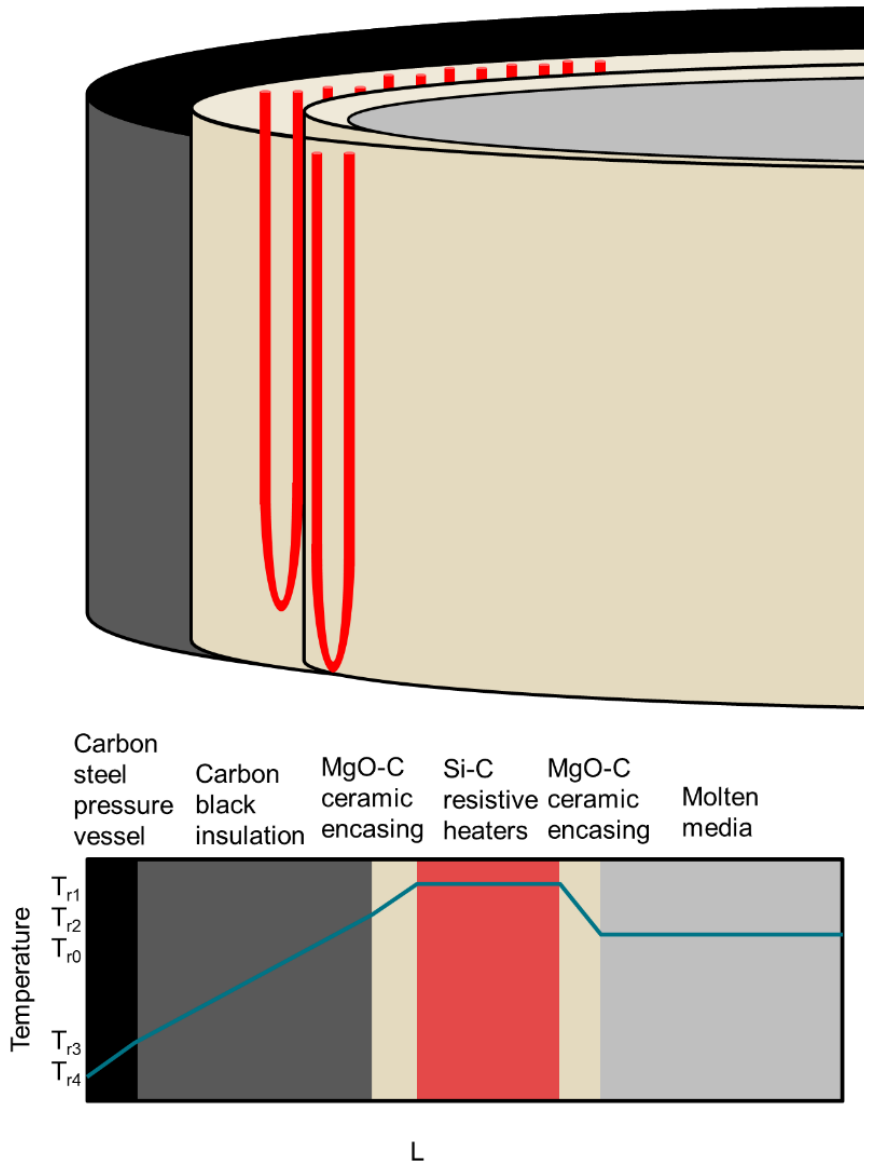

Figure 3.2: Concept diagram of resistive heating reactor design for liquid-media methane pyrolysis. A representative cross-sectional temperature profile is displayed. T_{r0} is the temperature of the isothermal molten media. The Si-C resistive heaters are modeled as isothermal at T_{r1}. T_{r2} is the temperature at the MgO-C ceramic interface with the carbon black insulation, Tr3 is the temperature at the insulation interface with the pressure vessel, and Tr4 is the temperature at the pressure vessel interface with the ambient conditions.

Here, d_p is the particle diameter (0.1 mm), ρ_G is the density of the gas phase (0.55 kg/m3 for H_2 at 1100 C and 30 bar), D is the diameter of the exit orifice (D=2r_e), and Ar is the Archimedes number, as a function of the particle density ρ_p (2200 kg/m3 for solid carbon) and the gas viscosity μ_G (1.84*10-5 for H_2).

$$Ar = \frac{\rho_{H_2}(\rho_p - \rho_{H_2})gd_p^3}{\mu_{H_2}} \tag{3.34}$$

The superficial gas velocity at the reactor exit is constrained to be greater than or equal to the threshold velocity, V_{mp}.

$$\frac{\dot{V}_{g2}}{\pi r_e^2} \geq V_{mp} \tag{3.35}$$

The flow of product gas is passed through a heat exchanger to recover the sensible energy and preheat the inlet CH_4. Any remaining fine carbon is removed with a bag filter, sized according to $\dot{V}_{g2}$. The minimum thickness of the carbon-steel reactor shell is governed by the hoop stress equation for a cylindrical vessel as specified by ASME BPV Code (Sec. VII D.1 Part UG-27) with a weld efficiency, E of 0.85 and a max allowable stress, S of 88.94x106 Pa [226].

$$L_s \geq \frac{P_r 2\,(R + 2L_{MgO} + L_i)}{2SE - 1.2P_r} \tag{3.36}$$

Finally, we constrain the rate of low-carbon gaseous energy output to be greater than or equal to that desired by the end use consumer. In this case, we use a 50 MW_{LHV} boiler as the design capacity, Cap, at efficiency, η_b, of 85% (on an LHV basis) as the modeled consumer, but this scale can similarly represent supplemental H_2 production of 10 kta for use at a refinery.

$$\eta_b\,(LHV_{H_2}M_{H_2}y_{H_2} + LHV_{CH_4}M_{CH_4}y_{CH_4})\,\dot{n}_{g2} \geq Cap \tag{3.37}$$

3.3.2 Estimating levelized costs of operation

For a fixed production capacity capable of supplying a thermal load of 50 MW_{LHV}, several design variables of the pyrolysis energy system are determined with a nonlinear optimization program to minimize the H_2 price which yields zero net present value (NPV) at a fixed rate of return. The optimization is implemented in Julia [227] utilizing the JuMP [180] framework and the Artelys Knitro® [228] solver. As the problem is nonlinear with many locally optimal solutions, a multi-start optimization method was employed to improve confidence that the proposed solution is a global optimum: the global solution is assumed to be the lowest objective function constraint-satisfying solution out of 200 randomly-seeded optimization runs.

The system is parameterized by pressure at the inlet, P_{g0} (30 barg) and temperature inside the

reactor, T_{r0} (1100 °C). The model-selected design variables include the dimensions of the reactor (height, H, radius, R and exit radius, r_e) and the thickness of insulation and steel reactor walls (L_i, L_s). In addition, the inlet molar flow rate, $\dot{N}_{g0}$, and the gas temperatures T_{g1} and T_{g3}, are design variables (total design variables = 8). In order to solve the physics of the system, supplemental decision variables are required such as the temperatures at each layer of the reactor wall ($T_{r1}, T_{r2}, T_{r3}, T_{r4}$) and the achieved CH_4 molar conversion efficiency, η_{CH_4}, and are computed in-line to ensure that energy balance and molar conservation constraint equations are satisfied.

The total electric power consumption of the system can be computed by summing across components. The ceramic resistive heat diffusion is assumed to be 100% efficient.

$$P_{e-} = \dot{Q}_{loss} + \dot{Q}_{reactor} + \dot{W}_{blower} + \dot{W}_{cyclone} \tag{3.38}$$

The rate of gaseous energy introduced to the system, $P_{g,i}$, and low-carbon energy produced by the system, $P_{g,o}$, are calculated.

$$P_{g,i} = HHV_{CH_4} M_{CH_4} \dot{n}_{g0} \tag{3.39}$$

$$P_{g,o} = \left(HHV_{H_2} M_{H_2} y_{H_2} + HHV_{CH_4} M_{CH_4} y_{CH_4}\right) \dot{n}_{g2} \tag{3.40}$$

Further, the rate of carbon flow as solid carbon, $\dot{m}_{C,solid}$ [kg C/sec], and in terms of CO_2 emissions equivalent sequestered, $\dot{m}_{CO_2,seq}$ [kg CO_2/sec] are calculated as shown below.

$$\dot{m}_{C,solid} = M_C \eta_{CH_4} \dot{n}_{g0} \tag{3.41}$$

$$\dot{m}_{CO_2,seq} = M_{CO_2} \eta_{CH_4} \dot{n}_{g0} \tag{3.42}$$

Using the above terms, we aggregate the annual OpEx [$/year] and the annual revenues, Rev [$/year], using the capacity factor, cf, and the assumed price for solid carbon, $p_(C_solid)$ [$/tC], incentives for sequestered CO_2, $p_(CO_2seq)$ [$/t$CO_2$], and incentive for lifecycle CO_2 emissions avoided, $p_(CO_2av)$ [$/t$CO_2$]. Additional fixed operations and maintenance costs, FOM, are included to account for labor and maintenance costs [$/yr]. Annual maintenance costs were estimated to be 3% of the total capital requirement. For labor expenses, it was assumed that two shift operators would be necessary to operate the facility, each earning $50,000 per year. Supervisory labor cost is assumed to be 25% of operating labor expenses, and overhead expenses are assumed to be 40% of operating & supervisory labor costs [226]. Labor costs are a small fraction (¡5%) of total annual cash flows. Molten media losses have been observed in previous studies due to vaporization and deposition on the produced

solid carbon [190]. Recent work has demonstrated that design choices such as employing a membrane bubble column and/or incorporating a layer of lower density molten media (such as a molten salt) above the reactive media can reduce the loss of catalytic material [214, 215]. However, such material losses can have an outsize impact on project economics. As such, we treat these costs explicitly using the commodity cost of the metal c_m. We test sensitivity of results to various loss rates included as contamination factors on the solid carbon flow exiting the reactor, ζ_m [kg metal/kg carbon].

$$OpEx = 3600\frac{sec}{hr}8760\frac{hr}{yr}cf\left(p_{e-}\frac{P_{e-}}{3.6\frac{MJ}{kWh}} + p_{NG}\frac{P_{g,i}}{1055\frac{MJ}{MMBtu}} + c_m\zeta_m\dot{m}_{C,solid}\right) + FOM \quad (3.43)$$

For simplicity of exposition, we introduce an additional term Rev_C for the revenues from carbon emissions avoided, carbon emissions equivalent sequestered, and solid carbon sold:

$$Rev_C = p_{CO_2,av}\dot{m}_{CO_2,av} + p_{CO_2,seq}\dot{m}_{CO_2,seq} + p_{C,solid}\dot{m_{C,solid}} \quad (3.44)$$

$$Rev = 3600\frac{sec}{hr}8760\frac{hr}{yr}cf\left(LCOE\frac{P_{g,o}}{1055\frac{MJ}{MMBtu}} + \frac{Rev_C}{1000\frac{kg}{tonne}}\right) + FOM \quad (3.45)$$

Capital costs for most equipment are estimated from correlation equations in the chemical engineering literature [219, 226]. The capital cost for the transformer is estimated based on reported values from San Diego Gas and Electric to the California Independent System Operator [229]. Components for which reliable costs could not be found were estimated from their materials or commodity prices. All purchased cost estimates are escalated to 2017 US$ using Chemical Engineering Plant Cost Indices (CEPCI). A full table of capital cost estimation equations can be found in Appendix B.

The installed costs are estimated using the factorial method. The estimates for purchased cost of equipment were adjusted using Lang factors meant to capture ISBL costs and offsites. A Lang factor (LF) of 8 was applied, however sensitivity to this assumption is also explored. A design & contingency factor of 1.3 is applied based on values for a fluids-solids process referenced in [226].

The total capital requirement (TCR) of the system can be computed by summing the purchased cost of each piece of equipment (PC_e) which are all designated in Appendix B.

$$TCR = 1.3LF\sum_e PC_e \quad (3.46)$$

With the above, we specify the net present value (NPV) of this energy system and employ a

constraint such that NPV is equal to zero:

$$NPV = \sum_{t} \frac{Rev - OpEx}{(1 + IRR)^t} - TCR = 0 \tag{3.47}$$

The objective function of the optimization program is to minimize the levelized cost of energy (LCOE), representative of the sale price of H_2-rich fuel, subject to the above design constraints, and the economic constraint that the net present value (NPV) equals zero. This optimization then computes the effective break-even levelized cost of energy such that the system exactly covers its costs with NPV of 0.

$$\begin{aligned}
\min \quad & LCOE \\
\text{s.t.} \quad & \text{design constraints: (3.5), (3.27), (3.31) - (3.32), (3.36) - (3.37)} \\
& \text{physical constraints: (3.10), (3.17) - (3.18), (3.28) - (3.30), (3.38) - (3.42)} \\
& \text{heat exchange constraints: (3.6) - (3.8)} \\
& \text{bubble column flow constraints: (3.11) - (3.16)} \\
& \text{kinetic reaction constraints: (3.19) - (3.26)} \\
& \text{carbon-gas flow entrainment constraints: (3.33) - (3.35)} \\
& \text{economic constraints: (3.43) - (3.47)}
\end{aligned} \tag{3.48}$$

In the base case, the nominal internal rate of return (IRR) is 15% and the lifetime of the project, T, is 15 years, with an up-time capacity factor of 80%. All annual cash flows are assumed to escalate with inflation, so the IRR represents the nominal weighted average cost of capital for the project. Further, operating expenses include electricity costs at an assumed price of \$40/MWh based on the average wholesale electricity price observed in the California Independent System Operator (CAISO) territory in 2018. Natural gas feedstock cost was assumed to be \$6/MMBTU based on the approximate industrial customer tariff from the Pacific Gas & Electric Company [230].

LCOE is evaluated on a higher heating value (HHV) energy content of gas basis, as this is typical for the gas industry. However, this can be converted into a price of H_2 in terms of \$/kg for use in a refinery. The project is also compensated by some combination of revenue-streams associated with the generated carbon. In the base case scenario, we assume a value for $p_{C,solid}$ of \$150/tonne of solid carbon as sold as a feedstock for other manufacturing processes. Our base case includes no value of avoided CO_2 emissions however sensitivity scenarios test a credit of \$50/tonne CO_2 offered based on (i) the tonnes of CO_2 emissions avoided on a lifecycle basis ($p_{CO_2,av}$), or (ii) the tonnes of CO_2 emissions equivalent sequestered ($p_{CO_2,seq}$).

The lifecycle emissions avoided, $\dot{m}_{CO_2,av}$ [kg CO_2e/sec], are computed as the sum of stack emissions avoided and upstream emissions avoided, however these will vary depending on the end-use

application. For the case of combustion applications, the stack emissions avoided are equal to the difference in emissions from stoichiometric combustion of the produced H_2-rich gas and a pure stream of CH_4 providing the same amount of energy. In order to account for the upstream emissions of the proposed pyrolysis process, life-cycle factors are applied for the natural gas transported, β_{NG} (15 gCO_2e/MJ CH_4 per [231]) and for the electricity consumed, β_{e-} (162 gCO_2/kWh e-), based on the average carbon intensity of the 2017 California electricity grid [232].

$$\dot{m}_{CO_2,av} = \frac{\dot{m}_{H_2} LHV_{H_2}}{LHV_{CH_4} M_{CH_4}} M_{CO_2} - \frac{EF_{NG}}{1000 \frac{g}{kg}} \left(P_{g,i} - \frac{P_{boiler}}{\eta_{boiler}} \frac{HHV_{CH_4}}{LHV_{CH_4}} \right) - \frac{EF_{e-}}{1000 \frac{g}{kg}} \frac{P_{e-}}{3.6 \frac{MJ}{kWh}} \quad (3.49)$$

However, in the case of a refinery, both combustion and process emissions are avoided. As such, we use emissions factors from the CA-GREET 3.0 model for gaseous hydrogen from centralized steam methane reforming to account for all avoided stack emissions and upstream emissions. The stack emissions from H_2 production via this pathway, $\alpha_(SMR - H2, stack)$ are estimated to be 85.7 gCO_2e/MJ H_2. The full life-cycle emissions from H_2 production via the baseline SMR pathway, $\alpha_(SMR - H2, lifecycle)$ are estimated to be 100.5 gCO_2e/MJ on an HHV basis [231].

$$\dot{m}_{CO_2,av} = CI_{SMR,stack} \quad (3.50)$$

Sensitivity of the levelized cost of energy was explored with respect to the price of natural gas, the internal rate of return, the Lang factor, the value of solid carbon, the lifetime of the facility, the capacity factor of the facility, and the price of electricity. Additionally, we consider cases where a carbon emissions credit is available in various forms, including credits for life-cycle carbon emissions avoided and alternatively credits for carbon sequestered, intended to represent the policy nuance of the 45Q tax credits mentioned in Section 3.2.

Once a levelized cost of energy, LCOE, is found, it can be converted from units of [$/MMBTU] into an LCOH in [$/kg H_2] using the mass flow rate of H_2 relative to the total rate of gaseous energy produced. While impurities are still present, as post-processing separations and gas clean-up are not included, this is intended to provide a useful point of comparison with other H_2 cost estimates in the literature for H_2 from SMR or electrolysis. For both combustion and refining end-uses, additional processes may be required to remove trace compounds generated during the high temperature, high pressure molten-media methane pyrolysis process.

$$LCOH = LCOE \frac{P_{g,o}}{\dot{m}_{H_2}} \quad (3.51)$$

Finally, these cost metrics are converted to an equivalent abatement cost for the emitting facility, $C_{abatement}$ [$/t$CO_2$ avoided] by using the avoided stack emissions at the emitting facility

Design parameter	Optimal design value
Preheat heat exchanger area (m^2)	9
Reactor internal radius (m)	2.2
Reactor height (m)	1
Reactor pressure vessel thickness (mm)	104
Reactor insulation thickness (m)	0.3
Preheat temperature (°C)	700
Reactor exit radius (m)	0.83
CH_4 molar conversion efficiency	0.90

Table 3.1: Optimal design parameter results for the base case molten-media pyrolysis reactor energy system.

and identifying the carbon tax that would be required for such a premium on energy or H_2 to be economical.

3.4 Results & discussion

For both the boiler and the refinery cases, the thermochemical pyrolysis system model is identical as it is indifferent to the consumer of the gas. Further, the results of the economic model only differ in cases where we consider carbon credits on the basis of emissions avoided, as these processes have distinct avoided emissions based on the end-use of the product H_2. Finally, the emissions abatement costs (assessed on the basis of stack emissions avoided) will vary between the combustion and the refinery use-cases as the two use cases have different avoided cost and emissions characteristics.

3.4.1 Energy systems design optimization

The numerical insights regarding process optimization for bubble column pyrolysis reactors are tabulated in Table 3.1. In all cases, the optimal energy system includes a bubble column of radius 2.2 m and height 1 m. The optimal reactor height is dictated by the residence time required to achieve the desired minimum CH_4 conversion efficiency of 90%. A gas exit radius of 0.83 m is selected to ensure homogenous, dilute phase transport of solid carbon via entrainment in the product gas flow. The radius of the reactor was governed by the empirical models for gas holdup as a function of superficial gas velocity and the constraint that gas holdup does not exceed 12.5% at the column entrance. In order for this constraint to be satisfied, the radius had to be larger than the model would have otherwise selected.

The system incorporates a heat exchanger to recover sensible heat from the H_2-rich gas, preheating the inlet CH_4 to 700 °C and producing the H_2-rich fuel gas at a temperature of 523 °C after the pre-heat exchanger. This heat exchanger recovers 4.1 MW of thermal energy. The optimal design requires an electricity demand of 11.6 MW to power the reactor and 110 kW for ancillary electrical loads. The electric resistive heating elements reach 1147 °C to maintain isothermal conditions inside

of the reactor. This is well-within operating limits of such Si-C resistive heaters which can sustain temperatures up to 1625°C and would require approximately 460 25 kW units each 1.5m in length and 25 mm in diameter [224]. The 14 m circumference of the reactor should provide ample room to accommodate these heaters. Internal resistive heaters could also be introduced, provided that they are adequately protected from degradation in the molten media, but additional reactor volume may be required to accommodate internals.

A layer of carbon insulation 0.3 m thick is included to manage heat losses and results in 244 kW of thermal loss out of reactor walls, or 2.1% of the energy inputs to the reactor. A full accounting of the energy flows into and out of the system is presented in Figure 3.3. In order to abide by hoop stress limitations, the carbon steel pressure vessel requires a thickness of 100 mm. These optimal design decisions remain unchanged across the sensitivity scenarios tested, and the fundamental energy system design does not depend on the end-use of the produced low-carbon gas.

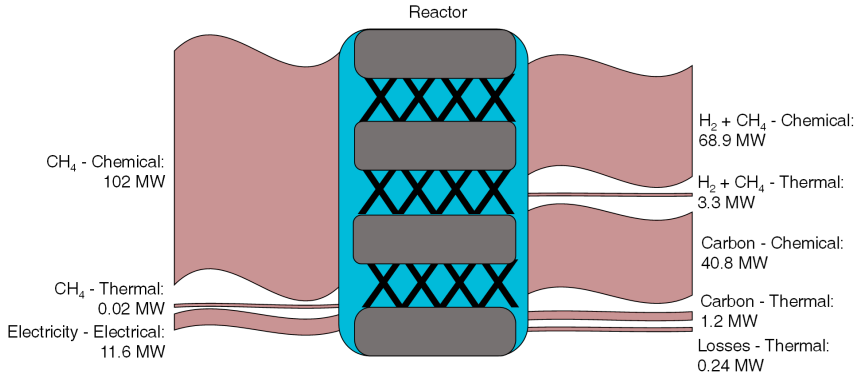

Figure 3.3: Energy balance diagram for pyrolysis energy system. Input and output flows at the system boundary are displayed in MW. Internal transfers that are omitted include 4.1 MW of thermal energy from the product gas stream to pre-heat the input gas stream. Numbers do not add up to unity due to rounding errors as well as use of empirical specific heat approximations. Note that the system is designed to provide 50 MW of thermal energy to an 85% efficient boiler (on an LHV basis), so 69 MW of chemical energy (on an HHV basis) is produced.

3.4.2 Discounted cash flow analysis

Under base case assumptions, the estimated capital costs for the proposed energy system align well with estimates from the literature for similar H_2 production systems. Our proposed system has a capital requirement of $28 MM for a capacity of 50 MWLHV which corresponds to 10.4 kta H_2 or $2.70/kta H_2 in the base case with 90% CH_4 conversion. In terms of capital cost, Parkinson et al. found a total capital requirement of $349.7 MM for a facility producing 100 kta of H_2 at a 91% on-stream factor, corresponding to $3.50/kta H_2 [212]. Our capital estimate is slightly lower, which is reasonable as the proposed system does not include any separation of H_2 from unreacted CH_4

and uses a simpler electric heater targeted for small scale industrial heating applications. Given the considerable uncertainties regarding the true costs of such a system, we consider this estimate within the margin of error.

As shown in Figure 3.4, if levelized over the 15-year lifetime using a capital recovery factor for the corresponding IRR, the annualized capital costs will be $4.8 MM, compared to annual operating expenses of $17 MM. The amortized capital costs comprise just 25% of annual expenses, which makes this system relatively insensitive to changes in the discount rate or lifetime of the equipment. However, the investor will be exposed to trends in the price of operational feedstocks like natural gas.

3.4.3 Levelized cost of energy and cost of abatement

The levelized cost of energy (LCOE) is shown for the full set of sensitivity cases in Figure 3.5. As mentioned above, the majority of the economic sensitivity results do not change when evaluated for different use-cases of the produced H_2. Provision of carbon credits on the basis of lifecycle GHG emissions avoided was the only sensitivity test that revealed differences between the combustion case and the refinery case.

We also express the LCOE as the levelized cost of hydrogen (LCOH), or the necessary sale price of the H_2-rich product gas. Under most economic sensitivities, both costs are at a premium to the costs of a baseline, emitting facility. For each use-case, the avoided stack emissions and the premium in cost above the avoided baseline marginal costs are used to evaluate the equivalent cost of abatement. This represents the tax on carbon emissions that would need to be imposed on the emitting facility for such a premium on energy to be economical.

For the case of distributed combustion applications, we use the carbon intensity of the produced H_2-rich fuel relative to CH_4 to calculate the stack emissions avoided by the industrial consumer, $\dot{m}_(CO_2av)$. The energy premium (above the assumed natural gas price) is expressed as an effective abatement cost, in terms of $/tonne CO_2 (Figure 3.6). For the case of a refinery application, we estimate the cost of H_2 from SMR to be the marginal cost of production of incremental H_2, as fixed costs of the plant are assumed to be sunk. Based on efficiency factors from CA-GREET 3.0, we estimate an all-in efficiency of 1.38 MJ CH_4/MJ H_2. In the base case, with natural gas prices of $6/MMBTU, this corresponds to $1.11/kg H_2. This provides a benchmark from which to assess the marginal abatement cost.

The LCOE for the base case assumptions was found to be $11.09/MMBTU of decarbonized gas, which is equivalent to $1.75/kg H_2. This represents a $5.09/MMBTU premium over the base case price of natural gas. As such, for a combustion use-case, there would need to be a carbon emissions tax of $115/tonne of CO_2 imposed on the industrial consumer in order for this additional cost to make economic sense. If applied to a refinery use-case, this corresponds to an abatement cost of $52.60/t$CO_2$.

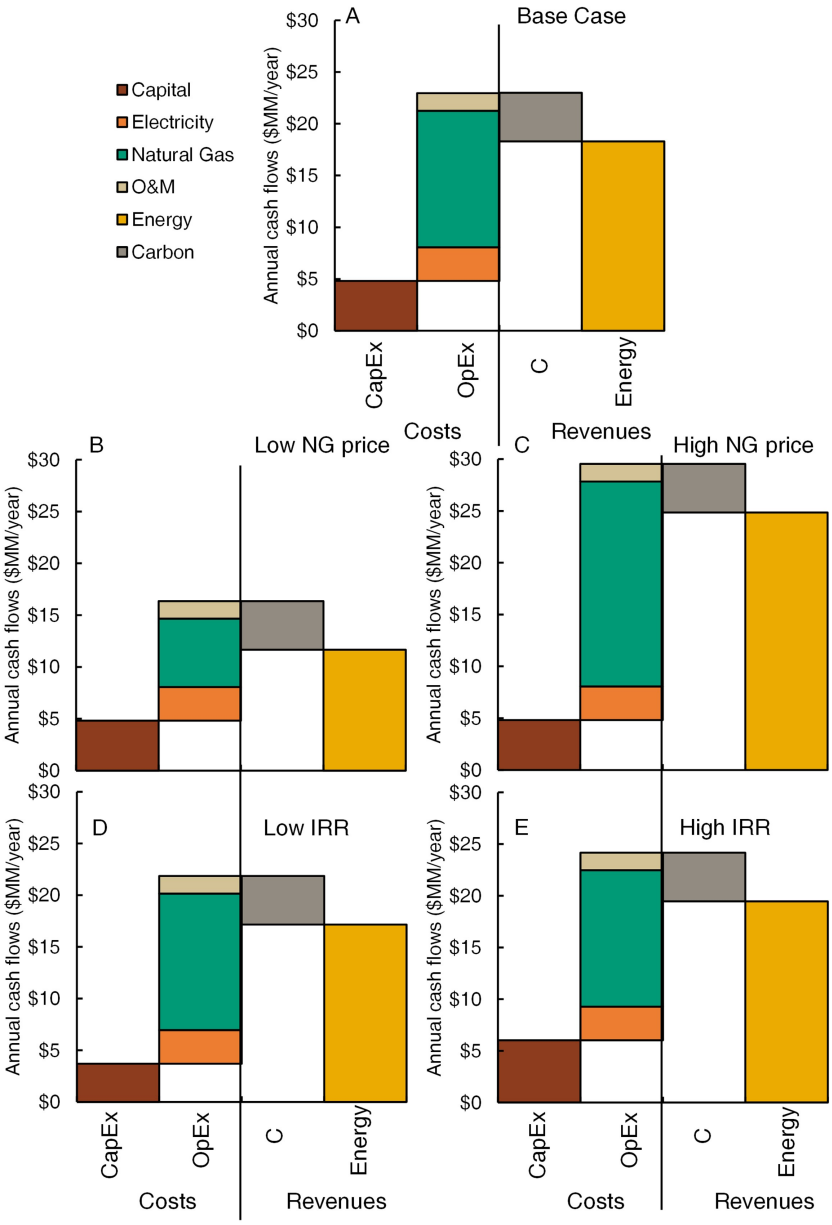

Figure 3.4: Annual cash flows for pyrolysis energy system in the base case (A) and under a variety of sensitivities (B-E). Selected sensitivity cases are natural gas prices ($3/MMBTU in B and $9/MMBTU in C) and internal rate of return (10% in D and 20% in E). The levelized cost of energy for each scenario is displayed in Figure 3.5

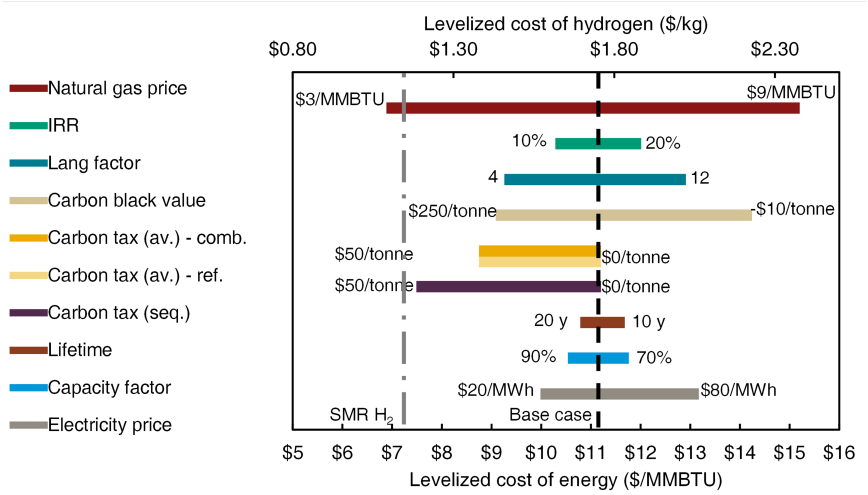

Figure 3.5: Levelized cost of energy from optimized pyrolysis energy system across various sensitivity scenarios. Sensitivities include natural gas price, internal rate of return (IRR), Lang factor, carbon black value, carbon tax on the basis of emissions avoided (for both combustion (comb.) and refinery (ref.) cases), carbon tax on the basis of emissions sequestered (seq.), lifetime, capacity factor, and electricity price.

As an upper bound, we test the scenario where there is no value to the carbon and instead there is an associated disposal cost of $10/tonne of solid carbon. In this case, the LCOE is $14.13/MMBTU with a corresponding abatement cost of $183/tonne of CO_2. In the case where carbon disposal incurs a cost of $10/tonne carbon, the LCOH increases to $2.23/kg H_2 and the estimated abatement cost nearly doubles to $92.00/tonne CO_2 avoided.

We also consider the specific case of a refinery in California using pyrolysis to generate H_2 and credits under the Low Carbon Fuel Standard (LCFS) program. We assume the refinery must pay $10/tonne carbon to dispose of the produced solids and receives LCFS credits worth $190/tonne CO_2e avoided on a lifecycle basis. In this case, the levelized cost of H_2 produced is $0.39/kg H_2. This lies below any reasonable estimate for costs of H_2 from SMR and could provide substantial returns. If the refinery is also permitted to sell the solid carbon into a secondary materials market at a price of $150/tonne carbon, the levelized cost of H_2 is estimated at -$0.08/kg H_2. The negative LCOH indicates that a positive NPV is provided solely from the revenues from carbon sales and the LCFS credits. Therefore, as incentivized by the LCFS framework, there is a notable opportunity for oil and gas industry to invest in clean H_2 for the refinery processes [188].

However, in any case with sale of solid carbon coupled with carbon credits, there would need to be rigorous verification that the solid carbon was permanently sequestered and did not return to the atmosphere as carbon dioxide. For example, current solid carbon products from refineries (petroleum coke) are sold to markets in Asia where they are burned for power generation. Secure

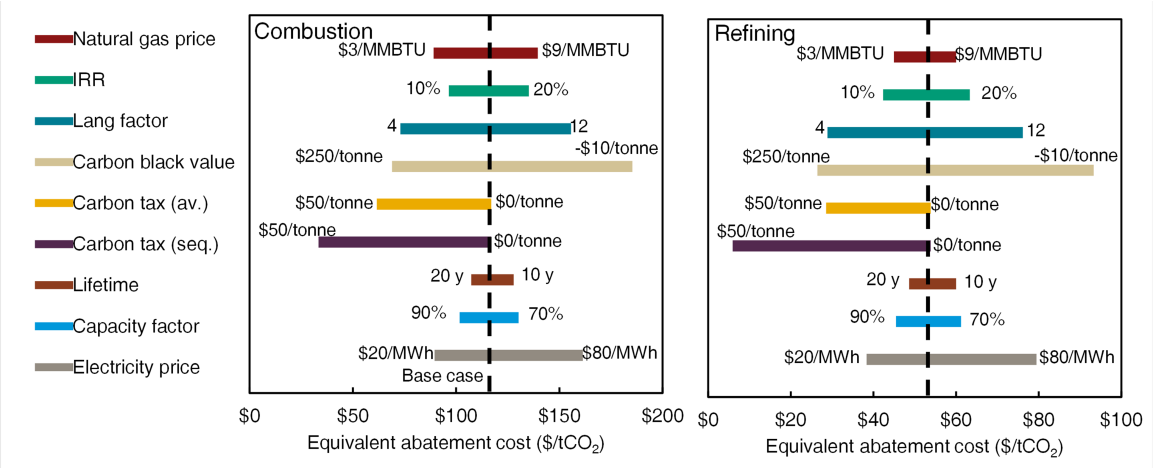

Figure 3.6: Levelized cost of abatement across sensitivity scenarios for the case of a combustion application (left) and a refinery application (right), evaluated on the basis of stack emissions avoided by the industrial consumer.

disposal practice would need to be verified as avoided in order to claim both types of value for the carbon.

All of the above results are presented for a system with a minimum CH_4 conversion efficiency of 90%. This results in a product stream that is 95 mol.% H_2. As it is unclear precisely what clean-up equipment would be required to remove all of the trace compounds generated in a high-pressure molten media pyrolysis process, we do not include any separations or gas clean-up processes on the back-end. However, here we illustrate the changes in optimal reactor design and costs as desired CH_4 conversion efficiency increases from 90% to 99.99% for a fixed energy demand of 50 MWLHV.

Finally, these economic results were found to be highly sensitive to any catalyst losses via removal with solid carbon. If the solid carbon is contaminated by as little as 0.0001 wt.% Ni-Bi, the process becomes uneconomic with LCOE of $38.50/MMBtu. At 0.0005 wt.% contamination, the LCOE is found to be $148/MMBtu. As such, great care must be taken to minimize and recover any catalyst losses by either including a molten salt cap as suggested by Parkinson et al. or exploring alternative approaches with lower cost catalytic materials.

With levelized costs of energy ranging from $9 to $15/MMBTU ($1.50 to $2.20/kg H_2) and equivalent abatement costs generally falling between $100 and $150/tonne CO_2 avoided, we compare these results to other retrofitted, "bolt-on" emissions reduction measures, including carbon capture and other technologies for low-carbon H_2 production. The Global CCS Institute produces estimates for the cost of CO_2 avoided for a variety of CCS use-cases. For the industrial boiler case, natural gas-fired combined cycle (NGCC) power generation may be the most analogous case from which to estimate CCS costs, with similar CO_2 mole fractions to the industrial combustion use case. The authors estimate the abatement costs for equipping a first-of-a-kind NGCC generator with CCS as

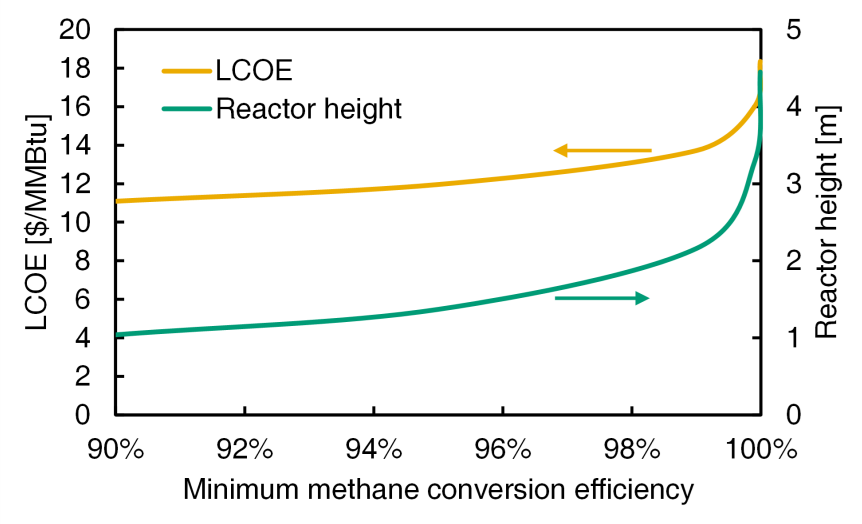

Figure 3.7: Sensitivity of levelized cost of energy (LCOE) and optimal reactor height to increased methane conversion efficiency requirements.

$89/tonne CO¬2 with real-world costs ranging from $80 to $160/tonne CO_2 [183]. These estimates also align with previous work of Rubin et al. [233]. The NGCC analyzed in this case had a net power output of 630 MW with a net plant efficiency of 51.5%. We scale the estimated costs down to act as a more direct comparison with the 50 MW combustion case (at 85% efficiency) explored here. For example, using a scaling factor of 0.6, and scaling by mass of CO_2 captured, the cost estimate of $89/tonne CO_2 scales up to $288/tonne CO_2. This would place the methane pyrolysis system examined in this work within the range of competition with more conventional CCS technologies at small scale. However, it is difficult to compare these options as they rely heavily on site-specific factors. In addition, retrofitting small-scale combustion appliances to enable carbon capture may be more challenging than switching the burner to accept an alternative fuel like H_2.

For low-carbon H_2 production, options include steam methane reforming equipped with CCS (SMR-CCS) and water electrolysis. Several studies have analyzed the additional cost of equipping SMR facilities with CCS and have found a levelized cost of H_2 to range from $1.22 to $2.81/kg H_2 [212]. This indicates that the costs of pyrolysis-generated H_2 are of the right order for magnitude for competition with legacy larger-scale SMR facilities. However, the superior option will largely depend on site-specific factors. For example, one additional benefit presented by a pyrolysis system would be the modularity, which would allow for minimal retrofits to existing technology and processes. Further, the production of solid carbon avoids the need for transmission pipeline infrastructure to transport supercritical CO_2 and could instead leverage train-based solids transport networks. This may allow pyrolysis technologies to be deployed on a shorter time horizon than conventional CCS technologies. However, even at the 50 MW scale explored here, the mass of carbon that would need

to be sequestered or transported off-site is 31.3 kilotonnes per year.

Electrolysis has been analyzed in the past finding costs of \$3/kg H_2 (\$22.31/MMBTU), which exceeds any of our sensitivity results [212]. Further, if electrolysis employs electricity from a grid with an average carbon intensity similar to that of California (162 gCO_2/kWh), the carbon emissions of the produced H_2 will be 37 gCO_2/MJ at a thermodynamic minimum. For the 2017 United States average grid carbon intensity (426 gCO_2/kWh), the emissions will be 98 gCO_2/MJ, which is similar to that of uncaptured SMR (100.5 gCO_2/MJ per CA-GREET 3.0).

As a final case, we consider the case of retrofitting a plant with a new electric boiler. Using the carbon intensity of the California grid (and assuming 100% efficiency) electrification would result in emissions of 45 gCO_2/MJ. If we employ the carbon intensity of the U.S. grid, the lifecycle emissions will be 118 gCO_2/MJ which is higher than the original 85% efficient boiler using direct combustion (73 gCO_2/MJ). If the boiler could leverage an emissions-free electricity source for all operations, the lifecycle emissions of electrification would compete with that of a pyrolysis retrofit. Using the operational expenses of pyrolysis, we estimate an upper bound on the electricity price at which an electric boiler would compete with a pyrolysis unit (on a marginal cost basis) is \$45/MWh.

Based on the relative cash flows, the LCOE and equivalent abatement cost are least sensitive to changes in the lifetime, capacity factor, and IRR (or cost of capital). This could represent an advantage over comparable CCS systems for which amortized capital costs make up the bulk of cash flows [234]. However, this means that the LCOE is highly sensitive to changes in operating expenses, such as the cost of natural gas, catalyst losses, or uncertainty regarding the future value of solid carbon.

The results of the sensitivity cases also highlight the importance of policy design nuances for carbon-capture projects. None of the retrofits results in a cost-competitive process in the absence of incentives, however some policy intended to motivate CCS would improve the economics for decarbonization. The current structure of the 45Q tax credits explicitly incentivizes the sequestration of CO_2 in the United States, rewarding projects on the basis of mass of CO_2 sequestered. As such, under the current language, this technology solution would not qualify to receive credits. Capture and utilization of solid carbon would require flexible incentives that recognize carbon emissions equivalent captured and sequestered. An additional consideration is whether policies recognize carbon-capture projects on the basis of emissions sequestered or emissions avoided. If the policy is designed to award credits on the basis of mass of carbon emissions sequestered there will be greater value for combustion applications. However, if the credits award value on the basis of mass of carbon emissions avoided, there is a substantial increase in the levelized cost of energy. This is because H_2 has a lower energy content relative to CH_4 and so the amount of emissions equivalent sequestered is not necessarily equal to, and in most cases is greater than, the amount of emissions avoided. Finally, depending on the structure of the carbon accounting, the end-use of the carbon could be important in determining whether the projects could be awarded credits for the permanent sequestration of

carbon or for substitution of an alternative source of solid carbon.

3.5 Conclusions

The proposed methane pyrolysis energy system may be one option for reducing greenhouse gas emissions in the near term while continuing to leverage existing infrastructure and minimizing stranded assets. The estimated emissions abatement costs of the pyrolysis energy system for small scale heating applications are similar to existing options for large-scale gaseous carbon capture and sequestration. In the case studies explored, results for the California transportation sector and California refinery hydrogen, where substantial credits are available for avoiding greenhouse gas emissions, indicate levelized cost of hydrogen could be as low as \$0.39/kg H_2 without carbon co-product value. However, even modest amounts of catalyst losses can make the process uneconomic. While unique engineering and design challenges remain and are unproven at any scale, a molten media-based methane pyrolysis process may offer advantages with respect to carbon supply chain and utilization of preferential economic characteristics and sensitivities.

Chapter 4

Accounting for GHG emissions of delivered electricity

4.1 Introduction

Accurately quantifying the embodied greenhouse gas (GHG) emissions of energy delivered to customers is essential for climate policy implementation. Regulating emissions associated with delivered electricity is further complicated by contractual arrangements for dynamic electricity transfer that confound emissions accounting approaches rooted in the physics of grid operations. This accounting exercise can be particularly challenging in the case of electricity transfers across regulatory jurisdictions.

In Section 4.2, we evaluate a new methodology adopted by the California Energy Commission to calculate the GHG emissions intensity of retail electricity providers. In the long run, the new regulations better align with the physical nature of grid operation than did past practices, but policymakers should monitor a set of potential challenges as market structures evolve. This work has been previously published in [22].

In Section 4.3, we propose a novel consumption-based accounting methodology to reconcile the nominal and the physical flows of electricity from generators to consumers. We also compare capacity factor-based and regression-based approaches for estimating default emissions factors, in the absence of fully specified nominal electricity flows. As a case study, we apply this approach to assess the methods by which California regulators quantify specified and unspecified electricity imports and their associated GHG emissions. Collectively, these efforts illustrate principles for a comprehensive, empirical accounting framework that could inform efforts to improve the accuracy and consistency of policies regulating regional electricity transfers. This work has been previously published in [23].

4.2 Emissions intensity of retail suppliers

The Power Source Disclosure (PSD) program is a consumer information program administered by the California Energy Commission (CEC) [235]. The PSD program requires load-serving entities (LSEs) to publish and disseminate information on the mix of generation sources used to satisfy their retail electricity sales in California. Regulated LSEs include investor-owned utilities (IOUs), publicly owned utilities (POUs), co-ops that offer bundled service, and generation-only community choice aggregators (CCAs).

4.2.1 Background

California Assembly Bill 1110 (AB 1110) was enacted in 2016 and required the CEC to update the PSD program to report the greenhouse gas (GHG) emissions intensity of each LSE's resource portfolio [236]. GHG emissions are reported in terms of the metric tons of carbon dioxide equivalent emitted per unit of retail electricity delivered [tCO_2e/MWh]. The purpose of the PSD program and the AB 1110 updates is to provide accurate, reliable, and simple to understand information regarding fuel sources for electricity generation offered for retail sales in California, as well as their associated environmental impacts [236]. Retail suppliers will begin disclosing the GHG emissions intensity of their portfolios on the 2021 calendar year Power Content Label, based on their 2020 procurement.

The new regulations are notable not just for their inclusion of GHG emissions, but also for how they respond to an important debate over how those emissions should be assigned. This question is particularly relevant with respect to long-term renewable energy contracts and their associated renewable energy credits (RECs) used for compliance with California's Renewables Portfolio Standard (RPS). The debate reflects the fact that both the physics of power system operations and the economics of wholesale electricity markets jointly determine the delivery of electric power to retail consumers, but physical power flows frequently do not match contractual agreements. As a result, LSEs can end up with a contractual (or nominal) supply of resources that does not fully align with the electricity physically delivered to their customers.

The PSD regulations borrow key definitions from the state's RPS. Both programs define electricity as being "delivered" to California if the underlying resource has a first point of interconnect in a California balancing authority or is dynamically transferred to a California balancing authority (as verified by e-tags from the North American Electric Reliability Corporation (NERC)) [235]. Procurement of qualified renewable energy from sources that are directly interconnected to a California balancing authority or dynamically transferred, with the corresponding NERC e-tags (i.e. "delivered"), are designated as portfolio content category (PCC) 1 for RPS compliance. PCC 2 contracts, also referred to as "firmed and shaped" renewable procurements, involve renewable energy purchases that are delivered to a non-California balancing authority, but for which associated

CARB – California Air Resources Board
CCA – Community choice aggregator
CEC – California Energy Commission
GHG – Greenhouse gas
IEMAC – Independent Emissions Market Advisory Committee
IEPR – Integrated Energy Policy Report
IOU – Investor-owned utility
LSE – Load-serving entity
NERC – North American Electric Reliability Corporation
PCC – Portfolio content category
POU – Publicly-owned utility
PSD – Power Source Disclosure
REC – Renewable energy credit
RPS – Renewables Portfolio Standard

Table 4.1: Acronyms

RECs are matched with an equivalent amount of energy that is scheduled for delivery to a California balancing authority. PCC 3 procurements refer to the purchase of "unbundled" RECs with no associated energy procurement.

The difference between the physical operation of the grid and the contractual operation of energy markets has led to a debate over how GHG emissions should be assigned in policy systems. Some researchers have suggested that emissions accounting could be based on purely physical flows using tools like consumption-based accounting or marginal emissions analysis [237, 238]. In practice, however, most legacy policy systems for renewable energy have relied, at least in part, on the use of contractual accounting mechanisms like RECs. However, some policy experts have highlighted the potential for the use of unbundled RECs to distort the true GHG emissions associated with physically delivered electricity [239]. In addition, California's Independent Emissions Market Advisory Committee (IEMAC) observed the potential for "double-counting" of zero-emissions electricity across different regulatory authorities if one agency accounts for emissions on the basis of physically delivered power while another associates the nominal transfer of a REC with the emissions attribute of electricity [240, 241]. Other stakeholders have argued that many contracting parties believe RECs should be associated with a zero-GHG attribute and therefore any decision that treats RECs as not including those environmental attributes could be problematic to existing marketplace actors [242, 243].

The PSD regulations focus primarily on reporting GHG emissions associated with the LSEs' delivered electricity, rather than their nominally contracted resource mix [243]. Critically, the PSD regulations require that LSEs' reported emissions intensity of PCC 2 purchases should be that of the delivered power, rather than the nominal, contractual procurement. This treatment extends to any specified contract that allows for substitute power to be delivered, including contracts for electricity from large hydro-electric generators that are not RPS-eligible but which otherwise fit the "firmed

and delivered" contract model. As PCC 3 purchases are unbundled RECs and not associated with the purchase of any power, they are not used to compute the fuel mix or GHG emissions intensity of an LSE's retail sales [235].

The PSD regulations' focus on physical emissions accounting, as opposed to contractual emissions accounting, has important implications for California's long-term climate policies. California's 100% clean electricity law, Senate Bill 100 (SB 100), sets a 2045 target of having 100% of retail electricity sales come from zero-GHG resources [168]. The CEC's new methodology for calculating the GHG emissions profile of LSEs' retail sales could thus take on additional importance as state policymakers develop an accounting structure and enforcement regime for the SB 100 target.

This section explores how the PSD program might perform going forward as a climate policy by evaluating how the program reports GHG emissions intensity. Section 4.2.2 summarizes the CEC-adopted calculation methodology, identifies the data and assumptions we use to estimate GHG emissions intensities based on the CEC's methods, and presents an alternative approach for calculating the GHG emissions intensity of an LSE's retail sales, as originally proposed by a CEC staff proposal [244]. Section 4.2.3 applies the calculation methodology to data from LSE-submitted supply forms to present a snapshot of potential emissions intensity values for a selection of California's largest LSEs. Because LSEs might decide to modify their procurement behavior in response to the new regulations, we develop a simple snapshot of the outlook based on 2019 reporting that occurred prior to the finalization of the regulations. Section 4.2.4 discusses some implications of the adopted calculation methodology in the near and long term and draws conclusions about the updates to the PSD program and provides recommendations for further analysis and monitoring.

4.2.2 Methods

CEC calculation methodology

The CEC's methodology characterizes the energy mix for each LSE by aggregating its specified electricity purchases on an annual basis. Specified purchases are transactions in which electricity is traceable to specific generating facilities by an auditable contract trail, including associated e-tags. Retail suppliers can employ annual data to meet this requirement instead of hour-by-hour matching of loads and resources. Any specified wholesale sales must be deducted from each specified gross purchase, per Eq. (4.1), to yield the specified net purchases NG_i [MWh] for the year.

$$NG_i = GP_i - WS_i \qquad \forall i \in \mathcal{SP} \tag{4.1}$$

We refer to an LSE as "under-procured" if its retail sales exceed total net specified purchases and "over-procured" if it has net specified purchases that exceed its retail sales.

If an LSE has total specified net purchases in an amount less than their retail sales (i.e., is

under-produced), then the remainder is assessed as unspecified power, per Eq. (4.2).

$$U = RS - TNP \tag{4.2}$$

If an LSE has total specified net purchases in an amount greater than their retail sales (i.e., is over-procured), then specified net purchases must be decremented in an amount such that the sum of all net purchases will equal total retail sales. The CEC's method allows entities that are over-procured to deduct natural gas specified purchases first, per Eq. (4.3a). If the natural gas procurements are smaller than the difference between total specified purchases and retail sales, then all other fossil-fueled purchases are decremented proportionately, per Eq. (4.3b). Finally, if the total amount of adjusted net purchases still exceeds retail sales, the remainder of specified purchases will be decremented proportionately, per Eq. (4.3c).

$$\text{if } 0 \leq (TNP - RS) \leq NP_{NG} \tag{4.3a}$$

$$\begin{cases} ANP_i = NP_i - (TNP - RS)\frac{NP_i}{NP_{NG}} \forall i \in \mathcal{SP}_{NG} \\ ANP_i = NP_i \forall i \notin SP_{NG} \end{cases}$$

$$\text{if } NP_{NG} \leq (TNP - RS) \leq NP_{NG} + NP_F \tag{4.3b}$$

$$\begin{cases} ANP_i = 0 \forall i \in \mathcal{SP}_{NG} \\ ANP_i = NP_i - (TNP - NP_{NG} - RS)\frac{NP_i}{NP_F} \forall i \in \mathcal{SP}_F \\ ANP_i = NP_i \forall i \notin SP_{NG} \cup SP_F \end{cases}$$

$$\text{if } NP_{NG} + NP_F \leq (TNP - RS) \tag{4.3c}$$

$$\begin{cases} ANP_i = 0 \forall i \in \mathcal{SP}_{NG} \cup SP_F \\ ANP_i = NP_i - (TNP - NP_{NG} - NP_F - RS)\frac{NP_i}{NP_Z} \forall i \in \mathcal{SP}_Z \end{cases}$$

A source-specific emissions factor, β_i [tCO_2e/MWh], is then applied to all adjusted specified net purchases in order to evaluate the amount of emissions associated with this portfolio of electricity. For any unspecified electricity purchases, a default emissions factor for electricity from unspecified sources, β_u [tCO_2e/MWh], is applied. Dividing these gross emissions by retail sales yields the emissions intensity estimate, EI [tCO_2e/MWh] for the LSE portfolio, as per Eq. (4.4).

$$EI = \frac{EF_u U + \sum_{i \in \mathcal{SP}} EF_i ANP_i}{RS} \tag{4.4}$$

For specified purchases with the corresponding NERC e-tags that are delivered to a California balancing authority, the source-specific emissions factor will reflect the emissions intensity associated

with the contracted generator. As mentioned above, some specified purchases of RPS-eligible renewable energy fall under PCC 2 and PCC 3, which do not involve electricity purchases delivered to a California balancing authority. PCC 3 procurements are excluded from the GHG emissions intensity calculations, as these unbundled RECs are financial instruments that do not reflect electricity procurement.

The PSD regulations specify that the emissions factor associated with "firmed and shaped" PCC 2 purchases—or any similar contracts that allow for power to be delivered that is not from the contracted source—should be that of the substitute (delivered) power, rather than the nominal (contractual) procurement. Unless the generator of the substitute power is identified with the associated e-tags, the delivered power will be deemed an unspecified import and assigned a default emissions factor. Unspecified power includes all unspecified spot market purchases (including those furnished by in-state generators), non-marginal imports from neighboring balancing authorities, or power from renewable sources that has been separated from its REC (null power).

The PSD's physical delivery accounting structure applies only to new contracts, with legacy contracts that pre-date the regulation grandfathered under an accounting structure that is based on contracted resources instead. For legacy contracts, LSEs must report the emissions associated with the contracted resource, even if another resource is physically delivered to serve its customers. This contract-based treatment applies until the underlying contract expires or is modified. Thus, once all grandfathered contracts reach maturity or are modified, the PSD program will have shifted the state's retail electricity emissions accounting structure to one based on the physical deliveries.

Unspecified purchases are assigned a default emissions factor developed by the California Air Resources Board (CARB) (β_u = 0.428 tCO_2e/MWh). CARB adopted this emissions factor in 2010, based on data from 2006-2008, and intended it to represent the marginal emissions associated with electricity imports from unspecified sources on the Western Interconnect (WECC) [245, 246]. Although CARB maintains that this factor remains accurate today [188], others have argued that the use of a static value based on data from 2006-2008 may not accurately reflect the operational realities of the WECC today due to changes in fuel and technology costs [246]. Reflecting these concerns, the IEMAC recommended CARB update its unspecified emissions factor [241, 240].

Estimating portfolio GHG emissions intensities

To explore the implications of the CEC-adopted methodology, we estimate what the reported emissions intensity would be for some of California's largest LSEs if the new methods were applied to reported data from the CEC's 2019 Integrated Energy Policy Report (IEPR) filings Forms S-1 and S-2 [247]. More details on these forms can be found in [248]. The IEPR supply forms include any contracts in place at the time of reporting and reflect actual procurement for 2017 and 2018 and planned procurement for 2019-2030. Actual procurement for 2019 and beyond may differ from these estimates, as contracts are transferred among LSEs in response to changes in retail sales forecasts.

In addition, LSEs could also modify their procurement behavior in response to the new PSD regulations or any new developments in western electricity markets. We analyze a static outlook based on 2019 reporting to provide one view of how the PSD labels for individual LSEs might evolve, rather than to predict expected outcomes.

Our analysis uses generic emission factors for each reported fuel type—unlike the PSD regulations, which apply source-specific emissions factors for each specified electricity purchase. For coal and natural gas, we use the average emissions intensity of generators of each fuel in 2018: 0.981 tCO_2e/MWh for coal and 0.415 tCO_2e/MWh for natural gas [128]. This assumption overstates the amount of emissions from some natural gas-fired generators, as some supply contracts involve combined heat and power (CHP) plants that will report lower facility-specific emissions in practice. Finally, as retail sales data are not publicly available for all LSEs, we use the firm load procurement requirement from IEPR Form S-1 as a proxy for this value. The firm load procurement requirement includes retail sales, utility uses, losses, and any wholesale obligations.

Some LSEs have redacted supply data for specific years or for the entire time horizon. In such instances, persistence estimates are used to characterize the missing information. Most notably, this is the case for the natural gas-fired procurements of Pacific Gas & Electric (PG&E) beyond 2018. As such, we assume that the natural gas-fired procurements for PG&E will remain constant at 2018 levels. San Diego Gas & Electric only provides procurement information for the years 2017 and 2018 and consequently is not included in the forward-looking analysis.

In the case of an over-procured LSE, it is necessary to decrement specified purchases in order that the contributions towards the portfolio sum to equal retail sales. The CEC's adopted methodology preferentially decrements first (1) specified natural gas and then (2) other fossil fueled purchases before (3) non-fossil purchases. As an alternative approach, we consider a methodology that would retain the proportionate representation of the full set of LSE-purchased resources. Instead of preferentially reducing fossil resources over clean energy, this alternative method would reconcile total specified purchases with retail sales by proportionately adjusting all specified purchases downward. This method was originally proposed by the CEC, but (according to the Final Statement of Reasons) elicited broad opposition from stakeholders who requested that the retail supplier be permitted to assign its preferred resources to customers [249]. This is expressed mathematically in Eq. (4.5).

$$\forall i \in \mathcal{SP}, \quad ANP_i = NP_i - (TNP - RS)\frac{NP_i}{TNP} \tag{4.5}$$

We also explore the treatment of firmed and shaped renewable energy contracts. The PSD program evaluates the emissions associated with new firmed and shaped contracts with respect to the substitute (delivered) power rather than the nominal (contractual) resource. But contracts signed before the new regulations were developed are assigned the emissions of the nominal (contractual) resource. We test the exposure of various LSEs to this policy decision, as well as the temporal

effects arising from the turnover of older contracts into new or modified contracts. We assume that all PCC 2 purchases identified in the IEPR supply forms will be grandfathered in and treated as zero-emissions renewables, not evaluated at the emissions intensity of the substitute power. We test the effect of treating PCC 2 procurements as unspecified power in order to characterize the extent to which results may change if existing contracts were not subject to grandfathering.

4.2.3 Results & discussion

Applying the CEC-adopted calculation methodology to the data from 2019 IEPR supply forms, we present the emissions intensity estimates for several of the largest California LSEs based on 2017 and 2018 procurement data in Figure 4.1.

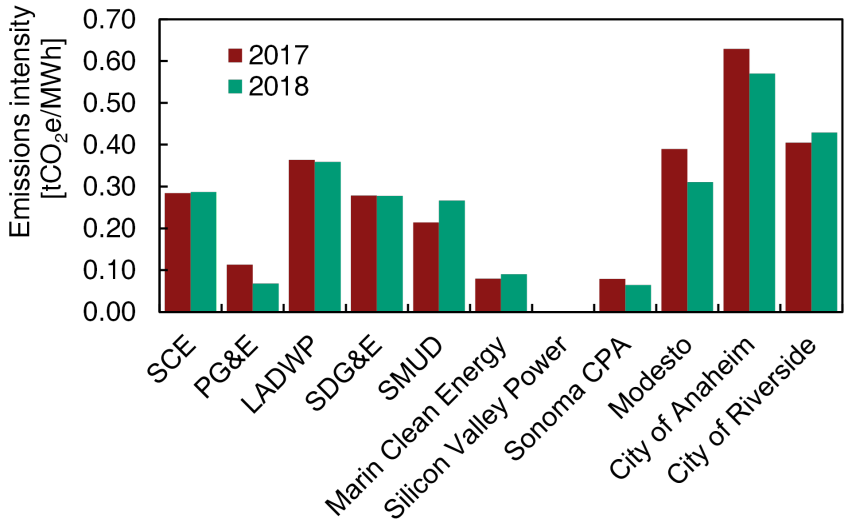

Figure 4.1: Calculated emissions intensities for several large California LSEs.

Additionally, we present the outlook for emissions intensity estimates, based on reported procurement plans and contracts in place from 2017-2030 (Figure 4.2). Any LSE with a 2018 procurement requirement above 2 TWh was included in the analysis, subject to data availability constraints described in Section 4.2.2.

Figure 4.2 illustrates three trends across different categories of LSEs. First, over-procured investor-owned utilities like PG&E would expect to see favorable application of the CEC's preferential reductions of natural gas purchases—causing PG&E's reported emissions intensity to drop to zero before increasing in later years due to the scheduled retirement of its Diablo Canyon nuclear generating units. In contrast, Southern California Edison (SCE) is expected to have constant emissions intensity estimates based on currently reported supply data. This is due to a high reliance on unspecified power and consistent under-procurement relative to their firm procurement requirement. California's third major IOU, SDG&E, has no public data available for this analysis.

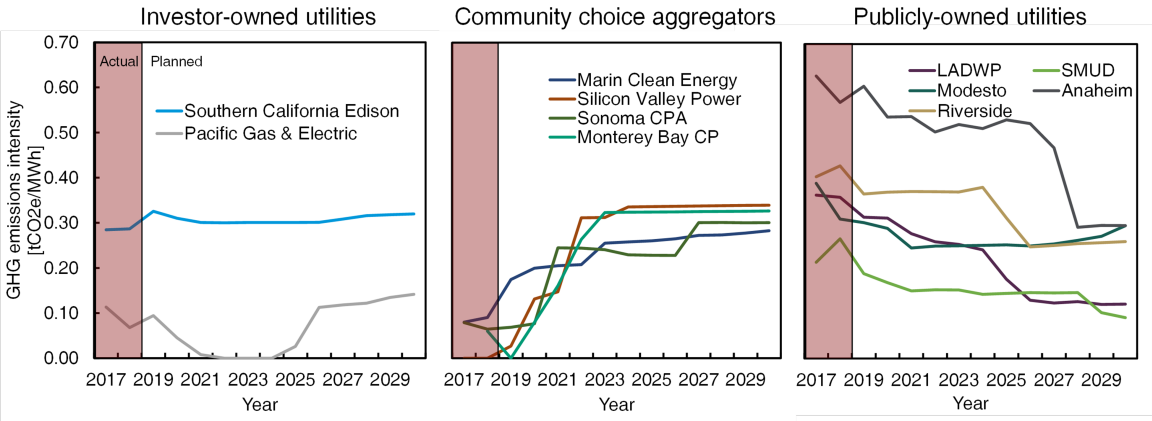

Figure 4.2: Calculated emissions intensities for the electricity supply planning forms submitted by IOUs, CCAs, and POUs. Data for years 2017 and 2018 are reflective of actual procurement, while the years 2019-2030 are reflective of planned procurement.

Second, several community choice aggregators—including Marin Clean Energy, Silicon Valley Power, and Monterey Bay Community Power—would report very low GHG emissions intensities in the immediate term, with emissions intensities rising rapidly in the early 2020s. Many of these CCAs rely on firmed and shaped contracts that will be treated as zero-emissions electricity for legacy contracts, but which would receive higher emissions factors associated with actual physical deliveries for new contracts. Third, some publicly-owned utilities, such as LADWP and SMUD, have emissions intensity values that trend downwards as planned shedding of coal-fired purchases and increased share of zero-emissions energy drives declines in average reported emissions intensity.

Figure 4.3 provides additional insights into the effects of over-procurement among some LSEs. This figure compares the results we project using (1) the CEC's adopted method of preferentially decrementing specified natural gas and then other fossil fueled purchases before non-fossil purchases for over-procured LSEs, and (2) the alternate method we described in which all resources are decremented proportionately. For most LSEs, the CEC's adopted method generally biases emissions intensity estimates downward from the true proportionate contribution of specified purchases. In the case of Anaheim Public Utility, however, the preferential deduction of natural gas-fired purchases biases emissions intensity upwards because this POU has significant coal resources in its planned portfolio for most of the 2020s.

Taking this one step further, an LSE could report an emissions intensity of 0 tCO_2e/MWh under the adopted method by procuring an annual volume of zero-emissions energy equal to its retail sales, regardless of when that generation is provided to the grid. Unless actual zero-emissions generation (with or without storage) closely matches real-time demand, such an LSE would still need to rely on additional procurement that would not be reflected in the reported emissions intensity. Figure 4.4 provides a stylized example. In the left panel, we calculate the emissions intensity for a hypothetical

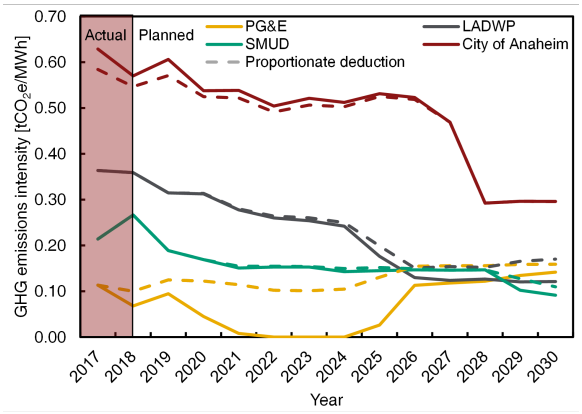

Figure 4.3: Comparison of estimated emissions intensity for major load serving entities that plan to be systematically over-procured over the next ten years.

LSE with various annual portfolios of specified purchases and/or reliance on system power using (1) the CEC-adopted methodology and (2) the proportionate deduction methodology. The right panel illustrates how annual procured generation could align with retail sales in real time.

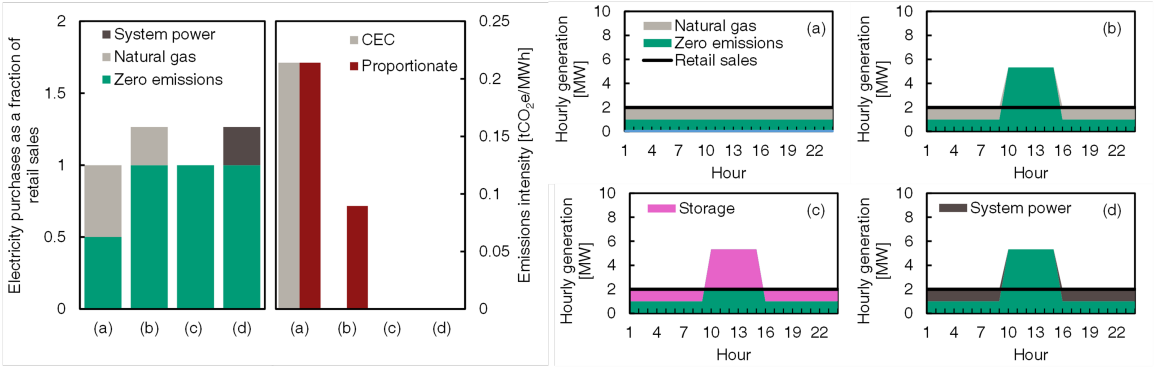

Figure 4.4: Left: Various portfolios of specified purchases and/or reliance on system power for a toy load serving entity and the emissions intensity, as calculated by the CEC-adopted method, and using a proportionate reduction for any over-procurement. Right: Illustrative temporal profiles displaying how procured generation for each scenario could align with retail sales in real-time.

In scenario (a), annual retail sales are met by equal shares of specified zero-emissions and natural gas purchases. If instead specified purchases from zero-emissions resources increase to equal annual retail sales as in scenario (b), the CEC's adopted methodology will report 0 tCO_2e/MWh—even if the LSE still relies on natural gas purchases to meet real-time demand. The CEC's adopted methodology will also not differentiate between scenario (b) and scenario (c), in which the LSE utilizes storage (or other load-shifting strategies) to align zero-emissions procurement with demand in real-time, irrespective of their very different consequences for electricity grid operations. The

proportionate deduction approach, on the other hand, will result in 0 tCO_2e/MWh if and only if an LSE's specified purchases come exclusively from zero emissions sources.

In scenario (d), the LSE meets real-time demand with unspecified spot market purchases, rather than specified natural gas purchases as in scenario (b). In this instance, neither the CEC-adopted method nor a proportionate reduction approach would allocate any emissions to the LSE, because unspecified power assigned to an LSE is calculated as the aggregate difference between specified purchases and retail sales. Improved temporal resolution, with hourly reconciliation of specified purchases and retail sales for example, is required to capture the reliance on system power visualized in Figure 4.4, scenario (d).

Finally, we evaluate the impact of grandfathering existing PCC 2 renewable energy contracts designated as such by three CCAs in the supply forms used in this analysis. Figure 4.5 estimates the GHG intensity of these CCAs' portfolios if their legacy contracts were assigned the emissions intensity of unspecified power, rather than renewable power under the CEC's new rules. This change has a substantial effect on 2017 and 2018 reporting, but the impact of this distinction quickly fades as LSEs do not report many long-term contracts designated as PCC 2.

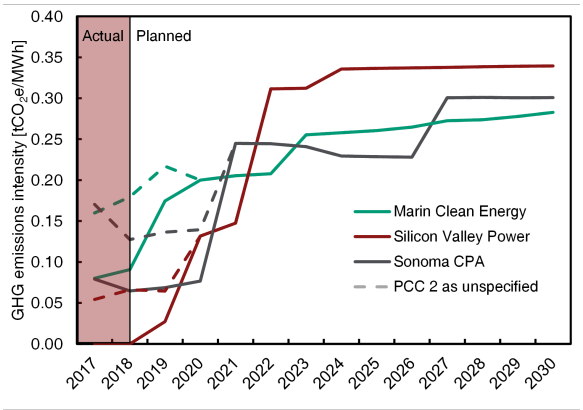

Figure 4.5: Alternative emissions intensity estimates for three community choice aggregators if PCC 2 renewable energy contracts are assigned unspecified power GHG emissions.

We note that this is an illustrative example of how sensitive the emissions intensity estimates could be to the CEC's decision to provide a more lenient emissions treatment for legacy "firmed and shaped" contracts. We do not have information on the true source of the delivered power for each of these firmed and shaped import contracts—which could plausibly be specified in some legacy "firmed and shaped" contracts—but we believe that unspecified power emissions offers a reasonable way to bound the possible range of impacts. While the impacts of this methodological decision could be substantial for near-term reporting of emissions intensity for several entities, the supply forms used in this analysis do not indicate that longer-term contracts for these resources will meaningfully distort the emissions intensity reporting thereafter. In the future, we would expect that LSEs may

evaluate whether to modify their procurement behavior because of changes in the PSD program regulations.

4.2.4 Conclusions

The CEC's new Power Source Disclosure methodology fundamentally orients the reporting of LSEs' GHG emissions intensities around the physical flows of power deliveries. As a means of establishing an emissions accounting framework that is reliable in the long run, the new methodology constitutes a meaningful step toward providing accurate, reliable, and simple to understand information regarding fuel sources for electric generation offered for retail sale in California and the associated GHG emissions. In the near term, however, GHG emissions intensities estimated by the new methods might not fully reflect the portfolio of generation resources procured for delivery to serve California customers for two reasons.

First, over-procured LSEs—most notably PG&E—are subject to preferential accounting rules. If these LSEs remain over-procured for the next few years, it is possible that some will report artificially low GHG intensities associated with the fact that they have procured a surplus of zero-carbon resources relative to their loads and may be selling these resources to other LSEs on the spot market. On the other hand, over-procured LSEs have generally been selling their procured resource contracts to other LSEs whose customer bases are growing. While LSEs have no fundamental economic interest in remaining over-procured, to the extent they are able to balance their supply and demand needs through reselling in wholesale electricity markets—including possible future exports throughout and expanded western market—then it is conceivable that some will maintain a procurement posture that produces biased GHG intensity estimates under the PSD program. The pace at which resource re-allocation progresses will likely determine whether this issue manifests at a meaningful scale. A recent proposal could re-allocate large portions of the zero-GHG procurements from IOUs to CCAs, which would alter the trends identified, potentially leaving the CCAs in an over-procured position relative to their retail sales [250]. State regulators should be well positioned to monitor these conditions and evaluate whether any methodological changes are needed in the future.

Second, the CEC made a policy decision to grandfather LSEs' firmed and shaped contracts. Legacy firmed and shaped contracts that provide non-zero-GHG delivered resources are treated as having zero emissions for the purpose of the PSD program, even though new contracts with identical provisions will be assessed at the emissions intensity of the physically delivered power. This decision will tend to bias downwards the reported emissions intensity of LSE portfolios in most cases where such contracts are present. Nevertheless, current supply data indicates that any such effects are likely to be transient: as long-term supply contracts and retail electricity load are transferred between IOUs and CCAs, the impact of these methodological decisions should be diminished because new or modified contracts will be assigned the emissions of the power they physically deliver.

We note that all our analysis is based on data and projections made in the IEPR reporting

process, which occurred prior to the final PSD program regulations. We anticipate that many LSEs will evaluate how the new regulations affect them and may choose to modify their procurements going forward. For example, firmed and shaped procurements may be less popular now that the emissions intensity of such purchases will be calculated with respect to the delivered energy, rather than the nominally contracted source. As a result, we would expect that actual procurement will vary from what is projected in the 2019 IEPR planning process. Our results should not be interpreted as a prediction, but rather as an empirically grounded scenario for exploring potential issues arising under the PSD program requirements.

It is also possible that LSEs might adapt their procurement behavior to achieve artificially low emissions intensity estimates under the PSD accounting methodology. For example, an LSE's over-procurement of long-term supplies relative to retail sales will tend to create GHG emissions intensity estimates that are biased downward. LSEs are permitted to count any "delivered" electricity as a specified purchase, which is broadly defined to include any generation with a first point of interconnection in a California balancing authority. It is likely that in the coming decades, enhanced regional coordination will increase spot export of electricity from in-state renewable generators to mitigate curtailment [251]. The current CEC-adopted methodology would allow LSEs to nominally achieve zero emissions associated with retail sales while maintaining specified purchases of fossil-fueled generation offset on an annual basis by an equal amount of over-procured renewables that are exported to serve out-of-state load. This would represent a divergence between the regulatory definition of "delivered" electricity and the electricity physically delivered to serve California customers. Such an outcome could also create inconsistencies in interagency GHG accounting. For example, the greenhouse gas emissions inventory conducted by CARB assesses emissions liabilities that reflect all in-state generation and gross electricity imports [169]. In a high-exports scenario, the CEC could report LSE emissions intensities approaching zero while CARB assesses nontrivial emissions liabilities to electricity importers and/or in-state merchant generators. While the spot market price risk of this financial position may not be attractive to LSEs, we offer this thought experiment as an illustration of how the CEC's new methodology could be exploited to bias reported emissions intensities downwards.

This potential divergence could be remedied by moving towards an hourly accounting system to reconcile LSEs' procured generation supplies and retail sales. Under this framework, hourly generation that exceeds demand would be credited according to the emissions avoided by displacing system power, while demand that exceeds specified purchases would be assessed liabilities at the emissions intensity of system power for that hour. This approach is taken for long term planning of future energy systems by the California Public Utilities Commission in the Clean System Power calculator [252]. In order to match this methodological approach in the PSD program, the nominal allocation of historical hourly generation to retail load would require additional data reporting from LSEs on the temporal generation of all specified purchases. In theory, generation curtailment

could eventually create the incentive for LSEs to pursue improved hourly matching. By adopting hourly accounting structures, however, policymakers could accelerate that trend, limit the nominal concentration of emitting generation among unregulated segments of load (losses, self-consumption, wholesale sales, exports, etc.), and improve consistency with other utility planning proceedings [253, 254].

The CEC's adopted regulations also include an exclusion such that newly established CCAs will not begin reporting the GHG emissions intensity of their retail sales portfolio until two years following service of their first retail customers [235]. As additional CCAs form, the PSD program will not produce public information during CCAs' initial years, when customers are most likely to decide whether to opt out of a newly formed CCA. CCAs often claim superior environmental attributes relative to the incumbent utility provider, but the lack of clear information on emissions characteristics during the initial phase of new CCAs' operations—as well as potential bias in the values reported for over-procured incumbents—could deprive consumers of relevant information.

In updating its Power Source Disclosure program, the California Energy Commission has taken meaningful steps to improve the reporting structures for GHG emissions intensity associated with retail electricity service to California customers. By assigning imported specified purchases of electricity the emissions associated with delivered power, the CEC aims to balance recognition of the physical and contractual elements of electricity system operation.

We find that the PSD program's methods are likely to produce a clear and reasonable basis for evaluating the emissions associated with physical deliveries of retail power over the long run. In the near term, however, two effects—both of which are likely transient—could lead to artificially low reported GHG emissions intensities for some LSEs. First, the PSD program rules reward LSEs that are over-procured by preferentially deducting the GHG emissions associated with emitting resources. This allows over-procured LSEs to claim a higher share of zero-carbon resources than is present in their total procurement profile. Until the process of re-allocating retail electricity load and long-term supply contracts among LSEs is complete, the CEC-adopted methodology could allow several LSEs to report artificially low emissions intensity estimates. Second, a decision to grandfather legacy firmed and shaped contracts under a preferential emissions accounting method will tend to produce artificially low GHG emissions estimates for LSEs that, like many community choice aggregators, have relied heavily on contracts that include renewable energy certificates but physically deliver other resources to retail customers. As these contracts reach maturity, however, the reported GHG emissions of their replacements will be increasingly based instead on the power that they physically deliver.

The PSD program's primary use is as a customer-facing retail labeling program, but its accounting structure could also be applied to other state policies. Notably, SB 100 set a target for all LSEs to deliver 100% of retail sales from zero-GHG resources by 2045. Because this target is expressed in the same terms as the PSD program, it is possible that the PSD methods could be adapted or

applied to inform an implementation strategy for SB 100.

Both in the context of evaluating the accuracy of the retail labeling program as well as any future application to deep decarbonization policy, the PSD program would benefit from ongoing regulatory monitoring and evaluation. As electricity markets evolve, some of the program's methodological choices could lead to unintentional bias that becomes more problematic than it appears today. For example, if an export-intensive spot market develops and some LSEs remain contractually over-procured, it might be possible that some of the challenges we identified in this paper become more problematic. In addition, there may be important opportunities to improve the PSD program by incorporating hourly analysis of generation and retail load matching, especially if this can be done in coordination with other state agencies. Meanwhile, by shifting to a retail electricity emissions accounting regime that is based on physical power deliveries, the PSD program is now set up to help policymakers and LSEs navigate the direct climate impacts of their procurement decisions.

4.3 Emissions intensity of regional transfers

Regional coordination and dynamic transfer of electricity can allow for expanded use of low-cost energy resources [164] and resource diversity can help improve reliability of electricity systems, particularly as policymakers and utilities strive to achieve environmental goals [255, 256]. Such interactions often cross jurisdictional boundaries, complicating the measurement of environmental impacts and attribution of these impacts to regulated entities.

4.3.1 Background

Consumption-based accounting is one method popularized for tracking embodied greenhouse gas (GHG) emissions across trade networks and allocating responsibility to consumers, rather than producers [257]. Due to the indistinguishable nature of electrical energy after injection to the electricity grid, consumption-based accounting is a useful mathematical tool for quantifying embodied emissions associated with electricity deliveries in complex networked systems. The motivation for this framework for electricity systems is conceptually outlined by Ji et al. (2016) [258]. Various studies have since exploited the networked architecture of the electricity grid to estimate emissions factors of delivered electricity using an input-output framework [259, 260], iterative methods [261], and consumption-based accounting techniques [237].

In the United States, constitutional limits apply to state governments' ability to regulate interstate, wholesale electricity transactions. State climate policies are designed, instead, to regulate the composition of retail electricity sales [168]. Attributing emissions to retail providers according to their electricity supply portfolio is complicated by the presence of nominal or contractual purchases that deviate from a strict interpretation of the physics of electricity grid operation [235, 22]. A

strictly physical interpretation of GHG accounting would assert that electricity injections to a synchronously managed grid are indistinguishable from one another. It is a mathematical impossibility to attribute a particular generation source to any specific customer as electricity does not flow from a source to a sink; all generators work in concert to energize the grid and supply all demands. As such, any deliveries from a balancing authority in a particular moment would have the emissions attributes of the generation-weighted average emissions intensity of generators producing electricity at that instant. However, electricity providers also enter contractual arrangements for nominal delivery of electricity from specific generators with associated renewable or emissions attributes.

This joint nominal and physical nature of electricity delivery is reflected in the composition of "specified" and "unspecified" purchases attributed to a retail supplier. Specified electricity purchases can be traced to a unique generator with measurable emissions attributes. The emissions consequences of this class of purchases are usually assessed on a nominal basis, directly allocating the source-specific emissions to the entity purchasing the electricity. Unspecified electricity purchases do not have a traceable contract path from a particular generator. Emissions intensity estimates for unspecified electricity usually reflect a physical interpretation of electricity grid operations. Jurisdictions may adopt a default emissions factor for unspecified purchases, intended to represent the marginal emissions associated with incremental electricity generation from the originating control area. Such techniques may use capacity utilization factors to estimate which plants may increase annual output in response to increased demand for electricity [262]. Several academic papers have also quantified the emissions impact of marginal electricity demand using regression-based techniques [263, 264, 238, 265]. Such approaches may account for temporal variation in marginal emissions attributes through independent analysis of similar time steps, segmented on an annual, monthly, or hourly basis [263, 238, 265, 266]. Regional heterogeneity can be controlled for, to an extent, by analyzing individual balancing authorities as opposed to entire synchronous electricity grids [267].

Physical paradigms for GHG accounting offer analytical clarity and consistency, but for these methods to be useful they must coexist with the nominal arrangements and attributes which differentiate electricity supplies. Accounting frameworks must balance the imperative for accuracy, consistency, and clarity, and the desire to align economic incentives for market participants with policy objectives.

California has committed to reduce statewide GHG emissions 40% below 1990 levels by 2030 [268], with even deeper targets for the electricity sector [269]. The electricity sector has also been the single biggest driver of California's falling statewide GHG emissions [270, 271] with changes in the composition of electricity imports accounting for nearly 73% of the observed declines in electricity sector emissions since their peak in 2008 [271, 272]. Although electricity imports play a critical role in state climate and energy policy, they are not subject to a uniform accounting regime for GHG emissions. The California Air Resources Board (CARB) regulates GHG emissions from electricity imports in the state's cap-and-trade program and tracks progress towards the state's economy-wide

climate goals. Imports are designated as either specified or unspecified in CARB's Mandatory GHG Reporting Regulation (MRR) [169], with distinct implications for emissions accounting. Because a specified resource involves electricity contractually identified as transferred from a particular power plant, CARB treats specified imports as having the source-specific emissions intensity of the known out-of-state generator. To qualify as a specified import, the electricity must either have a point of first interconnect within a California balancing authority or be dynamically transferred to a California balancing authority with importers holding the associated North American Electric Reliability Corporation (NERC) e-tags to verify its delivery [169].

In contrast, unspecified imports lack a traceable contract path from their buyer to a specified generation source. CARB assigns a default emissions factor to quantify the GHG emissions from unspecified imports (0.428 tonnes CO_2e/MWh). This factor is based on an estimate of which generating units are likely to serve marginal load in the Western Interconnect (WECC), drawing on analysis of data from Energy Information Administration (EIA) Form 860 and Form 923 for the years 2006-2008 [241]. CARB's default factor was estimated over a decade ago and has not been updated since [246]. In 2018, CARB staff indicated that they had evaluated the accuracy of the default emissions factor and concluded that no update was required [273].

Accounting differences also matter in the context of the broader western grid. Multiple California policies require that GHG emission reductions reported in the state do not result in increased emissions elsewhere, a phenomenon known as "leakage" [168, 268]. Accounting for, and mitigating, emissions leakage is a principal objective of any unilateral climate policy, whether economy-wide [274, 275] or specific to the electricity sector [276]. In the electricity sector, leakage can occur on operational time scales, due to changes in the generation dispatch schedule, or on planning time scales, due to the reallocation of carbon-intensive resources to unregulated entities, a phenomenon known as "resource shuffling" [277]. Implicit in any emissions leakage estimate is an assumed counterfactual baseline scenario describing what would have happened in the absence of those climate policies. Econometric [278] and equilibrium simulation techniques [279] have been used to characterize the potential electricity sector emissions leakage consequences of California's cap-and-trade regulations.

CARB does not assign an emissions leakage liability to specified imports in bilateral contracts but does in the case of imports from the CAISO Energy Imbalance Market (EIM). Currently, the CAISO EIM accounts for only a small fraction of imports—about 3% in recent years [280] - but the role of regional trading is expected to grow significantly, especially as CAISO considers an extended day-ahead market [240, 251]. Leakage is a concern in the EIM because the market preferentially allocates zero-emissions energy for nominal transfer to serve California load, which could result in secondary dispatch of emitting generators to serve out-of-state load. CARB and CAISO collectively aim to quantify and mitigate emissions leakage from the EIM today by (1) limiting the bid of a participating generator to a deviation from their committed base schedule and (2) treating this transfer as "unspecified" for the purposes of emissions accounting in an annual true-up [281].

Policy efforts are already underway to harmonize some of these inconsistencies, but the underlying reasons for these differences and opportunities for greater consistency have not been well-characterized in the academic literature. In California, three disparate accounting mechanisms are employed to measure the GHG emissions impacts associated with specified electricity transfers, unspecified electricity transfers, and the emissions leakage consequences.

New techniques are needed to reconcile the nominal and physical flows of electricity from generators to consumers to provide accurate information to customers about their retail provider's portfolio and to assess liabilities in climate policy enforcement. This paper proposes a novel methodological framework that allows for harmonized GHG accounting, recognizing both the nominal and physical attributes of electricity supply, including electricity from unspecified sources, and estimating emissions leakage impacts outside of the regulated jurisdiction. As a case study, this chapter analyzes the GHG accounting methods in use for electricity imports by California agencies to assess consistency with the best available evidence and methods. Collectively, these efforts illustrate principles of a comprehensive, empirical accounting framework that could inform efforts to improve the accuracy and consistency of policies regulating embodied emissions of interregional electricity transfers to California and across the West.

We present a two-part analysis. First, we propose a novel consumption-based accounting framework that (1) respects known contractual procurements of specified electricity transfers, (2) isolates the margin of unspecified electricity transfers and its associated emissions intensity, and (3) estimates GHG emissions leakage factors in a consistent manner for all specified electricity transfers. The result of this analysis is compared against a purely physical consumption-based accounting baseline, as well as the current accounting framework applied by California regulators. Second, we compare capacity factor-based and regression-based approaches to estimate marginal emissions factors for unspecified electricity transfers, for use in the absence of fully specified nominal electricity flows. Section 4.3.2 reviews our methods and data, and Section 4.3.3 reports our results and Section 4.3.4 discusses their policy implications.

4.3.2 Methods

Estimating GHG emissions of electricity transfers

Contract-adjusted consumption-based accounting A consumption-based accounting framework can be used to quantify the embodied emissions associated with electricity transfers, as demonstrated by de Chalendar et al. (2019) [237]. This method assumes that each balancing authority delivers undifferentiated electricity at every moment, and therefore that the emissions intensity of each MWh of delivered electricity is equal to the generation-weighted average of local generators and positive transfers to that balancing authority. The gross emissions, $E_{i,t}$ [tonnes CO_2] embodied in electricity generated at a given balancing authority ($i \in B$), in a given time step ($t \in T$), equals the sum of all generators' committed dispatch, $P_{g,t}$ [MWh] multiplied by their source-specific emissions

factors, α_g [tCO_2/MWh] for all generators in balancing authority ($g \in G_i \subset G$).

$$E_{i,t} = \sum_{g \in G_i} \alpha_g P_{g,t} \tag{4.6}$$

Any embodied emissions transferred to the balancing authority are calculated as the product of flows into the balancing authority, $u_{i,t}$ [MWh], multiplied by the emissions intensity of electricity delivered in the sending balancing authority, $x_{i,t}$ [tCO_2e/MWh]. These embodied emissions entering the balancing authority must equal the sum of embodied emissions as delivered to local demand at the balancing authority, $d_{i,t}$ [MWh] and as delivered to export transfers to other balancing authorities, $v_{i,t}$ [MWh].

$$E_{i,t} + \sum_{j} x_{j,x} u_{i,j,t} = x_{i,t} d_{i,t} + \sum_{k} x_{i,t} v_{k,i,t} \tag{4.7}$$

In addition to the above mass balance, an energy balance is imposed at every balancing authority.

$$\sum_{g \in G_i} P_{g,t} + \sum_{j} u_{i,j,t} = d_{i,t} + \sum_{k} v_{k,i,t} \tag{4.8}$$

Substituting and rearranging, we produce the linear system that can be solved for x in every time step.

$$x_{i,t} \left(\sum_{g \in G_i} P_{g,t} + \sum_{j} u_{i,j,t} \right) - \sum_{j} x_{j,t} u_{i,j,t} = E_{i,t} \tag{4.9}$$

The embodied emissions imports associated with the historical operating schedule can be determined for a desired balancing authority (or set of balancing authorities, $b \subset B$ through vector multiplication of the emissions intensities and the electricity transfer vector for that balancing authority.

$$I^G = \sum_{t \in T} \sum_{i \in \hat{B}} \sum_{j} x_{j,t} u_{i,j,t} \tag{4.10}$$

This consumption-based model evaluates the average embodied emissions of electricity interchanges on a physical basis. To account for the nominal characteristics of electricity supply and regulation, we introduce a novel contract-adjusted consumption-based accounting approach where known specified electricity transfers $\lambda_{g,i,t}$ [MWh/hour] (from source generator $g \in G$ to sink balancing authority $i \in B$, in time step $t \in T$), and their source-specific emissions are removed from the system of equations. All specified imports are dynamically transferred to the destination balancing authorities. As such, the implications of this nominal distinction can be explored with the physical consumption-based model by removing the associated generation, interchanges, and emissions, and re-assigning

them mathematically to the destination balancing authority.

$$E^*_{i,t} = \sum_{g \in G_i} \alpha_g \left(P_{g,t} - \sum_{j \in B} \lambda_{g,j,t} \right) + \sum_{g \in G_i} \alpha_g \lambda_{g,i,t} \tag{4.11}$$

Inferred nominal transfer pathways for each specified transfer are parameterized in the matrix, α with elements specified in Eq. (4.12).

$$\alpha_{g,i} = \begin{cases} 1 & \text{if transfer path for } g \text{ includes } i \\ 0 & \text{otherwise} \end{cases} \tag{4.12}$$

Contract-adjusted electricity import transfers $u^*_{i,j}$ are calculated using Eq. (4.13).

$$u^*_{i,j} = u_{i,j} - \sum_{g \in G_i} \sum_{k \in B} \alpha_{g,i} \lambda_{g,k,t} \tag{4.13}$$

$$x_{i,t} \left(\sum_{g \in G_i} P_{g,t} + \sum_j u^*_{i,j,t} \right) - \sum_j x_{j,t} u^*_{i,j,t} = E^*_{i,t} \tag{4.14}$$

Emissions intensity values found by the solving system of equations in Eq. (4.14) can be interpreted as the average emissions intensity for the margin of unspecified electricity delivered by each balancing authority. Note that for this interpretation to be strictly accurate, all specified procurements (for which the source-specific emissions attributes are claimed by a regulated entity) would need to be known and accounted for across all jurisdictions.

These accounting exercises can be done independently for each operating interval across the year to calculate the emissions intensity of electricity delivered in each balancing authority and across each interchange. Alternatively, an annual average can be computed by summing all transfers, generation, and emissions across the year, and solving a single system of linear equations. For each unique interchange, an annual calculation will only capture the emissions implications of net transfers across the entire year, rather than the gross transfer that would be represented by independently solving for any gross embodied emissions imports that occur across each operational time step.

Estimating emissions leakage for specified electricity transfers The proposed contract-adjusted consumption-based accounting computation also provides average emissions factors for electricity delivered in neighboring balancing authorities, excluding the distortive effects of any generation that is contractually designated for transfer to a different jurisdiction. These emissions factors represent the emissions intensity of electricity that could have otherwise been displaced by nominally transferred generation. This quantity offers one plausible counterfactual for assessment

of emissions leakage consequences. Any electricity importers procuring specified electricity transfers with a lower emissions intensity than that delivered by the generator's resident balancing authority could be considered liable for this difference as emissions leakage.

$$L_i = \sum_{g \in G} \lambda_{g,i} \max\{0, x_i - \alpha_g\} \tag{4.15}$$

CARB's current cap-and-trade program addresses leakage in different ways, depending on the type of electricity transaction involved. CARB makes no leakage estimation for in-state electricity generation nor for specified imports cleared for dynamic transfer in a bilateral or day-ahead context. In contrast, CARB treats imports from the CAISO Energy Imbalance Market as though the "true" delivery is unspecified electricity [273, 241]. When an out-of-state clean energy resource is dispatched via the CAISO EIM to serve California load, CARB reasons, then other emitting resources are dispatched to serve the out-of-state load that the clean energy resource might have served if it were not selected for dispatch to a California balancing authority. To account for this leakage, CARB makes importers responsible for the difference between the source-specific emissions from the nominal resource dispatched by the CAISO EIM market algorithm and CARB's default emissions factor for unspecified electricity. Thus, the full cap-and-trade liability imposed on electricity importers is assessed as though all CAISO EIM imports reflect unspecified electricity, rather than the particular resource CAISO EIM deems delivered to serve a California balancing authority.

The "true" value for leakage cannot be observed, varies by plant and context, and likely lies above a value of zero (implicit in CARB's approach for any specified imports scheduled for delivery outside of the EIM). The approach explored here can be thought of as one plausible scenario for comparison.

Data Hourly data on net generation and electricity transfers were obtained from EIA Form 930 [90]. Imputed and cleaned hourly electricity demand data are used from Ruggles et al., (2020) [91]. Data on hourly emissions from fossil-fueled plants were obtained from the Environmental Protection Agency (EPA) Continuous Emissions Monitoring System (CEMS) through the Air Markets Program Database (AMPD) [131]. Finally, annual data on emissions for each plant and balancing authority were obtained from the EPA's Emissions & Generation Resource Integrated Database (eGRID) 2016 [282]. A more thorough discussion of data cleaning efforts can be found in the Supplemental Information (Appendix C).

We used California Energy Commission (CEC) Power Source Disclosure (PSD) data for the years 2016 and 2017 to generate a list of specified imports from plants across the WECC [283]. Reconciling CARB's GHG emissions inventory [284] with the CEC's PSD reporting for 2016 and 2017 and the Qualified Fuel and Energy Resources (QFER) [285] produced a list of 38.9 TWh and

38.1 TWh of specified imports, respectively, that have identifiable source EIA Plant IDs and resident non-California balancing authorities. In addition, we include as specified imports an additional 18.9 TWh and 18.0 TWh from asset-controlling supplier (ACS) entities. Notable inconsistencies arise in reconciliation of CEC and CARB reporting on imports due to different labeling conventions - these are discussed in detail in the Supplemental Information.

Estimating marginal emissions factors for unspecified electricity transfers

Capacity factor-based emissions factors The EPA's eGRID includes non-baseload generation emissions factors for each balancing authority [282]. This analysis uses a capacity factor (ζ) threshold to establish a non-baseload factor γ_g, for each generating plant ($g \in G$), excluding those powered by renewable energy. For plants with utilization less than a cut-in threshold $\underline{\zeta}$ of 20%, the non-baseload factor is 1. For plants with utilization greater than a cut-out threshold $\overline{\zeta}$ of 80%, the non-baseload factor is 0. And for plants with utilization lying between the cut-in and cut-out threshold assumptions the non-baseload factor is found using Eq. (4.16).

$$\gamma_g = \frac{-5}{3}\zeta + \frac{4}{3} \tag{4.16}$$

This framework is used as a jumping off point for sensitivity testing to the administrative determination for what capacity factor threshold implicates a plant as "marginal." We generalize the formulation to test capacity factor cut-in thresholds ranging from 20% to 60% and adjust the linear transition region according to Eq. (4.17), holding the cut-out threshold static at 80%.

$$\gamma_g = \frac{1}{\underline{\zeta} - 0.8}\zeta + \frac{1 - \underline{\zeta}}{\underline{\zeta} - 0.8} \tag{4.17}$$

California policymakers also currently use a capacity factor-based approach to estimate marginal emissions impacts for application to unspecified electricity transfers. CARB assigns a default emissions factor (0.428 tonnes CO_2/MWh) to all unspecified imports. Using data from 2006-2008, CARB's approach identifies marginal generating units on the western grid (WECC) by selecting those that (1) do not have a combined heat and power component, (2) are powered by fossil fuels, and (3) have an annual capacity factor of less than 60%. Each identified unit receives an emissions factor based on its primary fuel type and net generation from EIA Form 923 [129]. As detailed in the Supplemental Information, CARB's methodology also includes a number of manual interventions. We reproduced the calculations to evaluate how different choices for capacity factor thresholds as well as updated data would affect the adopted emissions factor.

Regression-based emissions factors More rigorous methods are available to characterize the marginal emissions impact of changes in electricity demand, such as linear regressions on historical data. Such so-called "difference-in-differences" regressions express the change in CO_2 emissions, δE_t

[tonnes CO_2/hr], as a function of the change in fossil-fueled generation, δP_t [MWh/hr], across a set of intervals ($t \in T$). Because emissions are a direct consequence of fossil-fueled generation, the correlation identified by the regression is assumed to be causal. Further, if fossil-fueled generators are assumed to be serving marginal demand at all times, the regression coefficient (β) can be interpreted to represent the marginal emissions factor for meeting incremental demand for electricity in the set of included data points.

$$\Delta E_t = \beta \Delta P_t \tag{4.18}$$

We implemented this regression independently for each of the balancing authorities in the WECC, using hourly historical data from the years 2016-2020 in order to characterize the marginal emissions associated with incremental fossil generation that may serve unspecified transfers. Because plants fueled by biomass and plants with combined heat and power components are not expected to respond to incremental demand on the margin, we excluded plants with these designations according to EIA Form 860 data [126]. We used hourly data on plant-level emissions $E_{g,t}$ and power output $P_{g,t}$ for each hour of the time horizon ($t \in T$) and each generator in the balancing authority ($g \in G_i \subset G$).

$$\Delta E_t = \sum_{g \in G_i} E_{g,t} - E_{g,t-1} \tag{4.19}$$

$$\Delta P_t = \sum_{g \in G_i} P_{g,t} - P_{g,t-1} \tag{4.20}$$

We used data from the EPA's Air Markets Program Database for the hourly CO_2 emissions and electricity generation of the fossil-fueled fleet in each balancing authority [131]. In addition, diurnal and seasonal features in marginal emissions factors are explored by subsetting the full time series data set and conducting separate regressions for each hour of the day and across each month.

Finally, we conduct a similar suite of regressions across all non-California balancing authorities in the WECC for the years 2006-2008 and for the years 2016-2018. We compare this result to the original and updated capacity factor-based estimates, using the currently adopted regulatory framework. Results and discussion

4.3.3 Results & discussion

Specified import emissions

Using a pure consumption-based accounting approach, we estimate that embodied emissions of approximately 20.9 $MMtCO_2$ were imported via 79.5 TWh of transfers to the five California balancing

authorities from out-of-state balancing authorities in 2016. This figure includes, without distinction or delineation, any emissions associated with (1) specified electricity imports, (2) unspecified electricity imports, and (3) emissions leakage associated with specified electricity imports. An hour-by-hour computation estimates gross embodied emissions imports of 20.35 $MMtCO_2$ for 2016. The observed discrepancy is because evaluation of gross embodied emissions imports on an hour-by-hour basis will include emissions liabilities computed independently for every hour with positive imports to a California balancing authority, while an annual computation will only include those emissions associated with positive net imports to California averaged across an annual basis. The hour-by-hour calculation offers the best comparator to the gross import emissions assessed by CARB however we do not expect these estimates to align particularly well as consumption-based accounting does not explicitly respect any nominal attributes of electricity transfers, quantifying the embodied emissions imports on a purely physical basis. In other words, to a consumption-based model, all electricity transfers are unspecified at an average emissions intensity of 0.263 tCO_2/MWh for 2016. Figure 4.6 presents the supply of unspecified and specified transfers to California according to their nominal and physical emissions intensities.

Given the uncertainties regarding data quality for specified import transfers estimated at the hourly resolution, we proceed with the contract-adjusted consumption-based accounting on a gross annual basis. However, as exports grow, improved temporal resolution will be necessary to differentially assess the emissions implications of instantaneous imports and exports, rather than the aggregated annual net interchange.

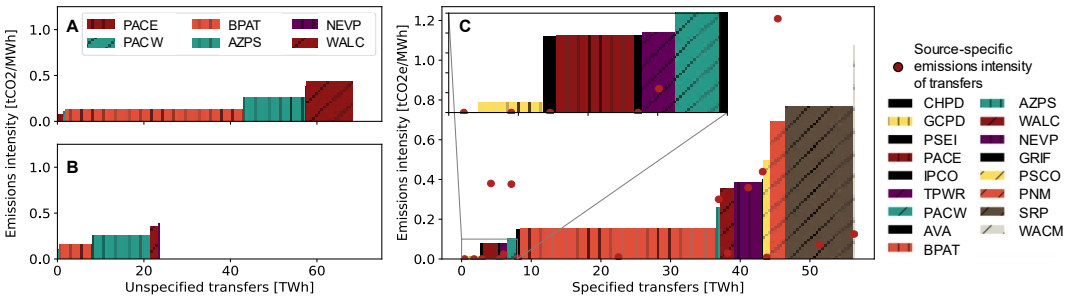

Figure 4.6: Left (A/B): Embodied emissions of unspecified transfers to California balancing authorities for 2016 evaluated using consumption-based modeling without (A) and with (B) contract-adjustments. Right (C): Embodied emissions delivered by neighboring balancing authorities with contract-adjustments, compared to the source-specific emissions intensity of specified transfers originating from these BAs in 2016.

With contract-adjusted consumption-based accounting, we find that the 2016 unspecified embodied emissions transfers to California decline to 9.2 $MMtCO_2$, as the volume of transfers to California balancing authorities is decreased by the amount of mathematically reassigned specified transfers (see Figure 4.6 (B)). The unspecified transfers have a decreased emissions intensity of

0.209 tCO_2/MWh. This emissions intensity value can be conceptually compared to the currently adopted default emissions factor for unspecified electricity transfers of 0.428 tCO_2e/MWh, as it intends to quantify the emissions associated with unspecified transfers according to an approximation of physical grid operations. Note that this is not a perfect comparator as the contract-adjusted consumption-based accounting factor represents an average emissions factor across unspecified electricity transfers to California, while the currently adopted default emissions factor is intended to estimate the emissions factor at the margin. In this analysis, contractual flows are only specified for California load-serving entities. As there is likely to be emissions-free electricity elsewhere in the West for which the emissions attributes have already been nominally claimed in other jurisdictions, the estimated emissions factors for the unspecified margin are likely biased downwards. However, as more contractual electricity flows are specified, a contract-adjusted consumption-based model will more accurately estimate emissions associated with unspecified electricity transfers across the West.

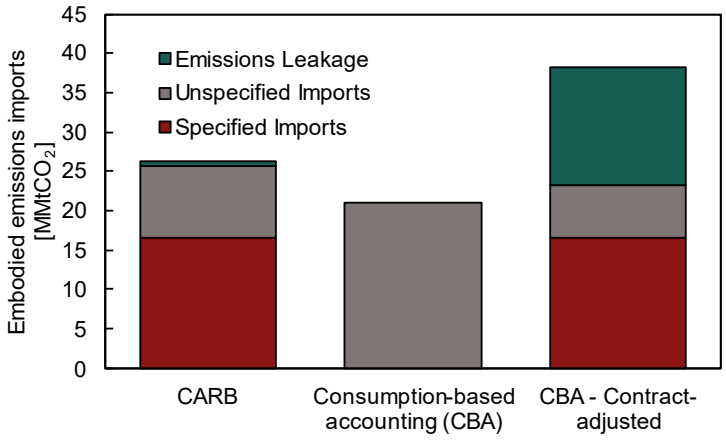

Figure 4.7: Comparison of consumption-based modeling results to the emissions liabilities assessed by the current framework employed by CARB for 2016.

The result presented in Figure 4.7 reflects emissions leakage as estimated relative to a purely physical accounting baseline. As discussed in Section 2.1.2, CARB assumes no emissions leakage for specified imports writ large, including bilateral contracting. In other words, the implicit counterfactual for specified electricity imports is that if California were not contracting for the energy, that power plant would not be generating and therefore emissions out-of-state would remain unchanged. That assumption is probably too strong in many circumstances. In contrast, the implicit counterfactual for a consumption-based accounting approach is that absent off-take agreements by California LSEs, the out-of-state resource would otherwise displace other emitting and non-emitting generators in its resident balancing authority or elsewhere in the WECC. Although CARB does not

currently assert this as the counterfactual scenario for specified imports, it does make that assertion when addressing transactions that clear the CAISO EIM. The CAISO EIM designates individual resources as being dispatched to serve California load, whereas CARB considers all transfers from the EIM as unspecified and applies a true-up emissions liability based on its default emissions factor [281]. The true-up resulted in an additional 0.58 $MMtCO_2e$ of liabilities in 2016 [284]. In the context of any potential leakage-related reforms to the cap-and-trade program, we are mindful that there are complex institutional and legal considerations that will inform any future policy deliberations. While consumption-based accounting is not the only technique for quantifying emissions, these results illustrate that the emissions leakage assessed across all specified imports (as presented in Figure 4.7) could be more than an order of magnitude larger than what CARB currently assesses in relation to EIM transfers.

While we do not explicitly analyze the economic incentives introduced by applying consumption-based modeling to emissions leakage quantification, any resource shuffling that swaps emissions-intensive purchases for non-emitting purchases would have the effect of increasing the emissions leakage factor assessed for the origin balancing authority. This feedback may reduce the potential emissions liabilities that can be avoided through resource shuffling. However, this approach may also disincentivize specified purchase of clean energy from carbon-intensive regions of the grid, as these purchases would be assessed large emissions leakage liabilities – such contractual arrangements may be important to catalyzing development of new clean energy resources.

As market operators may contemplate similar approaches, involving unique emissions leakage factors for each balancing authority applied to larger volumes of specified imports [251], future analysis should characterize the implications of such frameworks for market incentives.

Similar methods could be applied to account more explicitly for the emissions implications of electricity exports from balancing authorities in California to the rest of the western grid. With consumption-based modeling at hourly or sub-hourly time steps, the periods with exports across a given interchange can be characterized separately from those periods when imports are occurring across the interchange. However, this would require hourly or sub-hourly information about the dynamic transfer of specified electricity imports which is not publicly available at this time.

Marginal emissions factors for unspecified electricity

We estimate the hourly change in CO_2 emissions in neighboring balancing authorities as a linear function of the hourly change in generation of fossil-fueled plants that provide electricity to that balancing authority across the years 2016-2018 for comparison to the capacity factor-based methodology employed by the EPA. Figure 4.8 compares the range of factors obtained through sensitivity testing of eGRID non-baseload emissions factors to a regression-based alternative for a selection of balancing authorities in the WECC. We find no salient relationship between marginal emissions factors as estimated by a capacity factor threshold relative to a regression approach.

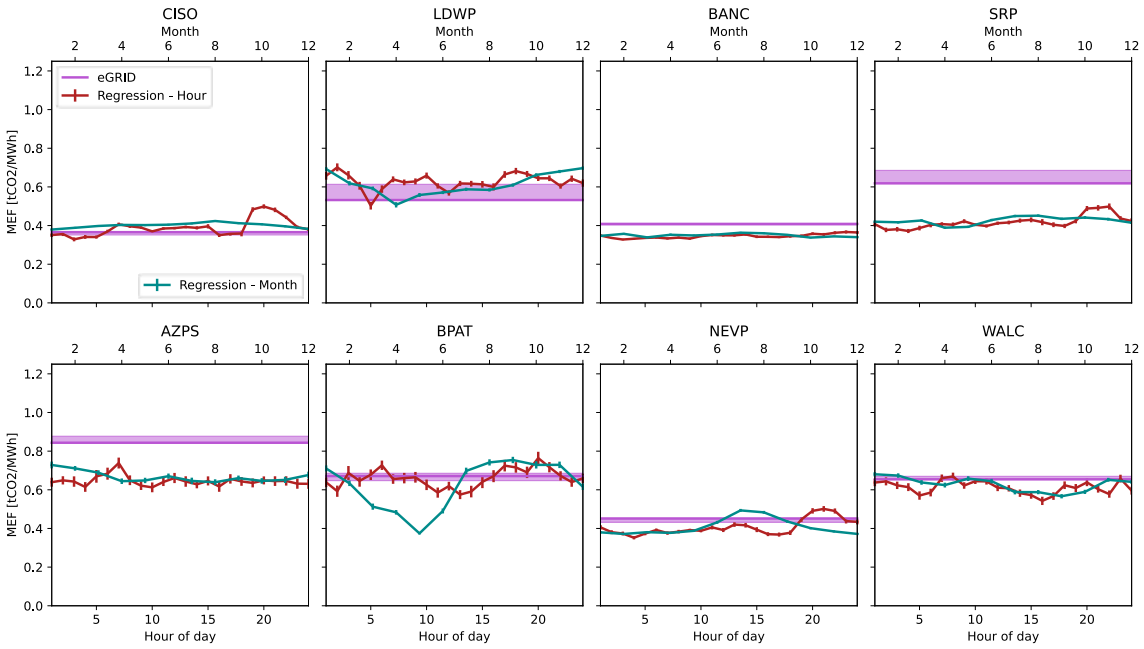

Figure 4.8: Marginal emission factors (MEFs) as estimated by capacity factor-based methods used in eGRID are compared to regression-based estimates that isolate diurnal and seasonal features in a selection of balancing authorities across the West. eGRID values are presented with a shaded sensitivity range in the cut-in capacity factor threshold from 20% to 60%. Regression coefficient values are presented with an associated 95% confidence interval.

Seasonal and diurnal patterns that emerge in regression analysis are expected to grow more pronounced as variable renewable energy resources comprise a larger fraction of total generation, driving features in net load magnitude served by dispatchable generators and energy storage resources.

We also replicate the original CARB method described in Section 4.3.2 to produce a nearly identical emissions factor (0.434 tCO_2e/MWh, which is slightly higher than the official 0.428 tCO_2e/MWh). The slight discrepancy is due to minor methodological differences, including the exclusion of Canadian plants as documented in Appendix C.

Employing the same method for more recent data from 2016-2018, we obtain an emissions factor of 0.635 tCO_2e/MWh, with the increase due to declining capacity factors for coal plants across the WECC. Because the original CARB method uses a capacity factor threshold of 60% to identify marginal units, low-capacity coal plants now identify as marginal resources and therefore increase the calculated emissions factor. Across the years 2006-2008, less than 1% of generation from the classified marginal generators was coal-fired—but that total exceeds 35% for the years 2016-2018 (see Figure C.5 in Appendix C). We similarly illustrate the sensitivity of CARB's legacy method to the selection of capacity factor threshold in the Supplemental Information (see Figure C.6).

The results for a regression on emissions and generation across all non-California balancing authorities in the western grid (meant to approximate the constraints employed in CARB's current capacity factor-based analysis) are displayed in Figure 4.9. Through either a capacity factor-based exercise or a regression-based analysis, we find that the estimated marginal emissions factor for fossil-fueled generation across the WECC has increased by approximately 20% over the past decade. The regression-based marginal emissions factor estimate for an updated time horizon is nearly 40% greater than the current adopted default emissions factor.

As recently as the 2018 MRR Final Statement of Reasons (FSOR), CARB staff indicated that they believe the default unspecified emissions factor is still an appropriate approximation for the emissions rate associated with power plants operating on the margin of western electricity markets [263]. Our results suggest that may not be the case and that additional analysis may be warranted.

Any change to the default emissions factor would need to address a number of additional challenges. For example, unspecified imports might not always operate solely on the economic margin, such that an analysis of marginal dispatch might not be useful for identifying the emissions profile of unspecified resources – in such cases the unspecified emissions factor as estimated through contract-adjusted consumption-based accounting may be more accurate. Marginal dispatch is also served by a wide range of resources in the west, including dispatchable hydroelectric generation that are omitted from this analysis due to data limitations. Finally, as California's Independent Emissions Market Advisory Committee has observed, the choice of default factors is not just a question of accuracy, but also incentives: a relatively high default factor provides an incentive for low-emissions resources to transact business such that they are identified as specified resources, whereas a low emissions factor provides an incentive for high-emission resources to transact through channels that

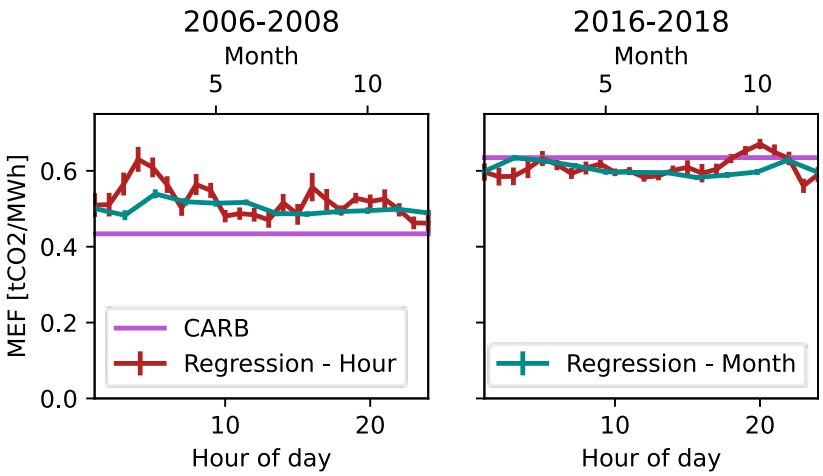

Figure 4.9: Replication of the CARB-adopted capacity factor-based marginal emissions factor for the time horizon 2006-2008 (left) is compared against regression-based estimates (across all non-California balancing authorities in the WECC) across the same time horizon and for an updated data set for 2016-2018 (right).

are designated as unspecified [240]. However, a high default factor may also offer incentive to engage in resource shuffling as highlighted by Bushnell et al. [279]. Although the analysis presented here does not explicitly address these potential challenges, we believe it illustrates the feasibility of improving the methods by which default emissions factors are assessed for electricity imports.

4.3.4 Conclusions

Regulating electricity imports is a critical area for energy policymakers in any dynamic, multi-jurisdictional electricity system and an increasingly complicated problem in California, which features ambitious climate policy, cross-border bilateral electricity transactions, and regional organized electricity markets. With the goal of supporting the effective and efficient implementation of climate and clean energy policy in the western United States, this paper proposes a novel, harmonized quantitative framework for estimating the emissions impacts of regional electricity transfers, respective of both the physical and contractual aspects of electricity supply and delivery. This work also elucidates several instances where substantive methodological improvements may be needed to achieve a consistent framework for regulating California's role in a rapidly evolving western electricity grid.

First, interagency coordination efforts should ensure consistent labeling of electricity imports, as inconsistency in data reporting can lead to confusion across overlapping agency missions and policy applications. Second, a consistent treatment for emissions leakage quantification should be employed across all specified imports; the approaches in use today are arguably inconsistent in their application

and means of mitigating leakage, specifically for specified imports that are cleared for nominal transfer in a day-ahead or bilateral context. However, further analysis is necessary to quantitatively characterize the consequent behavior incentives this accounting regime creates for regulated entities. Third, we find the default emissions factor for unspecified electricity imports does not reflect current conditions on the western grid and should be updated with a more accurate method and/or to better align economic incentives for identification of imports. With the potential introduction of a day-ahead wholesale electricity market in the western United States, policymakers have an opportunity to update and harmonize the accounting structures used to measure GHG emissions associated with electricity imports to California and serve as a positive example to regulators in other jurisdictions.

Chapter 5

Concluding remarks

5.1 Key findings

The principal contribution of this body of work is to provide a multi-model analysis of the challenges and opportunities for transitioning integrated natural gas and electricity energy systems to cost-effective net-zero emissions energy systems.

In Chapter 2, we find that electrification of greater than 80% of core gas demands is a component of the least-cost solution for modeled energy systems. Despite this substitution, the gas system is maintained to provide energy to difficult-to-electrify customers and to deliver net-zero emissions gas to electricity generators for use in times of peak electricity demand. Restricting electrification of gas appliances increases reliance on advanced gas technologies, such as power-to-gas transformation, and increases annual system costs by 15% in 2040. Neglecting practical constraints on pipeline blending of hydrogen can produce a misleading result that only transitions 20% of gas demands to electric appliance substitutes, relying on hydrogen blend fractions of greater than 50%. In all cases, we find average costs of delivered gas increase nearly 5-fold across the decarbonization transition in the test system, highlighting the importance of future work to address cost-allocation strategies for ensuring an equitable, affordable energy transition.

In Chapter 3, we find that the proposed methane pyrolysis energy system may be one option for reducing greenhouse gas emissions in the near term while continuing to leverage existing infrastructure and minimizing stranded assets. The estimated emissions abatement costs of the pyrolysis energy system for small scale heating applications are similar to existing options for large-scale gaseous carbon capture and sequestration. In the case studies explored, results for the California transportation sector and California refinery hydrogen, where substantial credits are available for avoiding greenhouse gas emissions, indicate levelized cost of hydrogen could be as low as \$0.39/kg H_2 without carbon co-product value. However, even modest amounts of catalyst losses can make

the process uneconomic. While unique engineering and design challenges remain and the technology is currently only developed at the lab scale, a molten media-based methane pyrolysis process may offer advantages with respect to carbon supply chain and utilization of preferential economic characteristics and sensitivities.

In Chapter 4, we draw several meaningful conclusions in a two-part analysis of greenhouse gas accounting quantitative frameworks and adopted regulations.

In Section 4.2, we show that in updating its Power Source Disclosure program, the California Energy Commission has taken meaningful steps to improve the reporting structures for GHG emissions intensity associated with retail electricity service to California customers. By assigning imported specified purchases of electricity the emissions associated with delivered power, the California Energy Commission (CEC) aims to balance recognition of the physical and contractual elements of electricity system operation. We find that the Power Source Disclosure (PSD) program's methods are likely to produce a clear and reasonable basis for evaluating the emissions associated with physical deliveries of retail power over the long run. In the near term, however, two effects — both of which are likely transient — could lead to artificially low reported GHG emissions intensities for some load serving entities (LSEs). First, the PSD program rules reward LSEs that are over-procured by preferentially deducting the GHG emissions associated with emitting resources. This allows over-procured LSEs to claim a higher share of zero-carbon resources than is present in their total procurement profile. Until the process of re-allocating retail electricity load and long-term supply contracts among LSEs is complete, the CEC-adopted methodology could allow several LSEs to report artificially low emissions intensity estimates. Second, a decision to grandfather legacy firmed and shaped contracts under a preferential emissions accounting method will tend to produce artificially low GHG emissions estimates for LSEs that, like many community choice aggregators, have relied heavily on contracts that include renewable energy certificates but physically deliver other resources to retail customers. As these contracts reach maturity, however, the reported GHG emissions of their replacements will be increasingly based instead on the power that they physically deliver.

Further, we identify three key conclusions on accounting for GHG emissions associated with dynamic electricity transfers in Section 4.3. First, interagency coordination efforts should ensure consistent labeling of electricity imports, as inconsistency in data reporting can lead to confusion across overlapping agency missions and policy applications. Second, a consistent treatment for emissions leakage quantification should be employed across all specified imports; the approaches in use today are arguably inconsistent in their application and means of mitigating leakage, specifically for specified imports that are cleared for nominal transfer in a day-ahead or bilateral context. However, further analysis is necessary to quantitatively characterize the consequent behavior incentives this accounting regime creates for regulated entities. Third, we find the default emissions factor for unspecified electricity imports does not reflect current conditions on the western grid and should

be updated with a more accurate method and/or to better align economic incentives for identification of imports. With the potential introduction of a day-ahead wholesale electricity market in the western United States, policymakers have an opportunity to update and harmonize the accounting structures used to measure GHG emissions associated with electricity imports to California and serve as a positive example to regulators in other jurisdictions.

5.2 Policy implications

The conclusions outlined in this dissertation have meaningful implications for regulatory policy across the transition to net-zero emissions gas-electric energy systems.

First, results in Chapter 2 indicate that continued expansion of natural gas distribution systems may not be a prudent investment given the magnitude of existing natural gas end-uses that currently outstrips supply of cost-effective net-zero emissions gas. Modeling results indicate that entire climate-zones may be most cost-effectively decarbonized by electrifying the vast majority of gaseous energy end-uses, particularly when supply constraints exist on non-electrolytic sources of net-zero emissions gas (e.g., biomethane). Barring expansive use of negative emissions technologies for carbon removal, the cost-effective fate of the natural gas distribution sector may be limited to serving peak-coincident, back-up, or otherwise case-specific transmission- or distribution-constrained energy demands.

Further, while redundant and hybrid energy infrastructure systems can provide immense value, policy-makers should consider all available alternatives including on-site storage of electrical or chemical energy. Pipeline networks are famously cost-effective for distributing large volumes of energy. However, as energy deliveries decline to quantities reflective of back-up energy needs during times of power-system stress or solely serving hyper-localized demands where electricity transmission constraints exist, the levelized economics of energy may favor options with lower fixed system costs such as distributed on-site liquified petroleum gas (LPG) back-up heat sources.

In Chapter 3, we show that in design of novel and breakthrough technologies for carbon-capture, the presence of policy support is critical to achieving cost-competitive economics with un-mitigated release of GHG emissions. Programs like the 45Q tax credits for carbon capture and sequestration or the Low Carbon Fuels Standard should be broadly designed to accommodate a range of technologies that may not fit the prescriptive definition of gaseous carbon dioxide capture and sequestration in geologic formations. The potential for solid carbon generation for permanent sequestration or as a manufacturing feed-stock should be recognized as a pathway for net emissions reductions.

Finally, as illustrated in Chapter 4, national and sub-national climate policy design must reckon with the dual contractual and physical nature of energy supply portfolios in assessing the emissions liabilities of regulated energy providers. Improved data transparency regarding specified energy purchases and dynamic transfer of energy across jurisdictions will allow for better greenhouse gas

accounting models to ensure that zero means zero. Similar frameworks must be applied to the natural gas sector such that regulated entities may experience economic incentive to purchase responsibly-sourced natural gas, biomethane, or hydrogen at a premium to more emissions-intensive sources of gas.

5.3 Future work

Critical questions remain regarding the cost-effective and equitable transition to net-zero emissions, integrated gas-electric energy systems. We have identified the following opportunities for future research:

- *Electric sector impacts of appliance electrification.* Future work should endeavor to improve the representation of gas and electric appliance demand profiles. Care should be taken to model realistic energy systems with correlated profiles for baseline energy demands, modeled appliance-level energy demands, and renewable energy availability. Tools such as NREL's ResStock and ComStock may be useful to simulate a set of representative appliances, as opposed to a generic template appliance for each region. However, novel approaches may be required to model hybrid energy solutions which use combustion back-up, relying on either distributed storage of liquefied petroleum gases or continued maintenance of the gas distribution system.

- *Role of hydrogen in cost-effective emissions-constrained energy systems.* The presented modeling framework can be used to characterize the degree to which direct consumption of hydrogen at diffuse end-use customers is a feasible strategy for decarbonizing gas distribution. Consumption of large shares of hydrogen in diffuse gas distribution end uses will require infrastructure upgrades from the pipeline to the burner tip and will be blend-limited by the least-permissive device in the supply chain. By comparing the savings of an unconstrained hydrogen blending scenario to the estimated fixed costs of necessary infrastructure upgrades, we can identify whether such investments are in the public interest.

- *Redundant infrastructures for resilient energy systems.* There is high value to having redundant and hybrid energy infrastructures. However, future work should aim to characterize the desirable attributes of a back-up/peaking energy infrastructure to serve low volumes of energy demand [MWh] during typical conditions, but to provide substantial energy delivery capacity [MW] during extreme conditions. Emphasis should be placed on systems that have low fixed costs of investment and maintenance and that have a high degree of reliability when called upon. Distributed liquified petroleum gas (LPG) for use in hybrid gas-electric heat pumps or on-site back-up generators could serve this role.

- *Cost allocation and rate-making to ensure equity across the transition.* As shown in Chapter 2, we find average costs of gas deliveries increase by as much as ten-fold across the transition to

a net-zero emissions gas-electric energy system. The equitable allocation of these costs across past and present customers is an essential area of study to ensure a just transition.

- *Co-optimization of electro-fuels production.* In practice, the design and operations of electro-fuels production facilities will be optimized to increase the operational hours for capital-intensive equipment and maximize profits. Similar technology-specific optimization routines as employed in Chapter 3 for molten-media methane pyrolysis may be necessary to accurately account for production costs of other low-carbon fuels.

- *Greenhouse gas accounting for integrated gas-electric energy systems.* The consumption-based accounting models proposed in Chapter 4 can be applied in future study to integrated gas-electric energy systems. This model will jointly solve for the embodied emissions of delivered gas and electricity for a system where gas is used to generate electric power and electric power is used to produce gaseous fuels. The contract-adjusted technique allows for regulated entities to take nominal credit for the emissions characteristics of contractual purchases and will help align incentives for purchasing responsibly-produced or net-zero emissions gas.

- *Experimental study in energy systems transition.* Energy system transitions do not occur in the sterile environment created by our mathematical models. Significant further study is required on the practical economic and policy tools to drive adoption of the enabling technologies for a cost-effective transition. For example, are incentive dollars for scaling new electric heat pump markets most effective when targeted at the customer, the contractor, or the manufacturer? An entire ecosystem of actors will determine the evolution of the energy system, and the effectiveness of various economic instruments is understudied and highly valuable for shaping policy. These questions can not be answered by more models. Rather, we need pilot programs designed rigorously to elucidate new information about the most effective ways to reduce emissions and move the needle towards a sustainable energy system.

Appendix A

Supplemental information: Gas-electric planning

A.1 Nomenclature

Sets and Indices:	
$n, e \in \mathcal{N}_P, \mathcal{E}_P$	Nodes and edges in electrical grid
$n, e \in \mathcal{N}_G, \mathcal{E}_G$	Nodes and edges in gas pipeline network
$x \in \mathcal{X}$	All existing and candidate energy supply and demand units
$x \in \mathcal{X}_n \subset \mathcal{X}$	All existing and candidate units at node n
$\omega \in \Omega \subset \mathcal{X}$	Electricity generation units
$\omega \in \Omega_G \subset \Omega$	Gas-fired generation units
$s \in \mathcal{S}_P, \mathcal{S}_G \subset \mathcal{S} \subset \mathcal{X}$	Electrical and gaseous storage units
$z \in \mathcal{Z} \subset \mathcal{X}$	Zero-carbon gas production units
$z \in \mathcal{Z}_b \subset \mathcal{Z}$	Biomethane gas production facilities
$a \in \mathcal{A} \subset \mathcal{X}$	Core (residential and commercial) gas customer appliances
$u \in \mathcal{U}$	Energy end-uses modeled at appliance-level
$a \in \mathcal{A}_u \subset \mathcal{A}$	Appliances that satisfy energy end-use u
$g \in \mathcal{G}$	Set of gas components tracked (e.g., H_2, CH_4, CO_2)
$i \in \mathcal{I}$	Investment time horizons
$r \in \mathcal{R}$	Representative operational periods
$o \in \mathcal{O}$	Linked operational time steps for each operational period
$c \in \mathcal{C}$	Sequential operational periods over an investment time horizon sampled from the representative set
$(i, r, o) \in \mathcal{T}$	Multi-index for time, where $\mathcal{T} \equiv \mathcal{I} \times \mathcal{R} \times \mathcal{O}$

Parameters:	
Network Configuration:	
$A^P \in \mathbb{R}^{N_P \times E_P}$	Nodal-edge incidence matrix for the electrical power grid
$A^G \in \mathbb{R}^{N_G \times E_G}$	Nodal-edge incidence matrix for the gas pipeline network

Operational Parameters:	
$\hat{\Phi}^P_{(i,r,o),n}$	Baseline demand for electrical energy [MW] at power node $n \in \mathcal{N}_P$
$\hat{\Phi}^G_{(i,r,o),n}$	Baseline demand for gaseous energy [MW] at gas node $n \in \mathcal{N}_G$
$\varphi^P_{(r,o),a}$, $\varphi^G_{(r,o),a}$	Electrical and gaseous energy demand profiles for modeled appliances [MW/appliance] $a \in \mathcal{A}$
$\underline{\Gamma}_\omega, \overline{\Gamma}_\omega$	Minimum and maximum stable electrical load [p.u] for dispatchable resource $\omega \in \Omega$
$\underline{\gamma}_{(r,o),\omega}$, $\overline{\gamma}_{(r,o),\omega}$	Minimum and maximum availability [p.u] for non-dispatchable resource $\omega \in \Omega$
$\overline{\rho}_\omega$	Maximum hourly ramp rate [p.u/hour]
$\underline{\upsilon}_\omega, \overline{\upsilon}_\omega$	Maximum down-time and up-time [hours]
$\overline{P}_e$	Maximum power flow [MW] for transmission line $e \in \mathcal{E}_P$
X_e	Reactance [p.u.] for transmission line $e \in \mathcal{E}_P$
$\overline{Q}_e$	Maximum gas flow [standard m^3/hour] on gas pipeline $e \in \mathcal{E}_G$
$\underline{\Pi}_n, \overline{\Pi}_n$	Minimum and maximum pressure (squared) [Pa^2] at gas node $n \in \mathcal{N}_G$
$\overline{\alpha}_e$	Maximum squared compression ratio for compressor at start of gas pipeline $e \in \mathcal{E}_G$
$\overline{S}_n$	Maximum rate of supply [MW] of fossil natural gas at each node $n \in \mathcal{N}_G$
K_e	Resistance factor for gas pipeline $e \in \mathcal{E}_G$
β_ω	Emissions factor for generation resource [tCO_2/MMBtu fuel]
β^G	Emissions factor for natural gas [tCO_2/MWh fuel]
$\chi_{n,g}$	Mole fraction of each gas component g produced by nodal fossil gas supply at node n [moles of g/moles of gas]
$\chi_{s,g}$	Mole fraction of each gas component g produced by gas storage unit s [moles of g/moles of gas]
$\chi_{z,g}$	Mole fraction of each gas component g produced by net-zero emissions gas production unit z [moles of g/moles of gas]
$\overline{\chi_g}$	Maximum molar blend of gas component $g \in \mathcal{G}$ [moles of g/moles of gas]
M_g	Molar mass of gas component $g \in \mathcal{G}$ [kg/kmol]
x_g	Energy content (on a LHV basis) of gas component $g \in \mathcal{G}$ [MJ/kg]
$C^{VOM}_{i,x}$	Variable operations and maintenance cost [$/MWh] of resource $x \in \mathcal{X}$
$C^{fuel}_{i,\omega}$	Fuel cost [$/MMBtu] of generation resource $\omega \in \Omega$
C^G_i	Cost of natural gas [$/MWh] in an investment period $i \in \mathcal{I}$
$w_{(i,r)}$	Representative weights for representative time period simulated [hours/year]

Design Parameters:	
$\hat{m}_x$	Number of existing units [no.] in resource $x \in \mathcal{X}$
u_x	Unit size [MW] for resource $x \in \mathcal{X}$
$\overline{\delta}_x$	Maximum units expanded per investment period [no./year] for resource $x \in \mathcal{X}$
$\overline{\Delta}_x$	Maximum units expanded across entire modeled investment horizon [no.] for resource $x \in \mathcal{X}$
τ_x	Average lifetime [years] for resource $x \in \mathcal{X}$
g_u	Forecast growth rate [%/year] for appliance sales by end-use $u \in \mathcal{U}$
$\hat{g}_a$	Historical growth rate for sales of appliance $a \in \mathcal{A}$
$f_{i,a,j}$	Cumulative failure fraction [%] between investment periods $i, j \in \mathcal{I}$ for population of appliances $a \in \mathcal{A}$
$\hat{m}_a$	Base year population [count] of appliance type $a \in \mathcal{A}$
$\hat{M}_a$	Base year sales [count] of appliance type $a \in \mathcal{A}$ (i.e., equipment entering service)
η_ω	Heat rate [MMBtu/MWh] for every generation resource $\omega \in \Omega$
η_z	Conversion efficiency [MWh gas/MWh elec.] for zero-emissions gas resource $z \in \mathcal{Z}$
η_s^+	Storage charge efficiency [%] of storage $s \in \mathcal{S}$
η_s^-	Storage discharge efficiency [%] of storage $s \in \mathcal{S}$
η_s^l	Storage hourly loss percentage [%] of storage $s \in \mathcal{S}$
d_s	Storage duration [hours] for storage $s \in \mathcal{S}$
h_z	Hydrogen fraction (by energy) [MWh H_2/MWh gas] of produced net-zero emissions gas by resource $z \in \mathcal{Z}$
$\overline{\beta}_i^G, \overline{\beta}_i^P$	Maximum emissions intensity of energy delivered [tCO_2/MWh] in gas and electricity sectors in an investment period $i \in \mathcal{I}$
$\overline{B}$	Maximum biomethane availability [MWh/year]
Y_i	Calendar year associated with investment period $i \in \mathcal{I}$
$\hat{Y}$	Calendar year associated with initial appliance population assumptions
κ_x	Capital recovery factor [year^{-1}] for resource $x \in \mathcal{X}$
ι^{WACC}	Weighted average cost of capital [%]
$\iota^{soc.}$	Societal cost discount rate [%]
$C_{i,x}^{cap}$	Capital cost [$/MW] of resource $x \in \mathcal{X}$ in an investment period $i \in \mathcal{I}$
$C_{i,x}^{FOM}$	Fixed operations and maintenance cost [$/MW-yr] of resource $x \in \mathcal{X}$ in an investment period $i \in \mathcal{I}$
C^{peak}	Cost of peak electricity distribution infrastructure [$/$kW_{peak}$/year]
C_n^{dist}	Cost of gas distribution network maintenance and reinvestment [$/node/year] at gas system node $n \in \mathcal{N}_G$
ϑ_i	Present value discounting factor [$\$_{2018}/\$_{Y_i}$] for investment time period $i \in \mathcal{I}$

Variables:	
$\delta_{i,x}$	Number of units built [no.] of a resource $x \in \mathcal{X}$ in investment period $i \in \mathcal{I}$
$\zeta_{i,x}$	Number of units retired [no.] of resource $x \in \mathcal{X}$ in investment period $i \in \mathcal{I}$
$m_{x,i}$	Remaining number of installed units [no.] of type $x \in \mathcal{X}$ and vintage $v \in \mathcal{V}$
$\Phi^{G}_{(i,r,o),n}$	Gas demand [MW] at gas node $n \in \mathcal{N}_G$ in time step $(i,r,o) \in \mathcal{T}$
$\Phi^{P}_{(i,r,o),n}$	Electricity demand [MW] at power node $n \in \mathcal{N}_P$ in time step $(i,r,o) \in \mathcal{T}$
$\Phi^{Z}_{(i,r,o),z}$	Electricity demand [MW] for production of net-zero emissions gas at production unit $z \in \mathcal{Z}$ in time step $(i,r,o) \in \mathcal{T}$
$\overline{\Phi}^{P}_{(i,r,o),n}$	Peak electricity demand [MW] at power node $n \in \mathcal{N}_P$ in time step $(i,r,o) \in \mathcal{T}$
$\Gamma^{P}_{(i,r,o),\omega}$	Electricity generation dispatch [MW] for resource $\omega \in \Omega$ in time step $(i,r,o) \in \mathcal{T}$
$\Gamma^{Z}_{(i,r,o),z}$	Net-zero gaseous fuel dispatch [MW] for resource $z \in \mathcal{Z}$ in time step $(i,r,o) \in \mathcal{T}$
$\nu_{(i,r,o),\omega}$	Units [no.] of resource $\omega \in \Omega$ committed in time step $(i,r,o) \in \mathcal{T}$
$\nu^{+}_{(i,r,o),\omega}$	Units [no.] of resource $\omega \in \Omega$ started up in time step $(i,r,o) \in \mathcal{T}$
$\nu^{-}_{(i,r,o),\omega}$	Units [no.] of resource $\omega \in \Omega$ shut down in time step $(i,r,o) \in \mathcal{T}$
$P_{(i,r,o),e}$	Power flow [MW] across transmission line $e \in \mathcal{E}_P$ in time step $(i,r,o) \in \mathcal{T}$
$v_{(i,r,o),e}$	Voltage angle [radians] across transmission line $e \in \mathcal{E}_P$ in time step $(i,r,o) \in \mathcal{T}$
$Q_{(i,r),e}$	Gas flow rate [standard m^3/hour] in pipeline $e \in \mathcal{E}_G$ in rep. time period (i,r)
$q_{(i,r),e,g}$	Nominal flow rate [kmol/sec] of gas component $g \in \mathcal{G}$ across pipeline $e \in \mathcal{E}_G$ in rep. time period (i,r)
$\phi_{(i,r,o),n,g}$	Nominal gas delivery rate [kmol/sec] of gas component $g \in \mathcal{G}$ at node $n \in \mathcal{N}_G$ in time step (i,r,o)
$\Pi_{(i,r),n}$	Nodal squared pressure [Pa^2] at gas node $n \in \mathcal{N}_G$ in rep. time period (i,r)
$\hat{\Pi}_{(i,r),e}$	Squared pressure [Pa^2] at start end of each pipeline $e \in \mathcal{E}_G$ after compression in rep. time period (i,r)
$\Gamma^{G}_{(i,r),n}$	Local slack supplies [MW] of natural gas at gas node $n \in \mathcal{N}_G$ in rep. time period (i,r)
$y_{(i,r),e}$	Flow direction [bin.] on pipeline $e \in \mathcal{E}_G$ in rep. time period (i,r)
$\lambda_{(i,r),e}$	McCormick relaxation pressure drop [Pa^2] across pipeline $e \in \mathcal{E}_G$ in rep. time period (i,r)
$\Psi_{(i,r,o),s}$	State of charge [MWh] of storage $s \in \mathcal{S}$ in time step $(i,r,o) \in \mathcal{T}$
$\overline{\Psi}_{(i,r),s}$, $\underline{\Psi}_{(i,r),s}$	Maximum/minimum nominal state of charge [MWh] of storage $s \in \mathcal{S}$ in rep. time period (i,r)
$\psi^{+}_{(i,r,o),s}$, $\psi^{-}_{(i,r,o),s}$	Charge/discharge rate [MW] of storage $s \in \mathcal{S}$ in time step $(i,r,o) \in \mathcal{T}$
$\Upsilon_{c,s}$	State of charge [MWh] in sequential period $c \in \mathcal{C}$ of storage $s \in \mathcal{S}$
ξ^{G}_{i}, ξ^{P}_{i}	Zero-carbon gas allocation [MWh/year] in the gas and electric sector in investment period $i \in \mathcal{I}$
ε^{G}_{i}, ε^{P}_{i}	Negative emissions offset use [tCO_2/year] in the gas and electric sector in investment period $i \in \mathcal{I}$

A.2 Cost assumptions

Specific information on the capital and operating cost assumptions used for the indicative case study are included below.

Capital Cost [2018$/kW]					
Resource	2020	2025	2030	2035	2040
Natural gas CT	934	887	862	844	830
Natural gas CC	1034	967	944	925	910
Coal	3593	3559	3516	3461	3398
Nuclear	6062	5906	5734	5545	5341
Solar PV	1325	1072	819	782	746
Wind	1786	1615	1412	1357	1300
Natural gas CC+CCS	2588	2346	2254	2156	2073
Biomethane	0	0	0	0	0
Electrolytic hydrogen	950	760	570	548	527
Electro-methane	950	760	570	548	527
Lithium ion battery	1455	1004	817	766	715
Long-duration storage	2225	1980	1765	1725	1690

Table A.1: Assumed capital costs for generation, power-to-gas, and storage units [2018$] for the planning time horizon

Fixed Operating Cost [2018$/kW-yr]					
Resource	2020	2025	2030	2035	2040
Natural gas CT	11	11	11	11	11
Natural gas CC	13	13	13	13	13
Coal	40	40	40	40	40
Nuclear	119	119	119	119	119
Solar PV	16	13	10	9	9
Wind	42	41	39	37	35
Natural gas CC+CCS	27	27	27	27	27
Biomethane	448	448	448	448	448
Electrolytic hydrogen	71.20	57.00	42.75	41.15	39.56
Electro-methane	71.20	57.00	42.75	41.15	39.56
Lithium ion battery	36.37	25.10	20.43	19.15	17.88
Long-duration storage	84.05	69.83	55.61	54.02	52.43

Table A.2: Assumed fixed operating costs for generation, power-to-gas, and storage units [2018$] for the planning time horizon

A.3 Transmission expansion optimization

In the presented model formulation, the network topology of the electric power and natural gas systems is fixed and immutable. New investment in transmission resources may be contemplated to

Variable Operating Cost [2018$/MWh]					
Resource	2020	2025	2030	2035	2040
Natural gas CT	2	2	2	2	2
Natural gas CC	4	4	4	4	4
Coal	4	4	4	4	4
Nuclear	2	2	2	2	2
Solar PV	0	0	0	0	0
Wind	0	0	0	0	0
Natural gas CC+CCS	6	6	6	6	6
Biomethane	0	0	0	0	0
Electrolytic hydrogen	0	0	0	0	0
Electro-methane	126.90	102.53	78.19	57.36	36.54
Lithium ion battery	0	0	0	0	0
Long-duration storage	0	0	0	0	0

Table A.3: Assumed variable operating costs for generation, power-to-gas, and storage units [2018$] for the planning time horizon

Installed Cost [2018$/unit]					
Residential appliances	Year				
	2020	2025	2030	2035	2040
Gas furnace [4 ton]	1980	1980	1980	1980	1980
Gas water heater [50 gal.]	737	737	737	737	737
Gas stove [4 9,500 BTU-burner]	2000	2000	2000	2000	2000
Electric heat pump [4 ton]	6922	6638	6355	6071	5788
Heat pump water heater [50 gal.]	1733	1662	1418	1347	1155
Electric induction stove [4 5kW-burner]	2000	2000	2000	2000	2000
Commercial appliances	Year				
	2020	2025	2030	2035	2040
Gas furnace [10 ton]	5230	5230	5230	5230	5230
Gas water heater [199 kBTU/hour]	6000	6000	6000	6000	6000
Gas stove [24 9,500 BTU-burner]	12000	12000	12000	12000	12000
Electric heat pump [10 ton]	10710	9954	9198	8694	8190
Heat pump water heater [74 kBTU/hour]	23652	21368	19192	17871	16550
Electric induction stove [24 5kW-burner]	12000	12000	12000	12000	12000

Table A.4: Assumed installed cost of gas and electric appliances [2018$/unit]

Fuel	2020	2025	2030	2035	2040
Natural gas	2.60	3.25	3.57	3.67	3.74
Coal	2	2	2	2	2
Nuclear	0.67	0.67	0.68	0.69	0.70

Table A.5: Assumed fuel costs [2018$/MMBtu] for electricity generation and commodity natural gas from [127]

accommodate the shift towards net-zero emissions energy systems. Similarly, the premature decommissioning and retirement of existing transmission interconnections may occur if contracted bulk gas deliveries decline to uneconomic quantities. Here, we present a preliminary model formulation that will accommodate transmission expansion and retirement planning in the presented optimization framework for integrated gas-electric energy systems.

First, expansion and retirement decision variables are introduced for each candidate and existing transmission edge. The total number of active transmission assets in each investment period is computed by summing the number of existing units, plus any new investments, less any retirements. Here, we enforce a maximum number of transmission assets of 1 (i.e., each edge must represent a single physical power line or transmission pipeline). This will accommodate multiple connections between the same two nodes, but will model each separately according to the physical flow equations rather than lumping their transmission capabilities into a single modeled asset.

$$\delta_{i,e} \geq 0, \;\; \zeta_{i,e} \geq 0, \;\; m_{i,e} \geq 0 \qquad \forall i \in \mathcal{I}, e \in \mathcal{E}_G \cup \mathcal{E}_P \tag{A.1a}$$

$$\sum_{i \in \mathcal{I}} \delta_{i,e} \leq 1, \qquad \forall e \in\in \mathcal{E}_G \cup \mathcal{E}_P \tag{A.1b}$$

$$\zeta_{i,e} \leq \hat{m}_e + \sum_{j \in [i-1]} (\delta_{j,e} - \zeta_{j,e}) \qquad \forall i \in \mathcal{I}, e \in \mathcal{E}_G \cup \mathcal{E}_P \tag{A.1c}$$

$$m_{i,e} = \hat{m}_e + \sum_{j \in [i]} (\delta_{j,e} - \zeta_{j,e}) \qquad \forall i \in \mathcal{I}, e \in \mathcal{E}_G \cup \mathcal{E}_P \tag{A.1d}$$

$$m_{i,e} \leq 1, \qquad \forall e \in\in \mathcal{E}_G \cup \mathcal{E}_P. \tag{A.1e}$$

Second, the constraints governing transmission of electricity and natural gas are modified to account for the endogenous decision dictating whether an active transmission asset is in operation.

For electric transmission, the box constraints delimiting power flow across an edge must now include the variable $m_{i,e}$ indicating whether a transmission line is in operation during this investment period. If $m_{i,e} = 0$ then the flow across the pipeline must be 0.

$$-\overline{P}_e m_{i,e} \leq P_{(i,r,o),e} \leq \overline{P}_e m_{i,e} \qquad \forall (i,r,o) \in \mathcal{T}, \; \forall e \in \mathcal{E}_{\mathcal{P}} \tag{A.2}$$

In addition, the equality constraint specifying power flows (Eq. (2.18)) must be replaced by a

set of inequality constraints.

$$P_{(i,r,o),e} \geq (m_{i,e} - 1)\overline{P}_e + \hat{P}\left(\frac{-1}{X_e}\right) \sum_{n \in \mathcal{N}_P} A_{n,e} v_{(i,r,o),n}, \qquad \forall (i,r,o) \in \mathcal{T},\ \forall e \in \mathcal{E}_P \tag{A.3a}$$

$$P_{(i,r,o),e} \leq (1 - m_{i,e})\overline{P}_e + \hat{P}\left(\frac{-1}{X_e}\right) \sum_{n \in \mathcal{N}_P} A_{n,e} v_{(i,r,o),n}, \qquad \forall (i,r,o) \in \mathcal{T},\ \forall e \in \mathcal{E}_P. \tag{A.3b}$$

When $m_{i,e} = 1$, these constraints will tightly bind $P_{(i,r,o),e}$ with equality. However, when $m_{i,e} = 0$ these constraints will permit the value of $P_{(i,r,o),e}$ to fall to zero in accordance with the box constraints in Eq. (A.2).

For gas transmission, the box constraint delimiting gas flow across an edge must now include the variable $m_{i,e}$ indicating whether a transmission pipeline is in operation during this investment period. If $m_{i,e} = 0$ then the flow across the pipeline must be 0.

$$-\overline{Q}_e m_{i,e} \leq Q_{(i,r),e} \leq \overline{Q}_e m_{i,e} \qquad \forall (i,r) \in (\mathcal{I} \times \mathcal{R}),\ \forall e \in \mathcal{E}_G. \tag{A.4}$$

As the gas flow equation constraints are already relaxed to inequalities in Eq. (2.39), no analogous inequalities (as employed in Eq. (A.3)) are required for the gas transmission expansion problem.

Third, the capital and operating costs associated with specific transmission assets are included in the objective function terms:

$$C_i^{exp} = \sum_{j \in [i]} \sum_{x \in \mathcal{X} \cup \mathcal{E}_P \cup \mathcal{E}_G} \left(\kappa_x C_{j,x}^{cap} \delta_{j,x}\{1 | Y_i \leq Y_j + \tau_x\} + C_{i,x}^{FOM} m_{i,x}\right) \qquad \forall i \in \mathcal{I}. \tag{A.5}$$

Including transmission expansion optimization with realistic binary variables for expansion and retirement will necessarily increase computational complexity of the optimization program. However, continuous relaxations for investment decision variables could be used to identify high-value transmission pathways that may be candidates for expansion.

A.4 Gas quality tracking

In the presented model formulation, the gas quality tracking problem (also known as a pooling problem) has been reduced to a simple set of linear constraints for nominal tracking of hydrogen injections and consumption. This approach is sufficient for preliminary investigations, however this results in several shortcomings discussed in Section 2.7. Specifically, the implications of hydrogen blending for operation and capture efficiency of CCS-equipped gas-fired generation units cannot be endogenously assessed. In addition, as lower-energy content sources of biomethane are incorporated into the pipeline network, pipeline operators may seek strategies for dynamic gas quality control through

blending of liquified petroleum gases to modulate combustion interchangeability characteristics.

The well-mixed gas quality tracking problem presents a nonlinear, non-convex modeling challenge that remains an area of active research. For a more thorough review of previous work on this problem see [286]. Versions of the below have been proposed in previous works including [287, 288] and [289].

Here, we present a preliminary formulation for one approach to linearize the full nonlinear, well-mixed gas quality tracking problem. We do so by using a discrete set of parameters that span the range of potential heating values delivered, paired with a set of binary decision variables to indicate precisely which of these heating values is delivered at each node in each operational time step. In this manner, we constrain the average molar energy content of gas entering the node to equal the average molar energy content of gas leaving the node. These energy content variables can also be constrained to reflect interchangeability limits of end-use consumption equipment.

First, we introduce a decision variable for the heating value of gas delivered in each time-point at each node, $h_{(i,r),n}$ [MJ/Sm^3]. This value will be found using the summation across a set of binary indicator variables $q_{n,k}$ that span the discretized range of acceptable heating values, characterized by their counterparts β^h_k.

$$\underline{h} \leq h_{(i,r),n} \leq \overline{h} \qquad \forall (i,r) \in (\mathcal{I} \times \mathcal{R}),\ \forall n \in \mathcal{N}_G \tag{A.6a}$$

$$h_{(i,r),n} = \sum_{k \in \mathcal{K}} \beta^h_k q_{(i,r),n,k} \qquad \forall (i,r) \in (\mathcal{I} \times \mathcal{R}),\ \forall n \in \mathcal{N}_G \tag{A.6b}$$

The mathematical approach here requires first partitioning the gas flow variable into a positive and negative value. These variables will explicitly identify where the flow direction comports with or confounds the nominal direction specified in the directional nodal-edge incidence matrix B (see Eq. (2.2)).

$$Q^+_{(i,r),e} \geq 0, \qquad Q^-_{(i,r),e} \geq 0 \qquad \forall (i,r) \in (\mathcal{I} \times \mathcal{R}),\ \forall e \in \mathcal{E}_G \tag{A.7a}$$

$$Q_{(i,r),e} = Q^+_{(i,r),e} - Q^-_{(i,r),e} \qquad \forall (i,r) \in (\mathcal{I} \times \mathcal{R}),\ \forall e \in \mathcal{E}_G \tag{A.7b}$$

Using these variables, we identify all molar gas flows entering each node $M_{(i,r),n}$, regardless of their emergent flow direction (i.e., the sign of $Q_{(i,r),e}$) or nominal flow direction (i.e., the sign of $A^G_{n,e}$):

$$\begin{aligned} M_{(i,r),n} = {} & \frac{\Gamma^G_{(i,r),n}}{LHV_{NG}} + \sum_{e \in \mathcal{E}_G} Q^+_{(i,r),e}\{1 | A^G_{n,e} = -1\} - Q^-_{(i,r),e}\{1 | A^G_{n,e} = 1\} \\ & \ldots + \sum_{z \in \mathcal{Z}_n} \left(\frac{\tilde{h}_z}{LHV_{H_2}} + \frac{1 - \tilde{h}_z}{LHV_{CH_4}} \right) \Gamma^Z_{(i,r,o),z} \\ & \ldots \forall (i,r) \in (\mathcal{I} \times \mathcal{R}),\ \forall n \in \mathcal{N}_G \end{aligned} \tag{A.8}$$

The molar quantity of fossil natural gas produced locally (or transferred from outside the modeled region) is computed using $\frac{\Gamma^G_{(i,r),n}}{LHV_{NG}}$. All gas flows *entering* the node are identified using the nominal nodal-edge incidence matrix A^G and the variables for positive and negative flows $Q^+_{(i,r),e}, Q^-_{(i,r),e}$. Finally, any local net-zero emissions gas production is included and adjusted by the average molar heating value of the gas (accounting for the share of hydrogen).

To assess the flows of energy on the system, we introduce new decision variables for the positive and negative flows of energy. We include constraints to set the value of energy flows equal to the molar flows multiplied by the energy content of gas delivered by the node that lies at the pipeline entrance.

$$E^+_{(i,r),e} \geq 0, E^-_{(i,r),e} \geq 0 \qquad \forall (i,r) \in (\mathcal{I} \times \mathcal{R}),\ \forall e \in \mathcal{E}_G \tag{A.9a}$$

$$E^+_{(i,r),e} = Q^+_{(i,r),e} \sum_{n \in \mathcal{N}_G} h_{(i,r),n}\{1|A^G_{n,e} = 1\} \qquad \forall (i,r) \in (\mathcal{I} \times \mathcal{R}),\ \forall e \in \mathcal{E}_G \tag{A.9b}$$

$$E^-_{(i,r),e} = Q^-_{(i,r),e} \sum_{n \in \mathcal{N}_G} h_{(i,r),n}\{1|A^G_{n,e} = -1\} \qquad \forall (i,r) \in (\mathcal{I} \times \mathcal{R}),\ \forall e \in \mathcal{E}_G \tag{A.9c}$$

For any variable, like $h_{(i,r),n}$, that is equal to a discretized summation across binary variables, we can linearize the product of this term with another continuous variable by introducing additional continuous variables to represent the tightly-constrained McCormick relaxation of the bilinear term.

In this case, we must linearize the term $Q^+_{(i,r),e} \sum_{n \in \mathcal{N}_G} h_{(i,r),n}\{1|A^G_{n,e} = 1\}$ by introducing a new set of continuous variables $p^+_{(i,r),e,k} = Q^+_{(i,r),e} \sum_{n \in \mathcal{N}_G} h_{(i,r),n}\{1|A^G_{n,e} = 1\}$ constrained by

$$p^+_{(i,r),e,k} \leq \overline{Q}_e(\sum_{n \in \mathcal{N}_G} q_{(i,r),n,k}\{1|A^G_{n,e} = 1\}) \tag{A.10a}$$

$$p^+_{(i,r),e,k} \leq Q^+_{(i,r),e} \tag{A.10b}$$

$$p^+_{(i,r),e,k} \geq Q^+_{(i,r),e} - \overline{Q}_e(1 - (\sum_{n \in \mathcal{N}_G} q_{(i,r),n,k}\{1|A^G_{n,e} = 1\})) \tag{A.10c}$$

$$p^+_{(i,r),e,k} \geq 0 \tag{A.10d}$$

Summing across $p^+_{(i,r),e,k} \forall k \in \mathcal{K}$ allows us to evaluate and constrain $E^+_{(i,r),e}$.

$$E^+_{(i,r),e} = \sum_{k \in \mathcal{K}} \beta^h_k p^+_{(i,r),e,k} \qquad \forall (i,r) \in (\mathcal{I} \times \mathcal{R}),\ \forall e \in \mathcal{E}_G \tag{A.11}$$

To ensure that only one discrete value is active, and the sum of the relaxation variables equals

the desired quantity, we include the following constraints:

$$\sum_{k\in\mathcal{K}} q_{(i,r),n,k} = 1, \tag{A.12a}$$

$$\sum_{k\in\mathcal{K}} p^{+}_{(i,r),e,k} = Q^{+}_{(i,r),e}, \tag{A.12b}$$

and an identical set of variables and constraints are included for $E^{-}_{(i,r),e}$.

Using these energy flow variables, we constrain each nodal heating value to equal the energy entering the node divided by the entering molar quantity:

$$h_{(i,r),n} = \frac{\Gamma^{G}_{(i,r),n} + \sum_{z\in\mathcal{Z}_n} \Gamma^{Z}_{(i,r,o),z} + \sum_{e\in\mathcal{E}_G} E^{+}_{(i,r),e}\{1|A^{G}_{n,e} = -1\} - E^{-}_{(i,r),e}\{1|A^{G}_{n,e} = 1\}}{M_{(i,r),n}} \tag{A.13}$$

by rearranging and using the same relaxation formulation for the product of $h_{(i,r),n}M_{(i,r),n}$ (using a new set of continuous relaxation variables $m_{(i,r),n,k}$:

$$m_{(i,r),e,k} \le M(\sum_{n\in\mathcal{N}_G} q_{(i,r),n,k}\{1|A^{G}_{n,e} = 1\}) \tag{A.14a}$$

$$m_{(i,r),e,k} \le M_{(i,r),n} \tag{A.14b}$$

$$m_{(i,r),e,k} \ge M_{(i,r),n} - M(1 - (\sum_{n\in\mathcal{N}_G} q_{(i,r),n,k}\{1|A^{G}_{n,e} = 1\})) \tag{A.14c}$$

$$m_{(i,r),e,k} \ge 0 \tag{A.14d}$$

We similarly constrain this evaluated quantity of energy delivered to be equal to the energy entering the node:

$$\sum_{k\in\mathcal{K}} m_{(i,r),e,k} = M_{(i,r),n} \tag{A.15a}$$

$$\sum_{k\in\mathcal{K}} \beta^{h}_{k} m^{+}_{(i,r),e,k} = \Gamma^{G}_{(i,r),n} + \sum_{z\in\mathcal{Z}_n} d_{(i,r,o),z}\eta_z + \sum_{e\in\mathcal{E}_G} E^{+}_{(i,r),e}\{1|A^{G}_{n,e} = -1\} - E^{-}_{(i,r),e}\{1|A^{G}_{n,e} = 1\}. \tag{A.15b}$$

Lastly, we modify the gaseous energy balance constraint using the computed energy flows across each pipeline:

$$\Gamma^{G}_{(i,r),n} + \sum_{z\in\mathcal{Z}_n} \Gamma^{Z}_{(i,r,o),z} + \sum_{e\in\mathcal{E}_G} A^{G}_{n,e}(E^{+}_{(i,r),e} - E^{-}_{(i,r),e}) + \Phi^{G}_{(i,r,o),n} + \sum_{\omega\in(\Omega_{NG}\cap\Omega_n)} \Gamma^{P}_{(i,r,o),\omega}\eta_\omega \tag{A.16}$$

Note that a molar balance constraint at each node is not necessary (and would be redundant) as we implicitly require that the average mole-weighted average heating value of gases entering a node is identical to the mole-weighted average heating value of gas delivered by a node. This logically

ensures that the energy balance implies a molar balance.

This same mathematical approach can be used to track any molar-weighted (or mass-weighted) gaseous fuel quantity throughout the network. This could include carbon emissions intensity, trace constituent concentrations, or mole fractions of hydrogen. Tracking more molar, nodal quantities necessarily introduces more binary variables. As such, relaxations should be explored as avenues to reduce computational complexity of the mixed integer quadratic program.

A.5 Alternative average cost of energy model

Here, we present an alternative approach to modeling the average cost of energy delivered to consumers. The formulation presented in Section 2.3.9 levelizes the costs of the electric power sector across all electricity generated. Consequently, the average cost of net-zero emissions gas is a function of this average cost of electric power. In this section, we present a formulation wherein the net-zero emissions gas production units are exposed to the wholesale electric power cost (as estimated by the variable costs of generation). Consequently, the fixed costs of the electric power sector are assumed to be recovered across the remainder of electricity generation not used for electro-fuels.

For simplicity of exposition, we re-introduce quantities for total generation of electrical power $\mathbf{\Gamma}_i^P$, core deliveries of gas $\mathbf{\Phi}_i^G$, and production of net-zero emissions gas $\mathbf{\Gamma}_i^Z$ on an annual basis:

$$\mathbf{\Gamma}_i^P = \sum_{r\in\mathcal{R}}\sum_{o\in\mathcal{O}}\sum_{\omega\in\Omega} w_{(i,r)}\Gamma^P_{(i,r,o),\omega} \qquad \forall i\in\mathcal{I} \qquad \text{(A.17a)}$$

$$\mathbf{\Phi}_i^G = \sum_{r\in\mathcal{R}}\sum_{o\in\mathcal{O}}\sum_{n\in\mathcal{N}_G} w_{(i,r)}\Phi^G_{(i,r,o),n} \qquad \forall i\in\mathcal{I} \qquad \text{(A.17b)}$$

$$\mathbf{\Gamma}_i^Z = \sum_{z\in\mathcal{Z}}\sum_{r\in\mathcal{R}}\sum_{o\in\mathcal{O}} w_{(i,r)}\Gamma^Z_{(i,r,o),z} \qquad \forall i\in\mathcal{I} \qquad \text{(A.17c)}$$

In addition, we introduce a new quantity for total annual electricity consumed for production of electro-fuels:

$$\mathbf{\Phi}_i^Z = \sum_{z\in\mathcal{Z}}\sum_{r\in\mathcal{R}}\sum_{o\in\mathcal{O}} w_{(i,r)}\Phi^Z_{(i,r,o),z} \qquad \forall i\in\mathcal{I} \qquad \text{(A.18)}$$

and a set of terms quantifying the revenue requirement for the electric power sector, and natural gas sector, excluding any costs associated with elecro-fuels consumption:

$$RR_i^P = C_i^{gen,P} + C_i^{fuel,P} + C_i^{stor,P} + C_i^{T\&D,P} + C_i^{CO_2}\varepsilon_i^P \qquad \forall i\in\mathcal{I} \qquad \text{(A.19a)}$$

$$RR_i^G = C_i^{fuel,G} + C_i^{stor,G} + C_i^{T\&D,G} + C_i^{CO_2}\varepsilon_i^G \qquad \forall i\in\mathcal{I} \qquad \text{(A.19b)}$$

Using the total societal cost terms defined in Eq. (2.73) - (2.74), we define the average costs of delivered electric power for wholesale sales $\mu_i^{P,ws}$, the average cost of electric power for retail sale

$\mu_i^{P,rs}$, and gas μ_i^G as a function of the average cost of net-zero emissions gas production μ_i^Z.

$$\mu_i^{P,ws} = \frac{C_i^{fuel,P} + C_i^{CO_2}\varepsilon_i^P + \xi_i^P(\mu_i^Z - C_i^G)}{\mathbf{\Gamma}_i^P} \qquad \forall i \in \mathcal{I} \qquad \text{(A.20a)}$$

$$\mu_i^Z = \frac{C_i^{gen,G} + \mathbf{\Phi}_{(i,r,o),z}^Z \mu_i^{P,ws}}{\mathbf{\Gamma}_i^Z} \qquad \forall i \in \mathcal{I} \qquad \text{(A.20b)}$$

$$\mu_i^G = \frac{RR_i^G + \xi_i^G(\mu_i^Z - C_i^G)}{\mathbf{\Phi}_i^G} \qquad \forall i \in \mathcal{I} \qquad \text{(A.20c)}$$

$$\mu_i^{P,rs} = \frac{RR_i^P + \xi_i^P(\mu_i^Z - C_i^G) - \mu_i^{P,WS}\mathbf{\Phi}_{(i,r,o),z}^Z}{\mathbf{\Gamma}_i^P - \mathbf{\Phi}_{(i,r,o),z}^Z} \qquad \forall i \in \mathcal{I} \qquad \text{(A.20d)}$$

The average cost of wholesale electric power $\mu_i^{P,ws}$ is estimated in Eq. (A.20a) to be the sum of variable operating costs $C_i^{fuel,P}$, negative emissions offsets $C_i^{CO_2}\varepsilon_i^P$, and the incremental cost of net-zero emissions gas purchases ξ_i^P, assessed at the average cost of net-zero emissions gas production μ_i^Z, relative to the cost of commodity gas already included in $C_i^{fuel,P}$. These costs are then levelized across total electricity generation $\mathbf{\Gamma}_i^P$. This bifurcated cost-allocation structure for wholesale electricity costs allows the cost of net-zero emissions gas μ_i^Z to be computed as a function of wholesale electric power costs $\mu_i^{P,ws}$ in Eq. (A.20b). The cost of net-zero emissions gas is equal to the sum of capital investments and operating costs of net-zero emissions production $C^{gen,G}$ and the costs of electric power inputs $\mathbf{\Phi}_i^Z$ (as assessed at the wholesale cost). These costs are levelized across the total production of net-zero emissions gas $\mathbf{\Gamma}_i^Z$.

The average costs of gas delivered can be straightforwardly computed in Eq. (A.20c) using the fuel costs of commodity natural gas to serve core demands $C_i^{fuel,G}$, the costs of gas storage $C_i^{stor,G}$, the costs of distribution infrastructure $C_i^{T\&D,G}$ and the costs of negative emissions offsets for the gas sector $C_i^{CO_2}\varepsilon_i^G$. In addition, the gas sector purchases of net-zero emissions gas ξ_i^G are assessed at the incremental cost of net-zero emissions gas μ_i^Z relative to commodity gas costs C_i^G. These costs are levelized for recovery across all core gas demands served $\mathbf{\Phi}_i^G$.

Finally, in Eq. (A.20d), the average cost of retail electricity is computed by taking the total revenue requirement for the electric power sector, subtracting any costs recovered through wholesale sale of electricity for net-zero emissions production, and dividing by the total electricity generated for final consumption.

The term in Eq. (A.20a) is substituted in Eq. (A.20b) to compute the value of μ_i^Z in closed form. Subsequently, the average cost of gas μ_i^G can be computed using Eq. (A.20c) and the value of μ_i^Z. Similarly, the average cost of electricity delivered for retail sales $\mu_i^{P,rs}$ can be computed using Eq. (A.20d) and the value of μ_i^Z.

The two cost-allocation formulations presented in this dissertation capture only two plausible simplifications of the cost recovery mechanisms that will ultimately govern the revenue sufficiency to fund the transition in regulated gas-electric energy systems. As such, these results are intended

as indicative, rather than definitive, to capture plausible trends in the evolution of costs of energy delivered to end-use consumers.

A.6 Endogenous consumer adoption modeling

The model formulation in Chapter 2 identifies the cost-optimal investment decisions for all gas and electricity sector investments as well as appliance investments made by populations of customers. Appliance investment decisions made by individual consumers can be shaped by policy through building codes and efficiency standards. However, consumer preferences and relative economics will also jointly govern investment.

Most prominent modeling efforts for simulation of economy-wide decarbonization pathways simplify these challenges by imposing policy decisions governing the sales share of new appliances. The sales penetration of desired emissions-free appliances for a future year is fixed by assumptions and a logarithmic s-curve is interpolated between present sales penetrations and the future value. This adoption curve is paired with a stock rollover tracking of appliance failure in order to compute the total demands for gas or electrical energy in a given year. These analyses similarly find a spiral in volumetric gas rates accompanies the transition to electric appliances for space and water heating.

One major shortcoming of this approach is the failure to address potential equity impacts across customers. Typically, sales share curves are applied uniformly across the entire appliance population. However, it is routinely hypothesized that a spiral in gas rates may disproportionately impact low-income customers without the upfront capital to transition to more expensive heat pump appliances or to finance the necessary building shell upgrades or structural retrofits [20].

With some additional effort, we can endogenously include such cost-allocation, rate-making, and consumer adoption features in the proposed modeling framework while preserving the convexity of the optimization program. In this section, we present a preliminary mathematical formulation to implement these policy and economic features alongside the set of centrally-planned investment decisions. First, we present the convexified formulation for cost-allocation and rate-making optimization in Section A.6.1. Next, we illustrate how these volumetric rates and fixed charges can be used to constrain appliance adoption decisions in Section A.6.2. Finally, in Section A.6.3, we discuss a relaxed version of this optimization program that will conduct scenario-based simulation of system evolution in a sequential, receding time horizon planning optimization.

A.6.1 Rate-making

Similar to the gas quality problem discussed in Section A.4, to evaluate the average cost of gas and electricity charged to ratepayers, we must compute a series of weighted average values endogenously. The total costs assessed to the electric or gas utility must be recovered across the optimized rate structure.

As illustrated in our ex-post calculations of average costs of gas and electricity delivered (see Section 2.3.9), we know that the total revenue requirement for gas and electric entities can be calculated as a closed form equation using the average cost of electricity delivered. These equations are replicated below for completeness:

$$\mu_i^P = \frac{C_i^{gen,P} + C_i^{fuel,P} + C_i^{stor,P} + C_i^{T\&D,P} + \xi_i^P(\mu_i^Z - C_i^G)}{\mathbf{\Gamma}_i^P} \qquad \forall i \in \mathcal{I} \qquad \text{(A.21a)}$$

$$\mu_i^G = \frac{C_i^{fuel,G} + C_i^{stor,G} + C_i^{T\&D,G} + \xi_i^G(\mu_i^Z - C_i^G)}{\mathbf{\Phi}_i^G} \qquad \forall i \in \mathcal{I} \qquad \text{(A.21b)}$$

$$\mu_i^Z = \frac{C_i^{gen,G} + \sum_{r\in\mathcal{R}}\sum_{o\in\mathcal{O}}\sum_{z\in\mathcal{Z}} w_{(i,r)}\Phi^Z_{(i,r,o),z}\mu_i^P}{\mathbf{\Gamma}_i^Z} \qquad \forall i \in \mathcal{I} \qquad \text{(A.21c)}$$

To compute these values endogenous to the optimization program without introducing non-convex terms, we adopt a slightly different approach. Here, we use a series of binary indicator variables with corresponding coefficients that are discretized across the plausible range of average costs of fuel delivered for net-zero emissions gas μ_i^Z, electric power μ_i^P, and gas μ_i^G. These terms compute the total revenue required to ensure cost recovery and divide it by the amount of energy produced or delivered.

First, the revenue requirements for each fuel production or delivery system are established using their fixed costs and inter-related average costs:

$$RR_i^Z = \alpha_i^Z + \beta_i^Z\mu_i^P \qquad \forall i \in \mathcal{I} \qquad \text{(A.22a)}$$

$$RR_i^P = \alpha_i^P + \beta_i^P\mu_i^Z \qquad \forall i \in \mathcal{I} \qquad \text{(A.22b)}$$

$$RR_i^G = \alpha_i^G + \beta_i^G\mu_i^Z \qquad \forall i \in \mathcal{I} \qquad \text{(A.22c)}$$

For simplicity of exposition, we use coefficients α and β to represent the following cost terms:

$$\alpha_i^Z = C_i^{gen,G} \qquad \forall i \in \mathcal{I} \qquad \text{(A.23a)}$$

$$\beta_i^Z = +\sum_{r\in\mathcal{R}}\sum_{o\in\mathcal{O}}\sum_{z\in\mathcal{Z}} w_{(i,r)}\Phi^Z_{(i,r,o),z} \qquad \forall i \in \mathcal{I} \qquad \text{(A.23b)}$$

$$\alpha_i^P = C_i^{gen,P} + C_i^{fuel,P} + C_i^{stor,P} + C_i^{T\&D,P} - \xi_i^P C_i^G \qquad \text{(A.23c)}$$

$$\beta_i^P = \xi_i^P \qquad \forall i \in \mathcal{I} \qquad \text{(A.23d)}$$

$$\alpha_i^G = C_i^{fuel,G} + C_i^{stor,G} + C_i^{T\&D,G} - \xi_i^G C_i^G \qquad \forall i \in \mathcal{I} \qquad \text{(A.23e)}$$

$$\beta_i^G = \xi_i^G \qquad \forall i \in \mathcal{I} \qquad \text{(A.23f)}$$

The decision variable for each average cost of energy μ_i is constrained to be equal to the sum of binary indicator variables $q_{k,i}$ across the set of $\mathcal{K}$ discretized coefficients for each fuel type, net-zero

emissions gas c_k^Z, electric power c_k^P, and natural gas c_k^G:

$$\mu_i^Z = \sum_{k \in \mathcal{K}} q_{k,i}^Z c_k^Z \qquad \forall i \in \mathcal{I} \tag{A.24a}$$

$$\mu_i^P = \sum_{k \in \mathcal{K}} q_{k,i}^E c_k^P \qquad \forall i \in \mathcal{I} \tag{A.24b}$$

$$\mu_i^G = \sum_{k \in \mathcal{K}} q_{k,i}^G c_k^G \qquad \forall i \in \mathcal{I} \tag{A.24c}$$

Finally, we constrain all average costs of energy to equal the total revenue requirement for each fuel system:

$$\mathbf{\Gamma}_i^Z \mu_i^Z = RR_i^Z \qquad \forall i \in \mathcal{I} \tag{A.25a}$$

$$\mathbf{\Gamma}_i^P \mu_i^P = RR_i^P \qquad \forall i \in \mathcal{I} \tag{A.25b}$$

$$\mathbf{\Phi}_i^G \mu_i^G = RR_i^G \qquad \forall i \in \mathcal{I} \tag{A.25c}$$

As such, McCormick relaxation schemes (as described in Section A.4) would be required for the following bilinear terms:

$$\beta_i^Z \mu_i^P \qquad \forall i \in \mathcal{I} \tag{A.26}$$

$$\beta_i^P \mu_i^Z \qquad \forall i \in \mathcal{I} \tag{A.27}$$

$$\beta_i^G \mu_i^Z \qquad \forall i \in \mathcal{I} \tag{A.28}$$

$$\mathbf{\Gamma}_i^Z \mu_i^Z \qquad \forall i \in \mathcal{I} \tag{A.29}$$

$$\mathbf{\Gamma}_i^P \mu_i^P \qquad \forall i \in \mathcal{I} \tag{A.30}$$

$$\mathbf{\Phi}_i^G \mu_i^G \qquad \forall i \in \mathcal{I} \tag{A.31}$$

With the above, we have presented a framework for evaluating the revenues collected by a gas or electricity utility and constraining this to equal the revenue requirement. Here, we use simple volumetric rates equal to the average cost of gas and electricity delivered. Implicit assumptions include that electricity generators are billed at the commodity cost of natural gas, with no contribution towards the gas utility revenue requirement. Also, producers of net-zero emissions gas pay the volumetric rate for electricity, and are not exposed to a wholesale price.

At the expense of computational complexity, it is obvious that this generalized formulation can be extended to include different rate classes, imposed on a range of customer classes, with fixed charge components if desired. This flexible framework would enable experimentation across a range of innovative co-optimized rate designs, however the computational burden of introducing additional binary variables for each component of the rate structure or customer-class may make the problem intractable.

A.6.2 Appliance-adoption

Retiring appliances in each investment period must then be replaced by substitute options. The adoption share of each candidate replacement can be assessed using the relative cost of ownership to the customer based on upfront capital costs, and ongoing expected costs of energy. The evaluated and/or co-optimized rate structures (as described in Section A.6 could be used to compute the expected total cost of ownership in each investment period for all of the candidate appliances $a \in \mathcal{A}$.

Appliance adoption shares can be modeled as a function of total cost of ownership, relative to the cost of substitute appliances. These adoption functions must be exogenously specified and will likely introduce additional nonlinear (or discretized binary) terms to evaluate the total number of new appliances entering the population in each investment period.

Consumer preferences could be incorporated through a downward or upward adjustment imposed on the total cost of ownership (i.e., an amount or percentage more they are willing to pay for one appliance as compared to another). Total cost of ownership calculations can also account for different discount rates of different customer classes through the set of appliances and end-use energy services. Expanding this set will require additional appliance classes $a \in \mathcal{A}$ for each customer class that you'd like to model. For example, in the presented case study, we include only one class of residential water heater for all customers. If you wanted to impose a different discount rate on high-income customers than for low-income customers, you would have two residential water heater classes in $\mathcal{A}$, but one would be designated to the end-use service $u \in \mathcal{U}$ "residential water heating for customers who make under $40,000" and the other would be designated "residential water heating for customers who make over $40,000."

Again, additional segmentation of customer classes and appliance populations will further expand the dimensionality of the problem and necessary number of binary variables and their McCormick relaxation counterparts. However, segmentation of the customer population is essential to understand the differential impact of climate policies and energy transitions on low-income populations or disadvantaged communities.

A.6.3 Sequential, receding-horizon planning

The described framework would enable endogenously co-optimized utility investment decisions, rate structures, and (with some additional effort) agent-based appliance adoption decisions. However, this fully co-optimized approach will likely prove too computationally burdensome to solve on practical time scales. Additionally, this approach runs the risk of over-optimizing the system and may not be the most beneficial approach to produce practical insights for regulators and system planners.

Alternatively, a sequential, receding-horizon planning optimization may be used to test different discrete and exogenously-specified cost-allocation and rate-making approaches in scenario-based analysis. This optimization routine would solve the program in Eq. 2.1 for a sequence of forward-looking investment years. The investment decisions for the first year are then fixed at their optimal

values, and the total system costs are allocated across electric and gas rate-payers according to an exogenously specified formulation.

Using these rate structures, we compute the expected total cost of ownership of electric- and gas-powered appliances. The relative economics of all candidate appliances are then used to simulate agent-based consumer adoption decisions for the current investment year. These utility and customer investment decisions are incorporated as the initial conditions for all subsequent investment optimizations.

This sequential, receding-horizon approach does not offer the model perfect foresight and, in some respects, may reflect a more realistic trajectory of system evolution. This may allow for comparative analysis of different rate-making or cost-allocation proposals and how the central-planning process may adapt across the planning horizon to exogenous decisions made by private actors.

A.7 Binary relaxations

In order to ensure model tractability, we include several potential binary relaxation options for future experimentation. All binary variables in the optimization program can be relaxed to continuous variables between 0 and 1 with the introduction of one additional quadratic constraint. This approach is inspired by the work of [290].

This approach is illustrated for an arbitrary binary variable y below:

$$0 \leq y \leq 1 \tag{A.32a}$$

$$0 \leq \hat{y} \leq 1 \tag{A.32b}$$

$$(y - \hat{y})^2 = 1 \tag{A.32c}$$

$$\tag{A.32d}$$

The binary variable y is relaxed to a continuous variable bound by 0 and 1 (Eq. (A.32a)). In Eq. (A.32b), we introduce a helper decision variable $\hat{y}$ as another continuous variable bound by 0 and 1. And in Eq. (A.32c) the square of the difference between these two is constrained to equal unity. The only values that will satisfy this quadratic constraint with equality are $y = 0, \hat{y} = 1$ and $y = 1, \hat{y} = 0$.

This approach introduces non-convexity due to the quadratic equality constraint in Eq. (A.32c). However, as advances are made in non-convex solvers, it may prove more computationally practical to solve the local optimization with a gradient-based or interior point optimizer, rather than solving the mixed integer linear program to global optimality via branch-and-bound algorithms.

Appendix B

Supplemental information: Molten-media pyrolysis

B.1 Nomenclature

Design variables:	
$\dot{n}_{g0}$	Molar flow rate of gas from pipeline [mol/s]
A_{HXR}	Heat exchanger area [m^2]
H	Reactor height [m]
R	Reactor radius [m]
V_R	Reactor volume [m^3]
η_{CH_4}	Fractional CH4 conversion [mol CH_4 converted/mol CH_4 entering reactor]
r_e	Exit radius [m]
L_s	Thickness of steel pressure vessel [m]
L_{ins}	Thickness of insulation layer [m]
L_{MgO}	Thickness of Magnesium-Oxide ceramic layer [m]

Physical variables:	
T_{g1}	Temperature of gas at reactor entrance [°C]
T_{g2}	Temperature of gas at reactor exit [°C]
T_{g3}	Temperature of gas after heat recovery [°C]
$\dot{n}_{g2}$	Molar flow rate of gas exiting reactor [mol/s]
$\dot{V}_{g0}$	Volumetric flow rate of gas from pipeline [m^3/s]
$\dot{V}_{g1}$	Volumetric flow rate of gas at reactor entrance [m^3/s]
$\dot{V}_{g2}$	Volumetric flow rate of gas at reactor exit [m^3/s]
$\dot{m}_{g0}$	Mass flow rate of gas from pipeline [m^3/s]
$\dot{m}_{g1}$	Mass flow rate of gas at reactor entrance [m^3/s]
$\dot{m}_{g2}$	Mass flow rate of gas at reactor exit [m^3/s]
P_{g1}	Pressure of gas at reactor entrance [MPa]
P_{g2}	Pressure of gas at reactor exit [MPa]
x_{H_2}	Mass fraction of hydrogen [%]
x_{CH_4}	Mass fraction of methane [%]
$Q_{HXR,C}$	Rate of heat transfer from cold stream [MW]
$Q_{HXR,H}$	Rate of heat transfer from hot stream [MW]
r	Rate of reaction [mol s^-1 m^-3]
y_{H_2}	Mole fraction of hydrogen [%]
y_{CH_4}	Mole fraction of methane [%]
ϵ_1	Gas holdup [m^3 gas/m^3 reactor volume]
V_{gj}	Mean drift velocity [m/s]
j_g	Superficial gas velocity [m/s]
j_g^+	Dimensionless superficial gas velocity [-]
V_{gj}^+	Dimensionless drift velocity [-]
V_{mp}	Transition superficial velocity for homogenous dilute flow [m/s]
G_s	Flux of solid particles entrained [m^3/m^2]
D	Diameter of exit orifice [m]
Ar	Archimedes number [-]

Operational variables:	
$\dot{Q}_{loss}$	Thermal losses from reactor [MW]
$\dot{Q}_{steel}$	Heat transfer through steel layer [MW]
$\dot{Q}_{ins}$	Heat transfer through insulation layer [MW]
$\dot{Q}_{MgO}$	Heat transfer through MgO ceramic layer [MW]
$\dot{Q}_{reactor}$	Heat transfer into reactor [MW]
$\dot{W}_{blower}$	Electric power demand for blower [MW]
$\dot{W}_{cyclone}$	Electric p demand for cyclone [MW]
$\dot{m}_{H_2}$	Mass flow rate of hydrogen produced [kg/s]
$\dot{m}_{C,solid}$	Mass flow rate of solid carbon produced [kg/s]
$\dot{m}_{CO_2,seq}$	Mass flow rate of carbon dioxide (equivalent) sequestered [kg/s]
$\dot{m}_{CO_2,av}$	Mass flow rate of carbon dioxide lifecycle emissions avoided [kg/s]
$\dot{m}_{CO_2,avoidedstack}$	Mass flow rate of carbon dioxide stack emissions avoided [kg/s]
P_{e-}	Total rate of electric power demand from grid [MW]
$P_{g,i}$	Total rate of gaseous fuel demand from pipeline [MW]
$P_{g,o}$	Total rate of gaseous fuel produced [MW]
$LMTD_{HXR}$	Log mean temperature difference [K]
$OpEx$	Operational expenses [$/year]
Rev	Revenues [$/year]
FOM	Fixed operations and maintenance expenses [$/year]
TCR	Total Capital Requirement [$]
PC_e	Purchase cost of equipment [$]
NPV	Net Present Value [$]
$LCOE$	Levelized cost of energy [$/MMBtu]
$LCOH$	Levelized cost of hydrogen [$/kg H_2]

Physical parameters:	
c_{p,CH_4}	Specific heat coefficient [kg/kg-K]
c_{p,H_2}	Specific heat coefficient [kg/kg-K]
R	Universal gas constant []
ΔH_{rxn}	Reaction enthalpy [kJ/mol]
HHV_{H_2}	Higher heating value of hydrogen [MJ/kg]
HHV_{CH_4}	Higher heating value of methane [MJ/kg]
LHV_{H_2}	Lower heating value of hydrogen [MJ/kg]
LHV_{CH_4}	Lower heating value of methane [MJ/kg]
M_{H_2}	Molar mass of hydrogen [g/mol]
M_{CH_4}	Molar mass of methane [g/mol]
M_{CO_2}	Molar mass of carbon dioxide [g/mol]
M_C	Molar mass of carbon [g/mol]
k_{MgO}	Thermal conductivity of magnesium oxide ceramic layer [W/m-K]
k_{ins}	Thermal conductivity of insulation layer [W/m-K]
k_{steel}	Thermal conductivity of steel layer [W/m-K]
ρ_m	Molten media density [kg/m^3]
ρ_{CH_4}	Density of inlet methane gas [kg/m^3]
C_0	Unitless distribution parameter for round ducts [-]
σ	Surface tension of molten media [N/m]
ρ_{H_2}	Density of product hydrogen gas [kg/m^3]
ρ_p	Density of solid carbon particles [kg/m^3]
μ_{H_2}	Viscosity of product hydrogen gas [kg m$^-$1 s$^-$1]
E_a	Activation energy [kJ/mol]
A	Pre-exponential factor [mL cm$^-$2 s$^-$1]
k_B	Boltzmann's constant [m^2 kg s$^-$2 K$^-$1]

Design parameters:	
P_{r0}	Reactor pressure [bar]
T_{r0}	Reactor temperature [°C]
T_{g0}	Temperature of gas from pipeline [°C]
P_{g0}	Pressure of gas from pipeline [MPa]
U_{HXR}	Heat transfer coefficient
r_b	Bubble radius [m]
C_{CH_4}	Methane concentration in reactant
d_p	Particle diameter [m]
P_{boiler}	Rate of thermal power demand for boiler [MW]
η_{boiler}	Efficiency of boiler [%]
$\underline{\eta}_{CH_4}$	Minimum molar conversion fraction [%]
ζ_m	Loss rate of molten media [%]
Cap	Boiler capacity [MW]
IRR	Internal Rate of Return [%]
LF	Lang Factor [unitless]
T	Lifetime of project [years]
cf	Capacity factor [%]
p_{e-}	Price of electricity [$/MWh]
p_{NG}	Price of natural gas [$/MMBtu]
p_{Csolid}	Price of solid carbon [$/kg]
p_{CO_2av}	Price of carbon emissions avoided [$/kg CO_2]
p_{CO_2seq}	Price of carbon emissions sequestered [$/kg CO_2]
c_m	Cost of molten media [$/kg Ni-Bi]
EF_{e-}	Emissions factor for electricity [kg CO_2/MWh]
EF_{NG}	Emissions factor for natural gas [kg CO_2/MMBtu]
$CI_{SMR-H2,stack}$	Carbon intensity of hydrogen from steam-methane reforming [kg CO_2/kg H_2]

B.2 Heat exchange modeling

The below empirical specific heat equations are used for gaseous heat exchange per [218]:

$$c_{p,H_2}(T) = a_{H_2}T + b_{H_2}T^2 + c_{H_2}T^3 + d_{H_2}T^4 \tag{B.1a}$$

$$c_{p,CH_4}(T) = a_{CH_4}T + b_{CH_4}T^2 + c_{CH_4}T^3 + d_{CH_4}T^4 \tag{B.1b}$$

Coefficients				
Gas	a	b	c	d
H_2	29.11	-0.1916*10^{-2}	0.4003*10^{-5}	-0.8704*10^{-9}
CH_4	19.89	5.024*10^{-2}	1.269*10^{-5}	-11.01*10^{-9}

Table B.1: Coefficients for empirical specific heat equations.

B.3 Plug flow reactor model

In order to validate the mathematical model for the reactor kinetics, we employ Aspen HYSYS process simulation software. The Aspen HYSYS model was a kinetically controlled plug flow reactor with a single pyrolysis reaction. The kinetic parameters derived experimentally by Upham et al. (2017) were employed [190]. Various reactor dimensions, volumes, and gas holdup values were explored. The mole fraction produced was found to only be a function of the residence time. The residence time can be converted to a reactive volume by multiplying by the volumetric flow rate, allowing for various reactor configurations to be compared on an identical baseline. Several simulations were conducted and the mole fraction of H_2 in product gas stream is compared in Figure B.1 to that predicted by the model derived in Upham et al., 2017, and the model used in this work.

While the mathematical formulation used by Upham et al. (2017) and ASPEN HYSYS accounts for the changing concentration of reactants across the plug-flow reactor, it does not appear that these models account for any consequent changes as mole creation results in a larger volume and reactant surface area.

B.4 Capital cost correlations

The Chemical Engineering literature contains a well-established body of work on the topic of capital cost estimation for novel process equipment. Table B.2, below, includes all capital cost estimation equations employed and their source. Some equations include adjustment factors for materials, f_m, and all values were updated to 2017$ using CEPCI.

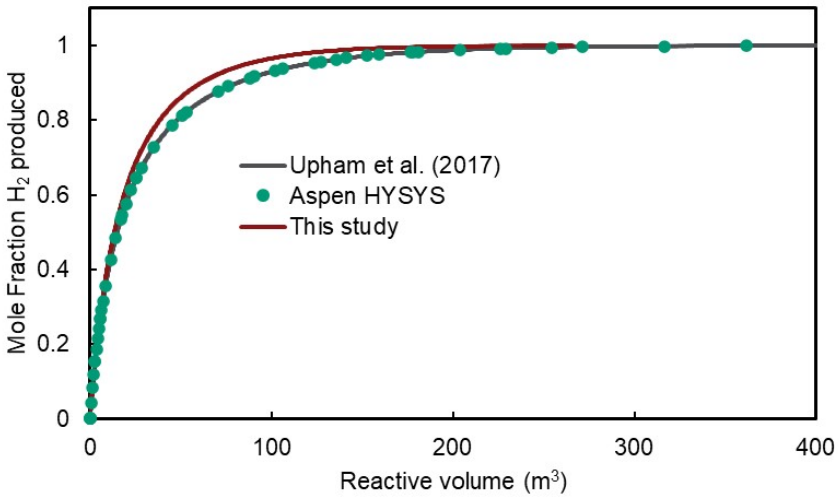

Figure B.1: Results of our mathematical model as compared to the model derived in Upham et al. (2017) and the outputs of a similarly tuned Aspen HYSYS reactor model.

Equipment (e)	Purchased cost (PC_e)	Source
Heat exchanger	f_m (28000+54$A_{HXR}^{1.2}$), $f_m = 1.7$	[226]
Pressure vessel	(11600+34$m_{shell}^{0.85}$)	[226]
Cyclone	$f_m\ e^{0.12 \ln \dot{V}_{g2}}$, $f_m = 9$	[219]
Bag filter	$e^{9.9+0.5575 \ln \dot{V}_{g2}}$	[219]
Transformer	$((\dot{Q}_{loss} + \dot{Q}_{reactor}))/((10^6 W)/MW)$ ($ 42850)/MW	[229]
Materials	Purchased cost (PC_e)	Source
Insulation	$C_(C-ins)\rho_(C-ins)V_(C-ins)$ $C_(C-ins)$=$0.1/kg	[184]
Ceramic (Mg-O)	$C_(Mg-O)\rho_(Mg-O)V_(Mg-O)$ $C_(Mg-O)$=$0.36/kg	[184]
Molten metal (Ni-Bi)	$(C_N i x_N i + C_B i x_B i)\rho_m(1-\epsilon)V_R$, x_{Ni}=0.1 x_{Bi} = 0.9 C_{Ni}=$6/lb, C_{Bi}=$5/lb	(InvestmentMine.com), (Rotometals.com)
Resistive elements (Si-C)	$C_(Si-C)$ $\rho_(Si-C)$ $V_(Si-C)$, $C_(Si-C)$=$36/kg	[223]

Table B.2: Capital cost estimation equations employed for a variety of equipment and materials.

B.5 Operational cost estimates

Power consumption of the cyclone, $\dot{W}_{cyclone}$ [W] is estimated from equations in[219].

$$\dot{W}_{cyclone} = 2000\dot{V}_{g2a} \tag{B.2}$$

B.6 Radial conduction modeling

A multi-layered radial conduction model was employed to estimate the shell losses from the pyrolysis reactor

$$\dot{Q}_{ceramic} = \frac{2\pi R^2 k_{MgO}(T_{r1} - T_{r2})}{L_{MgO}} + \frac{2\pi H k_{MgO}(T_{r1} - T_{r2})}{\ln \frac{R+2L_{MgO}}{R+L_{MgO}}} \tag{B.3a}$$

$$\dot{Q}_{insulation} = \frac{2\pi R^2 k_{ins}(T_{r2} - T_{r3})}{L_{ins}} + \frac{2\pi H k_{ins}(T_{r2} - T_{r3})}{\ln \frac{R+2L_{MgO}+L_{ins}}{R+2L_{MgO}}} \tag{B.3b}$$

$$\dot{Q}_{steel} = \frac{2\pi R^2 k_{steel}(T_{r3} - T_{r4})}{L_{steel}} + \frac{2\pi H k_{steel}(T_{r3} - T_{r4})}{\ln \frac{R+2L_{MgO}+L_{ins}+L_{steel}}{R+2L_{MgO}+L_{ins}}} \tag{B.3c}$$

$$\dot{Q}_{loss,rad} = 2\pi H \sigma_{rad}(T_{r4}^4 - T_{amb}^4)(R + 2L_{MgO} + L_{ins} + L_{steel}) + 2\pi R^2 \sigma_{rad}(T_{r4}^4 - T_{amb}^4) \tag{B.3d}$$

$$\dot{Q}_{loss,conv} = 2\pi H h_{conv}(T_{r4} - T_{amb})(R + 2L_{MgO} + L_{ins} + L_{steel}) + 2\pi R^2 h_{conv}(T_{r4} - T_{amb}) \tag{B.3e}$$

$$\dot{Q}_{loss} = \dot{Q}_{loss,rad} + \dot{Q}_{loss,conv} \tag{B.3f}$$

$$\dot{Q}_{loss} = \dot{Q}_{steel} = \dot{Q}_{insulation} = \dot{Q}_{ceramic} \tag{B.3g}$$

Appendix C

Supplemental information: Greenhouse gas accounting

C.1 Nomenclature

Nomenclature for Section 4.2:	
$i \in \mathcal{SP}$	Set of specified purchases
$\mathcal{SP}_{NG} \subset \mathcal{SP}$	Subset of specified purchases from natural gas-fired generators
$\mathcal{SP}_F \subset \mathcal{SP}$	Subset of specified purchases from fossil-fueled generators (excluding natural gas)
$\mathcal{SP}_Z \subset \mathcal{SP}$	Subset of specified purchases from non-fossil-fueled generators
GP_i	Specified gross purchase i [MWh/year]
WS_i	Specified wholesale sales of gross purchase i [MWh/year]
NP_i	Specified net purchase i [MWh/year]
U	Unspecified purchases [MWh/year]
RS	Retail electricity sales [MWh/year]
TNP	Total net purchases [MWh/year]
ANP_i	Adjusted net purchase for specified purchase i [MWh/year]
EF_i	Emissions factor for specified purchase i [tCO_2e/MWh]
EF_U	Emissions factor for unspecified purchases [tCO_2e/MWh]
EI	Emissions intensity estimate for a portfolio [tCO_2e/MWh]

Nomenclature for Section 4.3:	
$E_{i,t}$	Hourly emissions in time-step t for balancing authority i [tCO_2/hour]
α_g	Emissions factor for generator g [tCO_2/MWh]
$P_{g,t}$	Hourly power generation in time-step t for generator g [MWh/hour]
$u_{i,t}$	Electricity flows into each balancing authority i during time-step t [MWh/hour]
$v_{i,t}$	Electricity flows out of each balancing authority i during time-step t [MWh/hour]
$x_{i,t}$	Emissions intensity of electricity delivered in each balancing authority i during time-step t [tCO_2/MWh]
$d_{i,t}$	Demand for electricity in a balancing authority i during time-step t [MWh/hour]
I^G	Embodied emissions imports to a balancing authority i [tCO_2/year]
$\lambda_{g,i,t}$	Specified electricity transfers from generator g to balancing authority i in time-step t [MWh/hour]
$a_{g,i}$	Nominal transfer pathway indicator for whether power output from generator g is wheeled through or to balancing authority i [bin.]
$E^*_{i,t}$	Contract-adjusted emissions in time-step t for balancing authority i [tCO_2/hour]
$u^*_{i,t}$	Contract-adjusted flows into each balancing authority i during time-step t [MWh/hour]
$x^*_{i,t}$	Contract-adjusted emissions intensity of electricity delivered in each balancing authority i during time-step t [tCO_2/MWh]
L_i	Emissions leakage liability assessedfor balancing authority i [tCO_2/year]
γ_g	Non-baseload factor for each generator g
ξ_g	Capacity utilization factor for each generator g [%]
$\underline{\xi}$	Cut-in capacity utilization factor [%]
β	Regression coefficient [tCO_2/MWh]

C.2 Methodological comparison to de Chalendar et al., (2019)

The inspiration for this approach to emissions leakage quantification was drawn from the work of de Chalendar et al., (2019) [237], who leverage consumption-based accounting in the electric power sector to quantify emissions trans-shipments between balancing authorities and the associated divergence between production-bsased emissions and consumption-based emissions liabilities.

Several data quality issues required attention in the EIA Form 930 operating system data [90], including missing or inconsistent data on net generation, demand, and transfers between balancing authorities. To reconcile interchanges between balancing authority pairs where inconsistent data are reported, we used the average of the two reported numbers. To correct missing data entries, we replaced any missing hourly data with the value reported for the same hour of the preceding day.

After making these adjustments, we aggregated hourly continuous emissions monitoring system (CEMS) emissions for each unique EIA Plant ID and normalized the hourly values by total annual emissions reported. We multiplied the normalized emissions profiles by the annual emissions for that plant as reported in eGRID for 2016. This adjustment ensures that hourly emissions for biomass and combined heat and power plants are all adjusted appropriately to represent the CO_2 emissions that can be attributed to the electric power furnished by each plant, consistent with eGRID. This approach also assumes that any emitting units at the plant that do not meet reporting thresholds for CEMS will operate at similar times as the reporting units.

We then aggregated plants by their resident balancing authority and attributed hourly emissions to each balancing authority. As a last step, we compared annual emissions as estimated by this bottom-up method to the annual GHG emissions reported for each balancing authority in eGRID. The discrepancy between these figures represents emissions from plants that do not report hourly data to CEMS. We allocated these missing emissions for each balancing authority across each hour in the year, with the allocation proportionately weighted to total net generation for the balancing authority reported in each hour, according to EIA Form 930 [90].

Here, we adopt a similar approach with slight modifications for simplicity. Primary differences include the following:

In order to reconcile the EPA's Air Markets Program Data (AMPD) with the reported emissions for each plant in eGRID, we use AMPD solely for the normalized profile of emissions and leverage eGRID for the magnitude of annual anthropogenic emissions contributions assessed. Previous work has used additive and multiplicative adjustment factors for biomass and combined heat and power plants, respectively, based on the eGRID reporting for "adjusted" and "unadjusted" annual CO_2 emissions.

In order to account for emissions from plants that are not included in the AMPD data set, we quantify the difference in annual emissions at the balancing authority level between our hourly data set (developed as per the previous bullet point) and eGRID's reporting of balancing authority annual emissions. We incorporate these additional emissions with an hourly profile proportionate to hourly

net generation in the balancing authority. This assumes that emissions not reported to AMPD are generally proportionate in magnitude to total net generation. Previous work has observed the discrepancy but does not address it.

In cleaning of the hourly electricity system operating data, we adopt two systematic rules. If data are missing for an hour, we use the reported value for the same hour of the prior day. And if there are two reported values for the same interchange, we retain the average of the two present values. Previous work has inspected profiles visually and made manual adjustments to ensure that profiles match.

These changes cause our consumption-based estimates for embodied emissions to be higher relative to previous published work. Nevertheless, we consider the effect well within the margin of error given substantial uncertainties in data quality.

Our results for 2016 are compared to those of de Chalendar et al., (2019), and to the net generation and emissions recorded in eGRID 2016. Key differences in emissions exist between our results and previous work as we include all emissions reported in eGRID, and not just those contained in the CEMS data set. Additionally, the values for net generation diverge slightly from those in eGRID due to data quality issues in the EIA Form 930 dataset. Further, the annual net generation for both AZPS and SRP are substantially different from eGRID 2016 due to a misallocation of generation from Palo Verde Nuclear Plant which is owned by AZPS, but technically dispatches into SRP. However, these differences do not meaningfully affect the results presented, and more detailed analysis ought to be done before any emissions factors are adopted by policymakers.

Balancing Authority Code	This study		de Chalendar et al., (2019)		eGRID2016	
	Electricity [TWh]	Emissions [$MMtCO_2$]	Electricity [TWh]	Emissions [$MMtCO_2$]	Electricity [TWh]	Emissions [$MMtCO_2$]
AEC	5.7	3.8	5.7	3.5	5.7	3.8
AECI	21.1	16.6	21.3	15.0	21.3	16.6
AVA	6.6	0.7	7.5	0.7	7.5	0.7
AZPS	51.0	11.3	51.0	10.2	14.7	11.3
BANC	13.1	3.1	9.3	2.8	9.3	3.1
BPAT	113.2	13.8	125.0	13.8	121.6	13.8
CHPD	9.1	0.0	9.2	0.0	9.2	0.0
CISO	164.1	36.0	169.0	32.7	168.8	36.0
CPLE	65.7	20.9	62.6	18.9	62.6	20.9
CPLW	0.0	0.0	1.8	0.0	0.0	0.0
DEAA	1.9	0.8	1.9	0.8	1.9	0.8
DOPD	4.1	0.0	4.3	0.0	4.3	0.0

DUK	106.0	37.3	114.0	33.8	113.9	37.3
EEI	3.1	3.5	3.2	3.2	3.2	3.5
EPE	3.8	2.2	4.0	2.0	4.0	2.2
ERCO	352.1	192.5	383.0	175.0	383.3	192.5
FMPP	17.1	9.7	14.8	8.8	14.8	9.7
FPC	39.9	26.6	42.3	24.1	42.3	26.6
FPL	120.8	40.0	119.0	36.2	119.3	40.0
GCPD	10.2	0.0	10.2	0.0	5.4	0.0
GRIF	2.1	0.9	2.1	0.8	2.1	0.9
GRMA	7.0	3.3	7.0	3.0	7.0	3.3
GVL	1.6	1.2	1.6	1.1	1.6	1.2
GWA	0.6	0.0	0.6	0.0	0.6	0.0
HGMA	3.4	1.4	3.4	1.3	3.4	1.4
HST	0.0	0.0	0.0	0.0	0.0	0.0
IID	5.7	0.8	5.7	0.8	5.7	0.8
IPCO	11.5	0.8	11.2	0.7	11.2	0.8
ISNE	105.0	30.0	107.0	27.2	106.6	30.0
JEA	13.6	12.3	14.4	11.2	14.4	12.3
LDWP	23.1	13.2	20.8	12.0	20.8	13.2
LGEE	38.2	35.6	37.9	32.3	37.9	35.6
MISO	614.7	432.8	679.0	392.0	679.4	432.8
NEVP	30.3	14.5	34.1	13.1	34.1	14.5
NSB	0.0	0.0	0.0	0.0	0.0	0.0
NWMT	19.5	16.9	19.2	15.4	19.2	16.9
NYIS	135.8	33.4	140.0	30.3	140.1	33.4
OVEC	6.8	11.3	10.0	10.3	10.0	11.3
PACE	45.8	50.3	59.2	45.6	59.2	50.3
PACW	15.7	2.0	10.6	1.8	10.6	2.0
PGE	6.1	1.4	5.3	1.3	5.3	1.4
PJM	815.5	382.4	799.0	347.0	799.1	382.5
PNM	16.6	14.1	15.3	12.8	15.3	14.1
PSCO	38.0	16.3	28.5	14.8	28.5	16.3
PSEI	15.6	1.2	13.4	1.0	5.1	1.2
SC	18.2	16.5	18.5	15.0	18.5	16.5
SCEG	26.8	12.3	27.4	11.2	27.4	12.3
SCL	7.0	0.0	6.7	0.0	6.7	0.0
SEC	11.4	9.2	11.5	8.3	10.9	9.2

SEPA	1.5	0.0	1.8	0.0	1.4	0.0
SOCO	242.4	139.0	257.0	126.0	256.8	139.0
SPA	6.4	1.7	7.0	1.6	7.0	1.7
SRP	29.8	26.7	29.8	24.2	65.5	26.7
SWPP	260.4	168.1	257.0	152.0	257.5	168.1
TAL	2.6	1.2	2.6	1.1	2.6	1.2
TEC	22.8	15.8	23.2	14.4	23.2	15.9
TEPC	8.8	10.5	10.7	9.5	10.7	10.5
TIDC	1.6	0.7	1.6	0.6	1.6	0.7
TPWR	3.2	0.0	3.5	0.0	3.5	0.0
TVA	162.3	78.0	166.0	70.7	166.3	78.0
WACM	37.9	44.7	44.3	40.6	44.3	44.7
WALC	7.2	2.7	15.3	2.4	15.3	2.7
WAUW	0.4	0.0	3.5	0.0	3.5	0.0
WWA	0.7	0.0	0.7	0.0	0.7	0.0
YAD	0.7	0.0	0.7	0.0	0.7	0.0

Table C.1: Numerical results for net generation and emissions by balancing authority for the year 2016, as compared to previous work (de Chalendar et al., (2019)) and eGRID2016 reports.

C.3 Specified import subtraction from consumption-based accounting

In order to assess the emissions leakage associated with specified import transfers from out-of-state balancing authorities, we used Power Source Disclosure (PSD) forms, Quarterly Fuel and Energy Reports (QFER), and CARB's GHG Emissions Inventory to aggregate a list of source-identified specified imports from out-of-state balancing authorities. Table C.2 summarizes these results, presenting the disaggregation of imported electricity and embodied emissions. CARB's GHG Emissions Inventory reports gross imported electricity (line (A)) and identifies some portion of these gross imports as unspecified (line (B)). Of the specified imports, some transfers are from out-of-state plants that dispatch directly into California balancing authorities; these are quantified using the CEC's QFER and reported in line (C). No emissions leakage results from these imports, as they are interconnected directly to California customers and cannot directly transfer power to other balancing authorities without changes to the physical grid. Some CARB-reported specified imports are transfers from ACS entities (line (D)) and most of the remaining specified imports have been identified using the CEC's PSD reports (line (E)). Some residual imports could not be identified to

Specified electricity imports [TWh]	2016	2017
(A) Gross imports, per [271]	99.7	94.4
(B) Reported as unspecified, per [271]	21.0	19.0
(C) Identified from sources in CA balancing authorities, per [285]	19.2	18.7
(D) Asset Controlling Supplier imports, per [284]	18.3	17.0
(E) Identified from sources in out-of-state balancing authorities, per [283]	38.9	38.1
(F) Other non-identified [A-B-C-D-E]	2.3	1.6

Table C.2: Numerical results for consumption-based accounting simulations for the years 2016 and 2017 with specified imports included and removed from the system. Brackets indicate each row's data source or underlying computation, including results of the consumption-based accounting (CBA) analysis presented here.

a specific source with the available information (line (F)).

In order to manually remove these transfers from the system, we had to assume a transfer pathway by which these imports would reach California balancing authorities. The assumed transfer balancing authority is included for every balancing authority from which specified imports are sourced and was determined by using EIA Form 930 information to determine the most likely transfer pathway. When the below transfers are aggregated for each unique interchange between balancing authorities, any final transfers from Bonneville Power Authority were assumed to be split proportionately between CAISO, BANC, and LDWP based on the relative magnitude of total annual interchange. Finally, in addition to removing the electricity generation and transfers, the direct emissions from these specified imports must be removed from the resident balancing authority, as California entities take nominal responsibility for those GHG emissions. We use plant-specific emissions factors from eGRID2016 in order to ensure consistency with the other emissions estimates used. The answer may differ slightly if CARB-adopted source-specific emissions factors are used, but it is not expected to change the conclusions.

C.4 Reconciliation of CEC and CARB imports reporting

CARB and the CEC report different amounts and compositions of electricity imports to California. Figure C.1 demonstrates the differences between what is reported for zero-GHG emissions imports

2016				2017			
Resident BA	Electricity imports [TWh]	Direct emissions [tons CO_2]	Assumed Transfer BA	Resident BA	Electricity imports [TWh]	Direct emissions [tons CO_2]	Assumed Transfer BA
WALC	1.90	56298	LDWP	WALC	1.61	22045	LDWP
DEAA	0.00	1541	SRP	DEAA	0.00	0	SRP
GRMA	0.10	44475	AZPS	GRMA	0.00	0	AZPS
GRIF	0.11	47612	WALC	GRIF	0.11	49043	WALC
HGMA	0.00	0	SRP	HGMA	0.00	0	SRP
SRP	9.84	698711	CISO	SRP	9.41	141004	CISO
AZPS	0.61	183710	CISO	AZPS	0.56	154878	CISO
NWMT	0.00	2802	BPAT	NWMT	0.01	875	BPAT
NEVP	4.05	1453506	WALC	NEVP	4.32	1329276	WALC
PNM	2.12	2562239	WACM	PNM	2.28	2693261	WACM
BPAT	9.89	130848	CISO	PGE	1.25	94917	BPAT
PACW	1.25	470039	PACE	PACW	0.85	215427	PACE
PACE	2.22	843285	LDWP	BPAT	9.14	35353	CISO
AVA	0.66	2297	IPCO	PACE	1.97	616229	LDWP
PSEI	0.38	0	CHPD	AVA	0.72	3435	IPCO
TPWR	0.34	2651	PSEI	PSEI	0.37	0	CHPD
IPCO	0.23	0	PACW	PSCO	2.41	9047	PACW
PSCO	1.05	8159	PNM	IPCO	0.40	0	PNM
CHPD	0.87	0	BPAT	CHPD	1.13	0	BPAT
WACM	0.14	17438	WALC	SCL	0.03	0	PSEI
GCPD	1.85	0	BPAT	WACM	0.02	17367	WALC
EPE	0.05	0	PNM	GCPD	0.90	0	BPAT
GWA	0.58	0	NWMT	EPE	0.08	0	PNM
WWA	0.66	0	NWMT	SWPP	0.20	0	WACM
				TPWR	0.34	2625	PSEI

Table C.3: Specified imports nominally allocated to California and manually removed from the physical consumption-based accounting model to assess emissions leakage.

and for unspecified electricity imports.

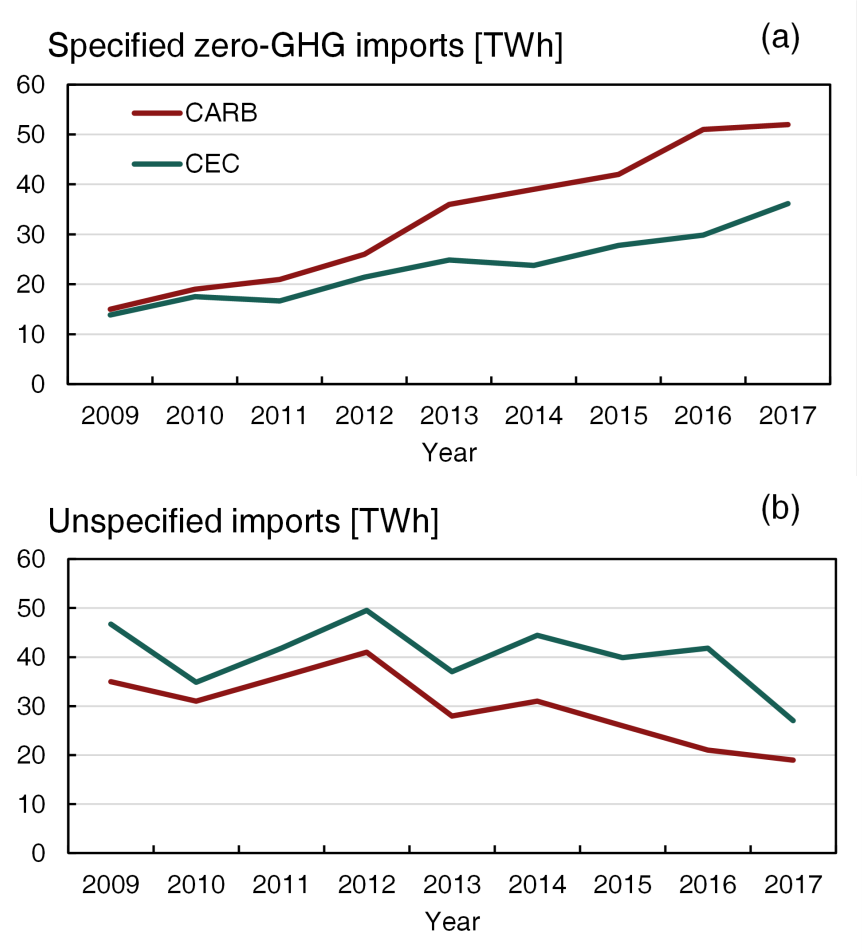

Figure C.1: Differences between CARB and CEC reporting for specified zero greenhouse gas imports (a) and unspecified imports (b). In order to explain these differences and produce a harmonized understanding of specified electricity imports, we reconcile three data sets from the CEC—Total System Electric Generation [272], Quarterly Fuel and Energy Report [285], and Power Source Disclosure (PSD) program [283]—with CARB's Mandatory GHG Reporting Regulation [169] and GHG Emissions Inventory [271, 284]. These results are then used to characterize downstream policy implications.

Our first task is to harmonize data from two different state agencies concerning the portfolio of resources providing electricity imports to California load serving entities (LSEs). The CEC publishes Total System Electric Generation (TSEG), based on LSE reporting from Power Source Disclosure (PSD) forms and the Quarterly Fuel and Energy Report (QFER) [285]. In addition, CARB maintains California's GHG Emissions Inventory and reports aggregated data on specified electricity imports from MRR reporting [169], with some emitting resources disaggregated in the

inventory documentation [271, 284].

CARB and CEC data diverge due to different conventions in assigning electricity attributes, as well as different treatment of gross imports and net imports. We identify all specified imports by their Plant ID where available in each data set. In Figure C.2, we present a disaggregated picture of specified imports to identify the relationship between these different accounting conventions. All categories prefaced with "other" are imports for which we could not identify a specific plant that was furnishing that electricity based on the available data. Our analysis identifies two main findings.

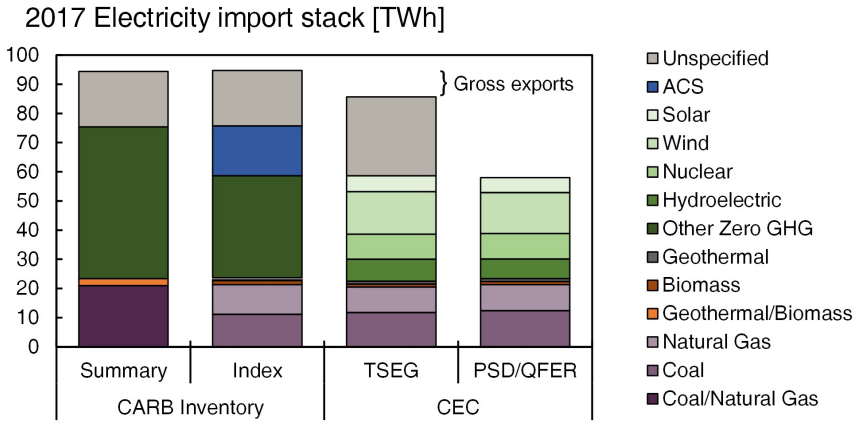

Figure C.2: Comparison of electricity imports as reported by the CARB GHG emissions inventory and the CEC in TSEG, PSD, and QFER data. The inconsistency between imports labeled "unspecified" can be accounted for by the use of ACS designations by CARB and the difference between gross and net imports.

First, the two agencies apply different treatment to so-called Asset Controlling Supplier (ACS) power entities. Pursuant to the MRR, CARB has designated the Bonneville Power Administration (BPA), Powerex, and Tacoma Power as ACS entities. CARB assigns all imports from each ACS entity a single emissions factor. CARB considers imports from ACS entities to be specified imports, which are classified as "primarily hydropower" and included in CARB's calculation of total zero-GHG imports from specified sources. (To clarify, CARB assigns small but non-zero emissions factors to these regions—for example, CARB assigned BPA an emissions factor of 0.0193 tonnes CO_2/MWh in 2017 [291].) In contrast, the CEC categorizes imports from ACS entities without a designated EIA Plant ID as unspecified imports and does not generically consider them zero-GHG resources. A similar outcome is observed for 2016 data, as documented in the Supplemental Information.

Second, the two agencies differ in whether they report net or gross imports, with the CEC reporting the composition of net imports and CARB reporting gross imports. The CEC uses quarterly reports from California balancing authorities to first quantify net electricity imports for the year and subsequently attribute fuel types based on PSD reporting. As a result, the unspecified imports reported in CEC TSEG are not derived from individual load-serving entities' reporting on unspecified

electricity transactions. Instead, they are determined in the negative: they represent the difference between the calculated net electricity imports to California and the sum of imports from specified sources as reported in the PSD and QFER programs.

The differences in the way the two agencies use identical terms to describe data on electricity imports can lead to confusion about their emissions implications in downstream policy programs, such as CARB's Low Carbon Fuel Standard. CARB's calculation for the lifecycle emissions of electricity as a transportation fuel relies on the CEC TSEG data. In the interagency translation, CARB's LCFS assumes that unspecified electricity as measured by CEC will have an emissions intensity similar to natural gas-fired generation [292]. As we have shown above, however, nearly 65% of the total unspecified imports in CEC data reflects about 18 TWh of electricity transfers from BPA, Powerex, and Tacoma Power that CARB treats as "primarily hydropower." Applying an emissions factor of natural gas-fired generation to about 18 TWh of primarily hydropower biases upwards the emissions intensity used in LCFS for electricity as a transportation fuel. Per recently adopted regulations implementing Assembly Bill 1110, the CEC will allow ACS entities to have their wholesale sales classified as "specified system power" with an associated fuel mix and emissions factor that comports with reporting to CARB under the MRR [169]. The CEC's new methodology should resolve much of the reporting discrepancy described above, although will not resolve the differences due to net versus gross imports.

An identical exercise can be completed for data from the year 2016 as well. 2016 was a year with lower hydroelectric generation, and so it is interesting to see this trend persist across years with diverse generation mixes. However, there is an additional inconsistency between reported imports from natural gas-fired sources. In 2016, the CEC Total System Electric Generation only appears to include a portion of imports from gas-fired generators that file Quarterly Fuel and Energy Reports and those included in the Power Source Disclosure filings. The reasons for this difference are unclear, and no such difference is evident in the 2017 data.

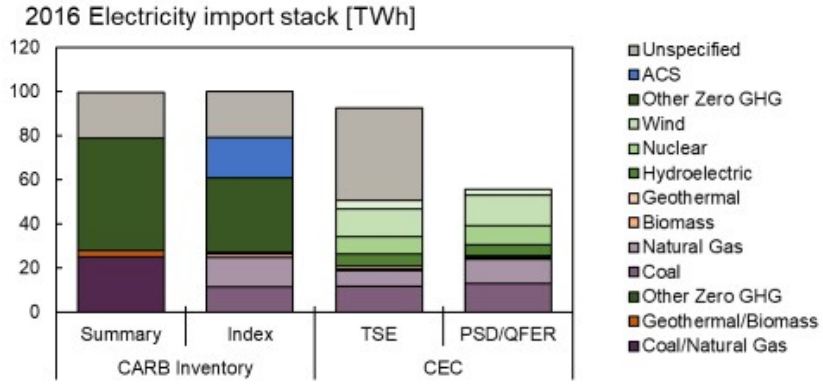

Figure C.3: Comparison of electricity imports as reported by the CARB GHG emissions inventory and the CEC Total System Electric Generation.

C.5 Replicating the WCI unspecified emissions factor workbook

To replicate the legacy default emissions factor as adopted by the California Air Resources Board, we identified two sets of manual adjustments those calculations made to the raw data sources from the Energy Information Administration (EIA) Form 923 and Form 860 worksheets [126, 129].

First, nameplate capacity values from Form 860 for each generating unit were de-rated to account for any partial operation during the year. For example, if a generator came online or retired in 2006, 2007, or 2008, then the nameplate capacity value was decremented to reflect the number of months the generator was operational in that year. Additional manual modifications were made to several nameplate capacity records for large coal-fired generators based on conversations with the plant owner or knowledge of long-duration shut-downs. For example, the Kennecott Utah Copper Corporation plant (EIA Plant Code 56163) was routinely shut down for 4 months of the year due to air quality restrictions. These changes increase the annual capacity factor for the plant and often result in the coal-fired plant no longer being considered "marginal."

We provide a sampling of screenshots from the workbook in Figure C.4 for illustrative purposes.

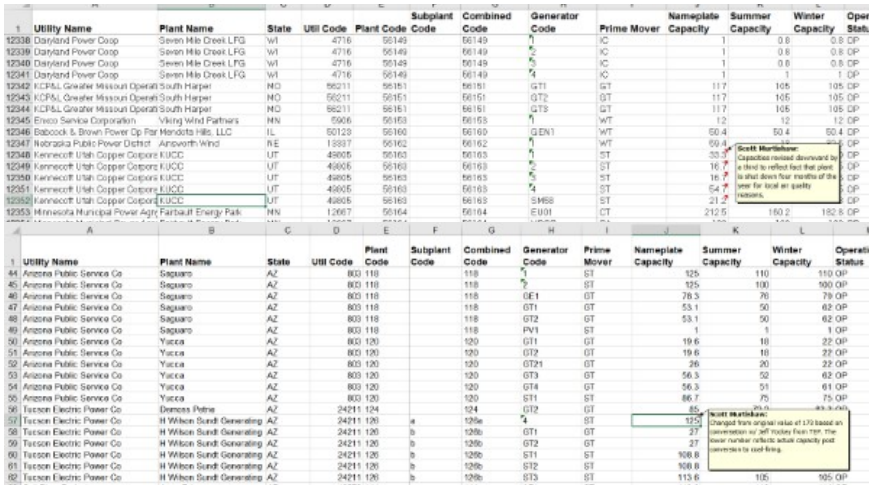

Figure C.4: Screen captures of manual adjustments to nameplate capacity values in Western Climate Initiative (WCI) workbook.

Second, CARB's analysis made certain assumptions about capacity factors. Because a capacity factor threshold is used as one of the criteria for inclusion in the set of "marginal" generators, an annual capacity factor must be estimated for every generator in the WECC. This calculation introduces additional nuance due to data limitations. EIA Form 923 records provide information on annual fuel consumption [MMBtu] and annual net generation [MWh], and each include, as unique identifiers, a Plant ID, a prime mover, and a fuel type. However, each record can represent more

than one physical generator at a single plant, so long as they have identical prime movers and fuel. For example, a combined cycle gas turbine (CCGT) generator will be split into two different Form 923 records, one for the combustion turbine (CT) prime mover and the other for the steam turbine (CA) prime mover. However, if a single plant has multiple CCGTs, the CT and CA components for each will be aggregated in their respective Form 923 records.

EIA Form 860 reports contain the set of generating units in operation during each year. Each record for a generator contains its plant code, nameplate capacity, prime mover, and primary fuel type. However, each generating unit may consume several different fuels and have corresponding records in Form 923 that do not align with their primary fuel type. As there is not a set of unique identifiers to merge Form 860 and Form 923 records, approximations must be made in order to estimate the capacity factor associated with each Form 923 record.

For the most part, the original WCI analysis aggregates nameplate capacity values for all generating units in Form 860 based on their Plant ID. By similarly aggregating the annual net generation values of all Form 923 records with that Plant ID, an annual capacity factor can be estimated for that plant. However, some plants contain multiple generating units with different operating regimes and, if separated, different annual capacity factors. This is particularly important for plants that have a natural gas-fired component and a coal-fired component. If combined, the full plant may have a lower annual capacity factor, thus classifying it as "marginal." If separated, the coal-fired units may have a higher capacity factor than the natural gas-fired units. To remedy this, the original WCI analysis split generating units at a single plant based on their primary fuel type. This modification was made for some but not all plants that burned both coal and natural gas, and the criteria for determining whether disaggregation was warranted or not are unclear. Further, attribution of fuel oil (DFO) generation (Form 923) records to either the coal or natural gas component of a plant was inconsistent in the WCI workbook.

Using this methodological foundation, we systematically replicate the results of the legacy analysis, update the data to reflect more recent years and test sensitivity of these results. For the purposes of this analysis, we omit Canadian plants due to data availability and solely look at plants that report to EIA. For the time horizon of 2006-2008, the original WCI analysis estimates the marginal emissions factor for plants in the United States portion of the WECC to be 0.4336 tCO_2e/MWh.

Additionally, in order to avoid manual adjustments, we systematically identify every plant that contains both a primarily coal-fired and a primarily natural gas-fired generator (according to Form 860). The Form 923 records for these plants are partitioned into a gas-fired component and a coal-fired component, for which annual capacity factors are evaluated separately. Any fuel oil (DFO) Form 923 records are allocated to the gas-fired component.

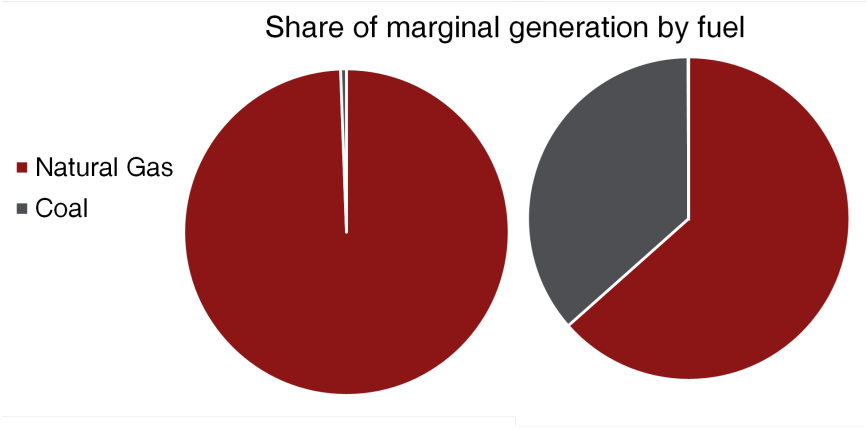

Figure C.5: Share of generation classified as "marginal" according to the legacy CARB methodology for the time horizons 2006-2008 (left) and 2016-2018 (right).

C.6 Default emissions factor supplemental figures

As Figure C.6 illustrates, the estimated emissions factor can vary substantially depending on what capacity factor threshold is selected to indicate a generator is "marginal." The threshold selected in the original CARB analysis (60%) produces an answer that is near a minimum for that time horizon, but not for the more recent time horizon.

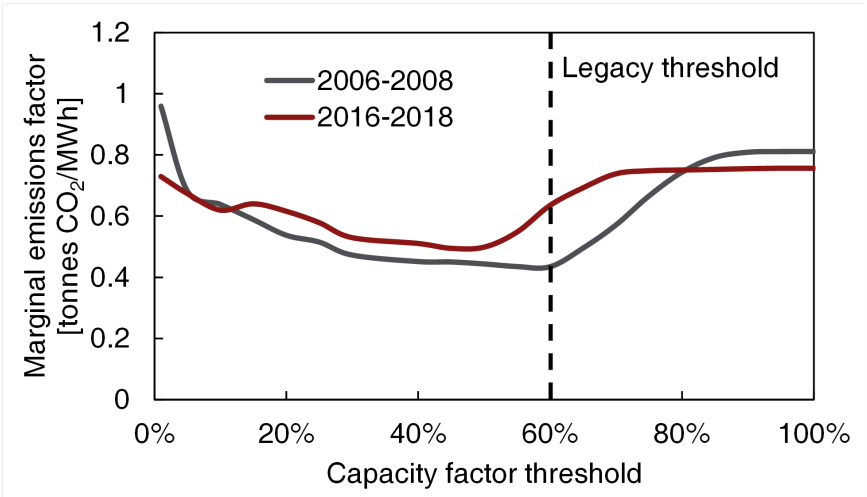

Figure C.6: Marginal emissions factors as estimated using EIA data and employing the capacity factor threshold method used to support the currently adopted default emissions factor.

Thus, we conclude that the legacy method for estimating emissions associated with unspecified electricity imports is based on outdated data and can be sensitive to the selected capacity factor

threshold. Although using a capacity factor threshold as a proxy for identifying marginal dispatch is intrinsically unreliable, it appears that higher default emissions factors would be obtained across a wide range of capacity factor thresholds that could reasonably be considered. This suggests there may be room for improvement in the calculation of the default emissions factor.

Bibliography

[1] John Theodore Houghton, Geoffrey J Jenkins, and Jim J Ephraums. "Climate change". In: (1990).

[2] IPCC Climate Change. "Climate change impacts, adaptation and vulnerability". In: *Contribution of working group II to the fourth assessment report of the Intergovernmental Panel on Climate Change. Summary for policymakers-Brussels-April* 23 (2007).

[3] Ottmar Edenhofer et al. "Working group III contribution to the fifth assessment report of the Intergovernmental Panel on Climate Change". In: *Intergovernmental Panel on Climate Change: Cambridge, UK, New York, NY, USA* (2014).

[4] Steven J Davis et al. "Net-zero emissions energy systems". In: *Science* 360.6396 (2018).

[5] *Munn v. Illinois*. 1877.

[6] Eric Hirst and Charles Goldman. "Creating the future: integrated resource planning for electric utilities". In: *Annual review of energy and the environment* 16.1 (1991), pp. 91–121.

[7] Charles Goldman et al. "Primer on Gas Integrated Resource Planning". In: (1993).

[8] Jesse D Jenkins, Max Luke, and Samuel Thernstrom. "Getting to zero carbon emissions in the electric power sector". In: *Joule* 2.12 (2018), pp. 2498–2510.

[9] Gregory A Von Wald et al. "Biomethane addition to California transmission pipelines: Regional simulation of the impact of regulations". In: *Applied Energy* 250 (2019), pp. 292–301.

[10] Ben Haley et al. "Pathways to Deep Decarbonization in the United States". In: (2015).

[11] AV Zlotnik et al. "Grid architecture at the gas-electric interface". In: *Los Alamos Natl. Lab., Santa Fe, NM, USA, Rep. LA-UR-17-23662* (2017).

[12] Mohammad Shahidehpour, Yong Fu, and Thomas Wiedman. "Impact of natural gas infrastructure on electric power systems". In: *Proceedings of the IEEE* 93.5 (2005), pp. 1042–1056.

[13] Ricardo Rubio-Barros et al. "Combined operational planning of natural gas and electric power systems: State of the art". In: *Natural gas, Sciyo* (2010), pp. 271–88.

[14] Jesse D Jenkins. "What's Killing Nuclear Power in US Electricity Markets". In: *Drivers of Wholesale Price Declines at Nuclear Generators in the PJM Interconnection* (2018), pp. 2018–001.

[15] Nestor A Sepulveda et al. "The role of firm low-carbon electricity resources in deep decarbonization of power generation". In: *Joule* 2.11 (2018), pp. 2403–2420.

[16] Jacqueline A Dowling et al. "Role of long-duration energy storage in variable renewable electricity systems". In: *Joule* 4.9 (2020), pp. 1907–1928.

[17] Adam R Brandt et al. "Blow wind blow: Capital deployment in variable energy systems". In: *Energy* 224 (2021), p. 120198.

[18] L Gacitua et al. "A comprehensive review on expansion planning: Models and tools for energy policy analysis". In: *Renewable and Sustainable Energy Reviews* 98 (2018), pp. 346–360.

[19] Michael Hubner and Hans-Jurgen Haubrich. "Long-term planning of natural gas networks". In: *2008 5th International Conference on the European Electricity Market*. IEEE. 2008, pp. 1–5.

[20] Dan Aas et al. *The Challenge of Retail Gas in California's Low-Carbon Future: Technology Options, Customer Costs and Public Health Benefits of Reducing Natural Gas Use*. Tech. rep. 2020. URL: `https://ww2.energy.ca.gov/2019publications/CEC-500-2019-055/index.html`.

[21] Gregory A Von Wald et al. "Optimization-based technoeconomic analysis of molten-media methane pyrolysis for reducing industrial sector CO 2 emissions". In: *Sustainable Energy & Fuels* 4.9 (2020), pp. 4598–4613.

[22] Gregory Von Wald et al. "Analyzing California's framework for estimating greenhouse gas emissions associated with retail electricity sales". In: *The Electricity Journal* 33.8 (2020), p. 106818.

[23] Gregory Von Wald et al. "Accounting for the Greenhouse Gas Emission Intensity of Regional Electricity Transfers". In: *Environmental Science & Technology* (2021).

[24] Bert Bolin and Bo R Doos. "Greenhouse effect". In: (1989).

[25] Martin Geidl et al. "Energy hubs for the future". In: *IEEE power and energy magazine* 5.1 (2006), pp. 24–30.

[26] J Carpentier. "Optimal power flows". In: *International Journal of Electrical Power & Energy Systems* 1.1 (1979), pp. 3–15.

[27] Pl Wong and R Larson. "Optimization of natural-gas pipeline systems via dynamic programming". In: *IEEE Transactions on Automatic Control* 13.5 (1968), pp. 475–481.

[28] Seungwon An, Qing Li, and Thomas W Gedra. "Natural gas and electricity optimal power flow". In: *2003 IEEE PES Transmission and Distribution Conference and Exposition (IEEE Cat. No. 03CH37495)*. Vol. 1. IEEE. 2003, pp. 138–143.

[29] Martin Geidl and Göran Andersson. "Optimal power flow of multiple energy carriers". In: *IEEE Transactions on power systems* 22.1 (2007), pp. 145–155.

[30] Martin Geidl. "Integrated modeling and optimization of multi-carrier energy systems". PhD thesis. ETH Zurich, 2007.

[31] Seyed Hamid Reza Hosseini et al. "Optimal planning and operation of multi-vector energy networks: A systematic review". In: *Renewable and Sustainable Energy Reviews* 133 (2020), p. 110216.

[32] Mark J O'Malley et al. "Multicarrier Energy Systems: Shaping Our Energy Future". In: *Proceedings of the IEEE* 108.9 (2020), pp. 1437–1456.

[33] Holger Teichgraeber et al. "Extreme events in time series aggregation: A case study for optimal residential energy supply systems". In: *Applied Energy* 275 (2020), p. 115223.

[34] Holger Teichgraeber and Adam R Brandt. "Clustering methods to find representative periods for the optimization of energy systems: An initial framework and comparison". In: *Applied energy* 239 (2019), pp. 1283–1293.

[35] Chuan He et al. "Coordination of interdependent electricity grid and natural gas network—a review". In: *Current Sustainable/Renewable Energy Reports* 5.1 (2018), pp. 23–36.

[36] Meisam Farrokhifar, Yinghui Nie, and David Pozo. "Energy systems planning: A survey on models for integrated power and natural gas networks coordination". In: *Applied Energy* 262 (2020), p. 114567.

[37] Wujing Huang et al. "Multienergy Networks Analytics: Standardized Modeling, Optimization, and Low Carbon Analysis". In: *Proceedings of the IEEE* 108.9 (2020), pp. 1411–1436.

[38] Anatoly Zlotnik et al. "Coordinated scheduling for interdependent electric power and natural gas infrastructures". In: *IEEE Transactions on Power Systems* 32.1 (2016), pp. 600–610.

[39] Omar Jose Guerra Fernandez et al. *Electric Power Grid and Natural Gas Network Operations and Coordination*. Tech. rep. National Renewable Energy Lab.(NREL), Golden, CO (United States), 2020.

[40] Michael Craig et al. "Valuing intra-day coordination of electric power and natural gas system operations". In: *Energy Policy* 141 (2020), p. 111470.

[41] Omar J Guerra et al. "Coordinated operation of electricity and natural gas systems from day-ahead to real-time markets". In: *Journal of Cleaner Production* 281 (2021), p. 124759.

[42] Saeed D Manshadi and Mohammad E Khodayar. "Coordinated operation of electricity and natural gas systems: A convex relaxation approach". In: *IEEE Transactions on Smart Grid* 10.3 (2018), pp. 3342–3354.

[43] Rong-Peng Liu et al. "Extended convex hull-based distributed optimal energy flow of integrated electricity-gas systems". In: *Applied Energy* 287 (2021), p. 116551.

[44] Anatoly Zlotnik et al. "Pipeline transient optimization for a gas-electric coordination decision support system". In: *PSIG Annual Meeting*. Pipeline Simulation Interest Group. 2019.

[45] Anatoly Zlotnik, Michael Chertkov, and Scott Backhaus. "Optimal control of transient flow in natural gas networks". In: *2015 54th IEEE conference on decision and control (CDC)*. IEEE. 2015, pp. 4563–4570.

[46] Line A Roald et al. "An uncertainty management framework for integrated gas-electric energy systems". In: *Proceedings of the IEEE* 108.9 (2020), pp. 1518–1540.

[47] Kaarthik Sundar et al. "Robust Gas Pipeline Network Expansion Planning to Support Power System Reliability". In: *arXiv preprint arXiv:2101.10398* (2021).

[48] Andreas Belderbos et al. "Facilitating renewables and power-to-gas via integrated electrical power-gas system scheduling". In: *Applied Energy* 275 (2020), p. 115082.

[49] Mohammad Amin Mirzaei et al. "A novel hybrid framework for co-optimization of power and natural gas networks integrated with emerging technologies". In: *IEEE Systems Journal* 14.3 (2020), pp. 3598–3608.

[50] Zexing Chen et al. "Coordinated optimal dispatch and market equilibrium of integrated electric power and natural gas networks with P2G embedded". In: *Journal of Modern Power Systems and Clean Energy* 6.3 (2018), pp. 495–508.

[51] Russell Bent et al. "Joint electricity and natural gas transmission planning with endogenous market feedbacks". In: *IEEE Transactions on Power Systems* 33.6 (2018), pp. 6397–6409.

[52] Modassar Chaudry et al. "Combined gas and electricity network expansion planning". In: *Applied Energy* 113 (2014), pp. 1171–1187.

[53] Mohammad Jooshaki et al. "Multistage expansion co-planning of integrated natural gas and electricity distribution systems". In: *Energies* 12.6 (2019), p. 1020.

[54] Qing Zeng et al. "A bi-level programming for multistage co-expansion planning of the integrated gas and electricity system". In: *Applied energy* 200 (2017), pp. 192–203.

[55] Conrado Borraz-Sánchez et al. "Convex relaxations for gas expansion planning". In: *INFORMS Journal on Computing* 28.4 (2016), pp. 645–656.

[56] Conrado Borraz Sanchez et al. "Convex optimization for joint expansion planning of natural gas and power systems". In: *2016 49th Hawaii International Conference on System Sciences (HICSS)*. IEEE. 2016, pp. 2536–2545.

[57] Jing Qiu et al. "A linear programming approach to expansion co-planning in gas and electricity markets". In: *IEEE Transactions on Power Systems* 31.5 (2015), pp. 3594–3606.

[58] Chuan He et al. "Robust coordination of interdependent electricity and natural gas systems in day-ahead scheduling for facilitating volatile renewable generations via power-to-gas technology". In: *Journal of Modern Power Systems and Clean Energy* 5.3 (2017), pp. 375–388.

[59] Qing Zeng et al. "Coordinated operation of the electricity and natural gas systems with bi-directional energy conversion". In: *Energy Procedia* 105 (2017), pp. 492–497.

[60] Huansheng Zhou et al. "Multi-stage contingency-constrained co-planning for electricity-gas systems interconnected with gas-fired units and power-to-gas plants using iterative Benders decomposition". In: *Energy* 180 (2019), pp. 689–701.

[61] Wentao Yang et al. "Coordinated planning strategy for integrated energy systems in a district energy sector". In: *IEEE Transactions on Sustainable Energy* 11.3 (2019), pp. 1807–1819.

[62] Aldo Bischi et al. "A detailed MILP optimization model for combined cooling, heat and power system operation planning". In: *Energy* 74 (2014), pp. 12–26.

[63] Aldo Bischi et al. "A rolling-horizon optimization algorithm for the long term operational scheduling of cogeneration systems". In: *Energy* 184 (2019), pp. 73–90.

[64] MT Rees et al. "Carbon constrained design of energy infrastructure for new build schemes". In: *Applied energy* 113 (2014), pp. 1220–1234.

[65] Zhipeng Li et al. "Multi-Stage Capacity Configuration Approach for Regional Integrated Energy System". In: *2020 7th International Conference on Information, Cybernetics, and Computational Social Systems (ICCSS)*. IEEE. 2020, pp. 667–671.

[66] Fatemeh Barati et al. "Multi-period integrated framework of generation, transmission, and natural gas grid expansion planning for large-scale systems". In: *IEEE Transactions on Power Systems* 30.5 (2014), pp. 2527–2537.

[67] Clodomiro Unsihuay-Vila et al. "A model to long-term, multiarea, multistage, and integrated expansion planning of electricity and natural gas systems". In: *IEEE Transactions on Power Systems* 25.2 (2010), pp. 1154–1168.

[68] GS Piperagkas, AG Anastasiadis, and ND Hatziargyriou. "Stochastic PSO-based heat and power dispatch under environmental constraints incorporating CHP and wind power units". In: *Electric Power Systems Research* 81.1 (2011), pp. 209–218.

[69] Da Xu et al. "Stochastic Optimal Operation of Low-Carbon Renewable Energy System". In: *2018 IEEE PES Asia-Pacific Power and Energy Engineering Conference (APPEEC)*. IEEE. 2018, pp. 417–421.

[70] Hongbo Ren et al. "Multi-objective optimization for the operation of distributed energy systems considering economic and environmental aspects". In: *Applied Energy* 87.12 (2010), pp. 3642–3651.

[71] Hong Fan et al. "Optimal Planning of Integrated Electricity-Gas System with Demand Side Management". In: *IEEE Access* 7 (2019), pp. 176790–176798.

[72] Jing Qiu et al. "Low carbon oriented expansion planning of integrated gas and power systems". In: *IEEE Transactions on Power Systems* 30.2 (2014), pp. 1035–1046.

[73] Yasaman Mozafari, Joule Bergerson, and William Rosehart. "Integrated Planning of Electricity, Heat, and Gas Infrastructure". In: *2020 IEEE Power & Energy Society General Meeting (PESGM)*. IEEE. 2020, pp. 1–5.

[74] Yaohua Cheng et al. "Planning multiple energy systems toward low-carbon society: A decentralized approach". In: *IEEE Transactions on Smart Grid* 10.5 (2018), pp. 4859–4869.

[75] Yaohua Cheng et al. "Planning multiple energy systems for low-carbon districts with high penetration of renewable energy: An empirical study in China". In: *Applied Energy* 261 (2020), p. 114390.

[76] Mathias Berger et al. "The role of power-to-gas and carbon capture technologies in cross-sector decarbonisation strategies". In: *Electric Power Systems Research* 180 (2020), p. 106039.

[77] Jesse D Jenkins and Nestor A Sepulveda. "Enhanced decision support for a changing electricity landscape: the GenX configurable electricity resource capacity expansion model". In: *An MIT Energy Initiative Working Paper. https://energy. mit. edu/wpcontent/uploads/2017/10/Enhanced-Decision-Support-for-a-Changing-Electricity-Landscape. pdf* (2017).

[78] Nils Baumgärtner et al. "RiSES3: Rigorous Synthesis of Energy Supply and Storage Systems via time-series relaxation and aggregation". In: *Computers & Chemical Engineering* 127 (2019), pp. 127–139.

[79] James H Williams et al. "Carbon-neutral pathways for the United States". In: *AGU Advances* 2.1 (2021), e2020AV000284.

[80] Holger Christian Philipp Teichgraeber. *Temporal Resolution in Energy Systems Optimization Models*. Stanford University, 2020.

[81] Allen J Wood, Bruce F Wollenberg, and Gerald B Sheblé. *Power generation, operation, and control*. John Wiley & Sons, 2013.

[82] Dimitris Bertsimas et al. "Adaptive robust optimization for the security constrained unit commitment problem". In: *IEEE transactions on power systems* 28.1 (2012), pp. 52–63.

[83] Kaarthik Sundar et al. "Unit commitment with n-1 security and wind uncertainty". In: *2016 Power Systems Computation Conference (PSCC)*. IEEE. 2016, pp. 1–7.

[84] Kenneth Van den Bergh, Erik Delarue, and William D'haeseleer. "DC power flow in unit commitment models". In: *no. May* (2014).

[85] Carlos M Correa-Posada and Pedro Sánchez-Martín. "Integrated power and natural gas model for energy adequacy in short-term operation". In: *IEEE Transactions on Power Systems* 30.6 (2014), pp. 3347–3355.

[86] Orin Flanigan. *Underground gas storage facilities: Design and implementation*. Elsevier, 1995.

[87] Sai Krishna Kanth Hari et al. "Operation of Natural Gas Pipeline Networks With Storage Under Transient Flow Conditions". In: *IEEE Transactions on Control Systems Technology* (2021).

[88] Leander Kotzur et al. "Time series aggregation for energy system design: Modeling seasonal storage". In: *Applied energy* 213 (2018), pp. 123–135.

[89] Diego A Tejada-Arango et al. "Enhanced representative days and system states modeling for energy storage investment analysis". In: *IEEE Transactions on Power Systems* 33.6 (2018), pp. 6534–6544.

[90] Energy Information Adminsitration (EIA). *Hourly Electricity Grid Monitor*. URL: `https://www.eia.gov/electricity/gridmonitor/dashboard/electric_overview/US48/US48`.

[91] Tyler H Ruggles et al. "Developing reliable hourly electricity demand data through screening and imputation". In: *Scientific data* 7.1 (2020), pp. 1–14.

[92] Michael Waite and Vijay Modi. "Electricity Load Implications of Space Heating Decarbonization Pathways". In: *Joule* 4.2 (2020), pp. 376–394.

[93] Trieu T Mai et al. *Electrification futures study: Scenarios of electric technology adoption and power consumption for the United States*. Tech. rep. National Renewable Energy Lab.(NREL), Golden, CO (United States), 2018.

[94] *Residential Energy Consumption Survey*. 2012.

[95] *Commercial Building Energy Consumption Survey*. 2012.

[96] Veena Subramanyam et al. "Energy efficiency improvement opportunities and associated greenhouse gas abatement costs for the residential sector". In: *Energy* 118 (2017), pp. 795–807.

[97] Paige Jadun et al. *Electrification futures study: End-use electric technology cost and performance projections through 2050*. Tech. rep. National Renewable Energy Lab.(NREL), Golden, CO (United States), 2017.

[98] Claire McKenna, Amar Shah, and Mark Silberg. *It's Time to Incentivize Residential Heat Pumps*. URL: `https://rmi.org/its-time-to-incentivize-residential-heat-pumps/`.

[99] Carl Shapiro and Srikanth Puttagunta. *Field Performance of Heat pump water Heaters in the Northeast*. Tech. rep. National Renewable Energy Lab.(NREL), Golden, CO (United States), 2016.

[100] Eric Wilson and Craig Christensen. *Heat Pump Water Heater Modeling in EnergyPlus (Presentation)*. Tech. rep. National Renewable Energy Lab.(NREL), Golden, CO (United States), 2012.

[101] H Willem, Y Lin, and A Lekov. "Review of energy efficiency and system performance of residential heat pump water heaters". In: *Energy and Buildings* 143 (2017), pp. 191–201.

[102] Michael Garrabrant et al. *Development and validation of a gas-fired residential heat pump water heater-final report*. Tech. rep. Stone Mountain Technologies, Inc., 2013.

[103] Kyle R Gluesenkamp. *Energy Factor Analysis for Gas Heat Pump Water Heaters*. Tech. rep. Oak Ridge National Lab.(ORNL), Oak Ridge, TN (United States). Building ..., 2016.

[104] Michael Mensinger Jr and Merry Sweeney. "Integrated Gas-fired Heat Pump Water Heaters for Homes: Results of Field Demonstrations and System Modeling". In: *ASHRAE Transactions* 126 (2020), pp. 325–332.

[105] Micah Sweeney et al. "Induction cooking technology design and assessment". In: *Small* 5 (2014), p. 800.

[106] Lawrence Berkeley National Laboratory. *Technical Support Document for Residential Cooking Products, Vol. 2: Potential Impact of Alternative Efficiency Levels for Residential Cooking Products*. 1998.

[107] Yung-Chang Ko and Ta-Hui Lin. "Emissions and efficiency of a domestic gas stove burning natural gases with various compositions". In: *Energy Conversion and Management* 44.19 (2003), pp. 3001–3014.

[108] Alex Wilson. *Efficient Cooking*. 2009. URL: `https://www.greenbuildingadvisor.com/article/efficient-cooking`.

[109] *Commercial and Residential Hourly Load Profiles for all TMY3 Locations in the United States*. Tech. rep. 2014. URL: `Retrieved%20from%20http://data.openei.org/submissions/153`.

[110] Michael A McNeil and Nicholas Bojda. "Cost-effectiveness of high-efficiency appliances in the US residential sector: A case study". In: *Energy Policy* 45 (2012), pp. 33–42.

[111] Craig Christensen et al. *BEopt (TM) software for building energy optimization: Features and capabilities*. Tech. rep. National Renewable Energy Lab.(NREL), Golden, CO (United States), 2006.

[112] Rheem. *Residential Gas Water Heater, 50.0 gal Tank Capacity, Natural gas, 38,000 BtuH.* URL: https://www.grainger.com/product/38UN60?ef_id=EAIaIQobChMIxq6Yp72A8AIViY%20jICh2mcQ5jEAQYAyABEgJD1_D_BwE:G:s&s_kwcid=AL!2966!3!496359977170!!!g!472905489998!&gucid=N:N:PS:Paid:GGL:CSM-2295:4P7A1P:20501231&gclid=EAIaIQobChMIxq6Yp72A8AIViYjICh2mcQ5j%20EAQYAyABEgJD1_D_BwE&gclsrc=aw.ds.

[113] Rheem. *Commercial Gas Water Heater, 100.0 gal Tank Capacity, Natural gas, 76,000 BtuH.* URL: https://www.grainger.com/product/2LAD2?ef_id=EAIaIQobChMI5p2cyNSA8AIVBI6%20zCh2hcwgpEAQYBCABEgI2O_D_BwE:G:s&s_kwcid=AL!2966!3!496359977191!!!g!471564520241!&gucid=N:N:PS:Paid:GGL:CSM-2295:4P7A1P:20501231&gclid=EAIaIQobChMI5p2cyNSA8AIVBI6%20zCh2hcwgpEAQYBCABEgI2O_D_BwE&gclsrc=aw.ds.

[114] Goodman Air Conditioning and Heating. *Goodman GMVM97 - 120kBTU - Modulating Gas Furnace.* URL: https://www.ecomfort.com/Goodman-GMVM971205DN/p26611.html?gclid=EAIaIQobChMIqv2spMeA8AIVUsvICh3oJA48EAQYAiABEgLlOPD_BwE.

[115] Lochinvar. *Air Source Heat Pump Water Heaters.* URL: https://www.lochinvar.com/products/commercial-heat-pump-water-heaters/air-source-heat-pump-water-heaters/.

[116] A.O. Smith. *CHP-120 Fully Integrated Heat Pump.* URL: https://www.hotwater.com/Water-Heaters/Commercial/Water-Heaters/Heat-Pump/CHP-120-Fully-Integrated-Heat-Pump/.

[117] Paige Jadun et al. *Electrification Futures Study Technology Data.* Tech. rep. National Renewable Energy Laboratory. https://data.nrel.gov/submissions/78, 2017.

[118] *2021 Cost to Replace Electrical Panel.* 2021. URL: https://homeguide.com/costs/cost-to-replace-electrical-panel.

[119] *Heat Pump Water Heaters.* 2021. URL: https://www.energy.gov/energysaver/heat-pump-water-heaters.

[120] Mikael Salonvaara et al. *Cost Assessment of Building Envelope Retrofits.* Tech. rep. Oak Ridge National Lab.(ORNL), Oak Ridge, TN (United States), 2020.

[121] United States Census Bureau. *American Community Survey.* URL: https://www.census.gov/programs-surveys/acs.

[122] United States Census Bureau. *County Business Patterns.* URL: https://www.census.gov/programs-surveys/cbp.html.

[123] Federal Emergency Management Agency (FEMA). *Hazus.* URL: https://www.fema.gov/flood-maps/products-tools/hazus.

[124] Steven Shultz. "Accuracy of HAZUS general building stock data". In: *Natural Hazards Review* 18.4 (2017), p. 04017012.

[125] Philip R White et al. "Quantifying the impact of residential space heating electrification on the Texas electric grid". In: *Applied Energy* 298 (2021), p. 117113.

[126] Energy Information Administration (EIA). *EIA Form 860*. 2020.

[127] Sertaç Akar et al. *2020 Annual Technology Baseline (ATB) Cost and Performance Data for Electricity Generation Technologies*. Tech. rep. National Renewable Energy Laboratory-Data (NREL-DATA), Golden, CO (United . . ., 2020.

[128] Energy Information Administration (EIA). *Electric Power Annual*. Tech. rep. 2020. URL: https://www.eia.gov/electricity/annual/.

[129] Energy Information Administration (EIA). *EIA Form 923*. 2020.

[130] *Emissions Factors for Greenhouse Gas Inventories*. Tech. rep. 2020. URL: https://www.epa.gov/sites/production/files/2020-04/documents/ghg-emission-factors-hub.pdf.

[131] *Air Markets Program Data*. Tech. rep. 2020. URL: https://ampd.epa.gov/ampd/.

[132] Independent System Operator of New England (ISONE). *Operations Reports*. URL: https://www.iso-ne.com/isoexpress/web/reports/operations/-/tree/daily-gen-fuel-type.

[133] Electric Reliability Council of Texas (ERCOT). *Generation*. URL: http://www.ercot.com/gridinfo/generation.

[134] Electric Reliability Council of Texas (ERCOT). *Resource adequacy*. URL: http://www.ercot.com/gridinfo/resource.

[135] California Public Utilities Commission (CPUC). *Unified RA and IRP Modeling Datasets 2019*. URL: https://www.cpuc.ca.gov/General.aspx?id=6442461894.

[136] Nate Blair et al. *System advisor model, sam 2014.1. 14: General description*. Tech. rep. National Renewable Energy Lab.(NREL), Golden, CO (United States), 2014.

[137] Nathan Parker et al. "Renewable natural gas in California: An assessment of the technical and economic potential". In: *Energy Policy* 111 (2017), pp. 235–245.

[138] Oliver Schmidt et al. "Future cost and performance of water electrolysis: An expert elicitation study". In: *International journal of hydrogen energy* 42.52 (2017), pp. 30470–30492.

[139] Adam Christensen. "Assessment of hydrogen production costs from electrolysis: United States and Europe". In: *Retrieved from the International Council on Clean Transportation: https://theicct.org/publications/assessment-hydrogen-production-costs-electrolysis-united-states-and-europe* (2020).

[140] Gunther Glenk and Stefan Reichelstein. "Economics of converting renewable power to hydrogen". In: *Nature Energy* 4.3 (2019), pp. 216–222.

[141] Evan D. Sherwin. "Electrofuel Synthesis from Variable Renewable Electricity: An Optimization-Based Techno-Economic Analysis". In: *Environmental Science & Technology* 55.11 (2021). PMID: 33983018, pp. 7583–7594. DOI: 10.1021/acs.est.0c07955. eprint: https://doi.org/10.1021/acs.est.0c07955. URL: https://doi.org/10.1021/acs.est.0c07955.

[142] Selma Brynolf et al. "Electrofuels for the transport sector: A review of production costs". In: *Renewable and Sustainable Energy Reviews* 81 (2018), pp. 1887–1905.

[143] David Peterson, James Vickers, and Dan DeSantis. *Hydrogen Production Cost From PEM Electrolysis 2019*. Tech. rep. National Renewable Energy Lab.(NREL), Golden, CO (United States), 2020. URL: https://www.hydrogen.energy.gov/pdfs/19009_h2_production_cost_pem_electrolysis_2019.pdf.

[144] Ilkka Hannula, Noora Kaisalo, and Pekka Simell. "Preparation of Synthesis Gas from CO2 for Fischer–Tropsch Synthesis—Comparison of Alternative Process Configurations". In: *C—Journal of Carbon Research* 6.3 (2020), p. 55.

[145] Jachin Gorre et al. "Cost benefits of optimizing hydrogen storage and methanation capacities for Power-to-Gas plants in dynamic operation". In: *Applied Energy* 257 (2020), p. 113967.

[146] Marc W Melaina, Olga Antonia, and Mike Penev. "Blending hydrogen into natural gas pipeline networks: a review of key issues". In: (2013).

[147] Wesley J Cole et al. "Utility-scale lithium-ion storage cost projections for use in capacity expansion models". In: *2016 North American Power Symposium (NAPS)*. IEEE. 2016, pp. 1–6.

[148] IRENA. *Green Hydrogen Cost Reduction: Scaling up Electrolysers to Meet the 1.5C Climate Goal*. 2020.

[149] Todd Ramsden, Ben Kroposki, and Johanna Levene. "Opportunities for hydrogen-based energy storage for electric utilities". In: *Proceedings of the NHA annual hydrogen conference. Sacramento*. 2008.

[150] Giuseppe Ripepi. "Hydrogen storage for variable renewable electricity integration: Techno-economic analysis of a Lined Rock Cavern system". MA thesis. 2018.

[151] D Steward et al. *Lifecycle cost analysis of hydrogen versus other technologies for electrical energy storage*. Tech. rep. National Renewable Energy Lab.(NREL), Golden, CO (United States), 2009.

[152] Anna S Lord. "Overview of geologic storage of natural gas with an emphasis on assessing the feasibility of storing hydrogen". In: *SAND2009-5878, Sandia Natl. Lab. Albuquerque, NM* (2009).

[153] Saeid Mokhatab, William A Poe, and John Y Mak. *Handbook of natural gas transmission and processing: principles and practices*. Gulf professional publishing, 2018.

[154] Ignacio Losada Carreño, Anna Scaglione, and Anatoly Zlotnik. "A Synthetic Test Instance for a US Natural Gas Network and Associated Power Grid". In: *2020 IEEE Power & Energy Society General Meeting (PESGM)*. IEEE. 2020, pp. 1–5.

[155] Robert L Fares and Carey W King. "Trends in transmission, distribution, and administration costs for US investor-owned electric utilities". In: *Energy Policy* 105 (2017), pp. 354–362.

[156] Erick Jones. "Decomposing Systems: Illustrating the Utility of Distributed Energy Resources with Decomposition Techniques". In: *IIE Annual Conference. Proceedings*. Institute of Industrial and Systems Engineers (IISE). 2020, pp. 1–6.

[157] A Mahone et al. "Renewable portfolio standards and cost-effective energy-efficiency investment". In: *Energy Policy* 37.3 (2009), pp. 774–777.

[158] Jim Lazar and Ken Colburn. "Recognizing the full value of energy efficiency". In: *Regulatory Assistance Project* (2013).

[159] *2021 Distributed Energy Resources Avoided Cost Calculator Documentation: Prepared by E3 for the California Public Utilities Commission*. 2021. URL: https://www.cpuc.ca.gov/general.aspx?id=5267.

[160] Energy Information Adminsitration (EIA). *Natural Gas Annual Respondent Query System (EIA-176 Data through 2019)*. URL: https://www.eia.gov/naturalgas/ngqs/#?report=RP1&year1=&year2=&company=&sortby=&items=.

[161] Tim Mason, Trevor Curry, and Dan Wilson. *CAPITAL COSTS FOR TRANSMISSION AND SUBSTATIONS Recommendations for WECC Transmission Expansion Planning*. 2012. URL: https://www.wecc.org/reliability/1210_bv_wecc_transcostreport_final.pdf.

[162] *Pipeline projects: Detailed information on the size and location of pipeline projects announced or under construction*. URL: https://www.eia.gov/naturalgas/pipelines/EIA-NaturalGas%20PipelineProjects.xlsx.

[163] Aaron Bloom et al. *The Value of Increased HVDC Capacity Between Eastern and Western US Grids: The Interconnections Seam Study*. Tech. rep. National Renewable Energy Lab.(NREL), Golden, CO (United States), 2020.

[164] Patrick R Brown and Audun Botterud. "The value of inter-regional coordination and transmission in decarbonizing the US electricity system". In: *Joule* 5.1 (2021), pp. 115–134.

[165] *California Executive Order B-55-18*.

[166] *New York, Senate Bill S6599 Climate Leadership and Community Protection Act*.

[167] *Massachusetts, Senate Bill 9 An Act Creating a Next Generation Roadmap for Massachusetts Climate Policy*.

[168] *California Renewables Portfolio Standard Program: emissions of greenhouse gases, Cal. S. B. 100 (2017-2018), Chapter 312, (Cal. Stat. 2018)*. 2018.

[169] *Mandatory Reporting Regulation. Cal Code Regs. tit. 17, § 95100-95163*. 2018. URL: `https://ww2.arb.ca.gov/mrr-regulation`.

[170] Pete Smith et al. "Biophysical and economic limits to negative CO 2 emissions". In: *Nature climate change* 6.1 (2016), pp. 42–50.

[171] Sabine Fuss et al. "Negative emissions—Part 2: Costs, potentials and side effects". In: *Environmental Research Letters* 13.6 (2018), p. 063002.

[172] Gregg Marland, Kristy Fruit, and Roger Sedjo. "Accounting for sequestered carbon: the question of permanence". In: *Environmental Science & Policy* 4.6 (2001), pp. 259–268.

[173] T Ruseva et al. "Additionality and permanence standards in California's Forest Offset Protocol: A review of project and program level implications". In: *Journal of environmental management* 198 (2017), pp. 277–288.

[174] Adam R Brandt et al. "Methane leaks from North American natural gas systems". In: *Science* 343.6172 (2014), pp. 733–735.

[175] Eric D Lebel et al. "Quantifying methane emissions from natural gas water heaters". In: *Environmental science & technology* 54.9 (2020), pp. 5737–5745.

[176] Emily Grubert. "At scale, renewable natural gas systems could be climate intensive: the influence of methane feedstock and leakage rates". In: *Environmental Research Letters* 15.8 (2020), p. 084041.

[177] New Constructs. *Weighted average cost of capital: explanation and examples*. Tech. rep. New Constructs, 2016.

[178] Energy and Environmental Economics. *RESOLVE User Manual*. Tech. rep. California Public Utilities Commission, 2017.

[179] Iain Dunning, Joey Huchette, and Miles Lubin. "JuMP: A modeling language for mathematical optimization". In: *SIAM review* 59.2 (2017), pp. 295–320.

[180] Miles Lubin and Iain Dunning. "Computing in operations research using Julia". In: *INFORMS Journal on Computing* 27.2 (2015), pp. 238–248.

[181] John Bongaarts. *Intergovernmental panel on climate change special report on global warming of 1.5° C Switzerland: IPCC, 2018*. 2019.

[182] A. Fernandez Pales, P. Levi, and T. Vass. *Tracking industry 2019*. 2019. URL: `https://www.iea.org/reports/tracking-industry-2019`.

[183] Lawrence Irlam. "Global costs of carbon capture and storage". In: *Global CCS Institute, Melbourne, Australia* (2017).

[184] Brett Parkinson et al. "Hydrogen production using methane: Techno-economics of decarbonizing fuels and chemicals". In: *International Journal of Hydrogen Energy* 43.5 (2018), pp. 2540–2555.

[185] *Credit for carbon oxide sequestration 26 U.S.C § 45Q.*

[186] Peter Franklin Folger. *Carbon capture and sequestration (CCS) in the United States*. Congressional Research Service, 2017.

[187] Clea Kolster et al. "CO 2 enhanced oil recovery: a catalyst for gigatonne-scale carbon capture and storage deployment?" In: *Energy & Environmental Science* 10.12 (2017), pp. 2594–2608.

[188] California Air Resources Board (CARB). *Staff report: initial statement of reasons*. 2018. URL: https://www.arb.ca.gov/regact/2018/lcfs18/isor.pdf.

[189] Alberto Abánades, Carlo Rubbia, and Delia Salmieri. "Technological challenges for industrial development of hydrogen production based on methane cracking". In: *Energy* 46.1 (2012), pp. 359–363.

[190] D Chester Upham et al. "Catalytic molten metals for the direct conversion of methane to hydrogen and separable carbon". In: *Science* 358.6365 (2017), pp. 917–921.

[191] Peter Folger. "Carbon capture: a technology assessment". In: LIBRARY OF CONGRESS WASHINGTON DC CONGRESSIONAL RESEARCH SERVICE. 2013.

[192] Ali Kargari and M Takht Ravanchi. "Carbon dioxide: capturing and utilization". In: *Greenhouse gases-capturing, utilization and reduction* 1 (2012), pp. 3–.

[193] DJ Barker et al. "CO2 capture in the cement industry". In: *Energy procedia* 1.1 (2009), pp. 87–94.

[194] Ottmar Edenhofer. *Climate change 2014: mitigation of climate change*. Vol. 3. Cambridge University Press, 2015.

[195] Leif Hockstad and L Hanel. *Inventory of US greenhouse gas emissions and sinks*. Tech. rep. Environmental System Science Data Infrastructure for a Virtual Ecosystem, 2018.

[196] John Gale and Paul Freund. "Greenhouse gas abatement in energy intensive industries". In: (2001).

[197] Duncan Leeson et al. "A Techno-economic analysis and systematic review of carbon capture and storage (CCS) applied to the iron and steel, cement, oil refining and pulp and paper industries, as well as other high purity sources". In: *International Journal of Greenhouse Gas Control* 61 (2017), pp. 71–84.

[198] SS Penner. "Steps toward the hydrogen economy". In: *Energy* 31.1 (2006), pp. 33–43.

[199] Alberto Abánades, Carlo Rubbia, and Delia Salmieri. "Thermal cracking of methane into hydrogen for a CO2-free utilization of natural gas". In: *International journal of hydrogen energy* 38.20 (2013), pp. 8491–8496.

[200] Clarke Palmer et al. "Dry reforming of methane catalysed by molten metal alloys". In: *Nature Catalysis* 3.1 (2020), pp. 83–89.

[201] Mun-Sing Fan, Ahmad Zuhairi Abdullah, and Subhash Bhatia. "Catalytic technology for carbon dioxide reforming of methane to synthesis gas". In: *ChemCatChem* 1.2 (2009), pp. 192–208.

[202] Daniel Tyrer. *Production of hydrogen, US Patent 1803221*. 1931.

[203] Meyer Steinberg. "Fossil fuel decarbonization technology for mitigating global warming". In: *International Journal of Hydrogen Energy* 24.8 (1999), pp. 771–777.

[204] Manuela Serban et al. "Hydrogen production by direct contact pyrolysis of natural gas". In: *Energy & fuels* 17.3 (2003), pp. 705–713.

[205] D Paxman et al. "Initial experimental and theoretical investigation of solar molten media methane cracking for hydrogen production". In: *Energy Procedia* 49 (2014), pp. 2027–2036.

[206] Zhang-Jing Zheng and Yang Xu. "A novel system for high-purity hydrogen production based on solar thermal cracking of methane and liquid-metal technology: Thermodynamic analysis". In: *Energy conversion and management* 157 (2018), pp. 562–574.

[207] Lionel JJ Catalan and Ebrahim Rezaei. "Coupled hydrodynamic and kinetic model of liquid metal bubble reactor for hydrogen production by noncatalytic thermal decomposition of methane". In: *International Journal of Hydrogen Energy* 45.4 (2020), pp. 2486–2503.

[208] M Plevan et al. "Thermal cracking of methane in a liquid metal bubble column reactor: Experiments and kinetic analysis". In: *International Journal of Hydrogen Energy* 40.25 (2015), pp. 8020–8033.

[209] T Geißler et al. "Experimental investigation and thermo-chemical modeling of methane pyrolysis in a liquid metal bubble column reactor with a packed bed". In: *International Journal of Hydrogen Energy* 40.41 (2015), pp. 14134–14146.

[210] T Geißler et al. "Hydrogen production via methane pyrolysis in a liquid metal bubble column reactor with a packed bed". In: *Chemical Engineering Journal* 299 (2016), pp. 192–200.

[211] Sarah Postels et al. "Life cycle assessment of hydrogen production by thermal cracking of methane based on liquid-metal technology". In: *International Journal of Hydrogen Energy* 41.48 (2016), pp. 23204–23212.

[212] B Parkinson et al. "Levelized cost of CO 2 mitigation from hydrogen production routes". In: *Energy & environmental science* 12.1 (2019), pp. 19–40.

[213] Dohyung Kang et al. "Catalytic methane pyrolysis in molten MnCl2-KCl". In: *Applied Catalysis B: Environmental* 254 (2019), pp. 659–666.

[214] Thomas C Farmer, Eric W McFarland, and Michael F Doherty. "Membrane bubble column reactor model for the production of hydrogen by methane pyrolysis". In: *International Journal of Hydrogen Energy* 44.29 (2019), pp. 14721–14731.

[215] Nazanin Rahimi et al. "Solid carbon production and recovery from high temperature methane pyrolysis in bubble columns containing molten metals and molten salts". In: *Carbon* 151 (2019), pp. 181–191.

[216] Energy and Environmental Analysis Inc. *Characterization of the US industrial commercial boiler population*. 2005.

[217] *CARB Pollution Mapping Tool*. 2019. URL: https://www.arb.ca.gov/ei/tools/pollution_map/#.

[218] Yunus A Çengel et al. *Fundamentals of thermal-fluid sciences*. Vol. 703. McGraw-Hill New York, 2008.

[219] Gael D Ulrich and Palligarnai T Vasudevan. *Chemical engineering process design and economics: a practical guide*. Process Publishing, 2004.

[220] Giorgio Besagni, Fabio Inzoli, and Thomas Ziegenhein. "Two-phase bubble columns: A comprehensive review". In: *ChemEngineering* 2.2 (2018), p. 13.

[221] Kataoka Isao and Ishii Mamoru. "Drift flux model for large diameter pipe and new correlation for pool void fraction". In: *International Journal of Heat and Mass Transfer* 30.9 (1987), pp. 1927–1939.

[222] Mamoru Ishii. *One-dimensional drift-flux model and constitutive equations for relative motion between phases in various two-phase flow regimes*. Tech. rep. Argonne National Lab., Ill.(USA), 1977.

[223] Daniel Christopher Stack. "Conceptual design and performance characteristics of firebrick resistance-heated energy storage for industrial heat supply and variable electricity production". PhD thesis. Massachusetts Institute of Technology, 2017.

[224] *Globar SiC Heating Elements*. 2020. URL: https://www.kanthal.com/en/products/furnace-products-and-heating-systems/electric-heating-elements/silicon-carbide-heating-elements/.

[225] HT Bi and JR Grace. "Flow regime diagrams for gas-solid fluidization and upward transport". In: *International Journal of Multiphase Flow* 21.6 (1995), pp. 1229–1236.

[226] Gavin Towler and Ray Sinnott. *Chemical engineering design: principles, practice and economics of plant and process design*. Elsevier, 2012.

[227] Jeff Bezanson et al. "Julia: A fresh approach to numerical computing". In: *SIAM review* 59.1 (2017), pp. 65–98.

[228] Richard H Byrd, Jorge Nocedal, and Richard A Waltz. "K nitro: An integrated package for nonlinear optimization". In: *Large-scale nonlinear optimization*. Springer, 2006, pp. 35–59.

[229] *Proposed 2018 SDGE Generator Interconnection Unit Cost Guide*. 2018. URL: `https://www.caiso.com/Documents/SDG-E2018DraftPerUnitCostGuide.xls`.

[230] Pacific Gas & Electric Company (PG&E). *Tariff*. 2018. URL: `https://www.pge.com/tariffs/index.page`.

[231] Timothy J Skone et al. *Life cycle analysis of natural gas extraction and power generation*. Tech. rep. NETL, 2016.

[232] Greg Schivley, Inês Azevedo, and Constantine Samaras. "Assessing the evolution of power sector carbon intensity in the United States". In: *Environmental Research Letters* 13.6 (2018), p. 064018.

[233] Edward S Rubin, John E Davison, and Howard J Herzog. "The cost of CO2 capture and storage". In: *International Journal of Greenhouse gas control* 40 (2015), pp. 378–400.

[234] Charles A Kang et al. "Assessment of advanced solvent-based post-combustion CO2 capture processes using a bi-objective optimization technique". In: *Applied Energy* 179 (2016), pp. 1209–1219.

[235] California Energy Commission. *Power Source Disclosure. Cal. Code Regs. tit. 20, § 1390-1394*. 2019. URL: `https://www.energy.ca.gov/programs-and-topics/programs/power-source-disclosure`.

[236] California State Legislature. *Greenhouse gases emissions intensity reporting: retail electricity suppliers, Cal. Assemb. B. 1110 (2015-2016), Chapter 656*. 2016.

[237] Jacques A de Chalendar, John Taggart, and Sally M Benson. "Tracking emissions in the US electricity system". In: *Proceedings of the National Academy of Sciences* 116.51 (2019), pp. 25497–25502.

[238] Kyle Siler-Evans, Ines Lima Azevedo, and M Granger Morgan. "Marginal emissions factors for the US electricity system". In: *Environmental science & technology* 46.9 (2012), pp. 4742–4748.

[239] S Weissman. "Knowing Your Power: Improving the Reporting of Electric Power Fuel Content in California". In: *Center for Sustainable Energy, available at https://energycenter.org/sites/default/files/docs/nav/policy/research-andreports/Knowing_Your_Power. pdf* (2018).

[240] Dallas Burtraw et al. *2019 Annual Report of the Independent Emissions Market Advisory Committee*. Tech. rep. 2019.

[241] Dallas Burtraw et al. "2018 Annual Report of the Independent Emissions Market Advisory Committee". PhD thesis. Environmental Protection Agency, 2018.

[242] Center for Resource Solutions (CRS). *Comments of Center for Resource Solutions (CRS) on October 9, 2018 Assembly Bill 1110 Implementation Proposal for Power Source Disclosure, Third Version*. 2018. URL: https://efiling.energy.ca.gov/GetDocument.aspx?tn=225090&DocumentContentId=55741.

[243] *Power Source Disclosure – AB 1110 Implementation Rulemaking: Initial Statement of Reasons*. 2019.

[244] *Assembly Bill 1110 Implementation Proposal for Power Source Disclosure*. 2017.

[245] California Air Resources Board (CARB). *Staff report: initial statement of reasons for rulemaking, revisions to the regulation for mandatory reporting of greenhouse gas emissions*. 2010. URL: https://www.arb.%20ca.gov/regact/2010/ghg2010/ghgisor.pdf.

[246] Joe Kaatz and Scott Anders. "The role of unspecified power in developing locally relevant greenhouse gas emission factors in California's electric sector". In: *The Electricity Journal* 29.9 (2016), pp. 1–11.

[247] California Energy Commission (CEC). *Utility Plans from 2019*. 2019. URL: https://ww2.energy.ca.gov/almanac/electricity_data/supply_forms_2019/.

[248] R Kennedy. *Forms and Instructions for Submitting Electricity Resource Plans: Prepared in Support of the 2019 Integrated Energy Policy Report*. 2018.

[249] California Energy Commission (CEC). *Final Statement of Reasons: Modification of Regulations Governing the Power Source Disclosure*. 2020.

[250] *Final Report of Working Group 3 Co-Chairs: Southern California Edison Company, California Community Choice Association, and Commercial Energy, February 21, 2020. R.17-06-026*. 2020. URL: https://docs.cpuc.ca.gov/PublishedDocs/Efile/G000/M335/K710/335710541.PDF.

[251] California Independent System Operator (CAISO). *Extending the Day-Ahead Market to EIM Entities: Issue Paper*. 2019. URL: http://www.caiso.com/InitiativeDocuments/IssuePaper-ExtendedDayAheadMarket.pdf.

[252] California Public Utilities Commission (CPUC). *Clean System Power Calculator (formerly "Clean Net Short Calculator")*. 2020. URL: https://www.cpuc.ca.gov/General.aspx?id=6442459770.

[253] The Utility Reform Network (TURN). *Comments of The Utility Reform Network on the draft regulatory amendments to the Power Source Disclosure Program. Retrieved from California Energy Commission Docket No. 16-OIR-05*. 2019.

[254] *Integrated Resource Planning: 2020 IRP Filings, Filing Requirements Overview. R.20-05-003.* 2020.

[255] Chen-Hao Tsai et al. "Challenges of planning for high renewable futures: Experience in the US midcontinent electricity market". In: *Renewable and Sustainable Energy Reviews* 131 (2020), p. 109992.

[256] Ella Zhou, Wesley Cole, and Bethany Frew. "Valuing variable renewable energy for peak demand requirements". In: *Energy* 165 (2018), pp. 499–511.

[257] Steven J Davis and Ken Caldeira. "Consumption-based accounting of CO2 emissions". In: *Proceedings of the National Academy of Sciences* 107.12 (2010), pp. 5687–5692.

[258] Ling Ji et al. "Greenhouse gas emission factors of purchased electricity from interconnected grids". In: *Applied Energy* 184 (2016), pp. 751–758.

[259] Shen Qu et al. "A Quasi-Input-Output model to improve the estimation of emission factors for purchased electricity from interconnected grids". In: *Applied energy* 200 (2017), pp. 249–259.

[260] Shen Qu et al. "Virtual CO2 emission flows in the global electricity trade network". In: *Environmental science & technology* 52.11 (2018), pp. 6666–6675.

[261] Evan Kodra et al. "The North American electric grid as an exchange network: An approach for evaluating energy resource composition and greenhouse gas mitigation". In: *Environmental science & technology* 49.22 (2015), pp. 13692–13698.

[262] Environmental Protection Agency (EPA). *The Emissions & Generation Resource Integrated Database (eGRID): Technical Support Document for eGRID with Year 2018 Data.* Tech. rep. 2020. URL: `https://www.epa.gov/energy/emissions-generation-resource-integrated-database-egrid`.

[263] Joshua S Graff Zivin, Matthew J Kotchen, and Erin T Mansur. "Spatial and temporal heterogeneity of marginal emissions: Implications for electric cars and other electricity-shifting policies". In: *Journal of Economic Behavior & Organization* 107 (2014), pp. 248–268.

[264] Adam D Hawkes. "Estimating marginal CO2 emissions rates for national electricity systems". In: *Energy Policy* 38.10 (2010), pp. 5977–5987.

[265] Maninder PS Thind et al. "Marginal emissions factors for electricity generation in the midcontinent ISO". In: *Environmental science & technology* 51.24 (2017), pp. 14445–14452.

[266] Jacques A de Chalendar and Sally M Benson. "Why 100% renewable energy is not enough". In: *Joule* 3.6 (2019), pp. 1389–1393.

[267] Duncan S Callaway, Meredith Fowlie, and Gavin McCormick. "Location, location, location: The variable value of renewable energy and demand-side efficiency resources". In: *Journal of the Association of Environmental and Resource Economists* 5.1 (2018), pp. 39–75.

[268] *Air pollution: greenhouse gases: California Global Warming Solutions Act of 2006. Cal. Assemb. B. 32 (2005-2006), Chapter 488 (Cal. Stat. 2006)*. 2006.

[269] *Assessing California's Climate Policies—Electricity Generation*. Tech. rep. 2020. URL: https://lao.ca.gov/Publications/Report/4131.

[270] Michael D Mastrandrea, Mason Inman, and Danny Cullenward. "Assessing California's progress toward its 2020 greenhouse gas emissions limit". In: *Energy Policy* 138 (2020), p. 111219.

[271] California Air Resources Board (CARB). *California Greenhouse Gas Emissions for 2000 to 2017, Trends of Emissions and Other Indicators*. Tech. rep. 2019.

[272] California Energy Commission (CEC). *Total System Electric Generation*. Tech. rep. 2019. URL: https://ww2.energy.ca.gov/almanac/electricity_data/total_system_power.html.

[273] California Air Resources Board (CARB). *Amendments to the Regulation for the Mandatory Reporting of Greenhouse Gas Emissions: Final Statement of Reasons*. 2018. URL: https://ww2.arb.ca.gov/rulemaking/2018/mandatory-reporting-greenhouse-gas-emissions-2018.

[274] David Weisbach, Samuel Kortum, and Michael Wang. "Optimal Unilateral Carbon Policy". In: (2020).

[275] Aaron Cosbey et al. "Developing guidance for implementing border carbon adjustments: Lessons, cautions, and research needs from the literature". In: *Review of Environmental Economics and Policy* 13.1 (2019), pp. 3–22.

[276] Stefan U Pauer. "Including electricity imports in California's cap-and-trade program: A case study of a border carbon adjustment in practice". In: *The Electricity Journal* 31.10 (2018), pp. 39–45.

[277] Danny Cullenward. "Leakage in California's carbon market". In: *The electricity journal* 27.9 (2014), pp. 36–48.

[278] C Lo Prete, Ashish Tyagi, and Cody Hohl. "California's cap-and-trade program and emission leakage in the electricity sector: an empirical analysis". In: *Work. Pap* (2019).

[279] James Bushnell, Yihsu Chen, and Matthew Zaragoza-Watkins. "Downstream regulation of CO2 emissions in California's electricity sector". In: *Energy Policy* 64 (2014), pp. 313–323.

[280] California Independent System Operator (CAISO). *Western EIM Benefits Reports (Q1-Q4 2018)*. 2018. URL: www.westernEIM.com.

[281] California Air Resources Board (CARB). *Final Regulation Order: Proposed Amendments to the Regulation for the Mandatory Reporting of Greenhouse Gas Emissions*. 2018. URL: https://ww2.arb.ca.gov/rulemaking/2018/mandatory-reporting-greenhouse-gas-emissions-2018.

[282] Environmental Protection Agency (EPA). *The Emissions & Generation Resource Integrated Database*. Tech. rep. 2018. URL: https://www.epa.gov/energy/emissions-generation-resource-integrated-database-egrid.

[283] California Energy Commission (CEC). *Power Source Disclosure data. Retrieved via personal correspondence*. 2019. URL: https://www.energy.ca.gov/programs-and-topics/programs/power-source-disclosure.

[284] California Air Resources Board (CARB). *Documentation of California's 2000-2017 GHG Inventory – Index*. 2019. URL: https://ww3.arb.ca.gov/cc/inventory/doc/doc_index.php.

[285] California Energy Commission (CEC). *QFER CEC-1304 Power Plant Owner Reporting Database*. 2019. URL: https://ww2.energy.ca.gov/almanac/electricity_data/web_qfer/index_cms.php.

[286] Roger Z Ríos-Mercado and Conrado Borraz-Sánchez. "Optimization problems in natural gas transportation systems: A state-of-the-art review". In: *Applied Energy* 147 (2015), pp. 536–555.

[287] Viet Pham, Carl Laird, and Mahmoud El-Halwagi. "Convex hull discretization approach to the global optimization of pooling problems". In: *Industrial & Engineering Chemistry Research* 48.4 (2009), pp. 1973–1979.

[288] Viet Pham. "A global optimization approach to pooling problems in refineries". PhD thesis. Texas A & M University, 2010.

[289] Mohammed Alfaki and Dag Haugland. "Comparison of discrete and continuous models for the pooling problem". In: *11th Workshop on Algorithmic Approaches for Transportation Modelling, Optimization, and Systems*. Schloss Dagstuhl-Leibniz-Zentrum fuer Informatik. 2011.

[290] Petra M Bartmeyer and Christiano Lyra. "A new quadratic relaxation for binary variables applied to the distance geometry problem". In: *Structural and Multidisciplinary Optimization* 62.4 (2020), pp. 2197–2201.

[291] California Air Resources Board (CARB). *Asset Controlling Suppliers*. 2019. URL: https://ww2.arb.ca.gov/mrr-acs.

[292] California Air Resources Board (CARB). *Low Carbon Fuel Standard Annual Updates to Lookup Table Pathways: California Average Grid Electricity Used as a Transportation Fuel in California and Electricity Supplied Under the Smart Charging or Smart Electrolysis Provision*. 2020. URL: https://ww3.arb.ca.gov/fuels/lcfs/fuelpathways/comments/tier2/elec_update.pdf.